# A STUDY ON SOIL-STRUCTURE INTERACTION OF AXIALLY LOADED SHEET PILES

by

Matthew Brian Sylvain

A dissertation submitted to the faculty of
The University of North Carolina at Charlotte
in partial fulfillment of the requirements
for the degree of Doctor of Philosophy in
Infrastructure and Environmental Systems

Charlotte

2019

Approved by:

______________________________
Dr. Miguel A. Pando

______________________________
Dr. Matthew J. Whelan

______________________________
Dr. Vincent O. Ogunro

______________________________
Dr. Harish Cherukuri

______________________________
Dr. Don Chen

# ABSTRACT

MATTHEW BRIAN SYLVAIN. A Study on Soil-Structure Interaction of Axially Loaded Sheet Piles. (Under direction of DR. MIGUEL A. PANDO)

Sheet piles are geotechnical structural elements often used in canals and rivers for soil retention and scour protection. Short span bridge abutment design in North Carolina and the U.S., for locations near bodies of water, typically uses sheet piles for soil retention and scour protection, while piles installed behind the sheet piles are used for axial load bearing. This dissertation investigates the feasibility of extending the function of these sheet piles to also act as axial load bearing foundation elements. Neglecting any axial load bearing potential provided by the sheet piles is likely a conservative design approach as Europe has successfully utilized the axial load bearing capacity of sheet piles in bridge abutment constructions for over fifty years (Carle and Whitaker 1989; Rybak and Zyrek 2013; SACILOR ; Skyline Steel LLC 2009; Yandzio 1998). Incorporating the axial load bearing capacity of sheet piles has the potential to significantly reduce construction costs and installation times by reducing the number or length of piles required for bridge abutment designs. This design approach has not been adopted in the U.S. partly due to the scarcity of full-scale axial load tests on instrumented sheet piles.

The main focus of this research is to help address this scarcity and assess the soil-structure interaction and axial load bearing capacity of axially loaded sheet piles. This research involves a series of full-scale axial load tests on well-instrumented sheet piles. The results are used to examine the soil-structure interaction behavior for this foundation system in detail and provide methods for predicting this behavior for design purposes. The first series of load tests are performed under controlled soil conditions at the

University of North Carolina at Charlotte (UNCC) Energy Production and Infrastructure Center (EPIC) geotechnical test pit, and the second set of tests are carried out under field settings at the equipment yard of the International Construction Equipment (ICE) facility in Matthews, North Carolina. The testing performed at the field site additionally included load testing of an H-pile to permit for comparisons between the axial stiffness and load capacity of a sheet pile pair and a pile section conventionally used for axial load bearing in bridge abutments. The results are compared with capacity predictions made using static methods and load-settlement curves obtained using different load transfer analyses. Additionally, the nature of the soil-structure interaction for a foundation with a wall or plate geometry is investigated further and compared to a cylindrical geometry. Analytical methods are used to study this behavior and it is found that the axially loaded foundation wall exhibits a different response than the cylindrical pile. The results for the foundation wall are used to develop new theoretical load transfer curves for load-settlement predictions of axially loaded sheet piles. Load transfer analyses using the developed *T-Z* and *Q-Z* curves are compared with measured load-settlement and load transfer curves resulting from pile load testing.

The load test results performed for this research, under the soil conditions at the laboratory and field sites, indicate that sheets piles have favorable axial load bearing characteristics and comparable performance to other driven pile types commonly used as axial load bearing foundations for short-span bridge abutments. Deep foundation methodologies for analysis and design of conventional driven piles are found to be applicable for assessing axial load capacity of sheet piles. The methods evaluated include static methods based on geotechnical in-situ tests, such as the standard penetration test

(SPT) and cone penetration test (CPT), and methods based on dynamic measurements obtained during pile installation, such as Pile Driving Analysis (PDA) and Case Pile Wave Analysis Program (CAPWAP). The level of accuracy of the different capacity prediction methods are compared and return similar levels of uncertainty for sheet pile capacity estimates as obtained for H-pile capacity estimates used in the field test program.

Plugging represents a key aspect when estimating the axial capacity of sheet piles. Plugging occurs when soil moves together with an axially loaded pile rather than shearing at the soil to pile interface. This behavior influences the areas involved in shaft and end-bearing. Plugging has the effect of increasing the load bearing surface near the toe of the pile, thereby increasing effective toe resistance, while shaft area and shaft resistance is typically reduced along the pile where plugging occurs. The change in end-bearing area for sheet piles due to plugging can be especially large due to the thin cross section of this foundation type. Plugging behavior for sheet piles can have significant implications for ultimate load capacity and is considered in greater detail as part of this study.

The applicability of load transfer methods to predict load-settlement curves and axial load transfer mechanisms for sheet piles is also assessed using the results of the different axial load tests performed in this research. Load-settlement curves predicted using load transfer analysis show good agreement with the behavior measured during load tests. Empirical as well as theoretical load transfer curves are considered and compared to experimental estimates obtained as part of this study.

# ACKNOWLEDGEMENTS

I am very thankful for the support I have received from numerous individuals and organizations during my time at UNC Charlotte. I'd like to thank my family for their tremendous support, encouragement, and understanding during my studies. Thank you to my advisor, Dr. Miguel Pando, for his guidance and support during my time here. I would like to thank my committee members for their dedication, time, and effort spent towards this project: Dr. Matthew Whelan, Dr. Vincent Ogunro, Dr. Harish Cherukuri, and Dr. Don Chen. I'd like to gratefully acknowledge support received from the Infrastructures and Environmental Systems program, the Civil and Environmental Engineering department, and from the North Carolina Department of Transportation (RP 2014-08) for financial support received during my program. I would also like to thank the Deep Foundation Institute and the Graduate School at UNC Charlotte for their financial support through awarded scholarships and financial support. Thank you to Mr. Dave Naylor, Dr. Rajaram Janardhanam, and Dr. Vincent Ogunro for the opportunity to serve as a teaching assistant for their courses, interacting with undergraduate students was an enriching experience. I'd like to especially thank the Geopier office in Davidson, North Carolina for the internship position that provided not only financial support but terrific experience that will benefit my career. Thank you to Dr. Youngjin Park and Mr. Mike Moss of the EPIC Highbay lab for their assistance with the full-scale pile load tests, their support and experience was much appreciated. Additionally, the numerous companies that have helped with materials and testing are very gratefully acknowledged, their assistance improved the quality of this research. And lastly, friends and colleagues are gratefully acknowledged for their valued support and company.

# TABLE OF CONTENTS

## LIST OF FIGURES

## LIST OF TABLES

# LIST OF SYMBOLS AND ABBREVIATIONS

## LIST OF SYMBOLS

| | |
|---|---|
| $\alpha$ | Coefficient used in the LCPC method for estimating unit shaft resistance |
| $\beta$ | Coefficient used in the beta method (effective stress based) for estimating shaft friction |
| $\gamma$ | Shear strain (%) |
| $\gamma_{dry}$ | Dry unit weight ($F/L^3$) |
| $\gamma_t$ | Total or moist unit weight ($F/L^3$) |
| $\delta$ | Interface friction angle (°) |
| $\upsilon$ | Poisson's ratio |
| $\rho$ | Density ($M/L^3$) |
| $\tau$ | Shear stress ($F/L^2$) |
| $\tau_{max}$ | Shear stress at failure ($F/L^2$) |
| $\tau_0$ | Vertical shear stress at the plate to soil interface ($F/L^2$) |
| $\phi$ | Friction angle (°) |
| $\phi'$ | Friction angle (in terms of effective stress) (°) |
| a | Area ratio of the CPT cone ($=A_n/A_c$) |
| A | Coefficient for empirical *T-Z* curve shape |
| $A_c$ | Projected area of the CPT cone tip ($L^2$) |
| $A_n$ | Cross-sectional area of the CPT load cell or shaft ($L^2$) |
| $A_s$ | Area of pile shaft that is in contact with soil (i.e. pile-soil interface) ($L^2$) |
| $A_t$ | Area engaged in toe bearing ($L^2$) |
| $A_{wall}$ | Cross sectional area of wall ($L^2$) |
| B (or b) | Pile width or diameter (L) |

| | |
|---|---|
| B | Coefficient for empirical *T-Z* curve shape |
| c’ | Cohesion (in terms of effective stress) (F/L$^2$) |
| c | Wave speed (L/T) |
| cm | Centimeter (L) |
| $C_c$ | Coefficient of curvature |
| $C_u$ | Coefficient of uniformity |
| D | Pile embedment (L) |
| $D_{10}$ | Grain diameter representing size at which 10% of the mass (or weight) of the material has a lesser diameter (L) |
| $D_{30}$ | Grain diameter representing size at which 30% of the mass (or weight) of the material has a lesser diameter (L) |
| $D_{50}$ | Grain diameter representing size at which 50% of the mass (or weight) of the material has a lesser diameter, or mean grain diameter (L) |
| $D_{60}$ | Grain diameter representing size at which 60% of the mass (or weight) of the material has a lesser diameter (L) |
| $E_D$ | Dilatometer modulus (F/L$^2$) |
| $E_m$ | Pressuremeter modulus (F/L$^2$) |
| $E_s$ | Modulus of Elasticity for soil (F/L$^2$) |
| f | Curve fitting parameter for modified hyperbolic soil model |
| $f_s$ | Unit pile shaft resistance (F/L$^2$) |
| ft | Feet (L) |
| $F_y$ | Yield strength (F/L$^2$) |
| g | Curve fitting parameter for modified hyperbolic soil model |
| G | Shear modulus (F/L$^2$) |
| $G_s$ | Specific gravity |
| $G_{sec}$ | Secant shear modulus (F/L$^2$) |

| | |
|---|---|
| $G_0$ | Maximum shear modulus ($F/L^2$) |
| h | Depth of pile cross section (L) |
| in | Inch (L) |
| $I_D$ | Dilatometer material index |
| $I_s$ | Rigidity and shape factor |
| $k_c$ | Coefficient used in the LCPC method for estimating unit toe resistance |
| kg | Kilogram, base unit of mass in the SI system (M) |
| kip | 1,000 lbf (F) |
| kN | Kilonewton (F) |
| kPa | Kilopascal ($F/L^2$) |
| ksi | Kip per square inch ($F/L^2$) |
| $K_0$ | Coefficient of lateral earth pressure at-rest |
| lbf | Pound force (F) |
| L | Length along centerline of foundation wall (L) |
| m | Meter, base unit of length in the SI system (L) |
| mm | Millimeter (L) |
| MPa | Megapascal ($F/L^2$) |
| N | Newton = $kg/s^2$, base unit of force in the SI system (F) |
| $N_c$ | Bearing capacity factor |
| $N_k$ | Cone factor |
| $(N_1)_{60}$ | SPT blow count corrected for overburden pressure and hammer energy |
| $p_1$ | Pressuremeter limit pressure ($F/L^2$) |
| Pa | Pascal = $N/m^2$, base unit of pressure in the SI system ($F/L^2$) |

| | |
|---|---|
| $P_{wall}$ | Perimeter of wall (L) |
| $q_c$ | CPT cone tip resistance ($F/L^2$) |
| $q_{ca}$ | Averaged CPT cone tip resistance using an averaging procedure outlined in LCPC method, used for estimating unit toe resistance ($F/L^2$) |
| $q_E$ | Cone tip resistance corrected for pore pressure ($\neq q_t$') ($F/L^2$) |
| $q_t$' | Corrected CPT cone tip resistance = $q_c$ + (1-a) $u_2$ ($F/L^2$) |
| $q_t$ | Unit pile toe resistance ($F/L^2$) |
| Q | Mobilized toe resistance as commonly denoted by load transfer methodology (F) |
| Qc | Calculated pile load capacity using static methods (F) |
| $Q_m$ | Measured pile load capacity corresponding to Davisson's failure criteria (F) |
| $Q_u$ | Ultimate load (F) |
| r | Distance away from centerline of pile (L) |
| $r_m$ | Radial distance at which deformations induced in the soil due to pile loading becomes negligible (L) |
| $r_0$ | Radius of pile (L) |
| $r_0$ | Half of wall thickness (L) |
| $R_s$ | Total pile shaft resistance (F) |
| $R_t$ | Total pile toe resistance (F) |
| s | Second, base unit of time (T) |
| $s_u$ | Undrained shear strength ($F/L^2$) |
| $S_{lat}$ | Area for shaft resistance ($L^2$) |
| $t_f$ | Thickness of flange for pile cross section (L) |
| $t_w$ | Thickness of wall for pile cross section (L) |

| | |
|---|---|
| $T$ | Mobilized shaft resistance as commonly denoted by load transfer methodology ($F/L^2$) |
| $u_2$ | Pore pressure measured behind the CPT cone ($F/L^2$) |
| $V$ | Applied vertical compression load (F) |
| $V_s$ | Shear wave velocity (L/T) |
| $w$ | Width of pile cross section (L) |
| $w_s$ | Total settlement of the pile (L) |
| $W_{opt}$ | Optimum water content (%) |
| $Z$ | Vertical pile movement as commonly denoted by load transfer methodology (L) |
| $Z_b$ | Vertical pile movement at the pile toe (L) |
| $Z_c$ | Critical movement required to mobilized maximum shaft and toe resistance for empirical load transfer method (L) |
| $\Delta Z$ | Depth of pile resisting applied load (L) |

# LIST OF ABBREVIATIONS

| | |
|---|---|
| API | American Petroleum Institute |
| ASTM | American Society of Testing and Materials |
| AZ | Arbed type sheet pile |
| BDI | Bridge Diagnostic, Inc. |
| BH | Bore hole |
| CAPWAP | Case Pile Wave Analysis Program |
| CASE | Case Western Reserve University, formerly Case Institute of Technology |
| CHT | Cross Hole Test |
| CME | Central Mine Equipment |
| CPT | Cone Penetration Test |
| CRP | Constant Rate of Penetration |
| CT | Computerized Tomography |
| CU | Consolidated Undrained triaxial test |
| DMT | Dilatometer Test |
| EOD | End of Driving |
| EPIC | Energy Production and Infrastructure Center |
| F | Frodingham type sheet pile |
| FHWA | Federal Highway Administration |
| GRL | Goble, Rausche, Likins |
| HP | H type pile |
| HSA | Hollow Stem Auger |
| ICE | International Construction Equipment, Inc. |

| | |
|---|---|
| JC | Case method damping factor |
| LL | Liquid Limit (%) |
| LCPC | Laboratoire Central des Ponts et Chaussees |
| LP | Larssen type sheet pile |
| MASW | Multichannel Analysis of Surface Waves |
| MKT | McKiernan-Terry |
| MTS | MTS Systems Corporation |
| NC | North Carolina |
| NCDOT | North Carolina Department of Transportation |
| OCR | Over Consolidation Ratio |
| PDA | Pile Driving Analysis/Analyzer |
| PI | Plasticity Index (%) |
| PL | Plastic Limit (%) |
| PVC | Polyvinyl Chloride |
| PXI | PCI eXtensions for Instrumentation |
| PZ | Ball and socket interlock sheet pile |
| RC | Relative Compaction |
| RX7 | Case method capacity with a damping factor of 0.7 |
| SCI | Steel Construction Institute (U.K.) |
| SCPTu | Seismic Cone Penetration Test with pore pressure (u) measurement |
| SD | Standard Deviation |
| SI | International System of Units |
| SP | Standard Proctor |

| | |
|---|---|
| SPT | Standard Penetration Test |
| UNCC | University of North Carolina at Charlotte |
| US | United States |
| USCS | Unified Soil Classification System |
| UU | Unconsolidated Undrained triaxial test |
| WC | Water Content (%) |

# CHAPTER 1: INTRODUCTION

## 1.1 Statement of Problem

Typical use of sheet piles in the U.S. involves soil-retaining structures where lateral loading and associated bending moments are most important when considering soil-structure interaction. For example, sheet piles are commonly used for marine construction, such as wharfs, harbors, and cofferdams, due to their excellent ability to retain soil and ability to interlock to form continuous walls. In recent years, sheet piles have increasingly been utilized not only for soil retainment and lateral load capacity but also for their axial load capacity (Abbondanza 2009; Carle and Whitaker 1989; Evans et al. 2012; McShane 1991; Underwood and Greenlee 2010; Yandzio 1998). This alternative application of sheet piles has substantial potential for use in short span bridge abutments where sheet piles are commonly used. In the U.S., short span bridge abutment design traditionally uses sheet piles mainly for scour protection, while conventional axial load bearing piles driven behind the sheet piles provide axial load capacity to the superstructure. Figure 1-1 presents an image of a typical North Carolina Department of Transportation (NCDOT) short span bridge design. Incorporating the axial load bearing capacity of sheet piles may help to reduce, or even eliminate, the need for H-piles in short span bridge construction. This dissertation stems from the recently completed NCDOT Research Project No. FHWA/NC/2012-08 titled ‘Determination of Vertical Resistance for Sheet Pile Abutments’. The objective of the NCDOT research project was to investigate design guidance and potential cost savings that could be realized by using sheet piles to carry axial loads in bridge abutments, an approach that has yet to be incorporated into common design practice in the U.S. Two separate dissertations are associated with this original NCDOT research project.

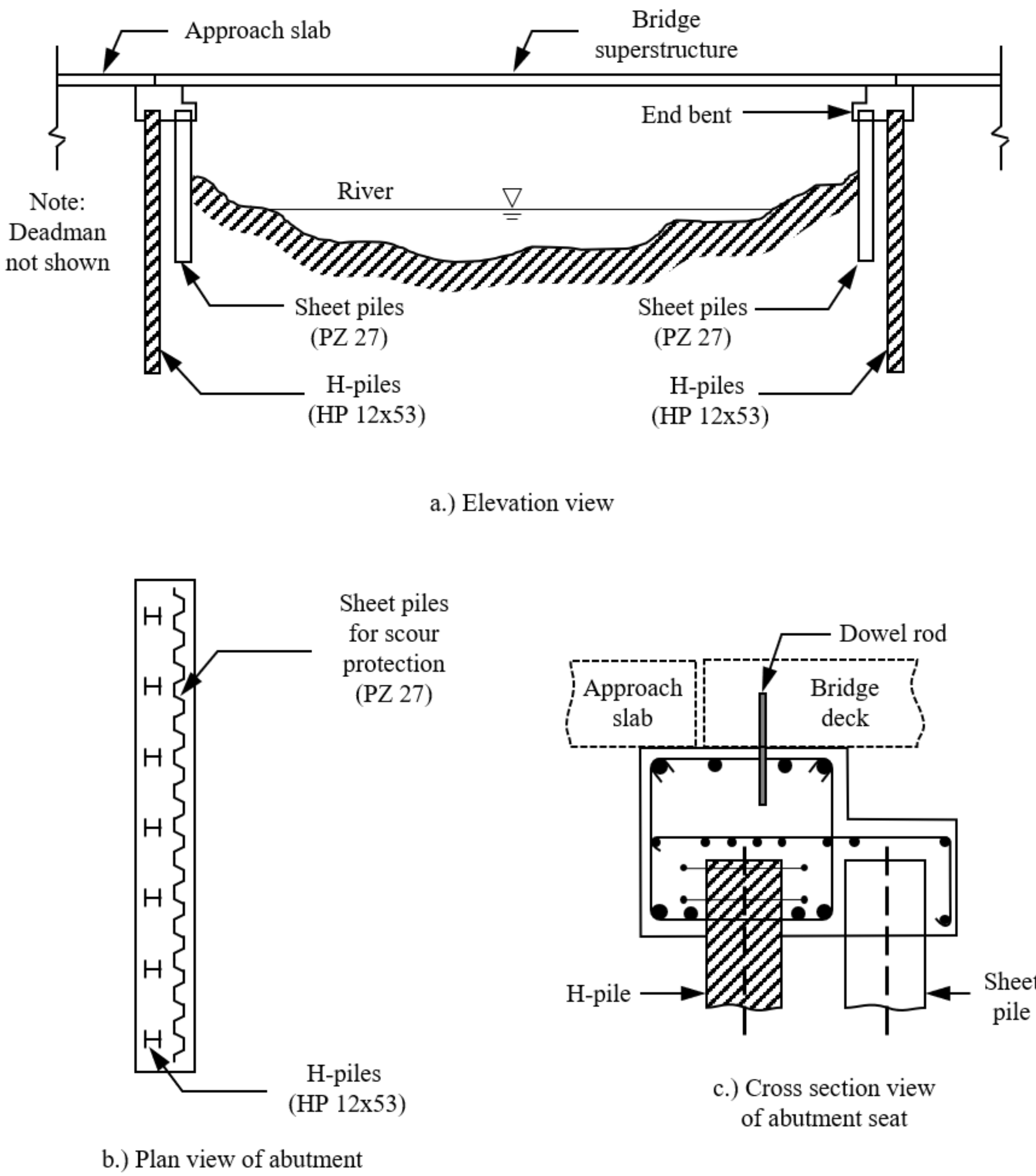


Figure 1-1. Schematic of a typical NCDOT short span bridge with sheet pile abutment

This design approach is likely inspired from recent bridge construction practices in Europe that have successfully made use of sheet piles for axial load bearing capacity for several decades. Several benefits can be realized by utilizing the axial load bearing capacity of sheet piles in bridge construction. Perhaps two of the most compelling advantages of this design approach are cost savings achieved through reducing the number and length of pile needed for construction and the reduced time required to construct the bridge due to reduction in the amount of pile driving. However, two significant technical gaps that need to be addressed to permit widespread adoption of this design approach are the lack of well-documented pile load tests of sheet piles and the lack of available, validated methods for predicting the axial load versus settlement behavior of sheet piles.

## 1.2 Objectives and Scope of Research

This dissertation investigates the geotechnical behavior of sheet piles under axial load. Specifically, the soil-structure interaction process that governs the axial load versus settlement response and axial load capacity. The main focus of this research is to investigate soil-structure interaction of axially loaded sheet piles using full-scale well-instrumented sheet piles. Full-scale pile load tests under laboratory and field settings are performed as part of this study. The first series of tests are conducted at the EPIC geotechnical test pit, and the second set of tests were performed at a field site located in Matthews, North Carolina. The test program at the field site includes pile load testing on a pair of sheet piles. Pile load testing is also performed on an H-pile section typical of those conventionally used for axial load bearing. Both test locations are well-characterized using conventional laboratory and in-situ geotechnical tests. The results of load testing are compared to conventional methods used to predict axial pile load capacity for design purposes. Results from the well-instrumented pile load tests are interpret using the load transfer method to further characterize the axial load bearing behavior of the test piles. Additionally, measured load transfer curves are compared to empirical curves developed for conventional axial load bearing piles. Design recommendations based on the literature review and experimental results are provided.

Additionally, analytical methods are used to further characterize the difference between the behavior of an axially loaded cylindrical pile and an axially loaded foundation wall. A newly derived expression for shear stress degradation with horizontal distance from the foundation wall is presented. This expression is used to develop new theoretical load transfer curves. Results from this analysis are compared to currently existing expressions in the literature for prismatic piles. Additionally, these theoretical load transfer curves are compared with measured results from field testing as part of this study and conclusions are drawn based on this comparison.

In summary, the main goal of this dissertation is to contribute to a better understanding of the load transfer mechanism that governs axially loaded sheet piles. This study aims to do this through full-scale load tests of well-instrumented piles in laboratory and field settings. An analytical approach is used to derive a new expression for the decay of shear stress with distance from an axially loaded plate pile in an effort to improve understanding of the load transfer mechanism involved for an axially loaded foundation wall.

## 1.3 Oranization of Dissertation

The organization of this dissertation in six chapters and three appendices is summarized as follows:

- Chapter 1, this introduction chapter.

- Chapter 2 presents the literature review and covers the current state of knowledge regarding this subject. This chapter presents research and case studies identified in the U.S. and in Europe that involve the axial load bearing capacity of sheet piles. Additionally, this chapter presents existing design guidance regarding the use of sheet piles for axial load resistance. Knowledge gaps are highlighted at the end of the chapter.
- Chapter 3 presents the experimental results of laboratory load testing performed on sheet piles. This chapter introduces details regarding laboratory tests, including descriptions of the piles and instrumentation, methods used for pile installation, soil characterization, measured load transfer curves, and load versus settlement results obtained from static pile load testing.
- Chapter 4 presents the experimental results of field load testing performed on sheet piles. This chapter provides information concerning the field site, characterization of the soils encountered, the instrumentation and piles used in the testing, measured load transfer curves, and load versus settlement results obtained from static pile load testing.
- Chapter 5 presents the results of the computational analysis performed as part of this study. Several empirical static methods are considered for comparison with measured pile load test results. The methods considered are based on CPT and SPT data. Experimentally obtained estimates for ultimate, shaft, and toe pile load capacities are compared to the corresponding quantities obtained using empirical methods for static capacity estimation. The load transfer curves measured from pile load testing are compared with empirically obtained curves. This comparison considers peak unit

resistance values for shaft and toe capacities based on the Meyerhof and LCPC methods. The functional form of the empirical load transfer curves are obtained from API (1993) and Vijayvergiya (1977). This chapter also presents the results from the analytical evaluation of an axially loaded foundation wall or plate and the derivation of a new expression for settlement. The degradation in shear stress with distance from the plate foundation was observed to differ from that observed for a cylindrical pile. This new expression for settlement is used to develop new theoretical *T-Z* curves to capture the load transfer behavior for an axially loaded wall geometry.

- Chapter 6 presents the summary and conclusions that present a comprehensive review of the key ideas presented in this dissertation. This chapter presents design recommendations based on the findings of this study as well as topics for further study.
- Appendix A presents supplementary material related to the literature review that is not included in the main body of this dissertation.
- Appendix B presents supplementary material related to the testing performed at the EPIC Highbay that is not included in the main body of this dissertation.
- Appendix C presents supplementary material related to the testing performed at the field site at Matthews, North Carolina. This material is not included in the main body of this dissertation.
- Appendix D presents material related to the static methods used for determining pile load capacity used in this study.

# CHAPTER 2: LITERATURE REVIEW

## 2.1 Introduction

This chapter presents a summary of the literature review conducted as part of this study on the axial load transfer behavior of sheet piles. The chapter is organized into four main sections:

1.) A summary of relevant identified case studies of worldwide bridge constructions that have used axially loaded sheet piles for bridge abutment design.

2.) A summary of axial pile load tests performed on sheet piles.

3.) Current existing guidance for the design of sheet piles to carry axial load.

4.) A review of plugging behavior observed in piles for both pile sections traditionally used for axial load bearing and sheet piles.

Supplementary material not presented in this chapter is included in Appendix A.

## 2.2 Bridge Case Histories

The use of sheet piles as the main axial load bearing elements in bridge abutments has been successfully reported in both Europe (Carle and Whitaker 1989; Rybak and Zyrek 2013; SACILOR ; Skyline Steel LLC 2009; Yandzio 1998) and the United States (Carle and Whitaker 1989; Evans et al. 2012; Hickman 2011; Skyline Steel LLC 2009). Several different sheet pile sections were encountered in the case histories. Typical sheet piles used in the identified European bridges were U-shaped sheet piles, such as the Larssen (LP) and Frodingham (F) types, while sheet piles used in the identified U.S. bridges were Z-shaped. Lateral loading is a very important design consideration for sheet piles serving as the only load bearing elements of a bridge abutment. In many of the bridge case histories from Europe, a “box” pile assembled with multiple sheet piles was used to increase the axial and lateral stiffness and strength of the foundation. Figure 2-1 presents schematics of U-shaped piles, Z-shaped pile, and boxed pile configurations for both of these pile types. A variety of different bridge abutment pile configurations involving the use of sheet piles were identified. These configurations are presented in Appendix A. A design alternative to box sections that was also identified in the literature involves the use of a “deadman”, which is an anchoring system used to provide lateral support to the abutment.

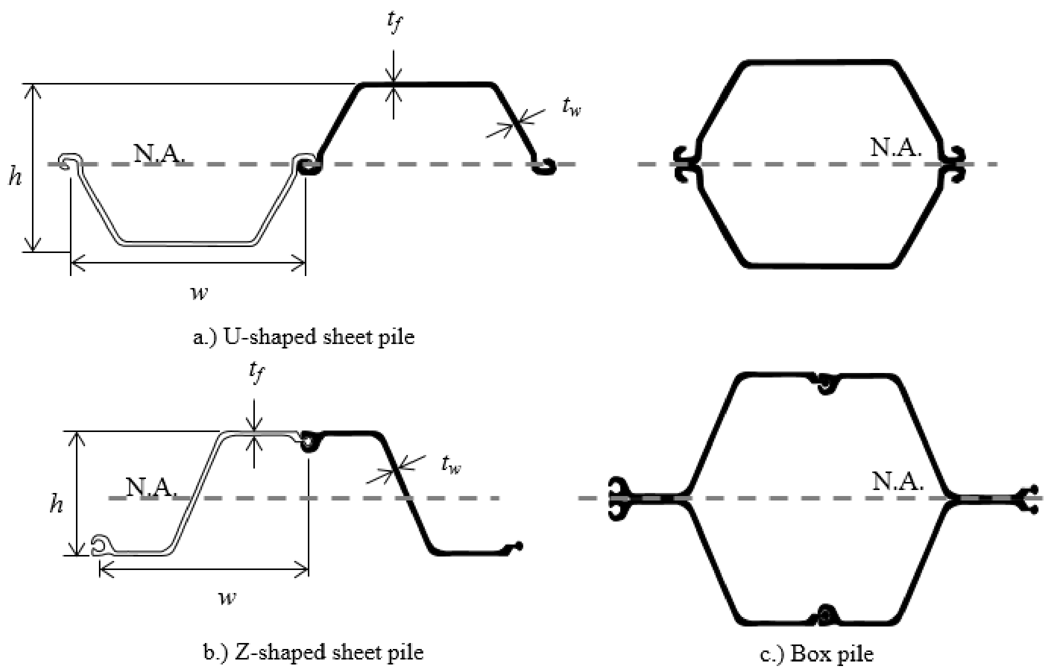


Figure 2-1. Configurations of sheet piles reported used in bridge case histories

A list of bridge case histories where sheet piles were reported as axial load bearing elements in the abutment is provided in Table 2-1. In general, bridges utilizing this design approach are more prevalent in Europe than in the U.S., and for these projects sheet piles are used in various and innovative ways to increase axial or lateral stiffness. Additional information regarding the case histories identified can be found in Appendix A.

Table 2-1. Bridge case histories where sheet piles are used as load bearing elements

| Structure Identifier | Region | Location | Abutment Details[1] | Reference |
|---|---|---|---|---|
| Pont de Chambiere | Europe | Chambiere Neighborhood, France | 14.02 m LP IV sheet piles with tieback | SACILOR (n.d.) Carle and Whitaker (1989) |
| A8 | | La Cagne River, Cagne-su-Mer, France | LP SL3 box columns | SACILOR (n.d.) |
| Somme River | | Amiens, France | 10.36 m LP IIn 17.98 m LP IIIn box every 3.2 m o.c. | SACILOR (n.d.) Carle and Whitaker (1989) |
| A31 | | Metz, France | LP IIs LP IIIs | Carle and Whitaker (1989) |
| Moselle Canal | | Neuves-Maisons, France | 12.19 m LP IV 12.80-15.24 m LPIII | SACILOR (n.d.) |
| Brenne River | | Venarey-Les-Laumes, France | 6 m LP IIIs | SACILOR (n.d.) |
| Saône River | | Seurre-Ecuelles, France | LP IVs | SACILOR (n.d.) |
| Humber Road | | Immingham, England | LP 20W LP 30W | Yandzio (1998) |
| Canal | | Stoke-on-Trent, England | F 3N F 4N | Yandzio (1998) |
| Capel St. Mary A12 Underpass | | Ipswish, England | High Modulus | Yandzio (1998) |
| Stockman's Lane | | Belfast, Ireland | LP IV box | Yandzio (1998) |
| S8 Express Road | | Warsaw, Poland | AZ 13, AZ 25, AZ 37-700 | Skyline Steel LLC (2009) Rybak and Zyrek (2013) |
| Taghkanic Creek | U.S. | Columbia County, NY | 4.88 m PZ 22 | Carle and Whitaker (1989) |
| Banks Road | | Tomkins County, NY | N/A | Carle and Whitaker (1989) |
| Small Creek | | Seward, AK | 8.84 m PZ 27 | Carle and Whitaker (1989) |
| Bryan Road | | Black Hawk County, IA | 4.57 m PZ 22 | Evans et al. (2012) |
| Lone Star Canal | | Chambers County, TX | 13.41 m AZ 14-770 | LEAP Engineering (2011) |
| Route 4 | | Paramus, Bergen County, NJ | AZ 36 w/ sheet pile deadman | Skyline Steel LLC (2009) |

Note: (1): Please refer to Figure 2-1 for an explanation of sheet pile acronyms

### 2.2.1 Summary of Bridge Case Histories

In total, eighteen bridge case studies were identified for locations in Europe and the U.S. Design approaches involved the use of both U and Z type piles configured as opened, boxed, or a mix of both configurations. Case studies identified in the U.S. made use of different sheet pile sections and pile type than what was typically found in Europe. Z type sections are typically used in the U.S. and the U type sections are typically used in Europe. All of the bridges identified were single span. Lateral support was an important design consideration for abutments using axially loaded sheet piles. Lateral support came from the use of a tie rod, deadman, or, in some cases, no lateral support was provided and the sheet piles behaved as a cantilever wall. For cases where sheet piles were used as the vertical load bearing member in an abutment, the piles had greater embedment depth into the concrete abutment compared to designs where sheet pile contributions to the vertical load resistance are neglected. In some of the U.S. cases, a bearing plate was used to transfer loads from the abutment to the sheet pile, however this was uncommon. Additionally, piles used to carry vertical loads were typically longer than those within designs where sheet piles were not used to carry vertical loads. For designs that incorporated both box and sheet piles, sheet piles lengths were reduced.

Based on the literature review, several bridges were identified that utilize the axial load capacity of sheet piles. In some cases, these bridges have been in operation for over 25 years, which suggests a strong potential for safely incorporating the axial load bearing capacity of sheet piles in bridge abutment designs. The case studies further suggest the potential for reducing or eliminating the number of bearing piles typically used in design. Incorporating the axial bearing capacity of the sheet piles may lead to considerable cost savings associated with reductions in both construction time and materials. Despite several successful case studies and the potential benefits of this approach, the axial load contribution from bridge abutment sheet piles is still routinely neglected in design assumptions by U.S. transportation agencies. Based on the literature review, much information concerning geotechnical conditions, long-term performance, and other details concerning the soil-structure interaction behavior of the sheet piles have not been thoroughly investigated. This indicates a need for additional well-documented case histories and, in particular, full-scale axial load tests to better understand the load transfer mechanism of this foundation element under axial loading. Appendix A presents additional information regarding this literature review.

## 2.3 Static Axial Load Tests on Steel Sheet Piles

There are relatively few axial load tests on sheet piles relative to axial load tests performed on other pile types. A few well-documented pile load tests reported by Bustamante and Gianeselli (1991) and by Evans et al. (2012) provide useful insight on the behavior of axially loaded sheet piles, but do not provide enough information to allow a comprehensive understanding of the mechanisms involved in the soil-structure interaction. Table 2-2 presents a summary of the identified axial load tests on sheet piles.

The table presents key information from the identified tests and a summary of the findings. The majority of the axial load tests involve full-scale piles, the same size as typically used in construction. In some cases, test piles were instrumented along their length to provide better insights regarding the load transfer behavior of the pile with depth. In-situ site characterization was performed using either Cone Penetrometer Tests (CPT), Standard Penetration Tests (SPT), or Pressuremeter tests to characterize the soils encountered, and the general type of soil is reported in the table. In some cases, a comparison pile was used to help evaluate how sheet piles performed in comparison to another type of pile under axial load testing at the same site. In many cases in Europe and the U.K. this involved a boxed sheet pile configuration that was used for bridge construction. The following subsections present each of the identified static axial load tests in more detail.

Table 2-2. Summary of identified axial load tests performed on sheet piles

| Reference | Type of Testing | Instrumentation Installed on Pile | Soil Characterization Tests | Type of Soil Encountered | Comparison Pile Used | Plugging Discussed | Summary |
|---|---|---|---|---|---|---|---|
| Bustamante and Gianeselli (1991) | Full-Scale | Strain gages along length of pile | CPT, SPT | Sand | Box pile | Yes, area bounded by flanges for calculating toe resistance, full shaft area used for shaft resistance. | Test site located in Dunkirk, France. Higher axial load bearing capacity observed in sheet pile compared to box pile |
| | Full-Scale | Strain gages along length of pile | CPT, SPT | Clay | Box pile | | Test site located in Merville, France |
| Borel et al. (2002) | Full-Scale | Strain gages along length of pile | Pressuremeter | Marly soils with cobbles | None | No | Test located in Cachan, France. Testing performed on impact and vibratory driven sheet pile pairs |
| | Full-Scale | Strain gages along length of pile | Pressuremeter | Dense gravels | None | | Test located in Erstein, France. Testing performed on impact and vibratory driven sheet pile pairs |
| Evans et al. (2012) | Full-Scale (live load testing) | Strain gages along length of pile | CPT, soil borings | Clay with sand seams | None | Plugging mentioned but expected to be negligible for | Results of live load testing resulted in axial and flexural stresses in pile comparable to calculated values |
| Taenaka et al. (2006) | Full-Scale | Strain gages along length of pile | SPT | Sand, silt, and gravel | Box pile | Yes, partial plugging present for sheet piles based on angle of folds in steel | Full-scale testing performed in Japan, model testing performed in laboratory. Higher axial load bearing capacity observed in sheet pile compared to box pile. Observations made regarding plugging behavior based on CT scans of model tests |
| | Model | None | Well-characterized test sand | Toyoura sand | Box pile | | |
| Rybak and Zyrek (2013) Skyline | Full-Scale | None | Not reported | Sand | Box pile | Yes, design values not provided | Test site located in Poland. Successfully demonstrated ample axial load bearing capacity of sheet piles |

2.3.1 Bustamante and Gianeselli (1991) - Dunkirk Test Site (Sand)

Bustamante and Gianeselli (1991) presents a static load test of a sheet pile wall and box pile driven at a site composed primarily of sandy soils conducted in Dunkirk, France (Figure 2-2). The test relevant to this research is the one on the sheet pile wall that consisted of four Larssen IIn sheet piles resulting in a wall width of 1.6 m. As shown in Figure 2-2, the wall was driven to a depth of approximately 7.42 m. Details concerning the driving process were not provided other than that conventional methods were used. CPT tip resistance values were obtained for the site and are presented in Figure 2-2.

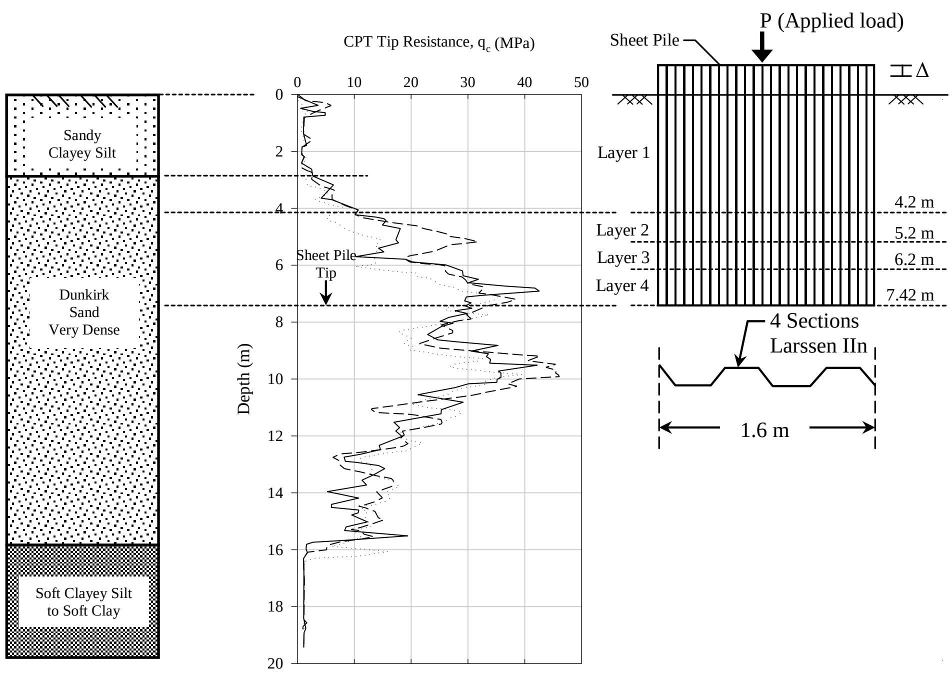


Figure 2-2. Geotechnical conditions at Dunkirk test site, adapted from Bustamante and Gianeselli (1991), obtained from Rice et al. (2014)

The soil profile consisted of a sandy, clayey silt layer with loose to medium density extending to a depth of 2.7 m and an average CPT tip resistance ($q_c$) value of approximately 2 MPa (290 psi). This was underlain by a very dense sand referred to by the authors as Dunkirk Sand that extended beyond the depth of the embedded sheet piles.

The $q_c$ values for this layer ranged from 2 MPa at a depth of 2.7 m to approximately 35 MPa at a depth of 7.4 m. Load test results, shown in Figure 2-3, indicated an ultimate load of 2,400 kN developed at a corresponding maximum measured pile head settlement of approximately 73 mm. Figure 2-4 presents the axial load distribution obtained from the instrumentation along the length of the sheet pile wall and Figure 2-5 presents the *T-Z* curves developed at each elevation of instrumentation.

In summary, a successful well-instrumented static axial load test was performed on a sheet pile wall at a test site in Dunkirk, France and is reported by Bustamante and Gianeselli (1991). Based on the measured load transfer, the majority of the applied axial load is carried towards the bottom of the pile wall where CPT rip resistance measured indicate denser sand. The authors note that the ultimate capacity reached was higher than expected and compare the results with box piles installed at the same test site. Box piles were formed from two welded sheet piles and two installations, one with a closed toe and one with an open tip, were evaluated in the field tests. The authors compare the ultimate capacity of the sheet pile wall with the box pile installations. Results indicate that the ultimate load of the sheet pile wall reached 210% and 120% of the ultimate load reached by the open and closed box pile, respectively. The authors indicate the higher capacity for the sheet pile wall may be partly due to the additional pile sections used to construct the sheet pile wall as compared to the box pile. Despite this, the authors note the measured capacity is high for the sheet pile wall, suggesting a strong potential for axial load bearing applications.

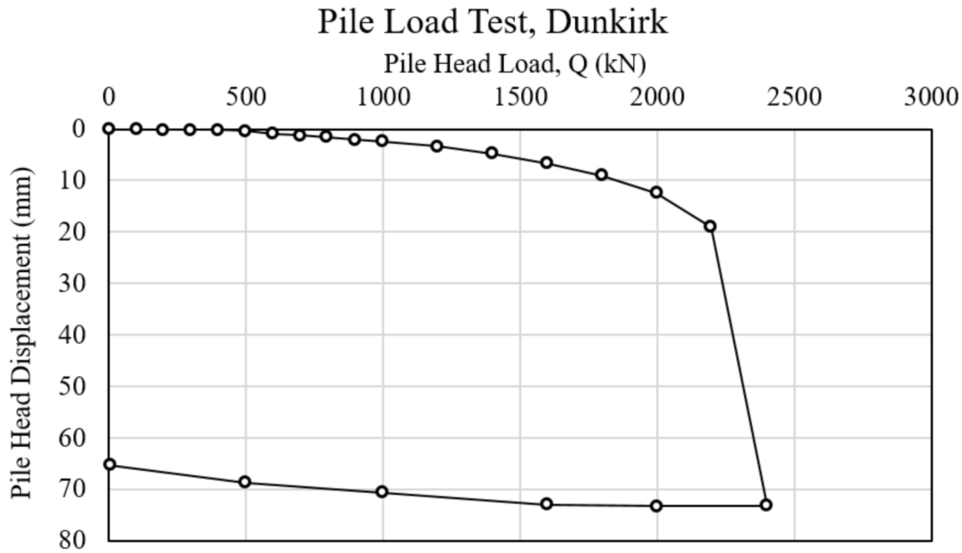


Figure 2-3. Pile head displacement versus head load for Dunkirk sand site (adapted from Bustamante and Gianeselli 1991)

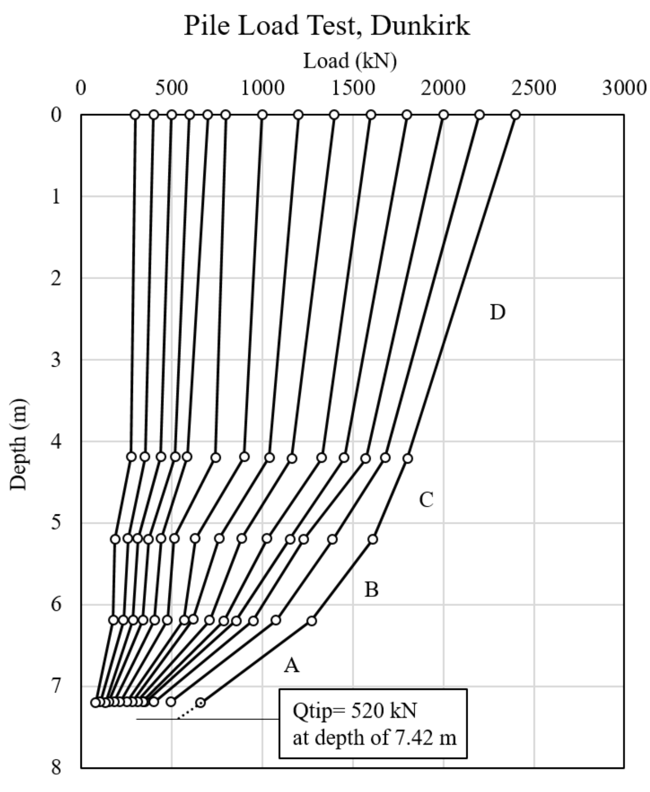


Figure 2-4. Load transfer measured for pile load test at Dunkirk sand site (adapted from Bustamante and Gianeselli 1991)

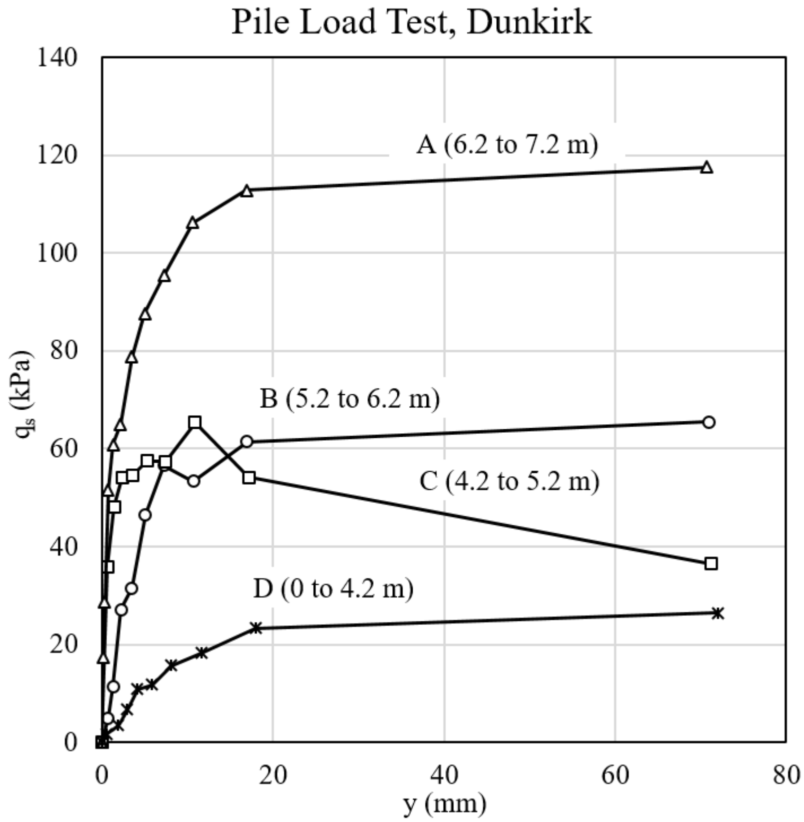


Figure 2-5. Experimental *T-Z* curves obtained from the pile test at Dunkirk sand site (adapted from Bustamante and Gianeselli 1991)

### 2.3.2 Bustamante and Gianeselli (1991) - Merville Test Site (Clay)

Bustamante and Gianeselli (1991) present a second static load test of a sheet pile wall and box pile driven into a clay soil profile at a site located in Merville, France. The sheet pile wall consisted of four Larssen IIs sheet piles, which resulted in a total wall width of 2 m that were driven to a depth of approximately 12 m. Details concerning the driving process were not provided other than that conventional methods were used. SPT blow counts as well as CPT tip resistance values were recorded and are reproduced in Figure 2-6. The soil profile consisted of a clayey silt layer with soft to medium stiff density extending to an approximate depth of 2 m and an average CPT $q_c$ value of approximately 1 MPa. This was underlain by a Flanders clay, which extended beyond the depth of the embedded sheet piles. The $q_c$ values for this layer ranged from 1 MPa at a depth of 2 m to approximately 4 MPa at a depth of 12 m. These $q_c$ values correspond to a clay layer with relative density of 18.2 to 19.1 kN/m$^3$. Load test results indicate an ultimate load of 3,000 kN corresponding to a pile head settlement of approximately 15 mm. Figure 2-7 reproduces the applied axial load versus pile head settlement response of the pile group. The instrumentation of the piles allowed for generation of *T-Z* curves along the length of the pile, which are reproduced in Figure 2-8.

In summary, a successful well-instrumented static axial load test was performed on a sheet pile wall at a test site in Merville, France and is reported by Bustamante and Gianeselli (1991). The authors do not report the measured loads along the sheet piles, however the measured *T-Z* curves indicates measured ultimate unit shaft resistance generally increases with depth. This is consistent with the measurements from CPT and SPT testing. The authors compare the ultimate capacity of the sheet pile wall with the box pile installations. Results indicate that the ultimate load of the sheet pile wall reached 280% and 230% of the ultimate load reached by the open and closed box pile, respectively. The authors mention the capacity of the sheet pile wall is extremely high compared to the box pile. Similar to the Dunkirk site, this may be partly due to the additional pile sections used to construct the sheet pile wall as compared to the box pile. The favorable performance of the sheet pile wall as compared to the box pile, a pile used to increase axial and lateral resistance in bridge abutments, suggest that sheet piles have favorable characteristics for resisting axial loads.

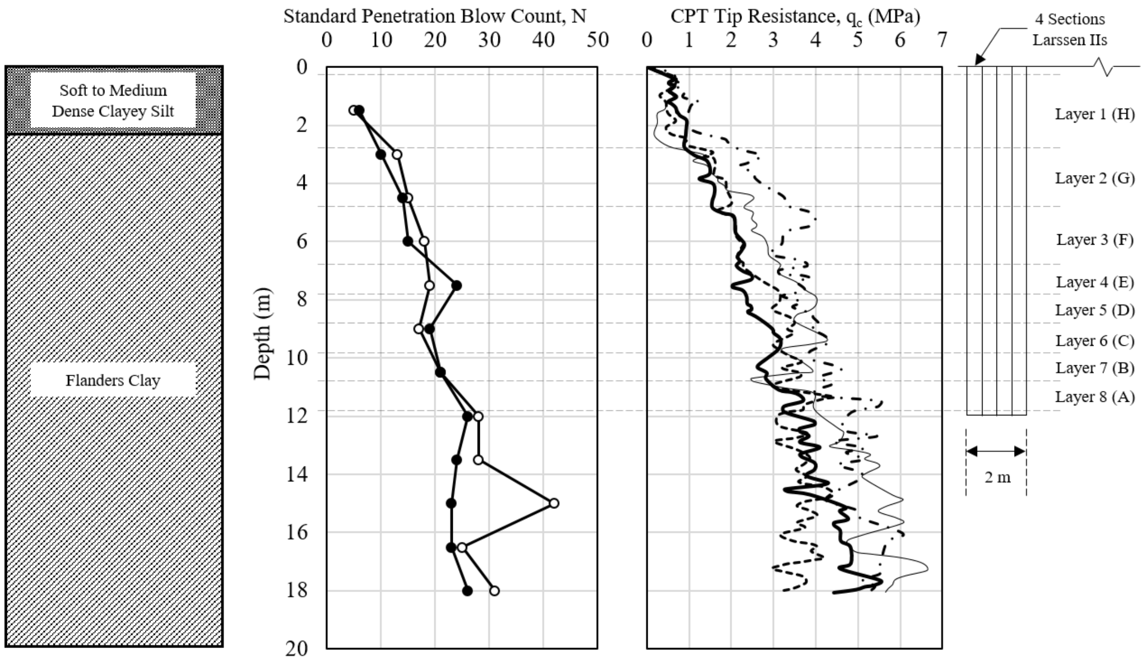


Figure 2-6. CPT and SPT in-situ results of Merville clay site (adapted from Bustamante and Gianeselli 1991)

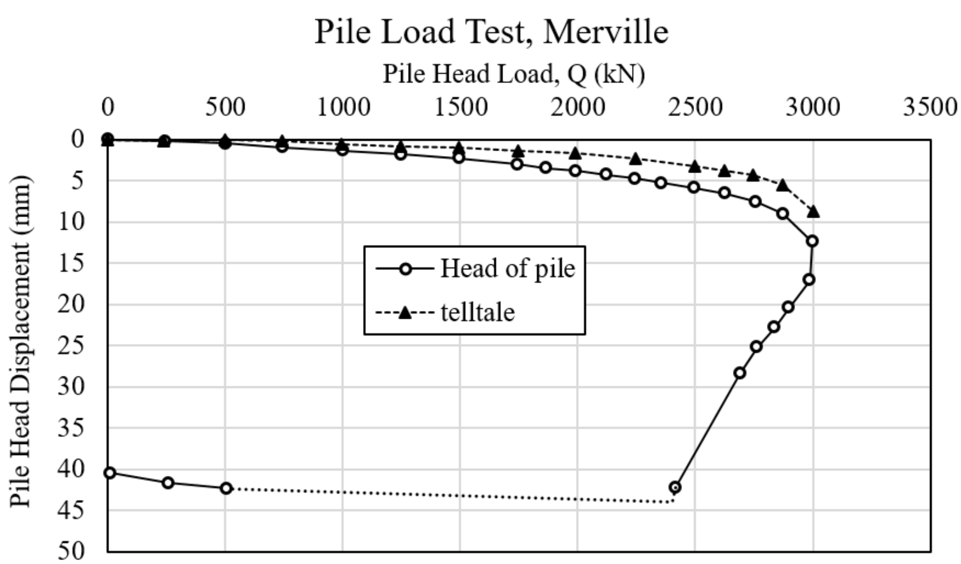


Figure 2-7. Pile head/tip displacements versus head load for Merville clay site (adapted from Bustamante and Gianeselli 1991)

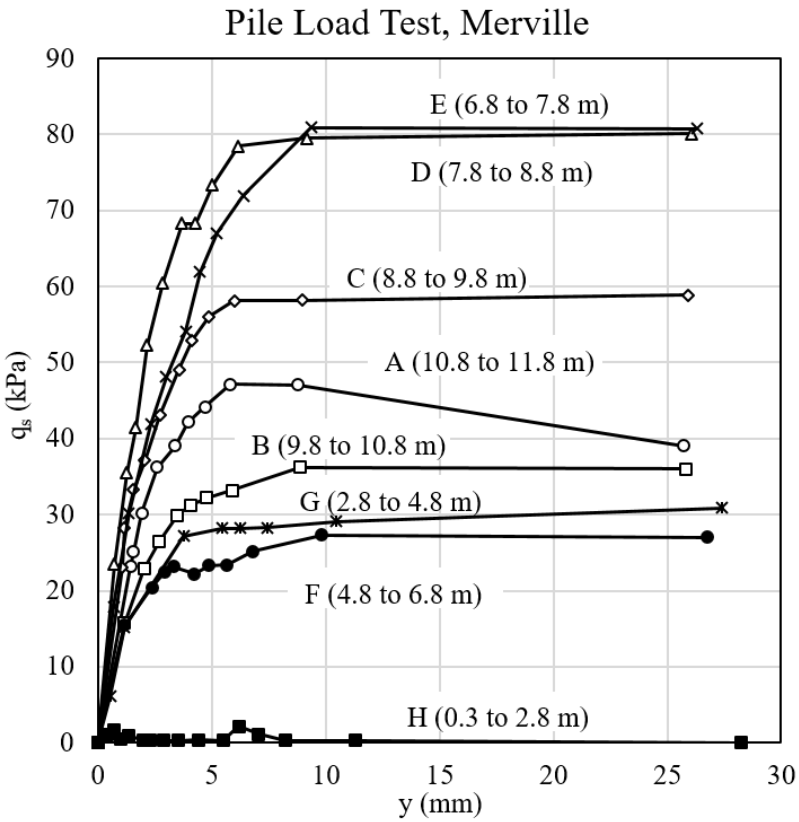


Figure 2-8. Experimental *T-Z* curves from the pile test at Merville clay site (adapted from Bustamante and Gianeselli 1991)

### 2.3.3 Borel et al. (2002) - Cachan Test Site (Clay (Plastic Marl) with Cobbles)

Borel et al. (2002) report load tests performed on sheet pile pairs installed using impact and vibratory driving. The authors use these tests to investigate the difference in pile capacity obtained between these two driving methods (Mosher 1987). The test site was located at a project site at Cachan, France (near Paris), where sheet piles were being used in support of excavation and axial load bearing foundations for a 6-story building with a two level basement. Due to associated cost savings, installation of the production sheet piles using vibratory driving was proposed. Pile load tests were conducted to address uncertainties regarding the difference in capacity between vibratory and impact driven sheet piles. The pile types used for testing were not specified by the authors, however it is implied that two pairs of L2S sheet piles were used. The piles were driven to 9 m embedment in a soil profile consisting of clayey sand to a depth of 3 m, sandy gravel to a depth of 5 m, and marly soils with cobbles to the maximum explored depth of 13 m. Pressuremeter soundings were conducted to characterize the site. The authors also present a driving record for the sheet pile pair that was driven using an impact hammer. Figure 2-9 presents a summary of these results.

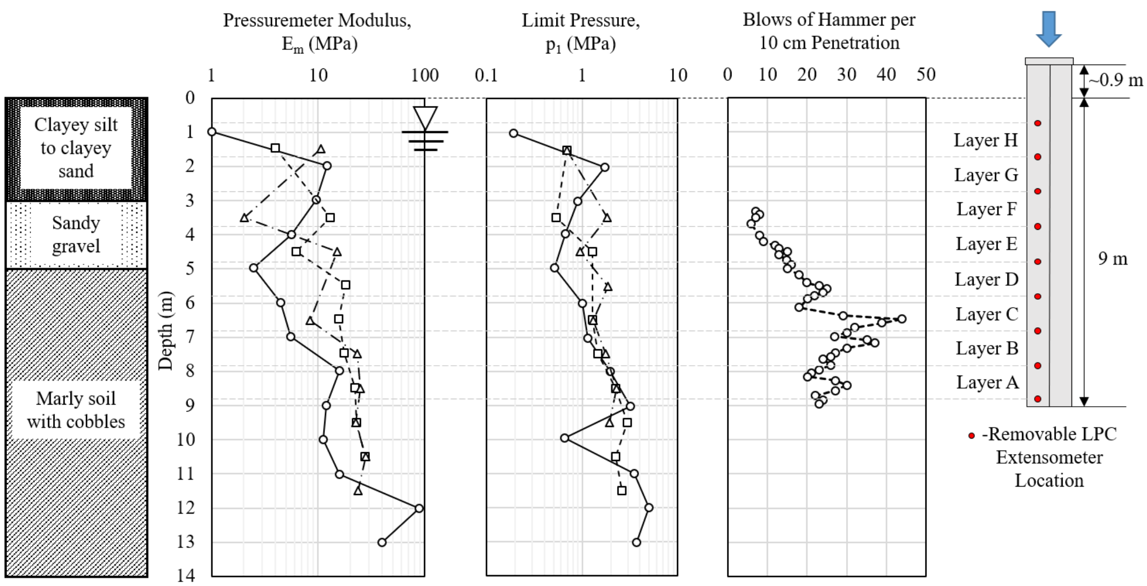


Figure 2-9. Soil profile and driving record recorded at Cachan site (adapted from Borel et al. 2002)

Compression load testing was performed on both sets of test piles after a period of twenty days. The results indicated that the piles driven by impact hammer had approximately 75% greater capacity than the piles driven by a vibratory hammer. Also, the axial load versus settlement curve shapes indicated a stiffer response for the piles driven by impact hammer. Figure 2-10 presents the measured head displacement versus pile head load for both pile groups. Facilitated by instrumentation installed along the shaft of the piles, axial force at different depths were measured and reported. Figure 2-11 presents these results for the impact and vibratory driven piles. Based on the results, the impact driven piles show higher axial load capacity mainly due to higher toe capacity, where the shaft resistance for both test piles is comparable. The authors mention that available case studies comparing vibratory and impact driven piles in sand have demonstrated lower capacity for vibratory piles mainly due to reduced toe resistance, consistent with the findings of this study. A possible reason for this behavior postulated by the authors is that vibratory driving does not densify soil in the region of the pile tip, unlike impact driving.

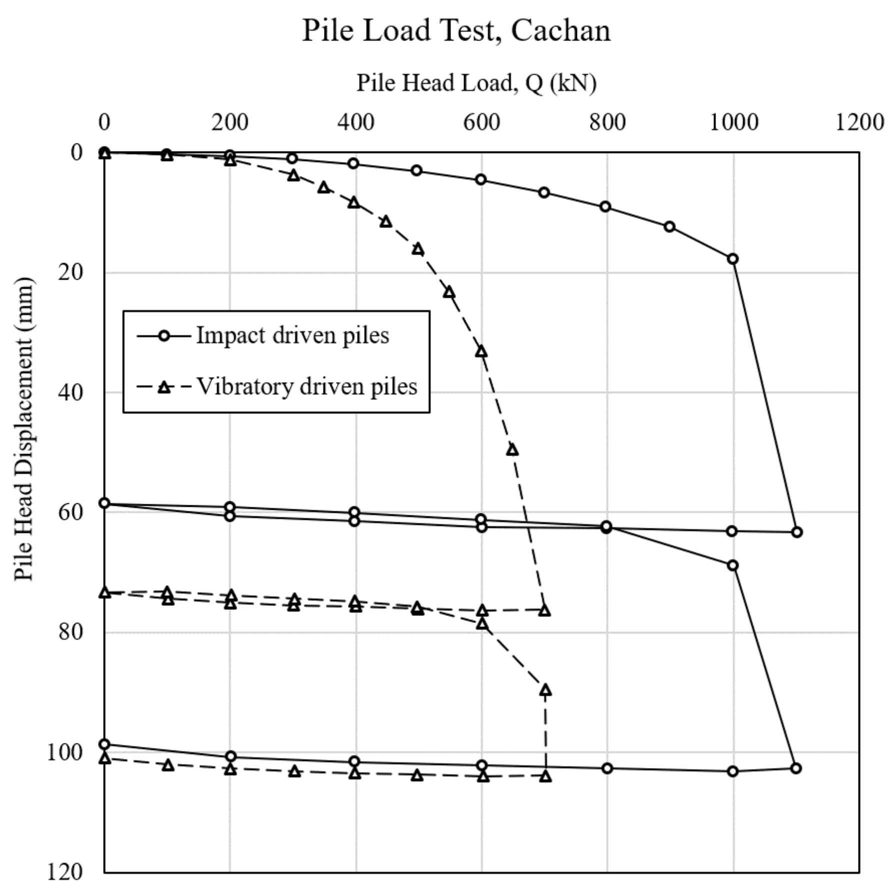


Figure 2-10. Pile head displacement versus pile head load, Cachan site (adapted from Borel et al. 2002)

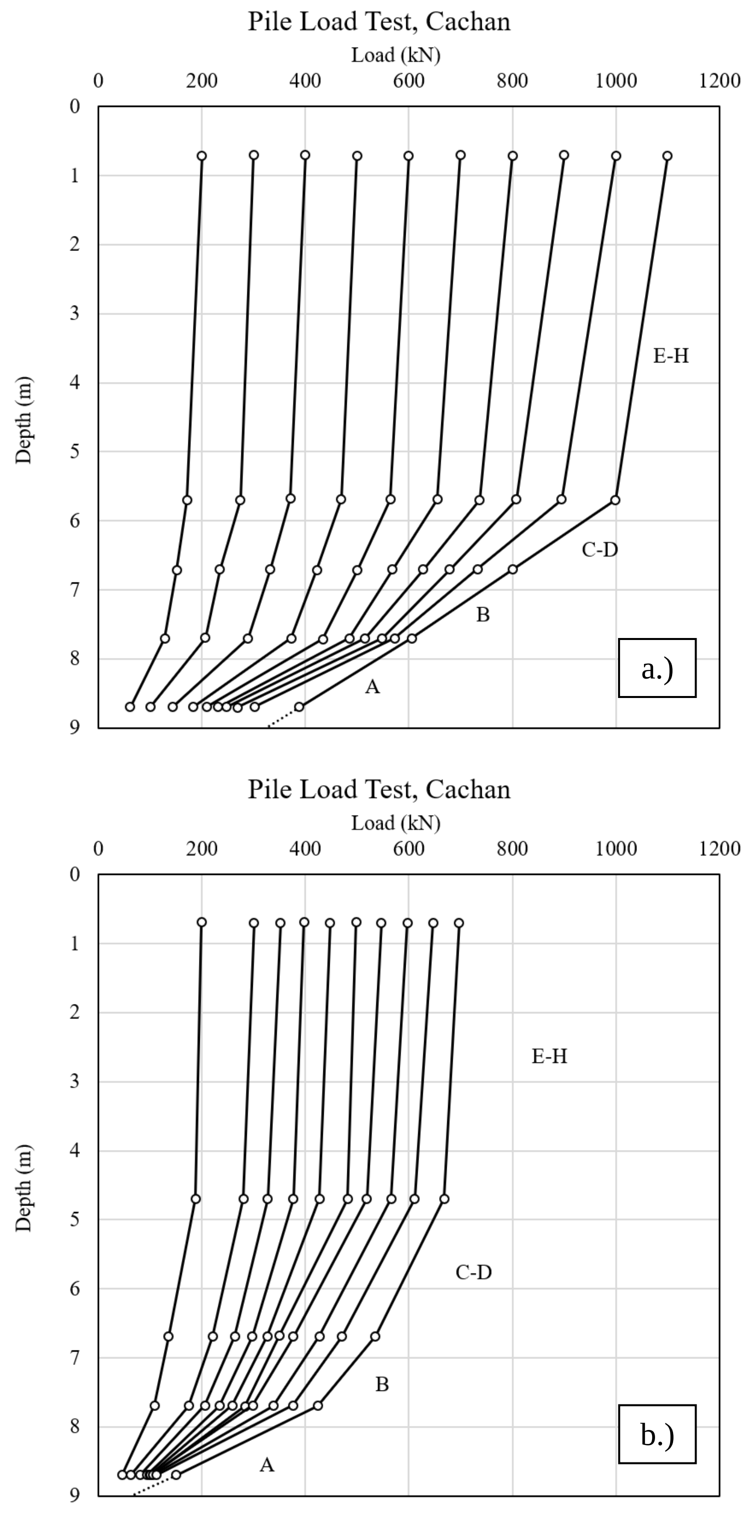


Figure 2-11. Depth versus load for a.) impact and b.) vibratory installed piles, Cachan site (adapted from Borel et al. 2002)

2.3.4 Borel et al. (2002) - Erstein Test Site (Gravel)

Borel et al. (2002) report an additional load test performed at the Rhine River in Erstein (Alsace, France). The testing was conducted as a means of foundation performance verification. Vibratory and impact driven sheet piles were also evaluated in this study. For these tests, two pairs of PU20 sheet piles were used for testing and driven to embedment depths of approximately 11 m. The soils encountered at the site consisted of 1.6 m of gravely fill over dense gravel of the Rhine River. Pressuremeter soundings were again conducted to characterize the site. The authors also present a driving record for the sheet pile pair that was driven using an impact hammer. Figure 2-11 presents these results.

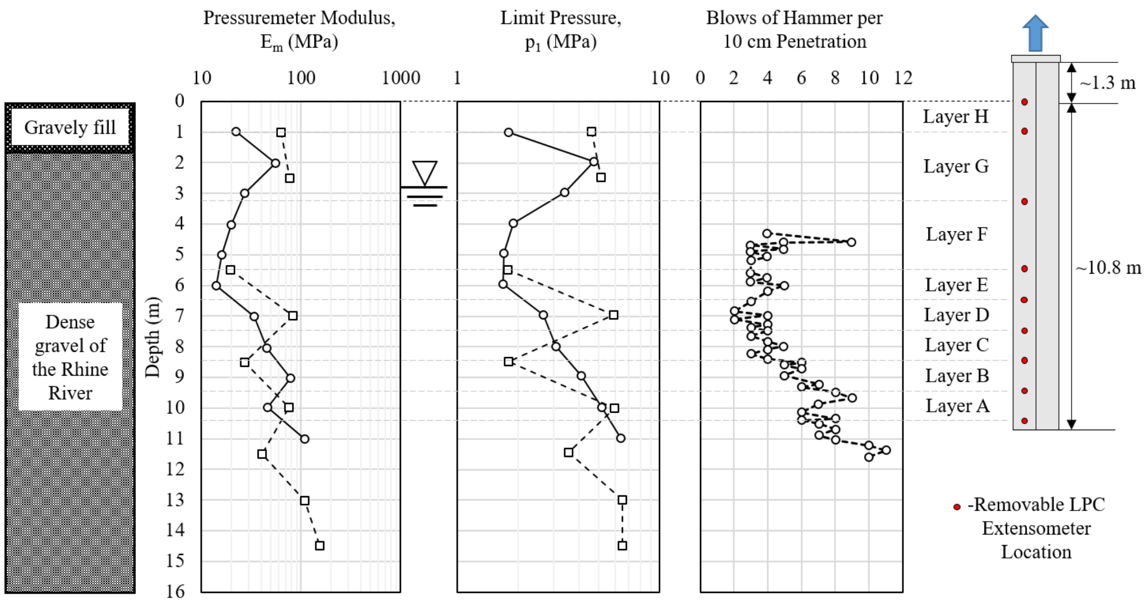


Figure 2-12. Soil profile and driving record recorded at Erstein site (adapted from Borel et al. 2002)

For this project, the piles were tested under uplift forces at one week after installation. Since uplift does not engage the toe resistance, these tests characterize the difference in shaft resistance between the two pile installation methods. Figure 2-13 presents the pile head displacement versus load for both test piles. The impact driven piles demonstrated greater axial capacity as compared to the vibratory driven piles, but to a lesser degree as compared to the compression tests performed at Cachan. The authors report for the vibratory driven sheet piles, the mean skin resistance measured was 25% lower than for the impact driven piles. These piles were instrumented allowing for measurement of the axial force distribution along the length of the piles. Figure 2-14 presents these load transfer measurements. Additionally, based on the axial force measurements along the length of the pile, *T-Z* curves were generated (Figure 2-15). The results from *T-Z* curve development lead to a few insightful conclusions regarding the behavior of impact versus vibratory driven piles. Based on the *T-Z* curves presented, it can be seen that ultimate frictional resistances are mobilized at larger displacements for the vibratory driven piles compared to the impact driven piles. Peak shaft resistances are reached at displacements ranging from 80 to 90 mm for the vibratory driven piles. These values are much higher than typically reported values for shaft mobilization of 5 to 10 mm (Das 2016). Additionally, the maximum unit shaft resistance is higher for nearly all *T-Z* curves for the impact test pile as compared to the vibratory test pile, in some cases by a factor exceeding two.

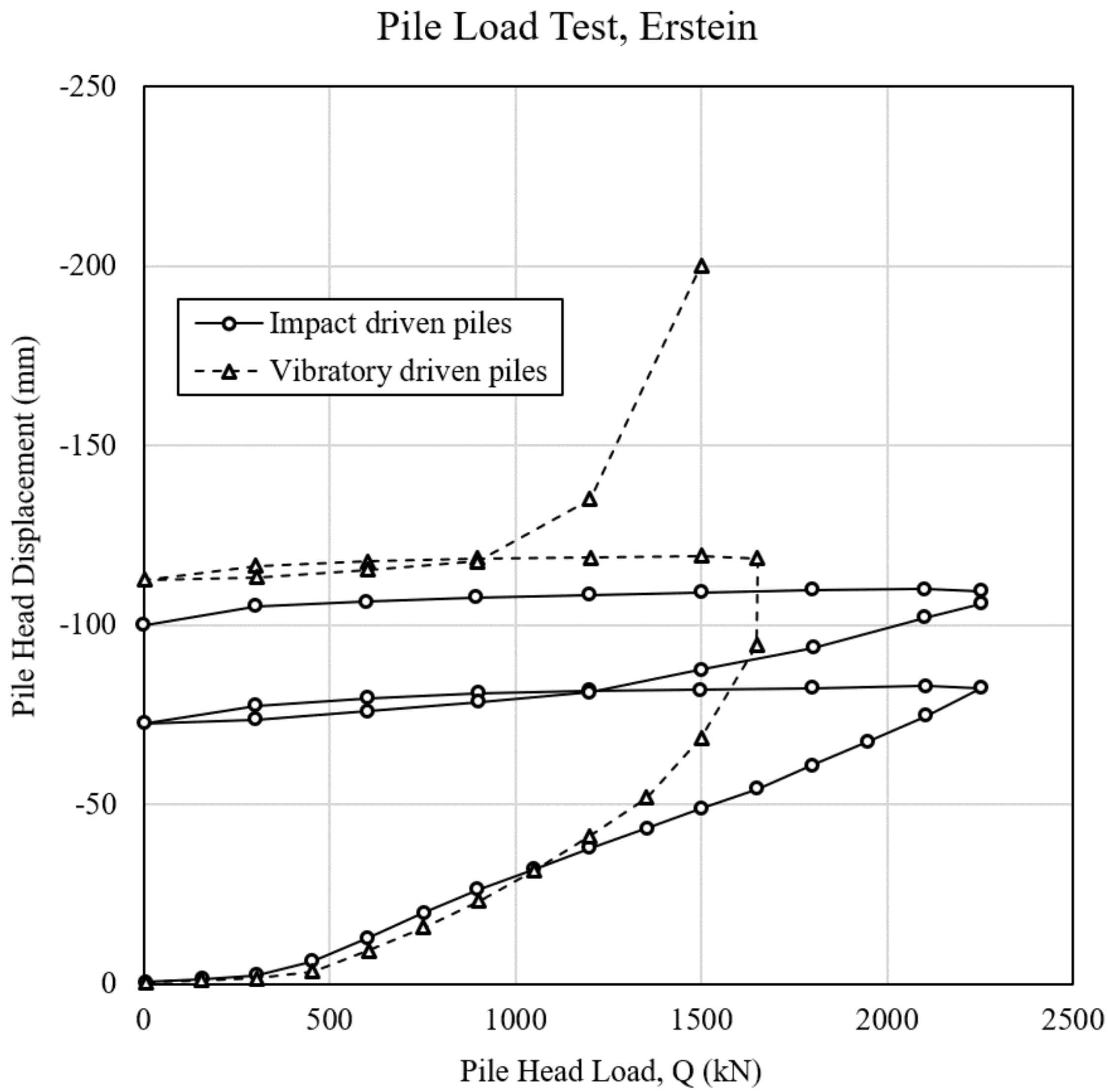


Figure 2-13. Pile head displacement versus pile head load, Erstein site (adapted from Borel et al. 2002)

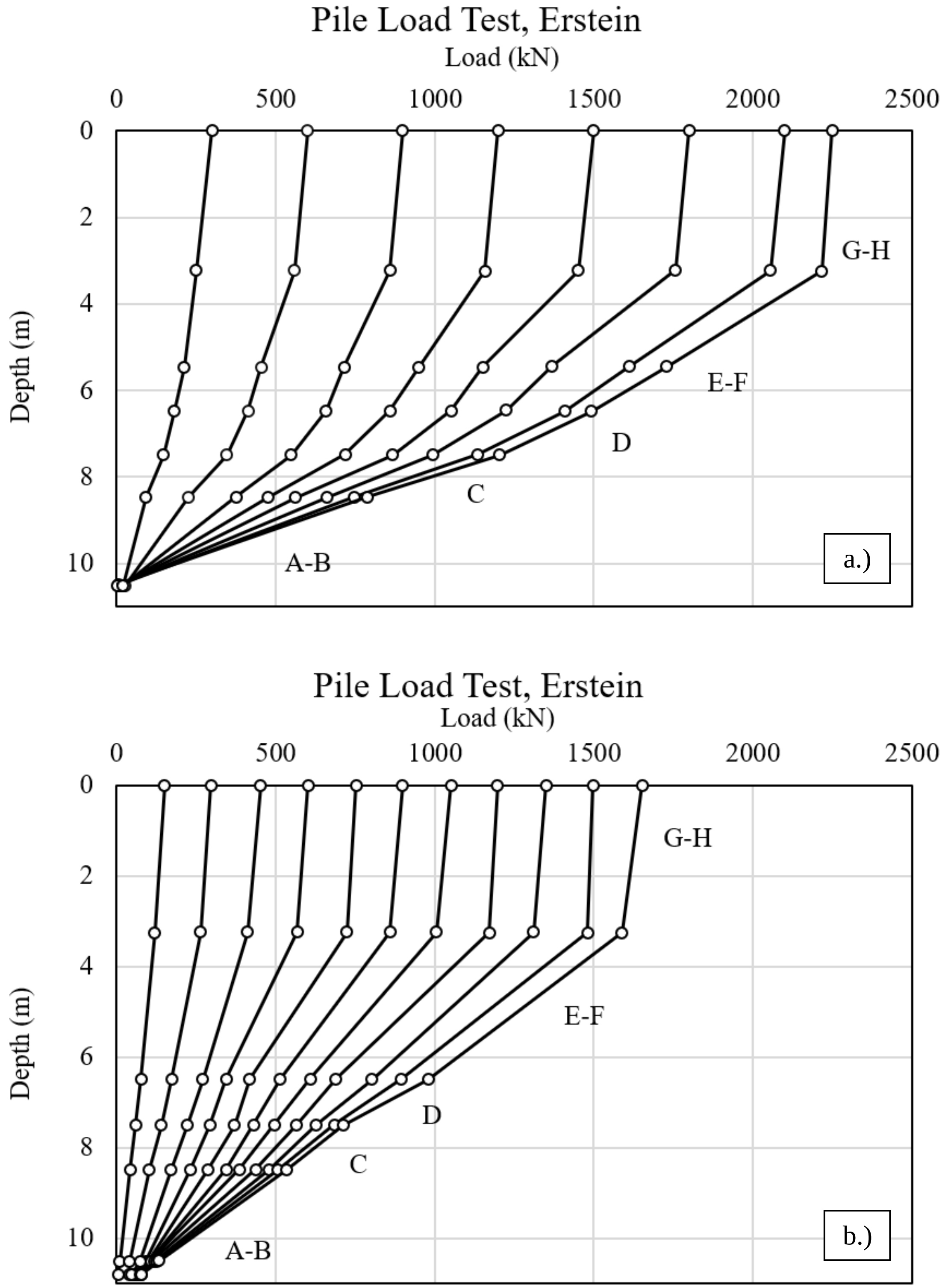


Figure 2-14. Depth versus load for a.) impact and b.) vibratory installed piles, Erstein site (adapted from Borel et al. 2002)

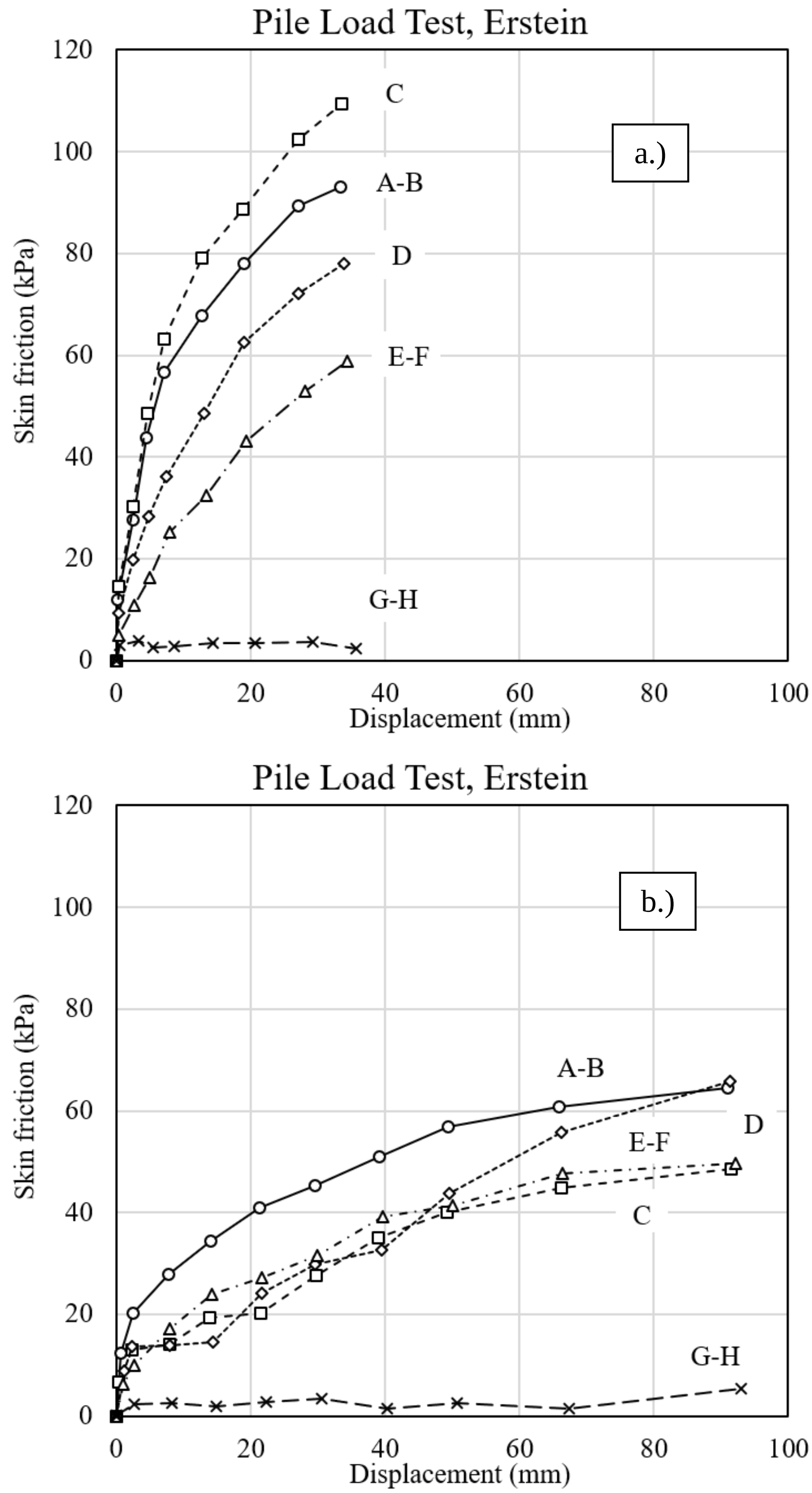


Figure 2-15. *T-Z* curves for a.) impact and b.) vibratory installed piles, Erstein site (adapted from Borel et al. 2002)

### 2.3.5 Taenaka et al. (2006) - Nippon Steel Test Site (Sand)

Taenaka et al. (2006) reported a load test case history performed at a test site located at the Technical Development Bureau of the Nippon Steel Corporation in Tokyo, Japan. The test program involved axial load tests on a sheet pile pair with the cross section shown in Figure 2-16 (a). The test program also included a load test on a box pile formed by two sheet piles, as shown in Figure 2-16 (b) (Nippon Steel & Sumitomo Metal Corporation 2012). The test piles were driven using vibratory equipment to an embedment of 11.2 m. Geotechnical conditions were investigated through the use of SPT and Figure 2-17 presents these results. A summary of the test pile dimensions is presented in Table 2-3. The authors report plugging conditions for the box pile with a plug area of 1,798 $cm^2$ (Table 2-3). In contrast, the authors indicate an unknown plugging condition for the sheet pile pair.

The authors do not report the location of the test piles at the site, however since both test piles were installed at the same site it is reasonable to assume comparable soil conditions for each test pile. The axial load test results are shown in Figure 2-18. It can be seen that the sheet pile pair exhibited a stiffer response and a larger axial load capacity compared to the box pile. From Figure 2-18, it is estimated that $Q_{ult}$ were 3500 kN and 2100 kN for the sheet pile and box pile, respectively. The axial load distributions with depth, as reported by Taenaka et al. (2006), are shown in Figure 2-19 (a.) and (b.) for the sheet pile and box pile, respectively. These axial load distributions with depth were used by the authors to obtain plots of mobilization of total shaft resistance ($Q_s$) as a function of pile head settlement (Figure 2-20 a.) and toe resistance ($Q_t$) as a function of pile toe displacement (Figure 2-20 b.).

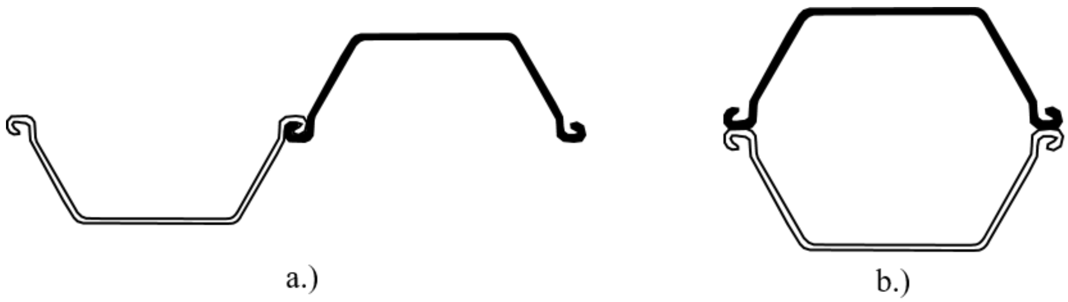


Figure 2-16. Pile configuration for a.) sheet pile pair and b.) box pile used for full-scale tests (adapted from Taenaka et al. 2006)

Table 2-3. Dimensions of test piles in Figure 2-16 (as reported by Taenaka et al. 2006)

| Pile Type / Item | Sheet pile pair (SP) | Box pile (BP) |
|---|---|---|
| Width of each pile (mm) | 600.0 | 600.0 |
| Embedment (m) | 11.2 | 11.2 |
| Steel cross sectional area ($cm^2$) | 207.8 | 207.8 |
| Perimeter (mm) | 3790 | 1895 |
| Theoretical toe plugged area ($cm^2$)* | Unknown** | 1798.0 |

Notes: *: Fully plugged
**: As reported by authors

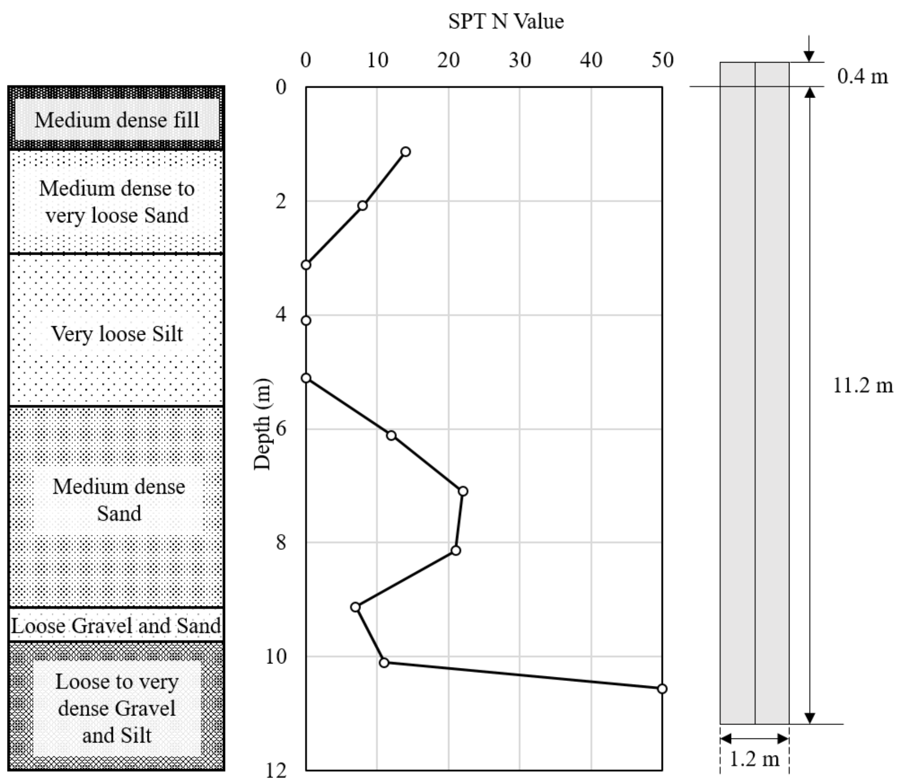

Figure 2-17. Soil at Nippon Steel Corporation test site (adapted from Taenaka et al. 2006)

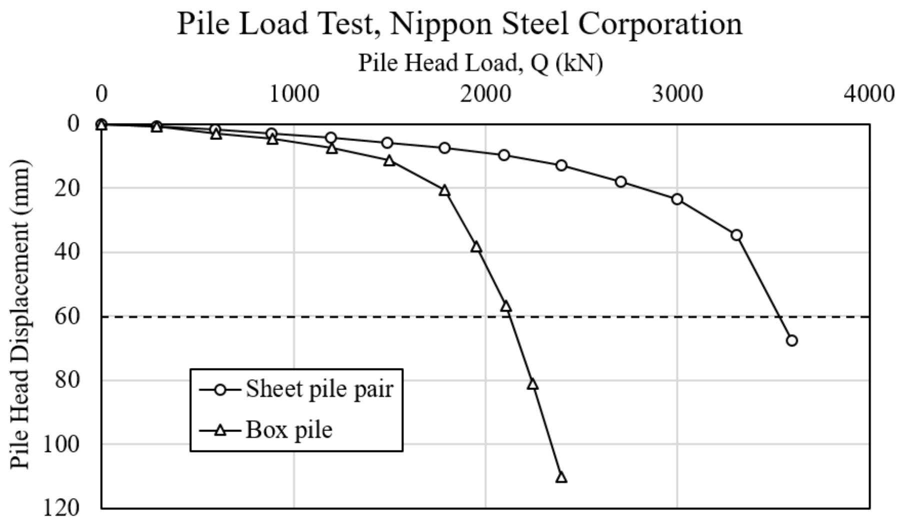


Figure 2-18. Pile head displacement versus head load for Nippon Steel Corporation test site for box pile and sheet pile pair (adapted from Taenaka et al. 2006)

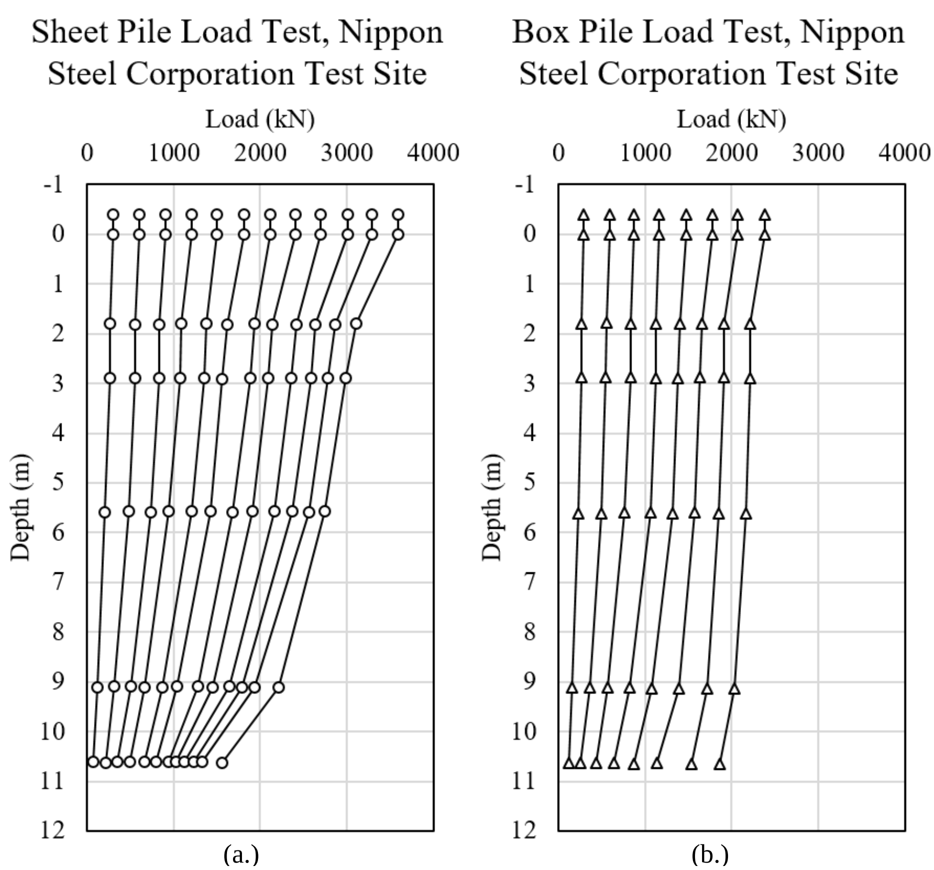

Figure 2-19. Results from pile load test at Nippon Steel Corporation test site for (a.) the sheet pile pair and (b.) box pile (adapted from Taenaka et al. 2006)

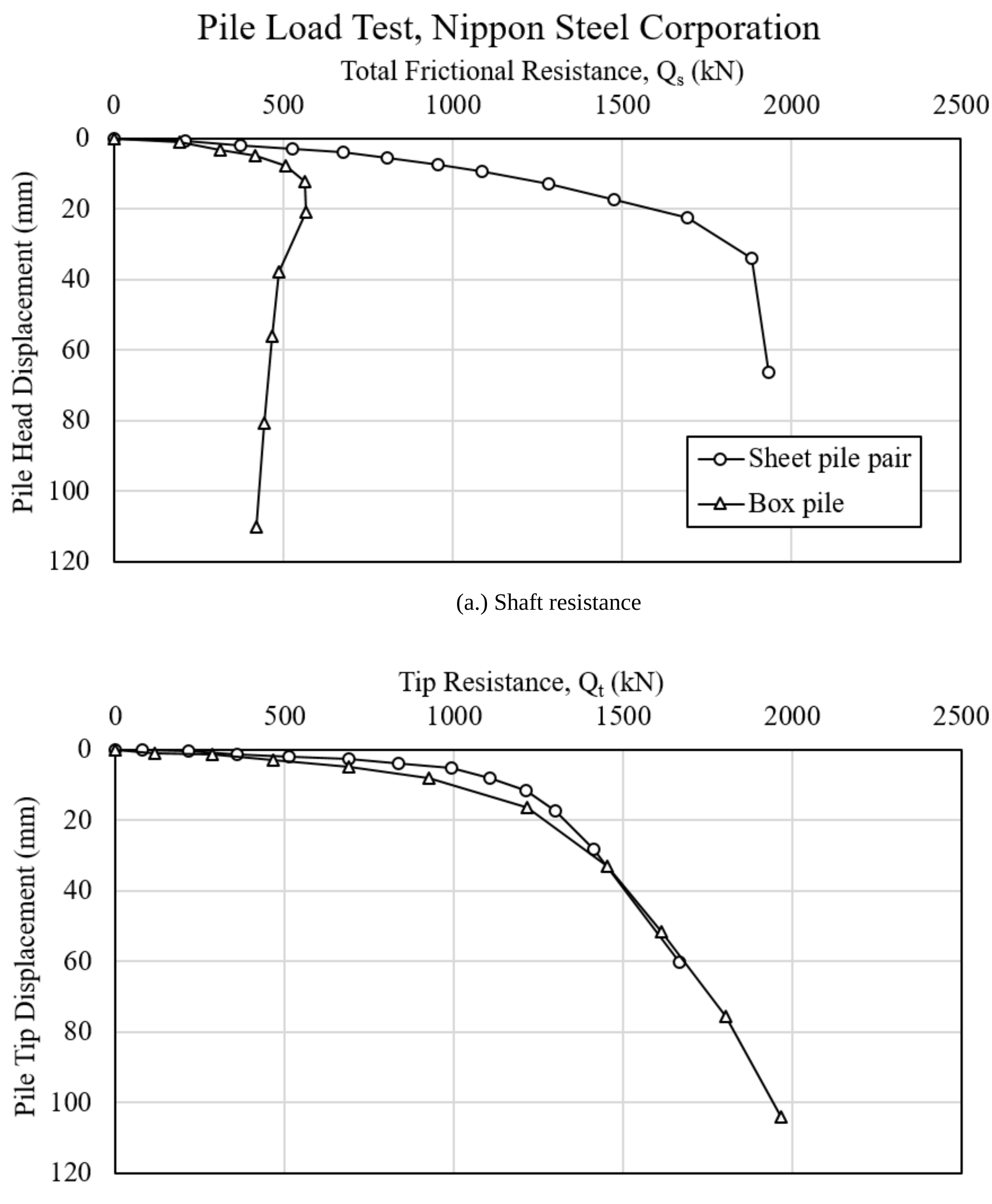


(b.) Tip resistance

Figure 2-20. Pile mobilized head displacement versus (a.) shaft resistance and (b.) toe resistance for both the sheet pile pair and box pile (adapted from Taenaka et al. 2006)

From the testing results shown in Figure 2-18, the capacity of the sheet pile pair was found to be higher than the box pile. The authors comment that the axial load distribution shows the box pile to be behave as an end-bearing pile, while the behavior of the sheet pile pair is more characteristic of a floating or friction pile. This behavior can be observed in the load transfer depicted in Figure 2-19, where the axial load changes only slightly with increasing depth as compared to the load measured near the toe of the pile for the box pile. This indicates that the box pile carries the majority of its load through toe resistance. The response measured from the sheet pile indicates that load changes with depth to a much greater degree than the box pile, indicating shaft resistance has a more significant role for the sheet pile pair than for the box pile. The authors commented on the ability of the sheet pile pair to carry larger frictional loads due to the larger shaft area when compared to a box pile that only has the outer surface for frictional skin resistance due to plugging. Additionally, the shaft and toe resistance shown in Figure 2-20 demonstrates that the sheet pile pair had greater shaft resistance and a comparable end-bearing capacity relative to the box pile, which suggests that a similar degree of plugging was occurring for both pile configurations. These results are promising when considering the potential of sheet piles for use as axial load bearing foundations. If sheet piles can resist applied axial load through greater shaft resistance and equal or comparable toe resistance compared to box piles, greater axial load bearing resistance can be provided by sheet piles in a wall configuration. Due to sheet piles having comparable axial load resistance compared with a conventional boxed pile configuration used for axial load bearing, sheet piles can have strong potential for use as axial load bearing members.

### 2.3.6 Rybak and Zyrek (2013) - Warsaw Test Site (Sand)

This section summarizes the field load test reported by Rybak and Zyrek (2013) as part of a bridge construction project for the S8 Express Road in Warsaw, Poland. Sheet piles were installed to function as soil retaining and axial load bearing foundation elements for a bridge abutment. This project involved field testing of piles to demonstrate the axial load capacity for the construction of the bridge, which utilized a double sheet pile wall. The use of sheet piles as axial load bearing foundations allowed for rapid construction time, which was ideal for the busy urban area of this project. The single span bridge superstructure had a span length of 15 m. Section sizes used for this project included Skyline Steel sections AZ 13, AZ 25, and AZ 37-700, all with grade S355GP steel (ArcelorMittal 2009; Skyline Steel LLC 2009). AZ 37-700 sheet piles were used for the construction of the abutments for the overpass. These sections consisted of two rows of sheet piles spaced 1.5 m apart and placed on both sides of the express road. The abutment design considered not only lateral loading produced by approximately 2 m of soil, but also the axial loading introduced by traffic.

The field test evaluated the axial bearing capacity of a non-production sheet pile pair driven into the free space between two parallel walls. This configuration was chosen to eliminate the effects of interlock friction and also to replicate the same soil conditions the abutment piles would experience during the service life of the structure. The authors note the soil consisted of medium dense coarse, medium, and fine sand to a depth of 17 m. Figure 2-21 presents the load test setup and Figure 2-22 presents the displacement versus load curve for this test.

The authors note some advantages to using sheet piles for axial load bearing, these include aesthetic considerations, dual functions of the piles for axial and lateral load resistance, and the large number of projects which already use sheet piles as temporary building elements that can consider sheet piles for use in the permanent foundation. Additionally, plugging is mentioned as an important design consideration that is difficult to predict and measure.

Figure 2-21. Sheet pile test setup (from Skyline Steel LLC 2009)

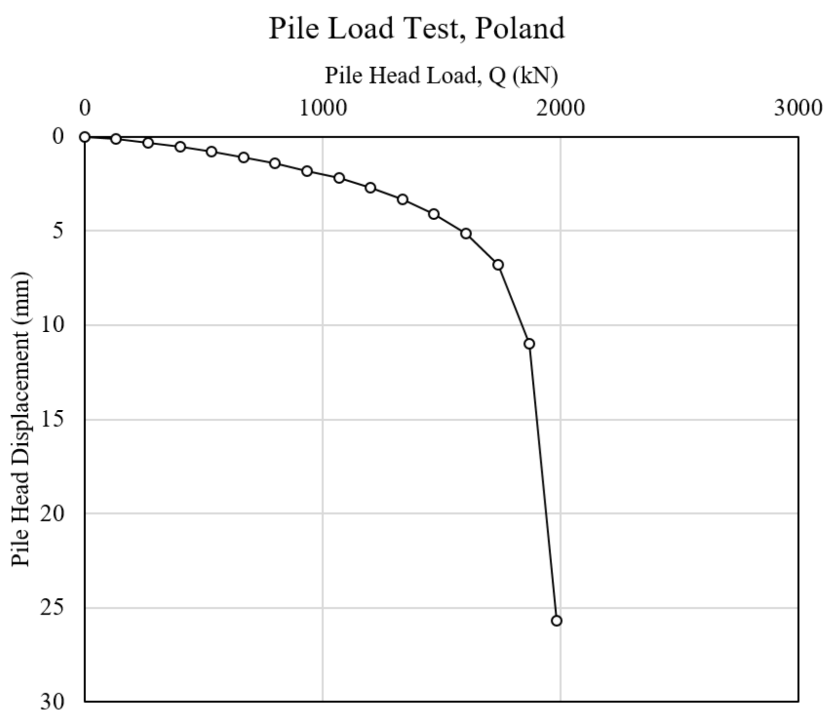


Figure 2-22. Pile head displacement (adapted from Rybak and Zyrek, (2013))

### 2.3.7 Summary of Full-Scale Field Load Test Case Studies

Seven full-scale axial load tests performed on sheet piles were identified in the literature. A summary of these tests is presented in Table 2-2. Two load tests were performed by Bustamante and Gianeselli (1991), one at a sand site and the other at a clay site. The authors present the results of the well-documented study and also provide interpretation of the results and design recommendations. The authors conclude that sheet piles can provide considerable axial load bearing capacity and should be utilized more often for this purpose in foundation design. Evans et al. (2012) did not perform a static pile load test, but performed a live load test on a sheet pile abutment. Results were used to determine axial and flexural stresses in the pile which were compared to calculated values. Taenaka et al. (2006) present the results of a full-scale and model tests involving sheet piles. Their study looked closely at the plugging mechanism involved for sheet piles driven as a wall and the authors found that sheet piles and boxed piles experience similar degrees of plugging, leading to similar end-bearing capacities. Rybak and Zyrek, (2013) present the results of a pile load test performed at a construction site utilizing a double sheet pile wall for a bridge construction project. Sheet piles performed as expected, demonstrating their viability for large construction projects.

In summary, the pile load tests that have been identified either illustrate the ample load carrying capacity of sheet piles for design loads or recommend further testing and analysis to better develop this design methodology. When compared to box piles, sheet piles were found to have greater axial load bearing capacity. In general, unless sheet piles are driven into dense/firm soils underlying loose/soft soils or driven to bedrock, they have been observed to primarily carry axially applied load through shaft resistance generated as a result of their large shaft area. Related to this, the extent of plugging experienced by sheet piles will affect the extent to which applied loads are carried by shaft resistance. Uncertainty regarding the plugging behavior was noted in several of the tests summarized in the literature review. A subsequent section provides more detail regarding the plugging behavior as it relates to sheet piles.

## 2.4 Current Existing Design Guidance

A few publications have been identified that offer recommendations regarding designing with sheet piles to carry axial load. This section presents examples in the literature of design guidance for the use of sheet piles for axial load bearing. Design recommendations for the use of sheet piles to carry axial loads have been developed primarily in Europe and the U.K. where the design practice of using sheet piles to carry axial loads in bridge abutments is more mature than in the U.S. As demonstrated in the previous sections, many more examples of bridge construction utilizing axially loaded sheet piles exist across Europe and the U.K. than in the U.S. It is important to consider current existing design guidance to better facilitate the adoption of this design approach in the U.S. A growing familiarity with current design practice will allow for a better understanding of any existing design challenges that may need to be addressed before introducing this design methodology to U.S. practice.

In general, the literature identified relating to design guidance can be grouped into shorter publications from conferences and journals and longer publications consisting of standards and design guides. The shorter publications identified provide useful commentary relating to case studies, important design considerations, and simplified methods of analysis relating to the design of sheet piles for axial loading in bridge abutments, while the longer publications provide more comprehensive discussion regarding best practices associated with use of sheet piles for axial load bearing. This section presents a summary of what has been identified in the literature concerning sheet pile axial load capacity, as it is a main focus of this research effort. Additional design guidance related to important considerations when designing with axially loaded sheet piles is presented in the Appendix A.

### 2.4.1 Predictive Methods for Determining Pile Axial Load Capacity

Several methods are presented in the reviewed literature for determining the axial load bearing capacity of sheet piles. These methods in many cases are identical to methods prescribed for similar steel bearing piles, such as H-piles and pipe piles. Publications providing guidance for determining axial capacities of sheet piles include Yandzio (1998) , ArcelorMittal (2008) , and Biddle (1997) . The methods can be categorized based on the type of soil, broadly defined as cohesionless or cohesive, with each method providing separate equations for shaft and toe capacities. The methods identified are summarized in Table 2-4.

Table 2-4. Summary of predictive methods identified in literature review.

| Reference | Soil type: Cohesionless | | Soil type: Cohesive | | Notes |
|---|---|---|---|---|---|
| | Maximum unit shaft resistance, $f_{s_{max}}$ | Maximum unit tip resistance, $q_{t_{max}}$ | Maximum unit shaft resistance, $f_{s_{max}}$ | Maximum unit tip resistance, $q_{t_{max}}$ | |
| Yandzio, 1998 | $=2\cdot N_b$[1] | $=q_c$[2] (when CPT data is available) $=400\cdot N_b$ | $=\alpha$[3]$\cdot c_u$[4] | $=9\cdot c_u$ | $\alpha$= 0.25 for undrained loading<br>0.5 for drained loading |
| Piling Handbook, 1998 | $=2\cdot N_s$[5] | $=400\cdot N_b$ | $=\alpha\cdot s_u$[6] | $=9\cdot s_u$ | • $N_b$= 0.5 ($N_1$[7]+$N_2$[8])<br>• For submerged sands, N must be reduced: $N_{red}$= 15+0.5·(N-15), where N>15 |
| Steel Bearing Piles Guide, 1997: API method | $=K_s$[9]$\cdot P_0'$[10]$\cdot\tan(\delta$[11]$)$ | $=P_0'\cdot N_q$[12] | $=\alpha\cdot c_u$ | $=9\cdot c_u$ | • $\alpha$= 1 for $0 \leq c_u \leq 24$ kPa<br>= 0.5 for 75 kPa < $c_u$ (based on API database)<br>• $\alpha$= 0.25 for undrained loading<br>= 0.5 for drained loading (based on SCI validation work) |
| Steel Bearing Piles Guide, 1997: SPT method | $=2\cdot N$ | $=400\cdot N$ | | | • N is factored by a value of 0.67 where soil is submerged<br>• Resistance values are in units of kPa |
| Steel Bearing Piles Guide, 1997: CPT method | $=q_c/300$<br>(in compression)<br>$=q_c/400$<br>(in tension)<br>$=0.35\ f_s$[13] | $q_c$ or $\overline{q_c}$ | $=\alpha\cdot c_u$<br>$=\alpha\cdot(q_c/N_k$[14]$)$ | | • For instances where no plugging occurs, use $q_c$ as measured.<br>• For instances where plugging occurs, use $\overline{q_c}$= $q_c$ averaged above and below pile tip using Schmertmann's method. |

Note:
(1): $N_b$= Standard Penetration Test value
(2): $q_c$= CPT cone tip resistance
(3): $\alpha$= Pile wall adhesion factor
(4): $c_u$= Undrained triaxial shear strength
(5): $N_s$= Average N along shaft length
(6): $s_u$= Average undrained shear strength for each layer
(7): $N_1$= Smallest N over 2 effective diameters below toe
(8): $N_2$= $\overline{N}$ over 10 effective diameters below pile toe
(9): $K_s$= Coefficient of lateral earth pressure on wall
(10): $P_0'$= Effective overburden pressure
(11): $\delta$= Effective interaction friction angle between pile wall and soil= $\phi'_{laboratory}$ - 5°
(12): $N_q$= Dimensionless bearing capacity factor
(13): $f_s$= CPT sleeve resistance
(14): $N_k$= 15 to 20 for overconsolidated clay

Yandzio (1998) presents a publication providing guidance for the design and construction of sheet pile embedded retaining walls for bridge abutments. The author suggests a method based on limit state principals that adheres to U.K. construction legislation, DETR Highways Agency Specifications, U.K. Codes of Practice, and European Standards. Other considerations are made in this publication regarding installation method for sheet piles, construction tolerances, and rates of corrosion. The publication references the Steel Construction Institute (SCI) publication ‘Steel bearing piles guide’ (Biddle 1997) regarding the axial capacity of sheet piles in different soil types. Design guidance provided utilizes a limit state approach and is based upon modes of failure at defined limit states. A number of useful design considerations are also presented.

The 8th edition of the ‘Piling Handbook’ from ArcelorMittal (2008) is written as a field guide and provides a comprehensive overview of important design considerations when using sheet piles in construction. These considerations include durability and corrosion considerations, installation methods, installation noise and vibration management, as well as design recommendations incorporating topics such as design of retaining walls and the design of axially loaded sheet piles.

Biddle (1997), through the SCI provides a publication offering design guidance relating to the selection, design, and installation of steel bearing piles for foundations in all types of structures. Their guide offers a limit state design approach and provides commentary on a number of practical aspects relating to the use of steel bearing piles, including specific considerations for H and sheet piles. Commentary is provided regarding U.S. and U.K. design methods in use for offshore structures, although these methods have been found applicable for onshore structures. This guide was also compiled based on the results of pile load test data gathered in the SCI database, including tests on steel H-piles and sheet piles, as a means to validate load capacity prediction methods.

Eurocode 7 (2004) provides design guidance for the design of steel sheet piles. The Eurocode provides guidance based on a limit state design approach, where partial factors are used to reduce design resistances and amplify applied loads based on uncertainty regarding selected design values. This method has many similarities to the Load and Resistance Factor Design (LRFD) design philosophy in U.S., which also uses factors to adjust design values based on the levels of uncertainty regarding design resistances and applied loads. Several of the references outside of the U.S. that offer design guidance relating to pile design and axially loaded sheet piles note the uncertainty of soil conditions and the importance of applying partial factors to loads and resistances or averaging soil properties to account for variations in measurements obtained from a wide range of sources (ArcelorMittal 2008; Biddle 1997; Yandzio 1998). The following Eurocode documents were reviewed in preparing this summary (European Committee for Standardization 2004; European Committee for Standardization 2005; European Committee for Standardization 2007):

- EN 1990:2002: Eurocode 1: Basis of Structural Design.
- EN 1997-1:2004: Eurocode 7: Geotechnical Design – Part 1: General Rules.
- EN 1993-1-1:2005: Eurocode 3: Design of Steel Structures – Part 1-1: General Rules and Rules for Buildings.
- EN 1993-5:2007: Eurocode 3: Design of Steel Structures – Part 5: Piling.

These publications and others demonstrate that the use of sheet piles in bridge abutments for resisting lateral and axial loads is a relatively mature topic in Europe. Several sections pertaining to the design of sheet pile structures is summarized in subsequent sections. Additional information regarding design considerations when using sheet piles in structures was identified as part of this literature review. While this information is useful for developing a familiarity with the design best practices, it is not central to topic of soil-structure interaction in axially loaded sheet piles and is presented in Appendix A.

In general, the most commonly recommended predictive methods include SPT based methods for cohesionless soils when determining shaft and toe resistances, and methods based on undrained shear strength for cohesive soil when determining shaft and toe resistances. Additional methods based on CPT or laboratory measured angle of internal friction are available, however due to the lack of this data being commonly available, the previous methods are recommended. The literature also notes that these empirical methods have a considerable amount of variability due to the inherent nature of soil. Depending on the project, validation of pile capacities through additional testing may be required (Biddle 1997).

### 2.4.2 Load Transfer

Several publications indicate the mechanism of load transfer from the superstructure to the foundation is an important design consideration for steel sheet pile abutments. Load bearing behavior of an axially loaded foundation wall may be fundamentally different from individually acting piles, requiring additional considerations for design. Even distribution of structural loads to the pile wall is required to avoid potential serviceability issues related to different loading and settlements of individual sheet piles. The recommendations are summarized below.

Biddle (1997) mentions a few different configuration for H-piles and High Modulus Piles used for bridge abutments. Load transfer is typically achieved through the use of shear studs installed on the pile and encasement in concrete. Greater attention must be given to projects where bending moments are applied to the head of the piles. Connection details from SCI and others are provided by the author and reproduced in Figure 2-23. Yandzio (1998) presents a similar configuration that utilizes bridge bearings to transfer loads from the superstructure to a reinforced concrete capping beam. Shear studs are used to improve the load tranfer between the capping beam and steel sections. Figure 2-24 presents an image provided in Yandzio showing a similar shear stud design being used to transfer loads. ArcelorMittal (2008) recommends that superstructure loads be transferred through the use of a capping beam. An alternative approach involves installing box piles and placing fill material into the boxed pile to a height equal to the required height of the abutment. The landing for the bridge beams can be formed directly into the boxed pile when such an approach is used. This method results in a stiffer pile wall, reduced soil stresses, and reduced settlements. An image of a completed sheet pile abutment is presented in Figure 2-25.

Carle and Whitaker (1989) mention in their paper the mechanics of load transfer at the head of the piles. In the case studies identified in Germany, it was noted that standards have been developed for a reinforced concrete capping beam to prevent the kniving action of piles and achieve more uniform load transfer to the piles. Additionally, a case from Alaska is presented where a steel channel is used to better achieve load transfer without the construction of a reinforced concrete capping beam. In either case, the load transfer from the structure to the sheet pile elements is treated with careful consideration suggesting this is an important aspect when designing with these types of piles for axial loads.

In summary, the load transfer mechanism involved in transferring loads from the superstructure to the foundation piles was noted in several of the publications reviewed, suggesting the importance of ensuring proper distribution of structural loads to the sheet piles. This load transfer has been accomplished in past projects through various means including the use of shear studs installed onto the bearing piles and casing the piles in concrete, using steel channel along the head of the piles, and including a pin connection between the bridge spans and the pile cap. This design challenge and the potential solutions should be taken into consideration when developing design guidance for the use of sheet pile abutments in the U.S.

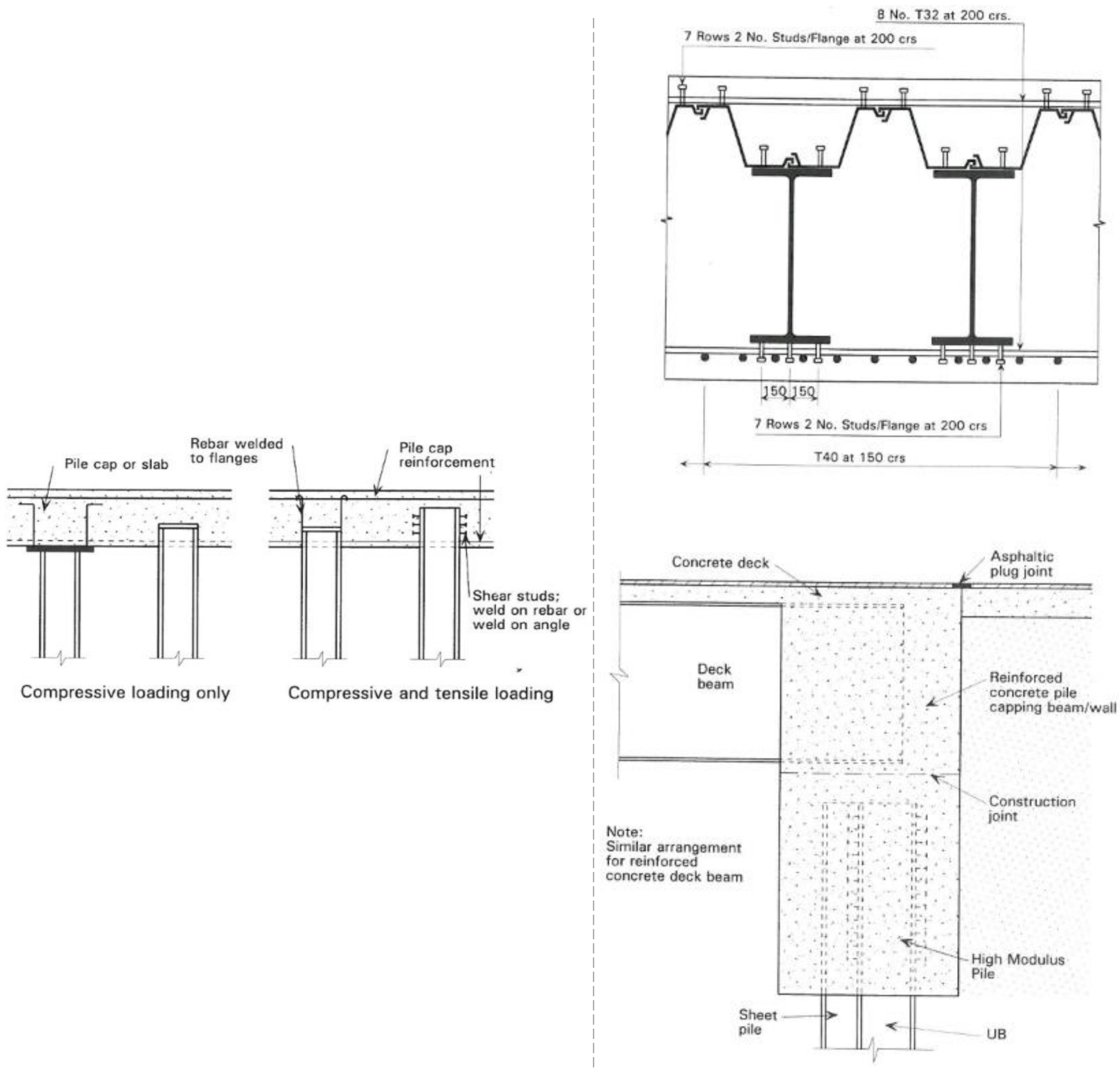


a.)

b.)

Figure 2-23. Steel pile and structure connections for a.) steel H-piles and b.) High Modulus Piles (from Biddle 1997)

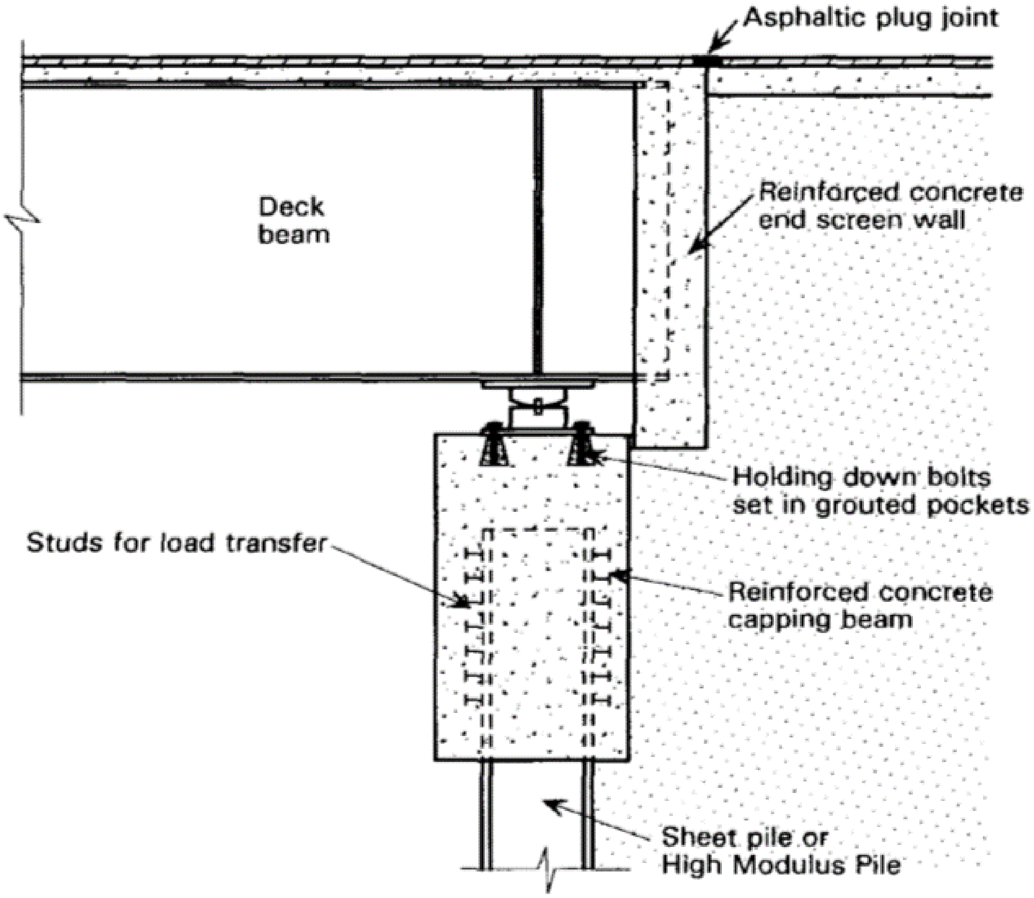


Figure 2-24. Configuration used to achieve load transfer between structure and foundation for bridge abutments (from Yandzio 1998)

Figure 2-25. Examples of steel sheet pile bridge abutments (from ArcelorMittal 2008)

## 2.5 Plugging Behavior in Piles

A pertinent topic when discussing the load transfer mechanism for axially loaded sheet piles is the occurrence of plugging. Plugging occurs when soil around an axially loaded pile does not shear at the soil to pile interface, but at a soil to soil interface some distance away from the pile surface. The volume bound by this interface is referred to as the soil plug which will move together with the pile (ArcelorMittal 2008). This behavior has significant implications when characterizing soil-structure interaction and influences what percentage of the applied load is carried through shaft and end-bearing. Plugging has the effect of increasing effective the load bearing area near the toe of the pile, thereby increasing toe resistance, while shaft area and shaft resistance are typically reduced along the length of the pile where the plugging occurs. For plugged pipe piles, the shaft area inside the pipe is not considered to contribute to shaft resistance and for displacement piles, such as H-piles or sheet piles, the formation of a plug can lead to reduced perimeter values and smaller shaft resistance. For non-displacement piles, plug formation can extend beyond the pile toe along the entire shaft length or some fraction. Additionally, the cross sectional area of the plug may change with depth with reduced plug area further from the pile tip. Plugging is a complex behavior thought to be affected by several factors including soil conditions, pile attributes and geometry, and the installation process used (Jeong et al. 2015). Plugging can be thought of as a range of soil behaviors at the pile tip, where plugging can occur fully, not at all, or partially occurring somewhere between these two extremes. Literature investigating the plugging behavior in sheet piles is fairly limited compared to what has been performed for pipe piles, however a few studies have been reported and are described below. Additionally, design guidance presented in publications introduced earlier in this chapter provide recommendations regarding plugging behavior in non-displacement piles, which is also presented in this section.

### 2.5.1 Plugging of Sheet Piles

The study by Taenaka et al. (2006) investigated plugging of sheet piles through a series of model tests. The authors used an aluminum soil box with a height of 445 mm and a diameter of 140 mm filled with Toyoura test sand. The index properties of Toyoura sand reported in this study are summarized in Table 2-5. A total of six different pile models were tested in order to observe the effect of different cross-sectional shapes on the failure pattern at the pile tip. Images of the different model piles are reproduced in Figure 2-26, and a summary of the properties of the model piles is presented in Table 2-6. From Figure 2-26 it can be seen that each series of tests were developed to test different aspects of pile design. Series-1 compared a model pile having a square cross section to another that had a rectangular cross section, both with approximately equal cross sectional areas. Series-2 compared the behavior of a model pile with a rectangular cross section to another model pile with a 'V' shaped cross section, again both models having equal cross sectional area. Lastly, series-3 compared the behavior of a model pile having a hollow square cross section to a model pile having an 'S' shaped cross section with the cross sectional areas being equal.

Table 2-5. Index properties of Toyoura sand used for model testing (from Taenaka et al. 2006)

| | |
|---|---|
| Dry density (kg/m$^3$) | Max 1,660 - Min 1,340 |
| Median particle size (mm) | 0.16 |
| Specific gravity | 2.64 |
| Relative density (%) | 85 - 90 |

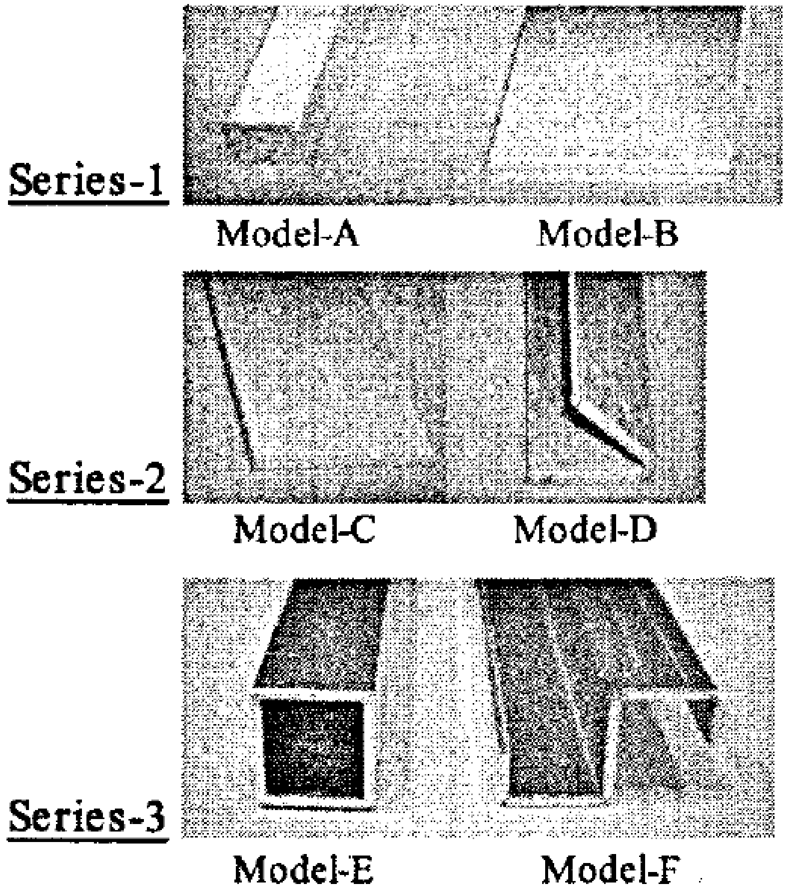


Figure 2-26. Images of model piles (from Taenaka et al. 2006)

Table 2-6. Property of model piles and test conditions (from Taenaka et al. 2006)

| | Series - 1: Focus on the shape | | Series - 2: Focus on the angle | | Series - 3: Simulate the full-scale tests | |
|---|---|---|---|---|---|---|
| Model | A | B | C | D | E | F |
| Property of model piles | | | | | | |
| Thickness of the plate (mm) | 10 | 3 | 3 | 3 | 1 | 1 |
| Width of the plate (mm) | 10 | 33 | 47 | 47 | | |
| Width of the model (mm) | | | | | 10 | 19 |
| Height of the model (mm) | | | | | 10 | 10 |
| Sectional area ($mm^2$) | 100 | 99 | 141 | 141 | 36 | 36 |
| Perimeter (mm) | 40 | 72 | 100 | 100 | 40* | 74 |
| Angle of fold (degrees) | - | - | 180 | 45 | | |
| Test conditions | | | | | | |
| Overburden pressure (MPa) | 2.88 | 2.88 | 2.88 | 2.88 | 6.03 | 6.03 |
| Embedment depth (mm) | 135 | 135 | 135 | 135 | 100 | 100 |

Note: *Friction area is estimated to be only outside, ignoring inside, of Model-E, as reported by authors

The soil box was filled using soil layers 275 mm thick placed with a free-fall method using multiple sieves. An overburden pressure was applied at the surface of the soil in the box using a dead load to better simulate conditions experienced by deep foundations. The model pile was then installed as a displacement pile. Two levels of overburden pressure were used: 2.88 and 6.03 MPa. Displacement controlled vertical loading was applied to the head of the model piles and computerized tomography (CT) scan imaging was performed at different displacements levels. Scans were made to monitor failure patterns at the toe of the pile and to capture the development of plugging for the different model pile geometries.

In general, shapes that had a square cross section (Model A and Model E) demonstrated a conical zone of increased soil density near the pile tip. Model piles that had a rectangular cross section (i.e., Model B and Model C) exhibited a zone of increased soil density in the shape of a triangular wedge extending along the length of the pile tip.

This zone was observed to be smaller than the zone developed for other pile types. Testing of Model D and Model F showed that introducing folds into the cross sectional shape of the pile led to larger areas of increased soil density near the pile tip. Figure 2-27 and Figure 2-28 show select results of the CT scans for Series-2 and Series-3, respectively. These figures are presented to highlight the effects of introducing angles into the pile cross section, which was observed to have a noticeable effect on the formation of a soil plug. The lighter regions of the scan presented in these figures represent areas of higher soil density, while darker regions indicate regions of decreased soil density. The authors associated these high density areas with areas in the soil where formation of a soil plug is occurring. Low density zones represent strain localization and the location of shear failure in the soil. It was observed that piles that included an angle (Model D and Model F) form a plug in a triangular wedge shape, as shown in Figure 2-27 (b) and Figure 2-28 (b). A generalized figure developed by the authors helps to illustrate this mechanism for a pipe and sheet pile and is reproduced in Figure 2-29. The results of this study indicate that angles introduced into pile cross sections promote plugging, although the formation of the plug is only partial. Due to corrugated shape of sheet piles, the numerous angles along the cross section likely encourage the formation of a partial plug in the form of a densified wedge of soil near the toe. For the clean sand considered in this study, this area of densified soil only occurred at the toe and did not extend along the pile shaft.

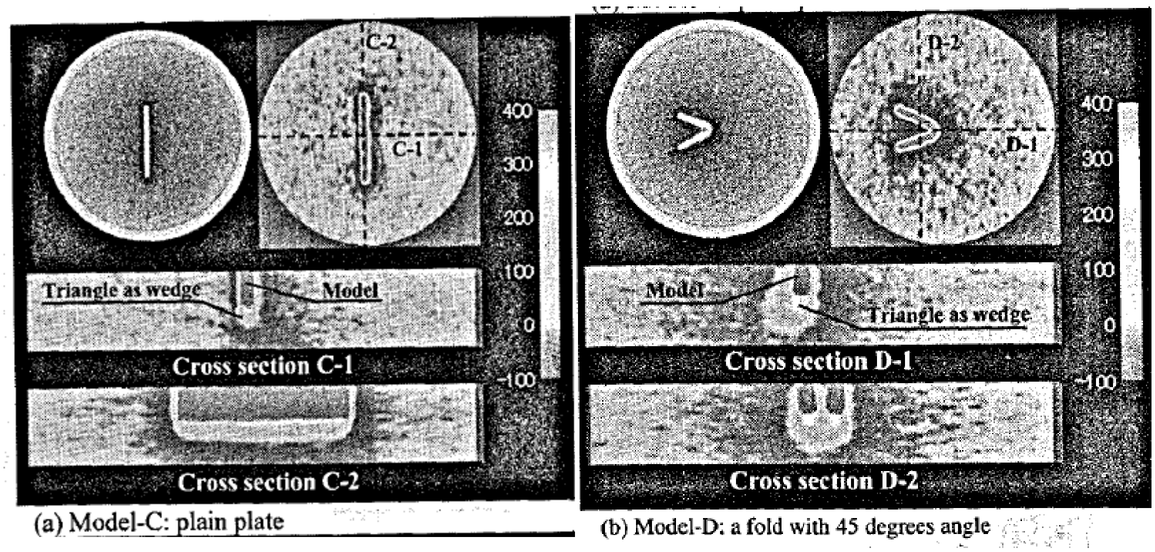


Figure 2-27. Results of CT scan (a) Model C and (b) Model D (from Taenaka et al. 2006)

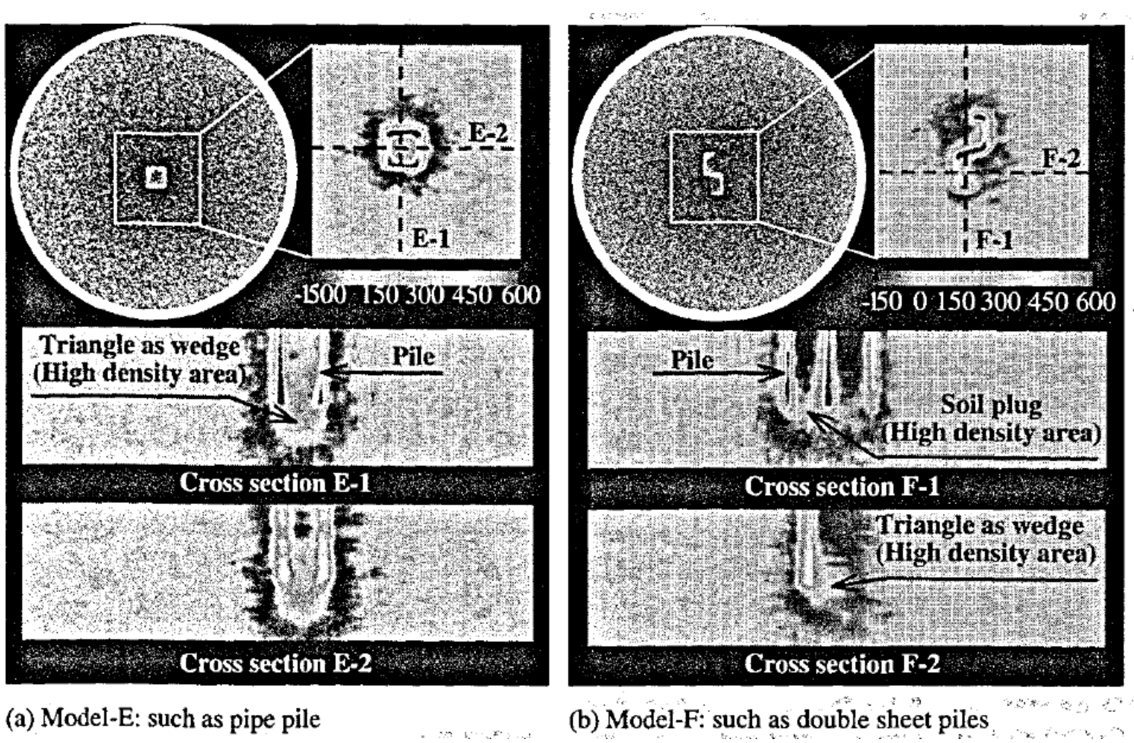


Figure 2-28. Results of CT scan (a) Model E and (b) Model F (from Taenaka et al. 2006)

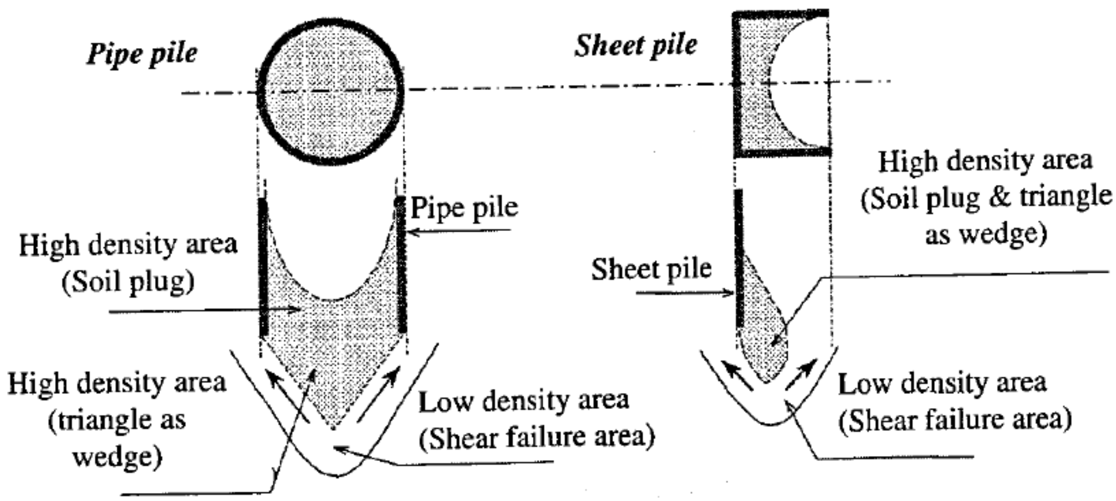


Figure 2-29. Schematics of plugging behavior based on measurements from CT test results (from Taenaka et al. 2006)

No other references were identified that specifically studied the plugging of sheet piles. However, Bustamante and Gianeselli (1991) indicate plugging had likely occurred in one of their load tests based on the measured axial load at the tip. Based on their test results, the authors proposed using a toe area equal to the shaded areas shown in Figure 2-30 for sheet piles with a plugged condition. The authors also recommend using the perimeter area denoted by the dashed line in Figure 2-30. This area for the shaft resistance ($s_{lat}$) only considers the perimeter of the steel, i.e. is based on an unplugged condition.

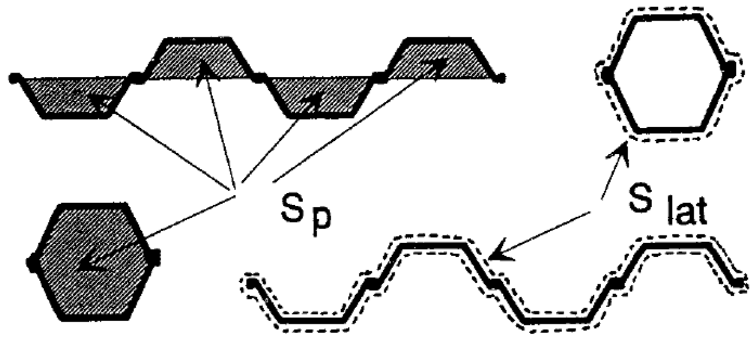


Figure 2-30. Definition of point cross section and lateral area for both sheet piles and box piles (Bustamante and Gianeselli 1991)

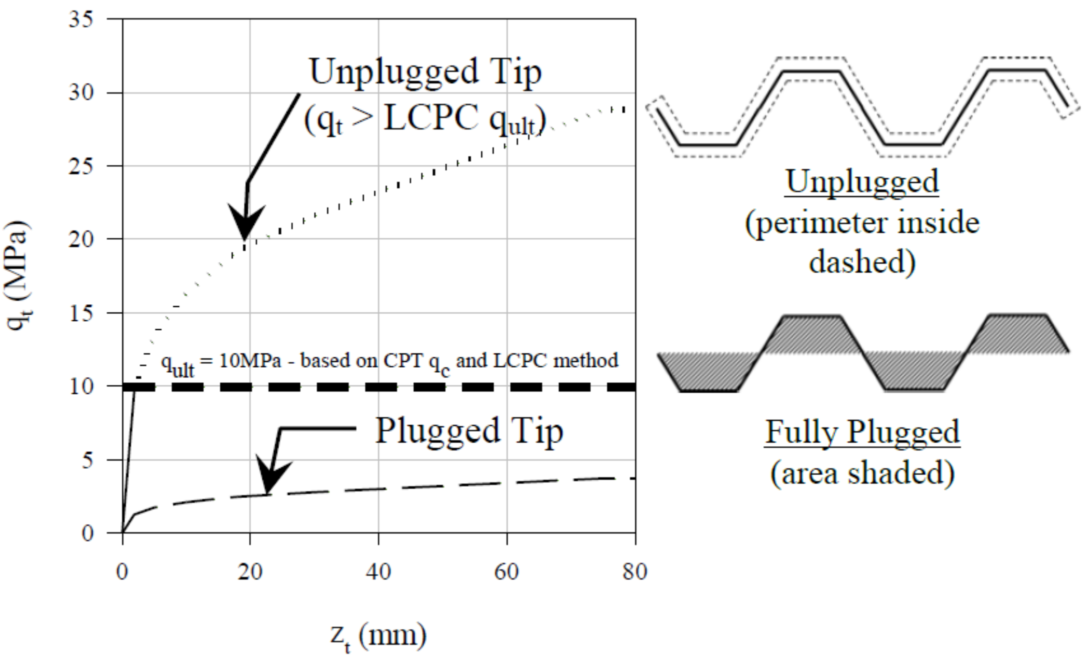


Figure 2-31. Unit toe resistance calculated for both unplugged and plugged conditions (left) and image showing unplugged and plugged areas for the sheet pile wall (right) (Rice et al. 2014)

This was further investigated in Rice et al. (2014). In this study, the load test results published in Bustamante and Gianeselli (1991) were analyzed using the load transfer method. The potential for soil plugging was considered based on the original data provided by Bustamante and Gianeselli (1991). It was found that the observed toe capacity of the sheet pile wall was large compared to values expected given the reported soil profile and associated in-situ testing. The measured load at the sheet pile toe was converted to unit toe resistance using the two possible extreme toe areas corresponding to "unplugged" and "fully plugged", as shown in Figure 2-31. For the unplugged toe condition, the unit toe resistance mobilizes to values exceeding 20 MPa for toe displacements of 20 mm or higher (see dotted line in Figure 2-31). In contrast, the mobilized unit toe resistance is less than 5 MPa if a plugged toe condition is assumed (long dashed line in Figure 2-31). The predicted unit toe resistance, using the field CPT tip resistance in conjunction with the LCPC method (Lunne et al. 1997) was found to be 10 MPa (horizontal dashed line in Figure 2-31). This figure suggests the formation of a partial plug at the sand test site was likely. However, the study by Bustamante and Gianesselli (1991) did not provide much discussion on the occurrence of plugging at their two test sites.

### 2.5.2 Design Guidance Concerning Plugging Behavior

The guidance provided in the literature concerning plugging behavior is summarized in this section. The total pile load resistance provided from shaft bearing will equal the product of unit shaft resistance and shaft area and the total pile load resistance provided from toe bearing will equal the product of unit toe resistance and toe area. Plugging will affect values for shaft and toe areas, and will have a strong influence over final calculated values for shaft and toe capacities, especially toe capacities where the increase in area due to plugging can be significant. Resistance and area values must both be reasonably accurate to obtain the best possible prediction for pile load capacity, understanding plugging behavior will lead to improved shaft and toe area values which will allow for improved values for predicted pile load capacities.

McShane (1991) mentions plugging as a design consideration for non-displacement piles, such as sheet piles, where the cross sectional shape of the pile will determine the propensity for plugging. For sheet piles, the more angular and deeper the corrugations in the steel, the greater the potential for plugging. Soil type will also determine plugging behavior, the author suggests cohesive soil has the greatest potential for plugging while cohesionless soil has the lowest. The author further suggests using a conservative estimate for plug area where 50% of the gross area can be assumed for cases where plugging is expected to occur. As mentioned, cohesionless soils tend to result in no plug formation. However, for cases where plugging is expected, use of 80% of the shaft perimeter is suggested. Load testing is advised to confirm these design values when plugging is expected to occur.

Yandzio (1998) references the British Steel Piling Handbook to determine the shaft area of sheet piles used in retaining wall abutments, when use of 80% of the coated area is recommended. The author further goes on to discuss that, due to the fact that wall friction is assumed to only act on the passive zone of soil along the wall, only 40% of the coated area of the shaft area below the point of full embedment should be used for determining shaft area. For the boxed pile configuration, the inner and outer shaft area can be used if a plug is not expected to form, and when plugging is expected to occur only the outer area should be used. Regarding toe area, for sheet piles acting in base resistance, no plugging is assumed. Beyond this discussion, no other recommendations are provided by the author regarding plugging behavior.

ArcelorMittal (2008) notes that plugging must be considered when determining values for shaft and toe load bearing areas. It is recommended that shaft area be calculated assuming no plug formation. When determining end-bearing resistance, it is recommended that full plugging is assumed but that reduction values of 0.5 for clay soil and 0.75 for sand soil be applied to selected values. A figure presented by the authors depicts the assumed toe and shaft bearing areas for different plug conditions and is replicated in Figure 2-32.

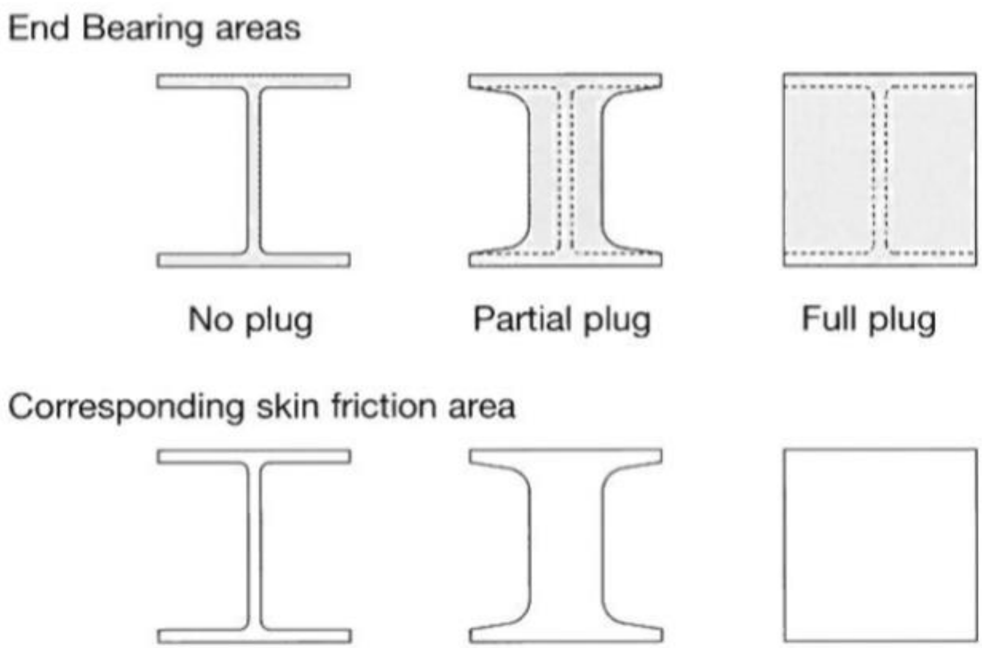


Figure 2-32. Toe and shaft bearing areas for an H-pile with no plugging, partial plugging, and full plugging from ArcelorMittal (2008) .

Biddle (1997) mentions that, based on collection and analysis of pile load tests carried out by the SCI, plugging is very rare for H-piles and should not be assumed unless there is evidence of plugging observed during driving. The API static method for shaft bearing resistance in cohesionless soil presented by the author requires that the whole steel surface area is used for both H-piles and sheet piles. Similarly, for base resistance, it is recommended that plugging should not be assumed. Similar shaft and toe areas are also recommended for the static SPT based methods recommended in the publication. For cohesive soils, the API static method for shaft bearing assumes total exposed shaft area unless evidence of plugging is encountered. Validation work carried out by SCI suggested static methods developed by API for pipe piles could be applied to H-piles and sheet piles. Calculations performed for this validation assumed no plugging had occurred for the H-piles. The base resistance estimates for cohesive soils also assume no plugging develops for sheet, H, tubular, or box piles. For tubular and box piles, it is recommended that the resistance provided by the interior shaft resistance from the soil plug plus the pile wall end-bearing be compared to the end-bearing across the whole cross section and to take the lesser of the two values. In general, plugging is assumed to not occur in most instances, especially for granular soils. In cohesive soils, plugging may occur for boxed or tubular piles, but is not expected to occur for sheet and H-piles.

The European Committee for Standardization (2004) recommends for the scenario of an open ended driven tube or pipe pile with an opening larger than 500 mm (19.7 inches) in any direction, the base resistance should be obtained by talking the smaller of:

- The shearing resistance between the soil plug and the inside face of the pile,
- The base resistance derived using the gross cross sectional area of the base

Beyond the recommendations for box or pipe piles, this document does not provide any additional recommendations regarding plugging.

In summary, several references outline the importance of understanding the plugging behavior of driven steel sheet piles. The implications of plugging can be significant for the calculation of shaft and toe resistances. In general, the design guides identified do not recommend the assumption of plugging unless there is evidence of its occurrence. When comparing cohesionless and cohesive soils, plugging will tend to have a greater effect in cohesive soils and occur more frequently in this soil type.

### 2.5.3 Summary of Plugging of Piles

In summary, plugging is a phenomenon experienced not only in pipe piles, but other non-displacement piles, such as H-piles and sheet piles. Plugging has significant implications for driving as well as load bearing for piles. The formation of a plug typically does not occur during the driving process, but will manifest under long term loading. Parameters that affect plug formation include, but are not limited to: soil properties, pile material and geometries, and loading conditions (during driving as well as after installation). Plugging is a behavior that is difficult to predict and also difficult to measure in non-pipe piles. For sheet piles, an evaluation of the toe load bearing relative to shaft bearing can provide indication of the formation of a plug. Plugging behavior has been observed through both field testing as well as laboratory testing of model piles and deserves closer examination as part of this study investigating the axial load bearing capacity of sheet piles.

## 2.6 Summary of Literature Review and Identified Knowledge Gaps

This section provides a summary of the literature review presented in this chapter on the current state of knowledge regarding the use of axially loaded sheet piles for the purposes of bridge abutments. This section also highlights major knowledge gaps currently existing regarding this topic. A summary of the topics covered in this chapter is presented below:

1. Bridge case histories
2. Static axial load tests on steel sheet piles

3. Currently existing design guidance
4. Plugging behavior in piles

The section discussing bridge case histories outlined the large difference in occurrence of bridge abutments constructed using axially loaded sheet piles within Europe and the U.K. relative to the U.S. This section highlighted the mature state of practice in Europe and the U.K. and demonstrates the viability of sheet piles for axial load bearing in bridge abutments. It is important to identify this gap in design practice as it provides incentive for maturing the state of practice in the U.S. Sheet piles have been used for over 50 years in bridge abutments within Europe and the U.K., demonstrating ample axial load carrying capacity for this foundation type. Incorporating the axial load bearing capacity of sheet piles in bridge abutment designs represents an improvement in currently existing design practice in the U.S. as it will lead to potential cost savings associated with reduced piles and construction time.

Regarding static axial load tests on steel sheet piles, only seven case studies were identified in the literature. This number is slim compared to axial load testing of other pile types. A lack of well-documented axial load tests of sheet piles represents a gap in the body of knowledge concerning this topic. This scarcity in axial load test results may contribute to the lack of understanding of the behavior of axially loaded sheet piles and may contribute to the exclusion of their axial load capacity in conventional abutment design in the U.S. This research effort will provide valuable data on several pile load tests to help address this need.

In general, currently existing design guidance treats sheet piles designed for axial loads as any other non-displacement pile. Sheet piles have many unique characteristics that set them apart from other displacement piles, such as their corrugated cross section, interlocking edges, and ability to form continuous walls. These characteristics may have important implications for the load transfer mechanism associated with axial loading. Current design guidance does not properly account for this difference. The load transfer mechanism involved with axially loaded sheet piles represents a knowledge gap this research project aims to address. This mechanism will be thoroughly investigated using results of well-instrumented full-scale tests. This research aims to provide theoretical load transfer curves to help model axially loaded sheet pile foundations and advance our understanding and design guidance associated with this topic.

Lastly, improved understanding of the load transfer mechanism from both an experimental and theoretical perspective is expected to address a knowledge gap concerning the plugging behavior of sheet piles. Existing design guidance has been identified that provides useful insight regarding this topic but does not provide comprehensive recommendations specific to axially loaded sheet piles. Plugging has been identified to be an important topic when it comes to understanding the load transfer mechanism governing axially loaded sheet piles but there has been relatively few studies on the subject, due in part to the difficulty in measuring this behavior. Results from this research effort will help provide additional insights regarding this behavior in axially loaded sheet piles and help address this knowledge gap.

In summary, the main knowledge gaps include:

- Lack of well-documented load tests of instrumented sheet piles.
- Lack of guidance regarding the design of axially loaded sheet piles that accounts for their unique characteristics.

- Lack of adequate understanding of the soil-sheet-pile interaction, and mechanics of load transfer for axially loaded sheet piles.
- Related to this, an improved understanding of the influence of plugging on axial load response of sheet piles is needed.

# CHAPTER 3: AXIAL LOAD TEST OF SHEET PILES- LAB TESTING

## 3.1 Introduction

As mentioned in the literature review, well-documented static axial pile load tests of sheet piles are relatively scarce. This scarcity possibly contributes to their lack of use for axial load bearing in bridge abutments within the U.S. Full-scale dynamic and static axial load testing was performed on well-instrumented sheet piles located at the Highbay facility of the University of North Carolina at Charlotte (UNCC) in order to help address this deficiency . These tests also served as a pilot study to help establish means and methods for pile load testing at a field location. Two walls consisting of four PZ-27 sheet pile sections were driven to an embedment depth of 2.44 m within a geotechnical test pit located within the EPIC Highbay laboratory. The concrete-lined geotechnical test pit had dimensions of 3.7 m by 3.7 m with a depth of about 3 m. The test pit base is natural ground consisting of residual soils and highly weathered rock. The test pit was backfilled with a selected soil in a controlled manner prior to pile installation and testing. Figure 3-1 presents an image of the test pit prior to backfilling. The pile load tests were performed in general accordance with the Constant Rate of Penetration Test procedures presented in ASTM D1143/D1143M, which require that a constant value of pile displacement per unit time be maintained for the duration of the test. Instrumentation installed along the pile length allowed information regarding the load transfer behavior to be measured and used to help characterize this behavior for sheet piles.

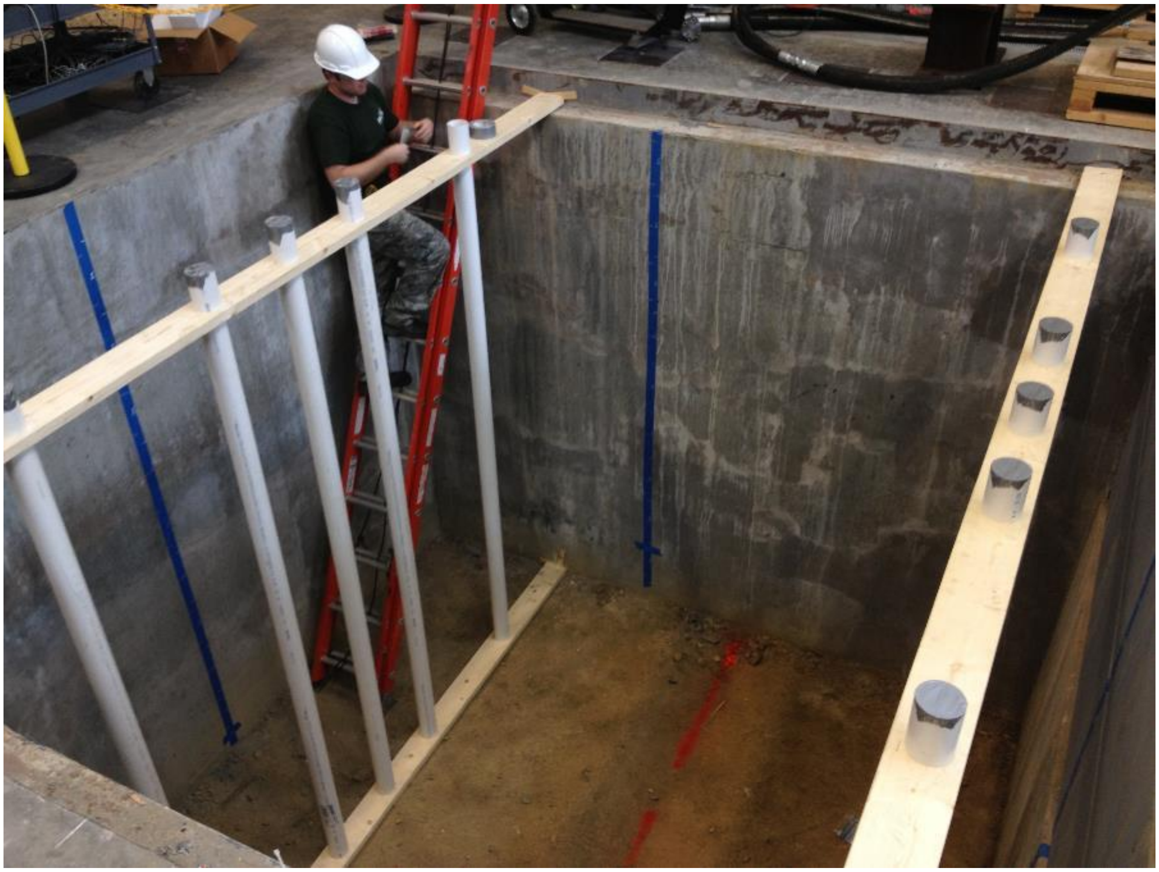

Figure 3-1. Geotechnical test pit at UNCC

## 3.2 Backfilling Process and Geotechnical Characterization of Test Pit Soil

The test pit was backfilled with compacted clayey to silty sand (SC to SC-SM). Index properties for the backfill soil were measured at UNCC using seven randomly selected samples. Table 3-1 summarizes the test results (ASTM 2007; ASTM 2010; ASTM 2011; ASTM 2012; ASTM 2014). Figure 3-2 presents grain size distribution curves obtained for the backfill soil. Compaction testing on this soil performed using Standard Proctor energy yielded a maximum dry unit weight ($(\gamma_{dry})_{max}$) of 18.7 kN/m$^3$ (118.8 lb/ft$^3$) and an optimum water content of 12.25% (See Table 3-1 for more information and Appendix B for additional results (ASTM 2011; ASTM 2014; ASTM 2014; ASTM 2015)).

Table 3-1. Summary of index properties and compaction results of backfill soil for pile load testing at UNCC

| Property | Value | ASTM Standard |
|---|---|---|
| Grain size distribution | Figure 3-2 (N=7) | D422 |
| $D_{10}$ (mm) | 0.0013-0.0088 | |
| $D_{50}$ (mm) | 0.18-0.54 | |
| $D_{60}$ (mm) | 0.38-0.82 | |
| $C_u$ | 77.4-294 | |
| $C_c$ | 0.86-4.86 | |
| Specific Gravity ($G_s$) | 2.68-2.72 (N=7) | D854 |
| USCS | SC to SC-SM | D2487 |
| Atterberg Limits | | |
| Liquid Limit (%) | 26-34 | D4318 |
| Plastic Limit (%) | 20-23 | |
| Standard Proctor Compaction Tests (N=2) | | |
| Max. Dry Unit Weight $(\gamma_{dry})_{max}$ (kN/m$^3$) | 18.66-18.86 | D698 |
| Optimum water content $W_{opt}$ (%) | 12.2-12.3 | |

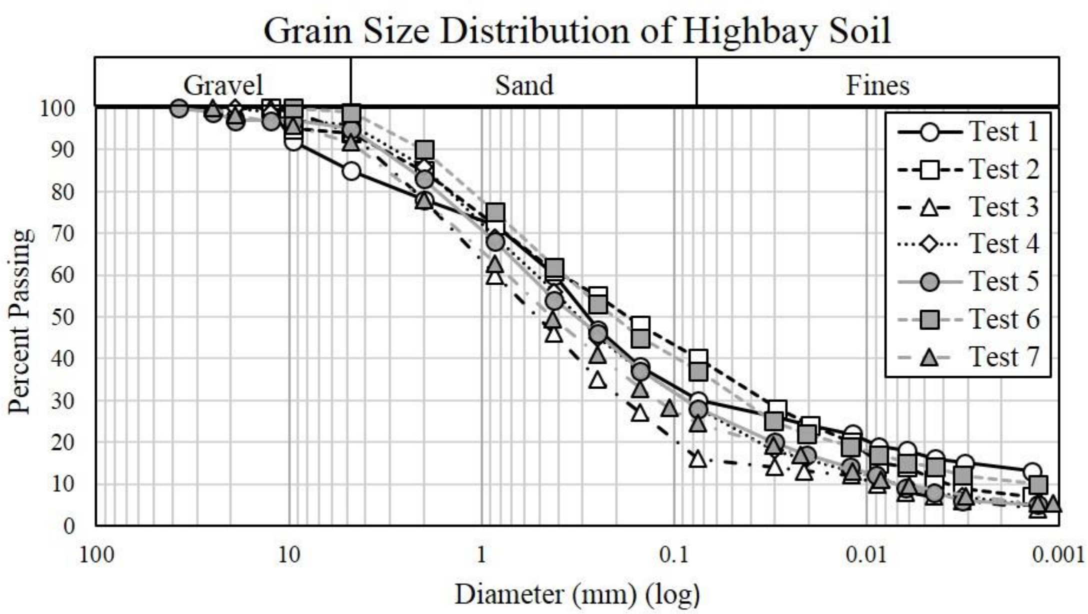


Figure 3-2. Grain size distribution for backfill soils used for pile load testing at UNCC

The clayey sand backfill was compacted in lifts with an average loose thickness of about 100 mm (4 in) (loose thickness refers to layer thickness before compaction). The soil was compacted by use of a vibratory plate and hand tampers. Compaction was controlled during the backfilling operation using nuclear density gage, sand cone, and drive cylinder tests (ASTM 2015; ASTM 2017; ASTM 2017). The average relative compaction achieved was approximately 92% with respect to the Standard Proctor maximum dry unit weight and the water content of the placed soil ranged between 11 to 13%, which was within one percentage point of the optimum moisture content. Figure 3-3 presents photos of the test pit during backfilling and Figure 3-4 presents an image of the test pit after backfilling was completed.

Figure 3-3. Images taken during backfilling of geotechnical test pit at UNCC

Figure 3-4. Photo of geotechnical test pit at the end of backfill placement

### 3.2.1 Geotechnical In-Situ Testing of the Compacted Backfill

In-situ characterization of the backfilled and compacted SC to SC-SM soil was conducted by standard geotechnical field investigations, including Standard Penetration Test (SPT), Seismic Cone Penetration Tests (SCPTu), and dilatometer tests (DMT) (ASTM 2011; ASTM 2012; ASTM 2015). Figure 3-5 indicates the locations where these tests were performed. As shown in this figure, the SC-SM backfill soil had an average corrected SPT blow $(N_1)_{60}$ of 12 blows per 0.3 m (1 ft). The SPT blow count of the basal in-situ residual soil located at the base of the test pit was in excess of 50 blows per 0.3 m (1 ft). The pre-installation CPT tests yielded average toe resistance values of 4.1 MPa (42.7 tsf) and 6.8 MPa (70.8 tsf) for the SW-SM backfill and native residual soil, respectively. Figure 3-6 presents the soil stratigraphy measured before and after pile installation.

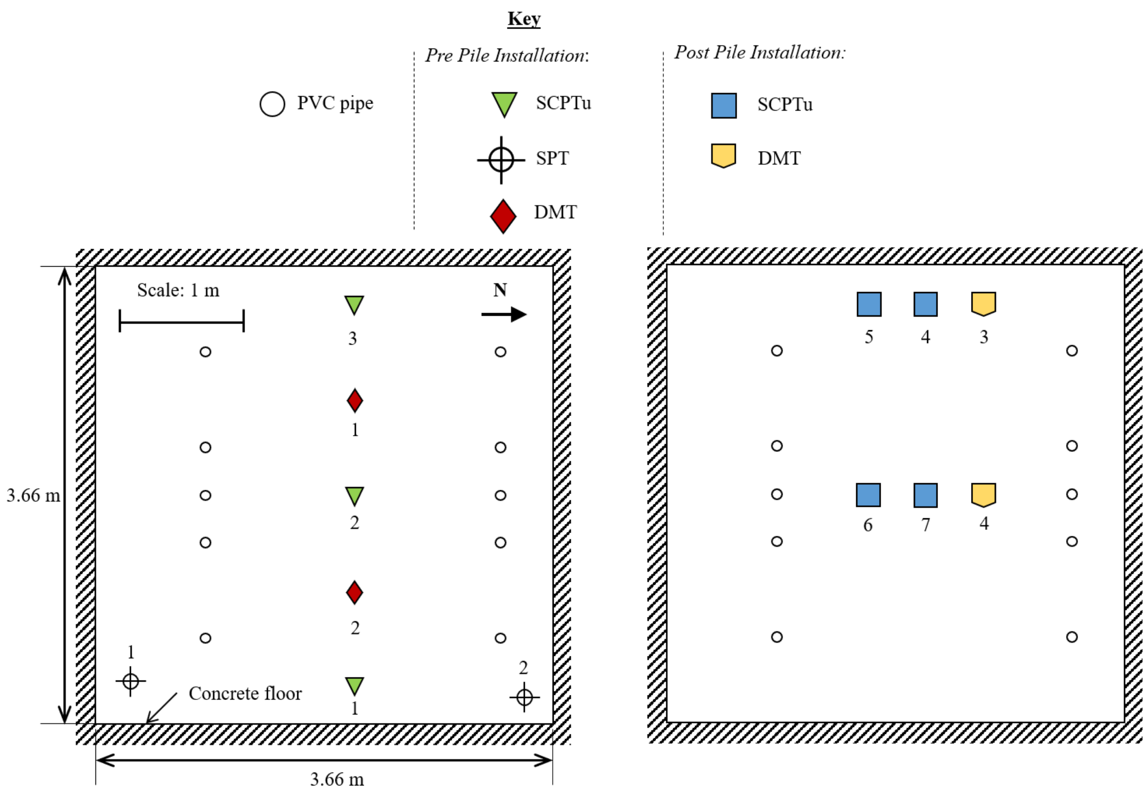


Figure 3-5. Location of in-situ geotechnical tests in UNCC geotechnical test pit

In addition to SPT borings and SCPTu soundings, flat plate dilatometer tests were performed before and after pile installation. These results are presented in Figure 3-7. Soil classification based on the DMT measured material index generally agree with index testing indicating this material is a sandy/clayey silt to silty sand. Test results indicate an increase in soil density after pile driving, this is observable through increased values of the Dilatometer Modulus value, $E_D$. Increased density of the backfill material was also apparent during DMT testing as lower maximum depths were observed during testing after pile installation.

In addition to DMT testing, densification in the backfill test pit soil was also evident through SCPTu testing. Measurement from tip resistance, $q_t$, as well as sleeve resistance, $f_s$, show on average higher values for post installation (SCPTu, 4 through 7) measurement as compared to pre-installation values (SCPTu, 1 through 3). This increase is especially pronounced at depths in the soil along the shaft of the sheet pile up to the embedment depth of 2.44 m, with less significant increases in values below the pile toe. The degree of increase is more noticeable for the $f_s$ values relative to $q_t$ values for the measured profile. These results suggest that the soil was significantly densified due to pile driving, with the greatest densification occurring along the shaft of the pile.

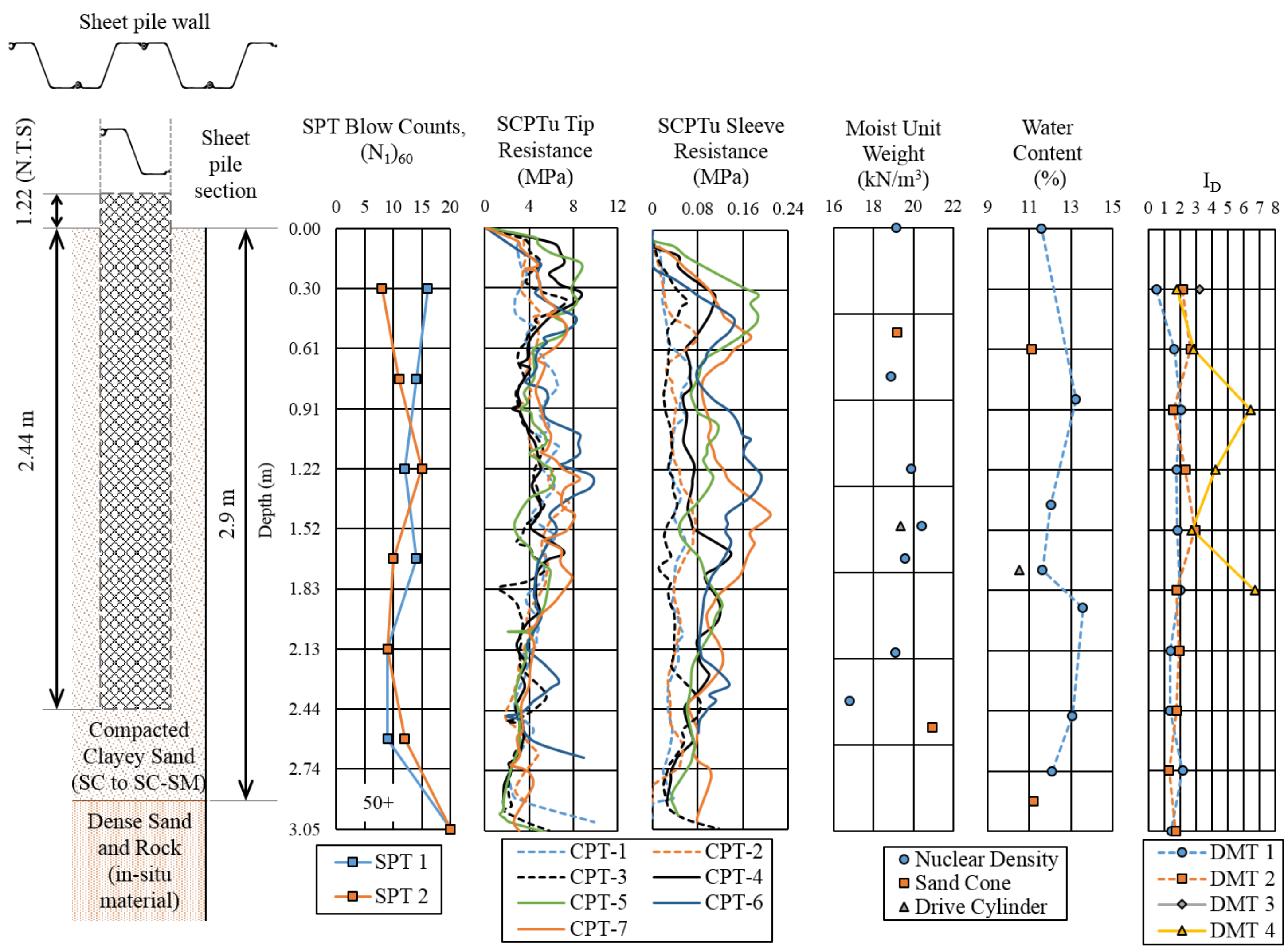


Figure 3-6. Soil stratigraphy at UNCC geotechnical test pit

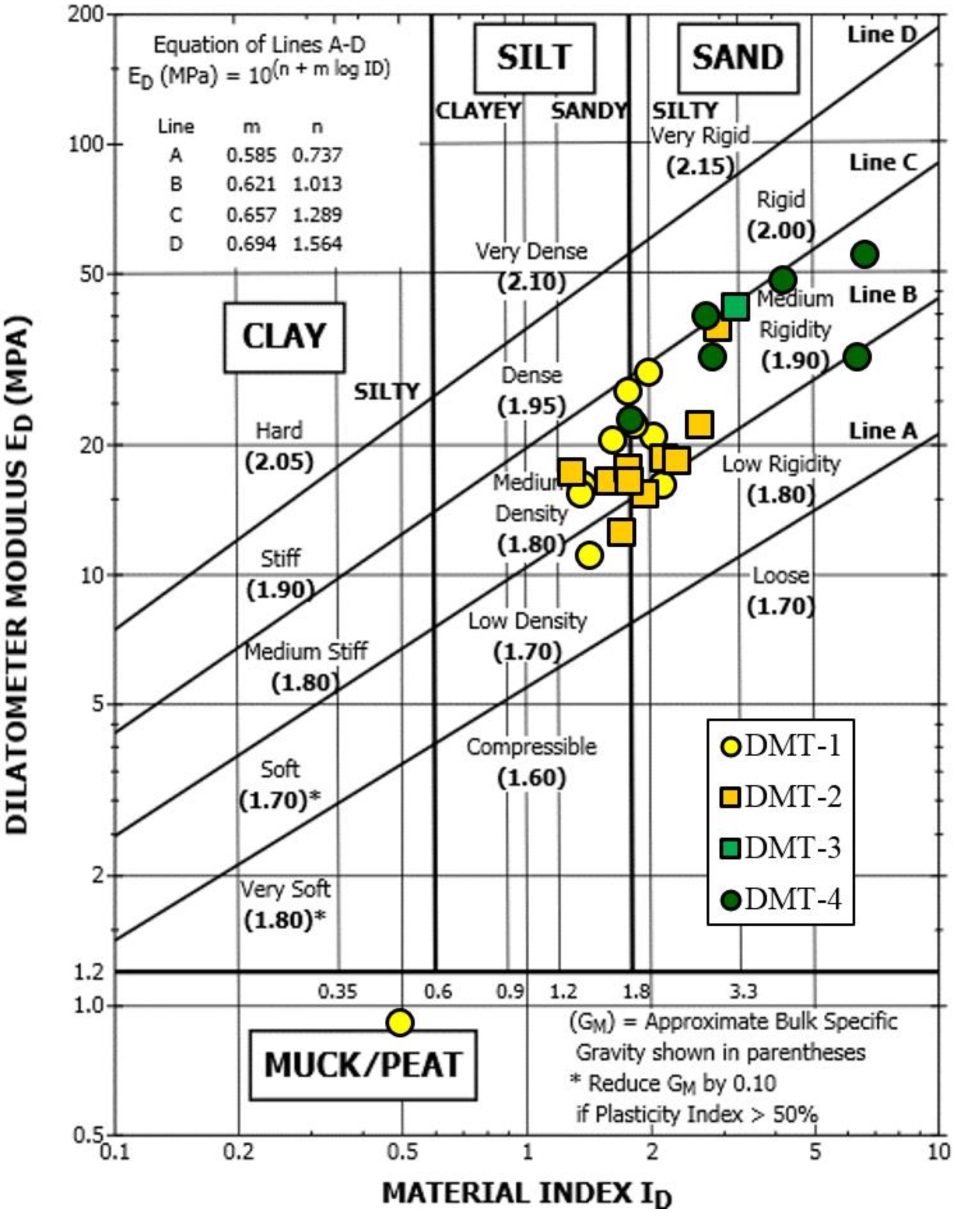


Figure 3-7. Summary of DMT test results performed at UNCC geotechnical test pit

### 3.2.2 Geotechnical Lab Tests on the Compacted Backfill

The shear strength properties for the backfill soil were measured using additional laboratory testing including direct shear testing and UU triaxial testing (ASTM 2011; ASTM 2015). Table 3-2 presents a summary of these tests, and additional information is presented in Appendix B.

Table 3-2. Summary table of direct shear and UU triaxial testing of compacted backfill soil

| Test | Value | ASTM Standard and Notes |
|---|---|---|
| Direct shear test (compacted sample at target dry unit weight and moisture; not inundated) | | |
| Peak $\phi'$ (deg) | 39.3 | ASTM D3080<br>Test rate = 0.0076 mm/min<br>$\gamma_{dry}$ = 17.18 kN/m$^3$<br>w.c. = 13.1% (RC = 92% S.P.) |
| Peak $c'$ (kPa) | 8.4 | |
| Residual $\phi'$ (deg) | n/a | |
| Residual $c'$ (kPa) | n/a | |
| UU Triaxial compression tests | | |
| Peak $\phi'$ (deg) | 32.2 | ASTM D2850<br>Strain rate = 1% /min.<br>$\gamma_{dry}$ = 17.04 kN/m3<br>w.c. = 12.2% (RC = 91% S.P.) |
| Peak $c'$ (kPa) | 22.9 | |
| Residual $\phi'$ (deg) | 31.4 | |
| Residual $c'$ (kPa) | 22.4 | |
| Tangential $E_s$ (MPa) | 7-9 | |

Note: RC = relative compaction. S.P. = Standard Proctor

The interface friction angle between the compacted back filled soil and the steel of the piles was measured using a steel coupon cut the steel piles. Interface shear tests were performed using the direct shear device with modifications, a summary of the results are presented in Figure 3-8. Additional details can be found in the Appendix B.

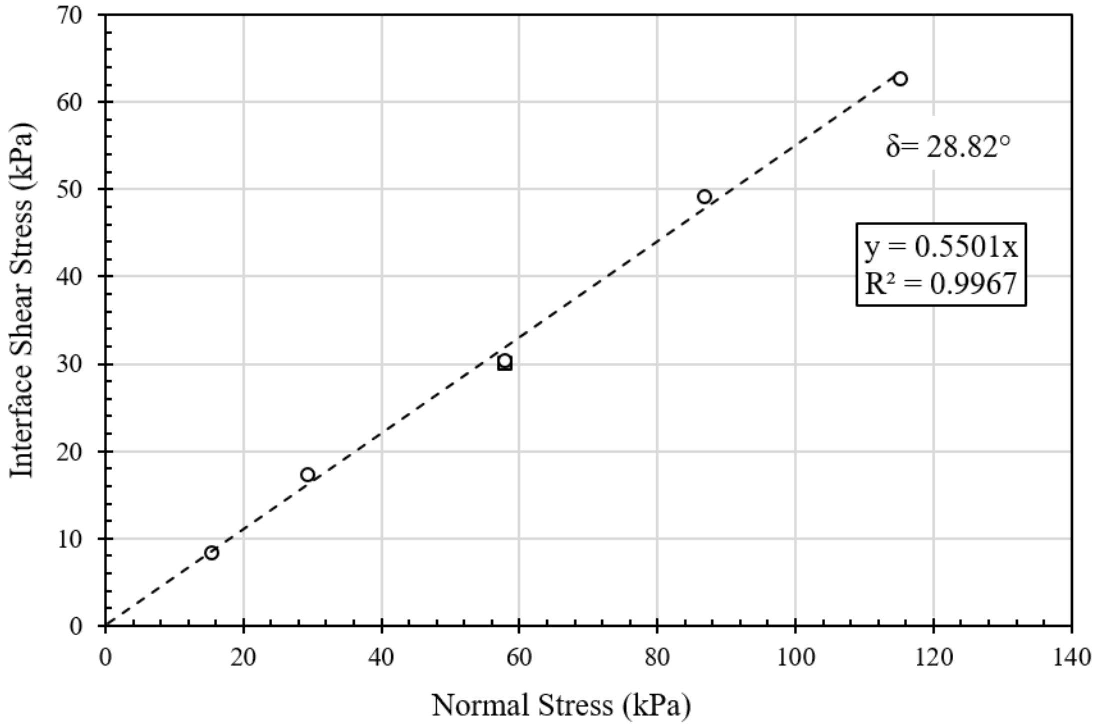


Figure 3-8. Results from interface testing for UNCC geotechnical test pit

### 3.2.3 Test Piles

The sheet piles used in this study were Skyline PZ 27 sections. These sheet piles are hot-rolled sections of Grade 50 steel ($F_y$= 345 MPa= 50 ksi) with a nominal cross sectional area of about 76.84 cm$^2$ per sheet (11.91 in$^2$). One sheet section is 0.46 m (1.5 ft) wide and each sheet pile wall consisted of 4 sections, as shown at the top of Figure 3-9, for a total wall width of 1.89 m. The total length of each steel sheet pile wall was 3.66 m and the piles were installed to a depth of 2.44m. Figure 3-9 indicates ground level with a dashed line. Before pile installation, the sheet piles were instrumented with Bridge Diagnostics Inc. (BDI) strain transducers and Vishay Micro-Measurements constantan grid resistance strain gages as shown in the top right of Figure 3-9. Details regarding strain gage, installation can be found in Appendix B. Figure 3-10 presents an image of the instrumented piles ready for installation.

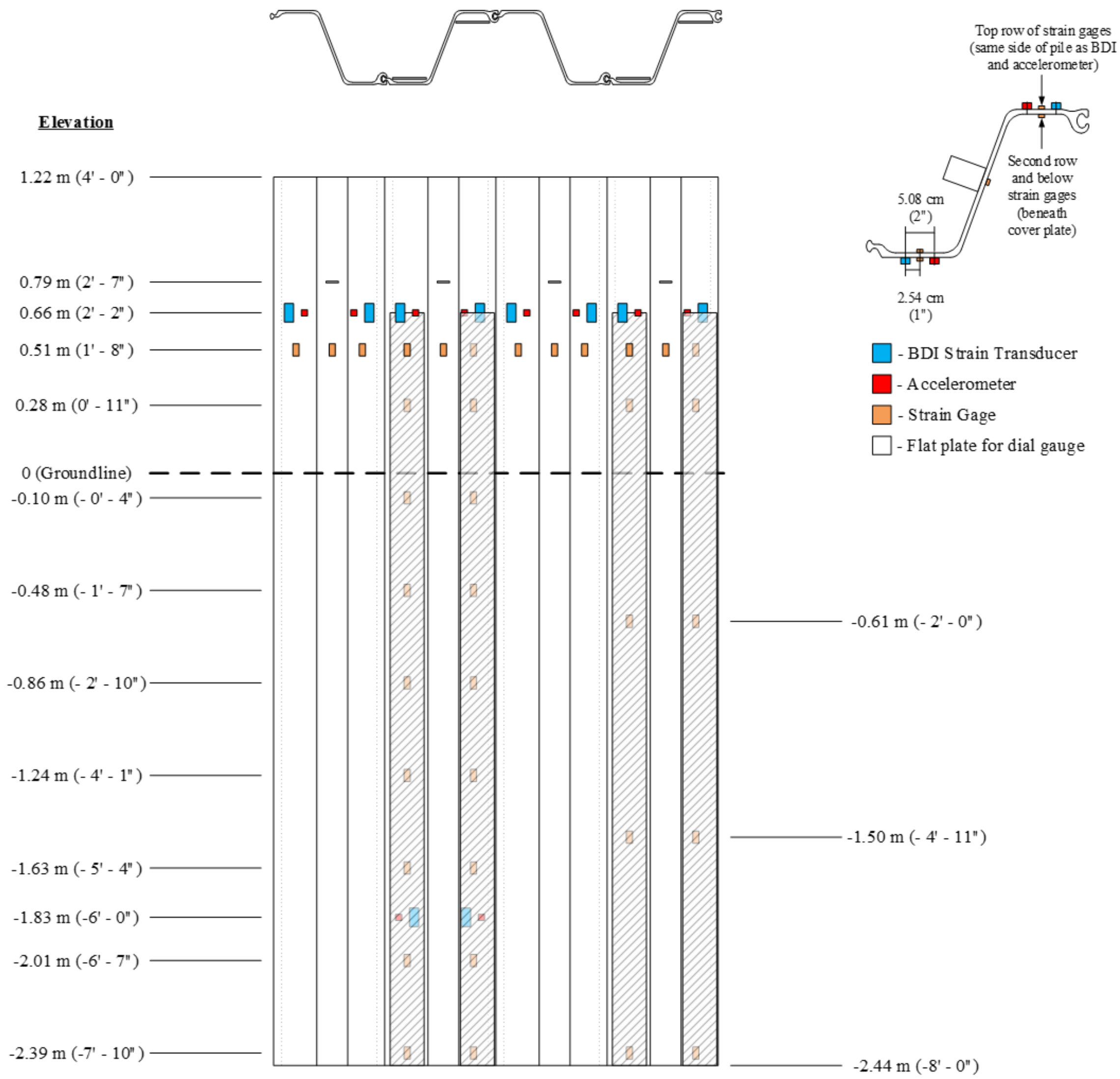


Figure 3-9. Sheet pile cross section and instrumentation layout for UNCC geotechnical test pit piles

Figure 3-10. Image of instrumented sheet piles ready for installation at UNCC geotechnical test pit

### 3.2.3.1 Pile Installation

The sheet piles were installed using a Model 6E International Construction Equipment (ICE) vibratory hammer. A MKT 9B3 impact hammer was also used on one of the sheet pile sections of Wall No. 1. Final embedment depth of 2.44 m was attained after driving resulting in an above ground length of pile of 1.22 m. Figure 3-11 presents and image of the hammers used for pile installation and Figure 3-12 presents an image of the driving record for wall No. 2 using the vibratory hammer. This figure labels the piles 1 through 4. Piles 1 and 3 featured instrumentation down the length of the pile section. These instrumented piles had the additional cross sectional area due to the cover plates placed over the sensors, this is likely a factor leading to the longer time required for installation, as shown in Figure 3-12. The installation process involved driving pile 2 to a depth of 1.22 m, followed by installation of pile 3 to the same depth. Pile 2 was then installed to the final embedment depth followed by pile 3. Pile 4 was then installed to the full embedment depth followed by pile 1.

a.)

b.)

Figure 3-11. Hammers used to drive sheet piles at UNCC geotechnical test pit: a.) ICE Model 6E vibratory hammer and b.) MKT 9B3 impact hammer

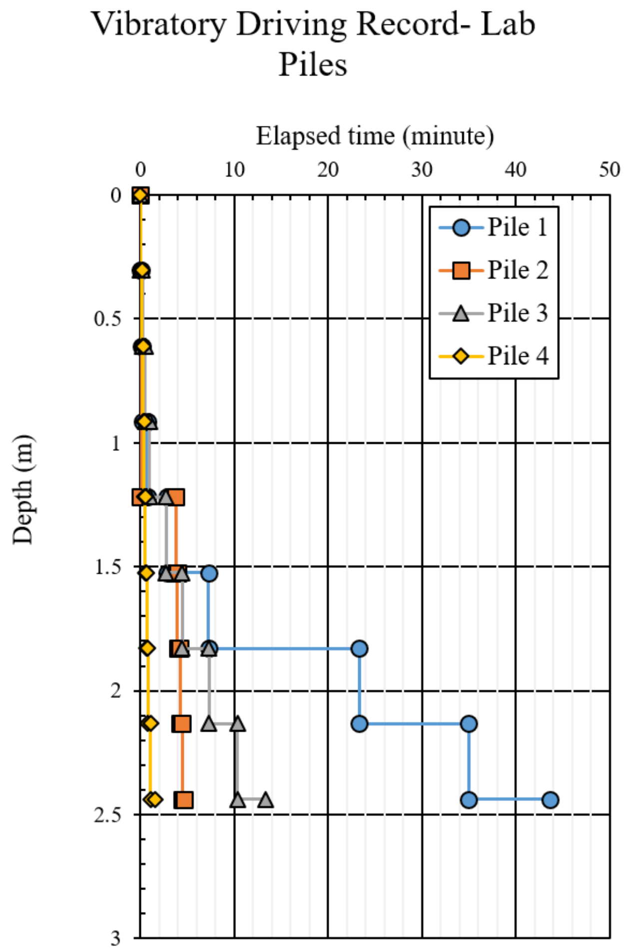


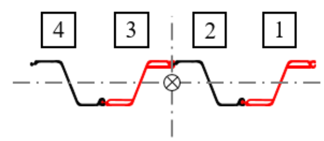


Figure 3-12. Driving record of UNCC geotechnical test pit piles

To allow for PDA and CAPWAP estimation of axial load capacity, a portion of sheet pile test wall No. 1 was installed with an impact hammer type MKT 9B3. PDA records from 15:55 to 16:02 on July 29, 2014 recorded a total of 178 blows for the installation of one sheet pile section. The PDA pile axial capacity estimate at End-Of-Driving (EOD), using the Maximum CASE Method Capacity with a JC = 0.7, was 253.5 kN (57 kips) for this single pile section. The CAPWAP analysis for hammer Blow 176, near EOD, yielded the results shown in Figure 3-13. The CAPWAP ultimate axial capacity for Blow 176 at EOD was estimated as 164.6 kN (37 kips) for this single pile section, with 74.7 kN (16.8 kips) (45.4 %) attributed to shaft resistance, and 89.9 kN (20.2 kips) (54.6 %) attributed to toe resistance.

Considering that each sheet pile wall consists of four PZ-27 sections, the estimated axial load capacity for the sheet pile walls based on the PDA and CAPWAP analyses for EOD conditions are 1048.2 kN (228 kip) and 658.3 kN (148 kip), respectively. Figure 3-13 presents these results and Figure 3-14 presents an image of the piles after driving.

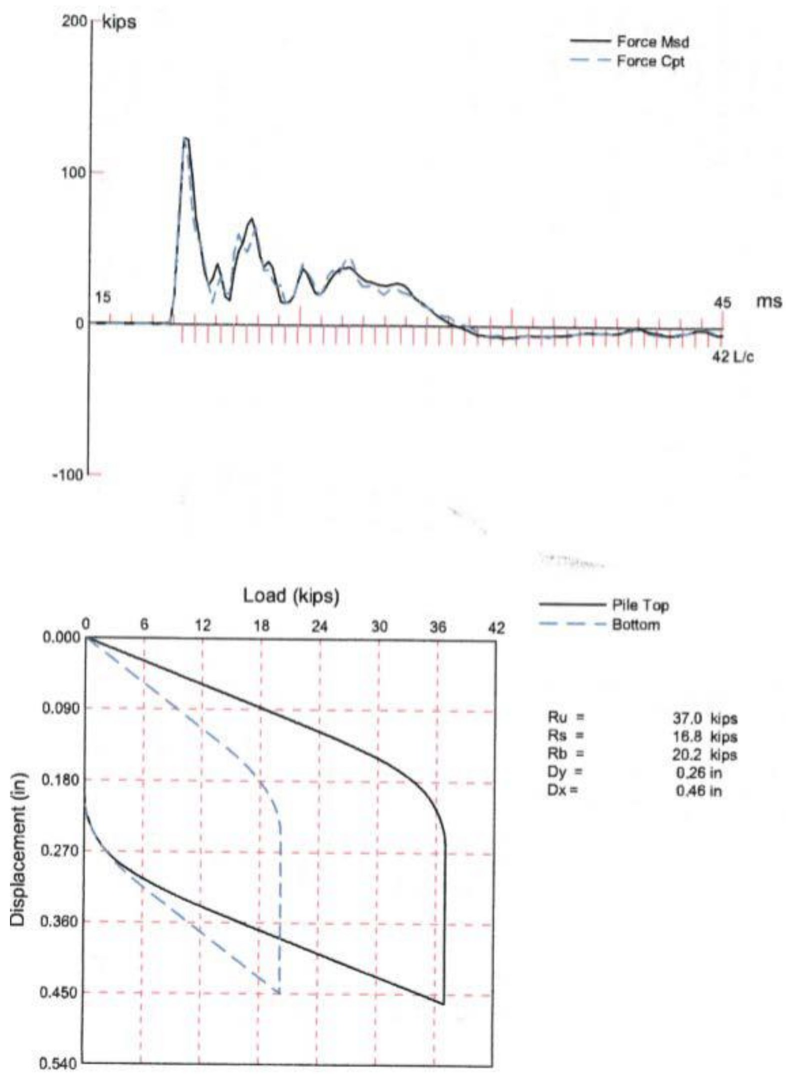


Results reported by GRL Engineering, Inc (PDA Set 2: Blow 176, July 29, 2014 at 16:02)

Figure 3-13. CAPWAP results for EOD PZ-27 section of Test Wall No. 1

Figure 3-14. Image of pile walls after driving at UNCC geotechnical test pit

3.2.3.2 Static Load Test Setup

The axial load test setup used to test the sheet pile walls is shown in Figure 3-16. The load was applied with a 1459 kN (328 kip) capacity MTS model 201.70 actuator and the pile head deflection was monitored with four digital dial gages offering 0.002 mm resolution. Figure 3-15 presents an image of the actuator. The static load test was performed at a constant rate of penetration (CRP) in general accordance with the procedure described in the ASTM Standard D1143 (ASTM 2013). The applied rate of pile head penetration was 0.635 mm/min (0.025 inch/min). The loading rate was input into MTS control software and actuator head loads and displacements were measured using internal sensors installed in the actuator. A 24-bit PXI-4330 bridge input module was used to provide excitation and signal conditioning for the resistive strain gages and the digital dial gauges which were measured concurrently using USB-to-signal communication.

Figure 3-15. Load actuator used for static axial pile load testing at UNCC geotechnical test pit

Figure 3-16. Image of static axial pile load test setup at UNCC geotechnical test pit

## 3.3 Static Axial Load Test Results

The two test walls were subjected to several axial load tests. Axial load versus pile head displacement curves for both test walls are shown in Figure 8. Both test walls exhibited similar axial load response in terms of initial stiffness and capacity. This is expected given that both walls had the same dimensions and were installed in the same controlled uniform soil conditions. The axial load capacities were approximately 1334.5 kN achieved at a head displacement of about 25 mm. This capacity is about 200% of the estimate obtained from the CAPWAP analyses of Wall No. 1 at EOD.

Further analysis of the second pile load test conducted on wall No. 2 was performed. Figure 3-18 presents an image of pile head load versus displacement. The failure load for this test was determined using Davisson's failure criteria and was found to equal 1218.9 kN at a displacement of 7 mm. Using strain gage measurements along the shaft of the pile, the axial force distribution along the length of the pile was determined. Figure 3-19 presents these results. As can be seen, the sheet pile wall carries applied load primarily through shaft resistance. Based on the measured load transfer and considering forces at the Davisson failure load, it was determined that contributions from shaft and toe resistances were equal to 1130.3 kN (93%) and 88.6 kN (7%), respectively.

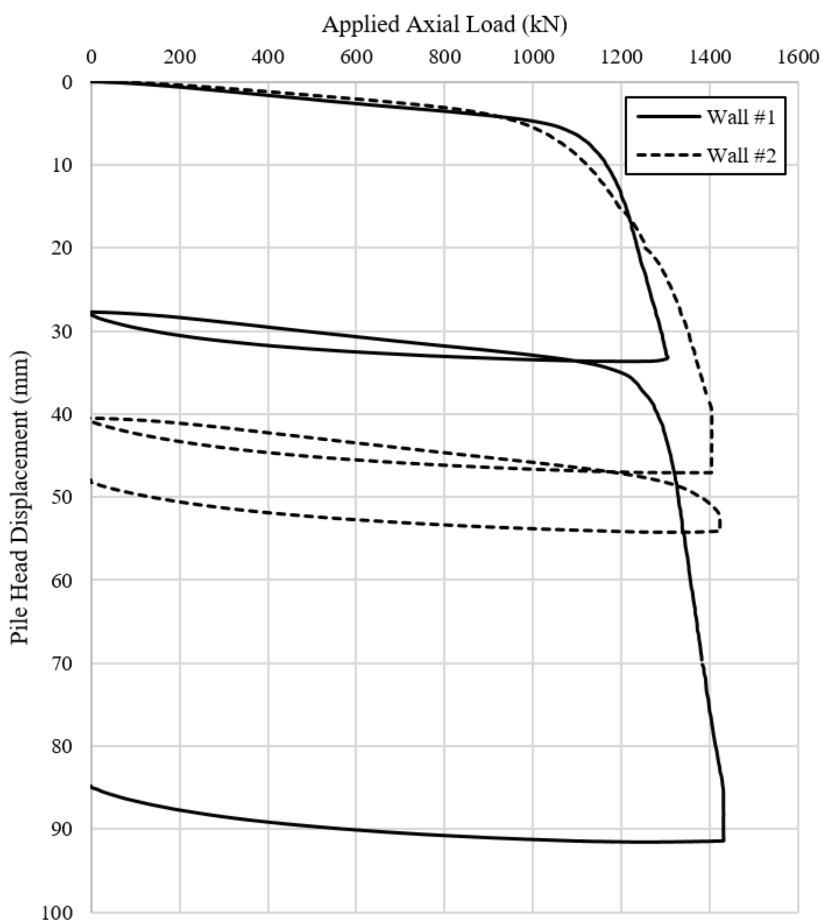


Figure 3-17. Pile head displacement versus applied axial load for pile load testing at UNCC geotechnical test pit

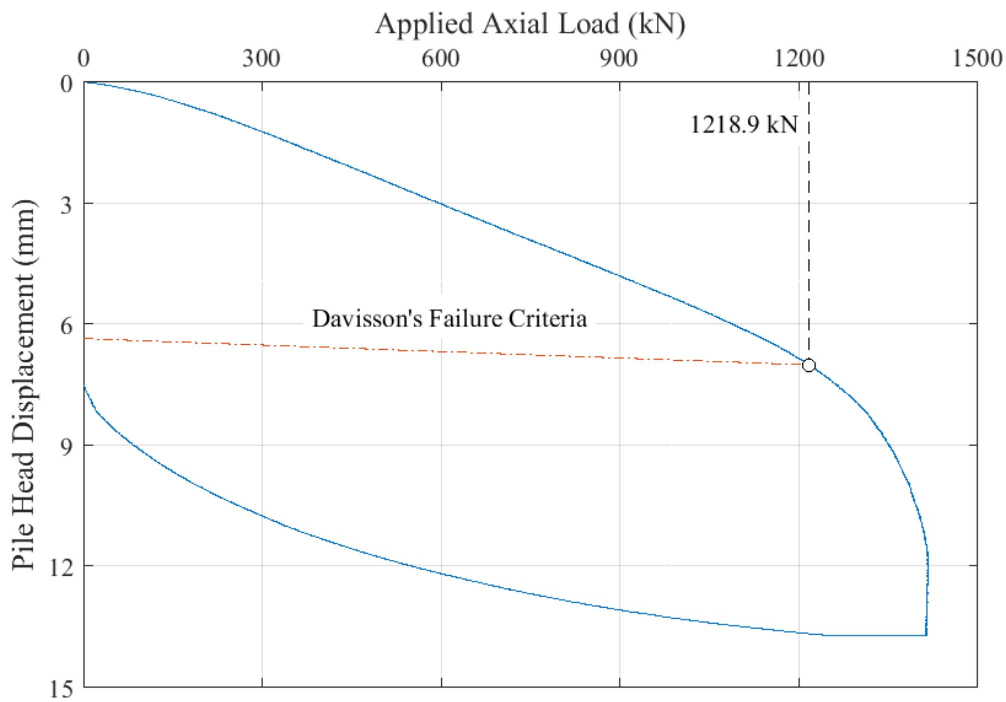


Figure 3-18. Pile head displacement versus load for static axial load test of sheet pile wall No. 2 at UNCC geotechnical test pit

Based on the measurements of force versus depth along the pile, experimental *T-Z* and *Q-Z* curves were developed. These curves offer additional information regarding the load transfer behavior for this pile type under static axial loading. *T-Z* curves were developed for regions along the pile from depths of 0 to 1.3 m and for 1.3 to 2.4 m. Figure 3-20 presents the experimental *T-Z* curves. The curves indicate increased shaft resistance at greater depths, which is consistent with expectations given the increase in overburden pressure, confinement, and soil density with depth. Additionally, the *T-Z* curves indicate that shaft resistance is fully mobilized around a displacement of 7.6 mm. This value agrees well with conventional values of 5 to 10 mm.

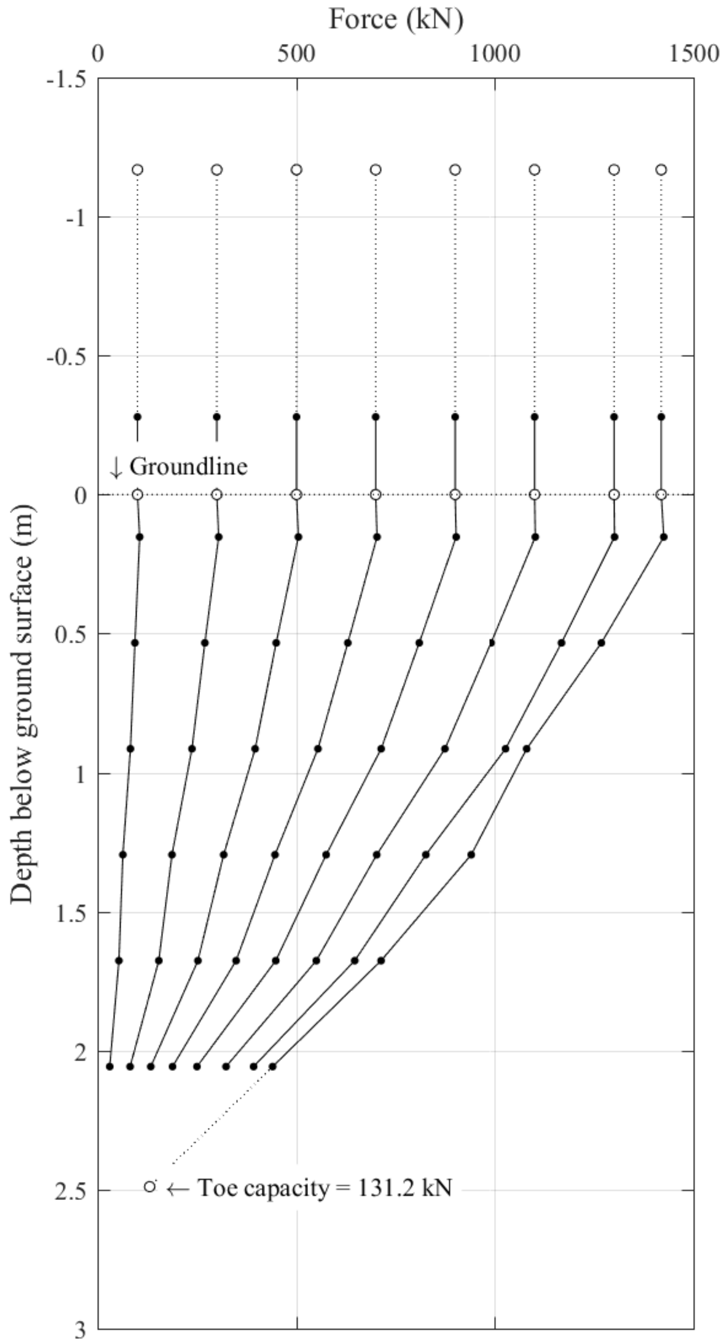


Figure 3-19. Load versus depth measured for Sheet Pile Wall No. 2 at UNCC geotechnical test pit

Developed *Q-Z* curves help characterize the load transfer behavior occurring at the pile toe. Figure 3-21 presents the experimentally developed *Q-Z* curve for this test. Based on this figure, the peak toe resistance of approximately 133.4 kN was reached at a displacement of approximately 12.7 mm. The magnitude of toe resistance is fairly low compared to the load carried through shaft resistance. The amount of displacement required to fully mobilize the toe resistance suggests that plugging may be occurring to some degree at the pile tip. Pile toe resistance is typically mobilized at displacement values equal to 10 to 25% of the diameter or width of the pile. It is unclear if this typical behavior applies to sheet piles or plugged piles. However, it is reasonable to assume larger displacements will be required to fully mobilize toe resistances acting over larger areas. The displacement measured to fully mobilize toe resistance of 12.7 mm is larger than the steel thickness of the pile of 9.5 mm. This comparison may indicate some degree of partial plugging is occurring at the toe but does not provide conclusive evidence.

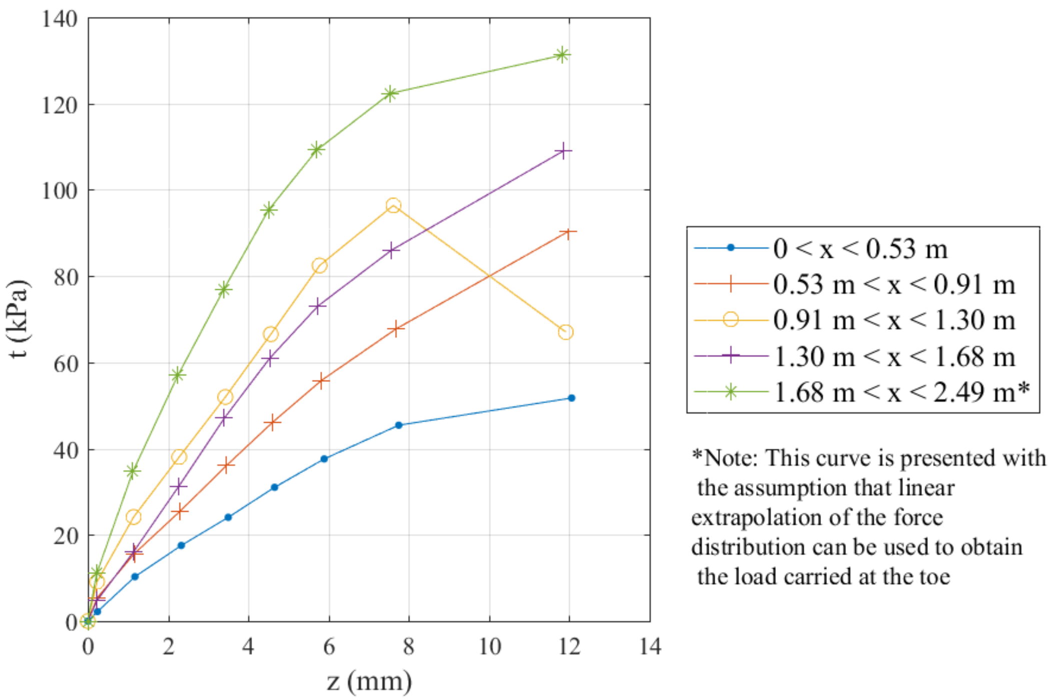


Figure 3-20. Experimental *T-Z* curves for test on wall No. 2 at UNCC geotechnical test pit

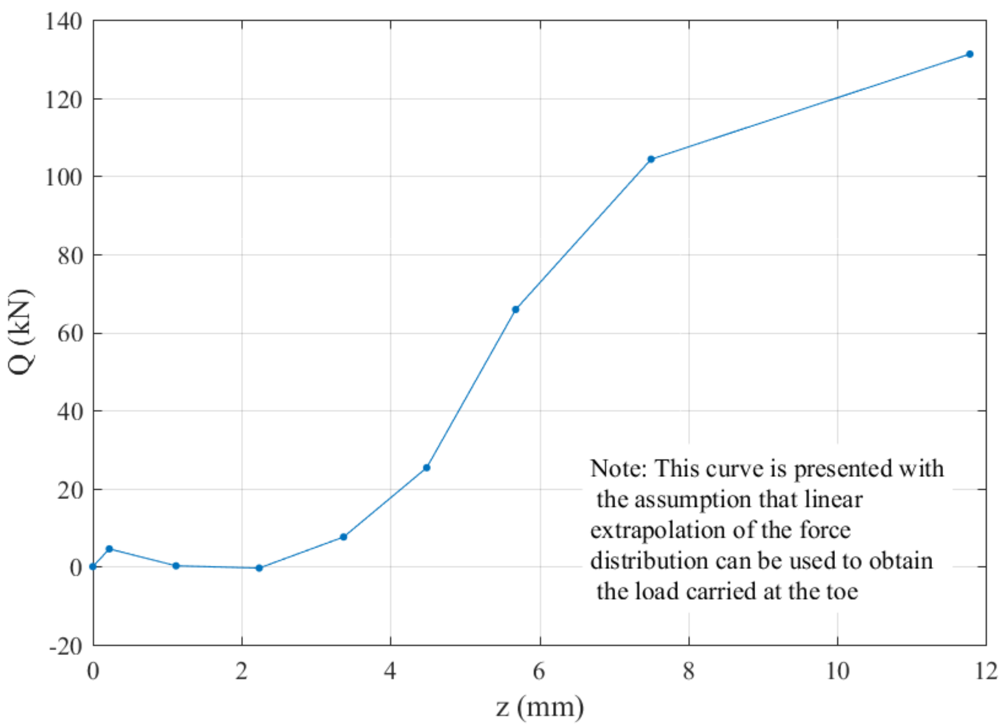


Figure 3-21. Experimental *Q-Z* curve for test on wall No. 2 at UNCC geotechnical test pit

## 3.4 Summary and Conclusions

A sheet pile load test performed on a sheet pile wall was successfully conducted at the geotechnical test pit of UNCC. Piles were installed into a compacted backfill consisting of native soils that classify as SC to SC-SM according to the USCS. Samples of the test soil were characterized using several geotechnical lab tests, these included index testing, direct shear, interface testing, and UU triaxial tests. The placed and compacted backfill was tested for density during backfilling operations using nuclear gauge testing, sand cone, and drive cylinder tests. After fill placement, conventional geotechnical field tests were used to the further characterize the test soil, these included SPT, SCPTu, DMT, and MASW. A few of these tests were conducted before and after pile installation. The PZ-27 sheet piles used for testing were 3.66 m in length and driven individually to an embedment depth of 2.44 m, two pile walls were installed each consisting of four sheet piles with 1.52 m of spacing separating the centerlines of the two walls.

Dynamic testing was performed during driving of select sheet pile and information from these tests was used to generate PDA and CAPWAP static capacity predictions. Strain gages were installed along the length of two of the sheet piles in each of the two walls and were used to measure axial force distribution with depth during static axial loading for both pile walls. This allowed for measurement of the mobilization of shaft and toe resistances. Moderate agreement was found between CAPWAP predictions and measured static axial load capacity. Moderate to poor agreement was found between PDA predictions and measured static axial load capacity.

Measurements of head load versus displacement were used to report the failure load as determined using the Davisson's criteria. Measured axial load versus depth was also reported based on the level of instrumentation installed along the sheet piles. Results from these measurements indicate that the piles were carrying load primarily through shaft bearing, with the majority of shaft resistance obtained from the lower 1.2 m of soil. The displacement required to fully mobilize shaft resistance was found to be approximately equal to conventional values reported for other pile types. Additionally, the measured values for peak toe resistance and displacement required for mobilization suggest that plugging is occurring at the toe but to a small degree.

The laboratory test program offers valuable insight into the axial load bearing characteristics of sheet piles. These tests are particularly significant given the relatively few studies on full-scale, well-instrumented, sheet piles. These tests, along with full-scale testing performed in the field, provide valuable contributions towards addressing identified knowledge gaps highlighted in chapter 2. The measured axial load capacities of the sheet piles walls were found to be significant and exceeded expected values.

# CHAPTER 4: AXIAL LOAD TEST OF SHEET PILES- FIELD TESTING

## 4.1 Introduction

One method used to reliably measure the relationship between axial load and the resulting pile displacement involves static axial pile load compression tests. When performed in the field, the test measures load-settlement behavior of individual or pile groups for the particular soil conditions existing at the test site, providing a high quality prediction of pile load-settlement behavior. With proper instrumentation, these tests also provide information regarding the distribution of shear stresses in the soil along the pile shaft and end-bearing capacity provided at the pile toe. Several test methods are possible and can outline different requirements regarding the application of axial loads to the pile over the duration of a test. These tests were performed in general accordance with the Constant Rate of Penetration Test procedures presented in ASTM D1143/D1143M, which require that a constant value of pile displacement per unit time be maintained for the duration of the test (ASTM 2013). Static axial pile load compression tests were performed at a field site in Matthews, North Carolina, for both a PZ-27 sheet pile pair and HP 12x73 H-pile (Sylvain et al. 2017). This chapter examines the load bearing characteristics of both pile types to compare the axial load versus settlement behavior of a sheet pile section typically used as a facing element and an H-pile section typically used as an axial load bearing element in short span bridge construction in North Carolina.

4.2 Project Details

4.2.1 Test Site

4.2.1.1 Geologic History of the Piedmont and Typical Soils

The test site was located in Matthews, North Carolina within the equipment yard of International Construction Equipment (ICE). Figure 4-1 presents the general location of this test site.

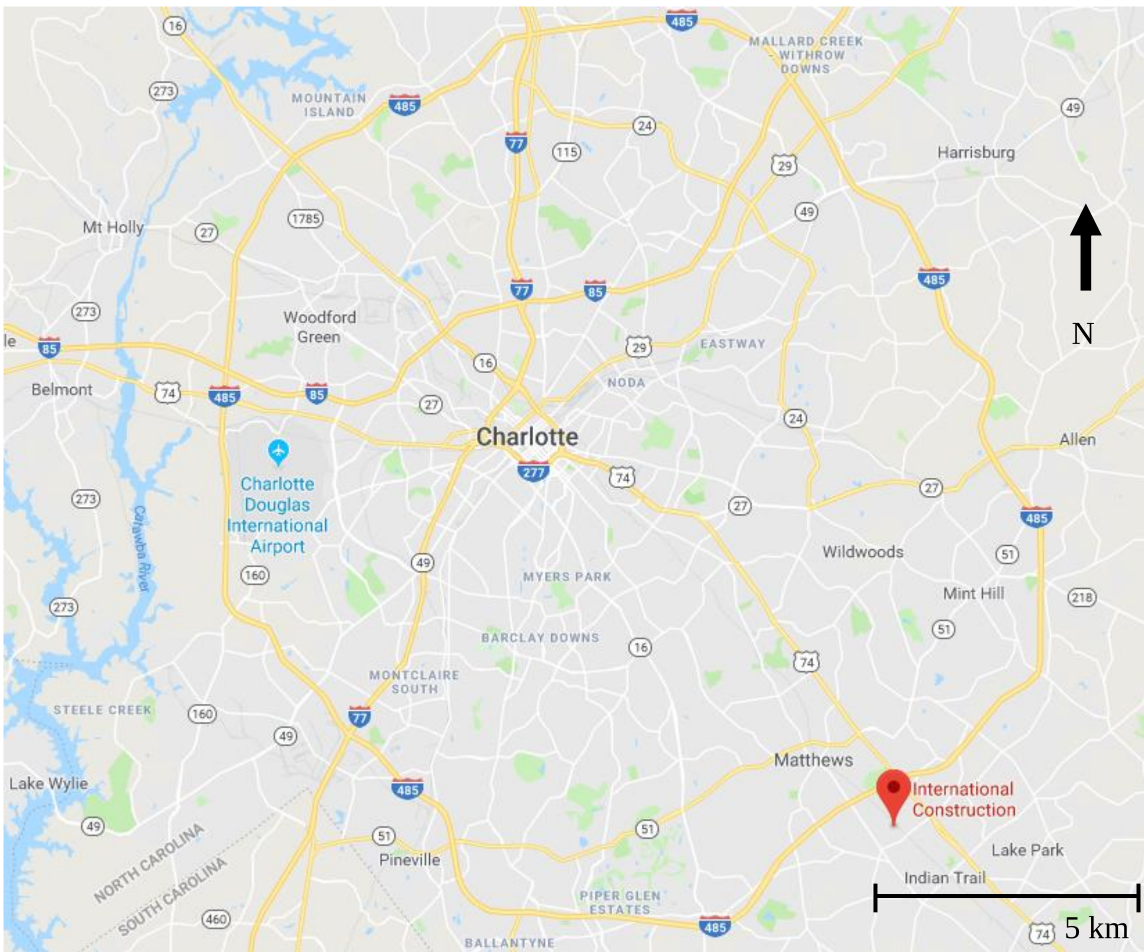


Figure 4-1. General location of field test site

The site is located within the Piedmont geology, which covers a region of the eastern United States extending from Alabama to Pennsylvania covering an area of approximately 1200 km long and 200 km wide. This geologic region is composed of rolling terrain and foot hills that formed as a result of the weathering of mountains. The parent rock is formed from metamorphic (gneiss and schist) and igneous (granite and gabbro) rock types, with occasional occurrences of phyllite, slate, greenstone, diabase, quartzite, and soapstone (Chew 1993).

Within the Piedmont geology, the test site is located more specifically within the Charlotte Belt of the Piedmont Physiographic Province of North Carolina. The Charlotte Belt and Piedmont Province generally consist of well-rounded hills and ridges, which are dissected by a well-developed system of draws and streams. The topography and relief of the Piedmont Province have developed from differential weathering of the underlying igneous and metamorphic rock. Because of the continued chemical and physical weathering, the rocks in the Piedmont Province are now generally covered with a mantle of soil that has weathered in place from the parent bedrock. These soils have variable thicknesses and are referred to as residuum. The residuum is typically finer grained and has higher clay content near the surface because of the advanced weathering. Similarly, the soils typically become coarser grained with increasing depth because of decreased weathering. As the degree of weathering decreases, the residual soils generally retain the overall appearance, texture, gradation, and foliations of the parent rock. Examples of possible foliation of different types of parent bedrock are presented in Figure 4-2. The boundary between soil and rock in the Piedmont is not sharply defined. A transitional zone termed “Partially Weathered Rock” is normally found overlying the parent bedrock.

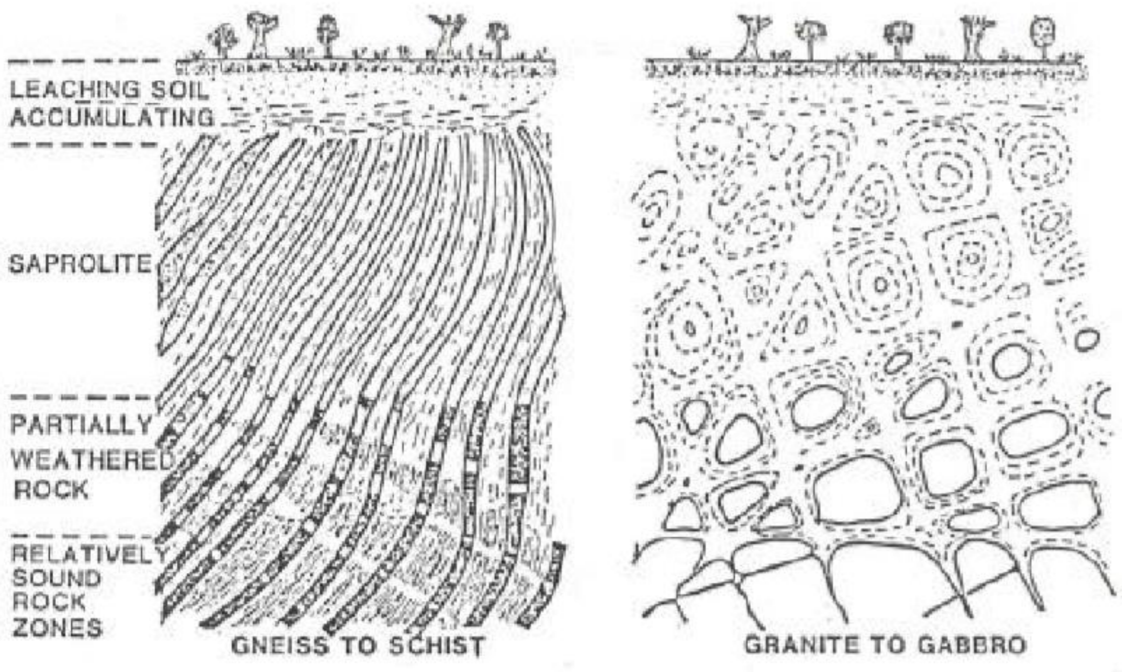


Figure 4-2. Parent bedrock foliation and weathering pattern from Piedmont metamorphic and igneous rock types (Sowers and Richardson 1983)

4.2.1.2 In-Situ and Laboratory Index Tests for Field Site

Site investigation included four conventional hollow stem auger borings with SPT testing and sampling (two preliminary borings were performed during field site evaluations, and two additional borings were performed after site selection), two SCPTu soundings, MASW geophysical testing, and the installation of a standpipe for monitoring groundwater elevation. The location of the field tests, as well as the location of the test piles, installed approximately 5.6 m apart, are shown in Figure 4-3. The borings were conducted using hollow stem auger flights advanced with a CME 550 drill rig. The SPT was conducted using an automatic hammer and field N-values were corrected for energy and overburden to obtain $(N_1)_{60}$ values. Test procedures were in general accordance with ASTM D1586 (ASTM 2011). CPT testing was performed using a cone manufactured by

Vertec with a cross sectional area of 10 cm$^2$ (1.55 in$^2$) and corresponding software installed on a field data acquisition unit.

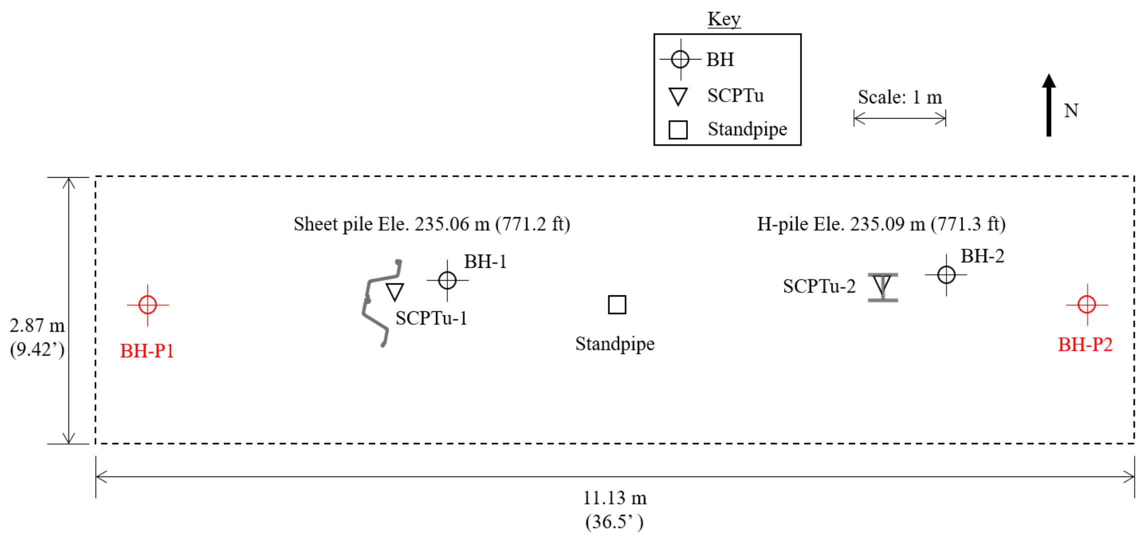


Figure 4-3. Location of test piles and in-situ tests at ICE

Various laboratory tests were conducted to characterize the engineering behavior of the soils encountered at the field site. Split spoon jar samples from SPT testing as well as a total of seven Shelby tube samples were collected from in-situ testing. Grain size distribution, Atterberg limits, and specific gravity testing were conducted to classify the soil. A summary of grain size distributions measured from samples obtained from BH-1 and BH-2 are presented in Figure 4-4. Results from Atterberg limit tests performed on samples obtained from BH-1 and BH-2 are presented in Figure 4-5. A summary of measured soil properties from index testing, as well as soil classification based on the Unified Soil Classification System (USCS), are presented in Table 4-1.

Based on the results of laboratory index testing and in-situ test results, the soil stratigraphy at the test site was established. The upper layer of the test pile site is a gravel fill with sand, approximately 0.15 m (6 inches) thick. The gravel fill is underlain by medium stiff, low plastic, sandy clay (CL) to a depth of about 1.2 m (4 ft). The sandy lean clay becomes softer with depth and also includes sandy silts. USCS classifications obtained for samples from this layer range from CL to ML. This CL/ML layer extends to a depth of 3.05 m (10 ft.) Beneath the CL/ML layer, a soft to stiff, low plastic, sandy silt (ML) extends to a depth of about 6.25 m (20.5 ft). The sandy silt layer is underlain by a medium dense to very dense silty sand (SM) layer that was encountered to the bottom of the four borings that extended to depths ranging from 9.91 m (32.5 ft) to 14.5 m (47.5 ft). The ground water level was monitored with a standpipe shown in Figure 4-3 and was found to fluctuate from 1.4 to 3.8 m (4.7 to 12.4 ft) below the ground surface. Figure 4-4 shows that the final depth of the toe for both test piles was approximately 5.2 m (17 ft). A summary of the main geotechnical test results along with a generalized soil profile based on exploratory borings and laboratory soil characterization tests is presented in Figure 4-6. In addition to SPT results, Figure 4-6 also presents toe resistance, sleeve resistance, and shear wave velocity measured from two SCPTu soundings.

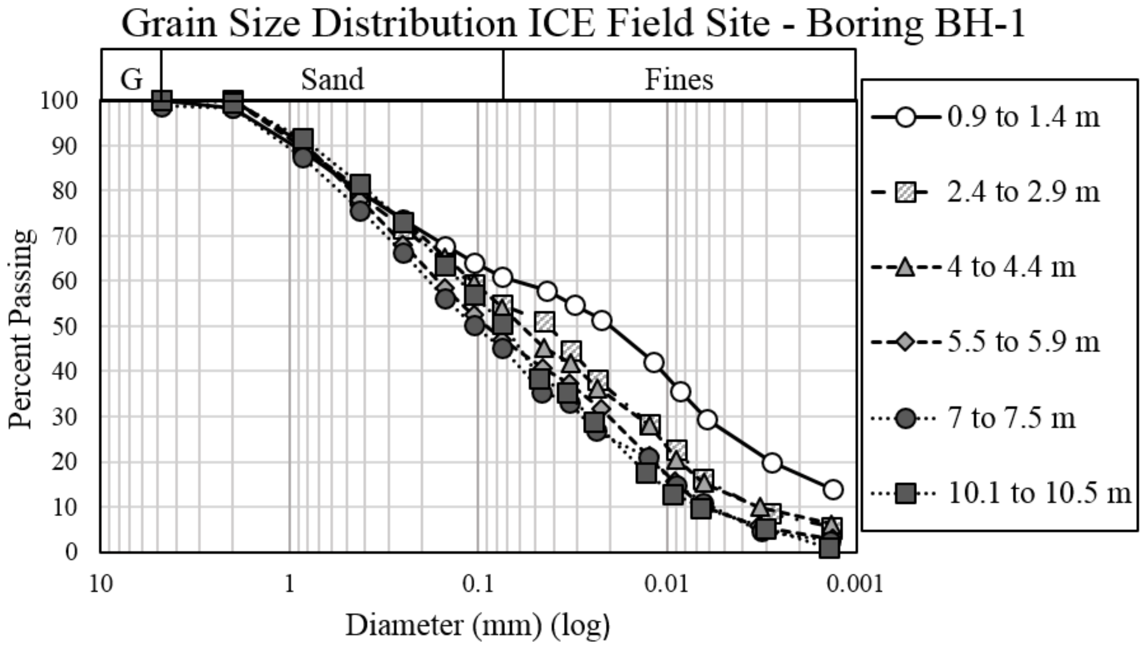


a.)

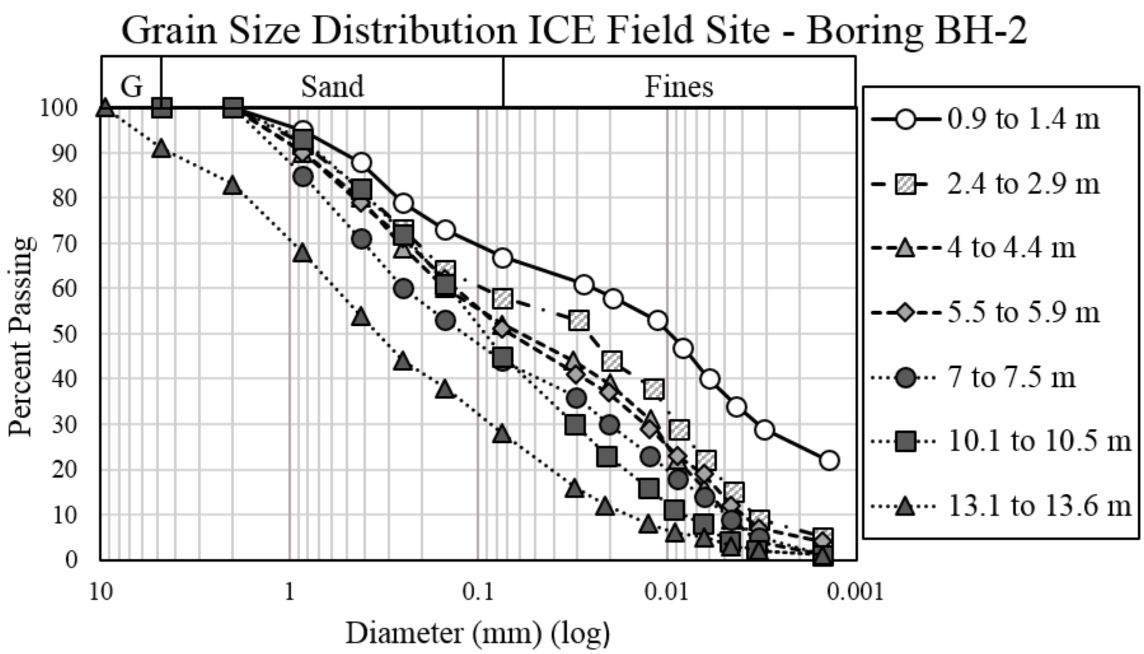


b.)

Figure 4-4. Grain size distribution for a.) soils obtained from boring BH-1, and for b.) soils obtained from BH-2

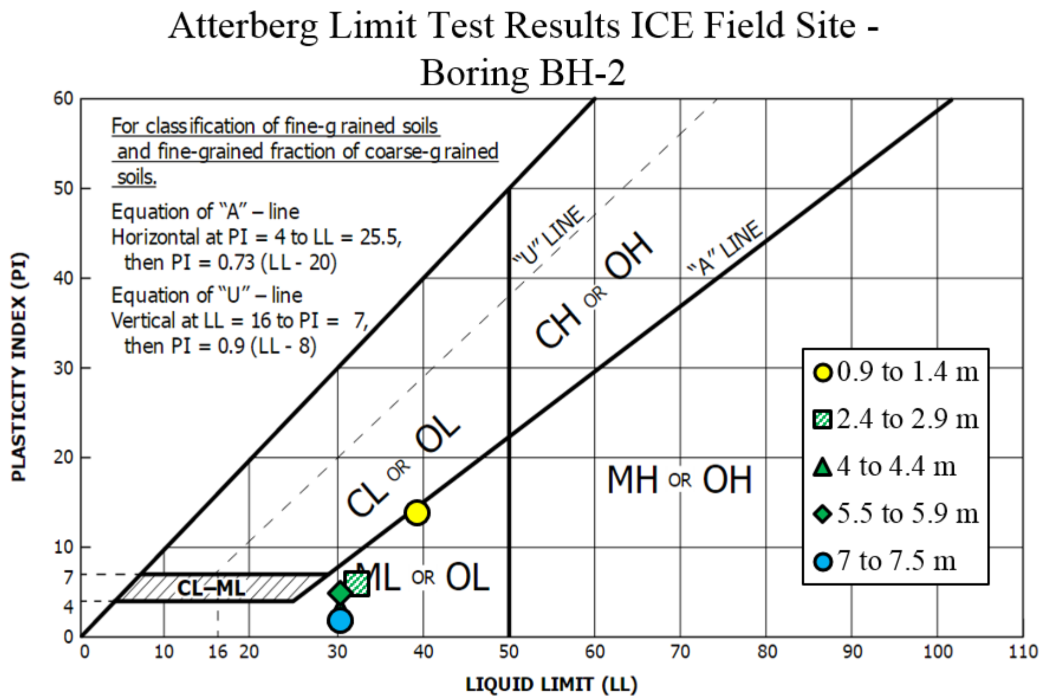


a.)

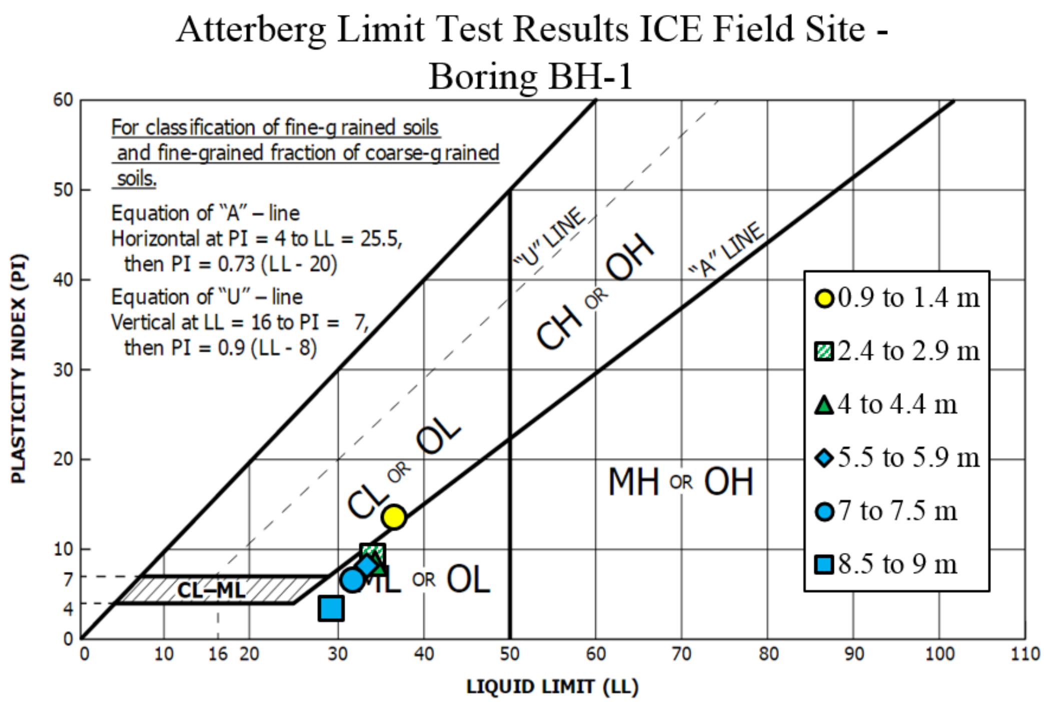


b.)

Figure 4-5. Atterberg limit test results for a.) soils obtained from boring BH-1, and for b.) soils obtained from BH-2

Table 4-1. Summary of measured soil parameters for a.) soil obtained from boring BH-1, and for b.) soils obtained from BH-2

a.)

| Summary of soil parameters ICE field site- Boring BH-1 | | | | | | | | | | | |
|---|---|---|---|---|---|---|---|---|---|---|---|
| Depth | | W.C. | LL | PL | PI | $G_s$ | Gravel (%) | Sand (%) | Fines (%) | USCS Classification | |
| From (m) | To (m) | | | | | | | | | Group Name | Group Symbol |
| 0.9 | 1.4 | 28.00 | 36 | 26 | 11 | 2.65 | 0 | 39.1 | 61.0 | Sandy Lean Clay | CL |
| 2.4 | 2.9 | 33.11 | 34 | 25 | 9 | 2.65 | 0 | 45.3 | 54.7 | Sandy Silt | ML |
| 4 | 4.4 | 32.29 | 34 | 26 | 8 | 2.65 | 0 | 46.0 | 54.0 | Sandy Silt | ML |
| 5.5 | 5.9 | 33.66 | 33 | 25 | 8 | 2.65 | 0 | 53.1 | 46.9 | Silty Sand | SM |
| 7 | 7.5 | 30.31 | 31 | 25 | 6 | 2.63 | 1.19 | 54.9 | 45.1 | Silty Sand | SM |
| 8.5 | 9 | 25.13 | 29 | 26 | 3 | 2.59 | 0 | 55.2 | 44.9 | Silty Sand | SM |

b.)

| Summary of soil parameters ICE field site- Boring BH-2 | | | | | | | | | | | |
|---|---|---|---|---|---|---|---|---|---|---|---|
| Depth | | W.C. | LL | PL | PI | Gs | Gravel (%) | Sand (%) | Fines (%) | USCS Classification | |
| From (m) | To (m) | | | | | | | | | Group Name | Group Symbol |
| 0.9 | 1.4 | 25.66 | 39 | 25 | 14 | 2.64 | 0 | 33.4 | 66.6 | Sandy Lean Clay | CL |
| 2.4 | 2.9 | 33.17 | 32 | 26 | 6 | 2.68 | 0 | 42.5 | 57.5 | Sandy Silt | ML |
| 4 | 4.4 | 32.63 | 30 | 27 | 3 | 2.67 | 0 | 47.7 | 52.3 | Sandy Silt | ML |
| 5.5 | 5.9 | 34.25 | 30 | 25 | 5 | 2.66 | 0 | 49 | 51 | Sandy Silt | ML |
| 7 | 7.5 | 30.01 | 30 | 28 | 2 | 2.66 | 0 | 55.9 | 44.1 | Silty Sand | SM |
| 10.1 | 10.5 | 24.63 | N/A | N/A | N/A | 2.65 | 0 | 54.8 | 45.2 | Silty Sand | SM |
| 13.1 | 13.6 | 13.29 | N/A | N/A | N/A | 2.73 | 9.5 | 62.3 | 28.2 | Silty Sand | SM |

Literature discussing site characterization of Piedmont soils indicates that the layering of this material does not occur in discrete strata but gradually due to the erosion process involved in its formation. The rate of erosion and nature of the layers formed depends on the nature of the parent rock from which the soils are formed (Vinson and

Brown 1997). Therefore, the defined layering chosen for this study should be considered to have gradual boundaries. It should also be noted that the Piedmont residuum is not well-characterized by the USCS based on findings in the literature (Mayne and Brown 2003). It is not uncommon to find soils within the Piedmont that narrowly classify as either coarse grained or fine grained material. These soils may behave as a dual soil type (SM-ML), demonstrating characteristics that are associated with undrained and drained soil behavior when loaded (Mayne and Brown 2003).

Many of the samples collected from the field site for this study were found to have mean grain sizes ($D_{50}$) close to 0.075 mm, which serves as a boundary between classifying a soil as coarse or fine grained. Figure 4-7 presents the mean grain diameter versus depth for samples collected from the ICE field site. As can be seen, a significant fraction of the samples tested have $D_{50}$ values that fall close to this boundary. The soils close to the ground surface had the largest percent of fines, while soils toward the bottom of the profile contained the highest percent of sand and decreasing plasticity. Soils between these two zones are narrowly defined as sandy silt or silty sand.

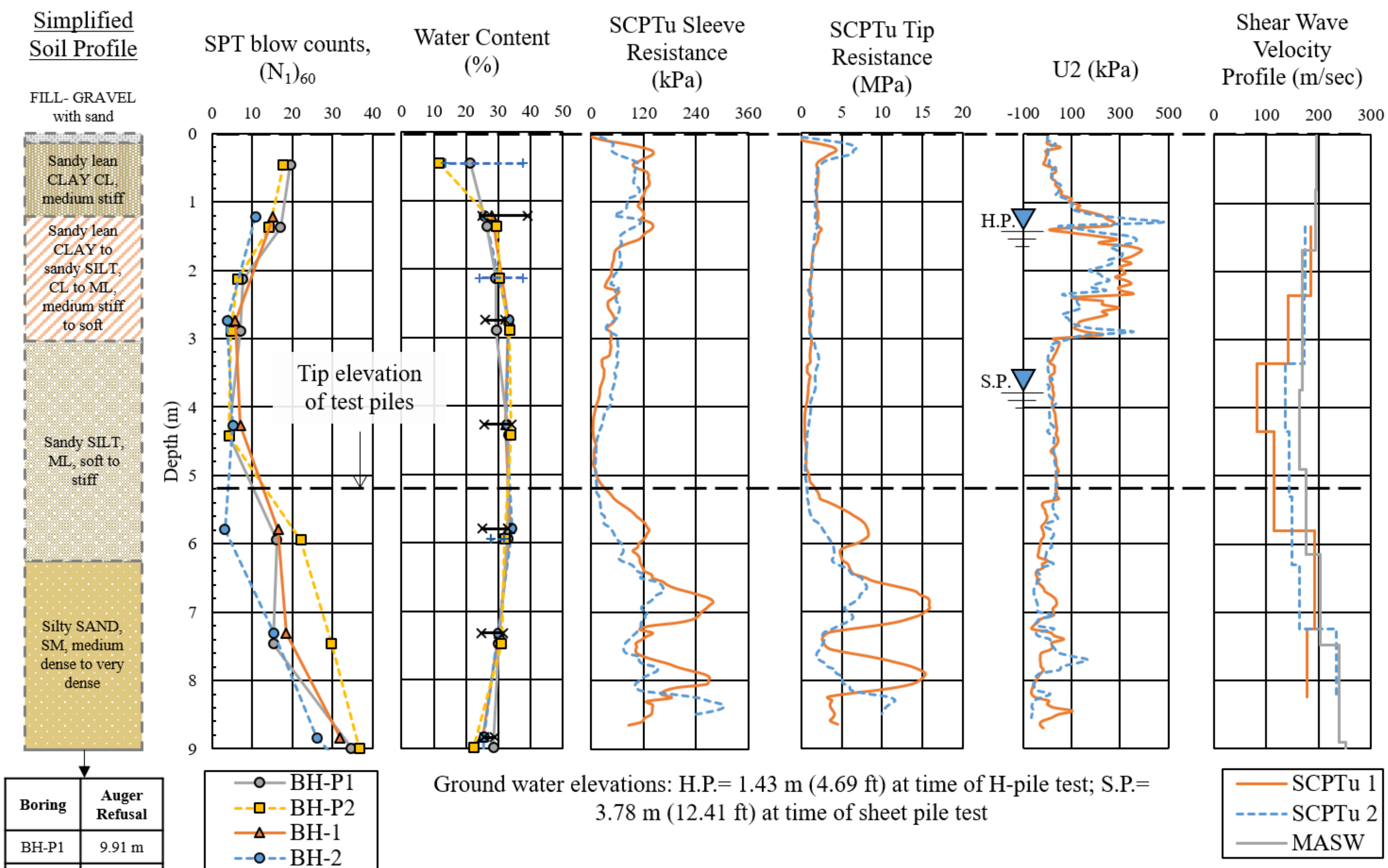


| Boring | Auger Refusal |
|---|---|
| BH-P1 | 9.91 m |
| BH-P2 | 10.52 m |
| BH-1 | 10.15 m |
| BH-2 | 14.48 m |

Figure 4-6. Soil stratigraphy at ICE site

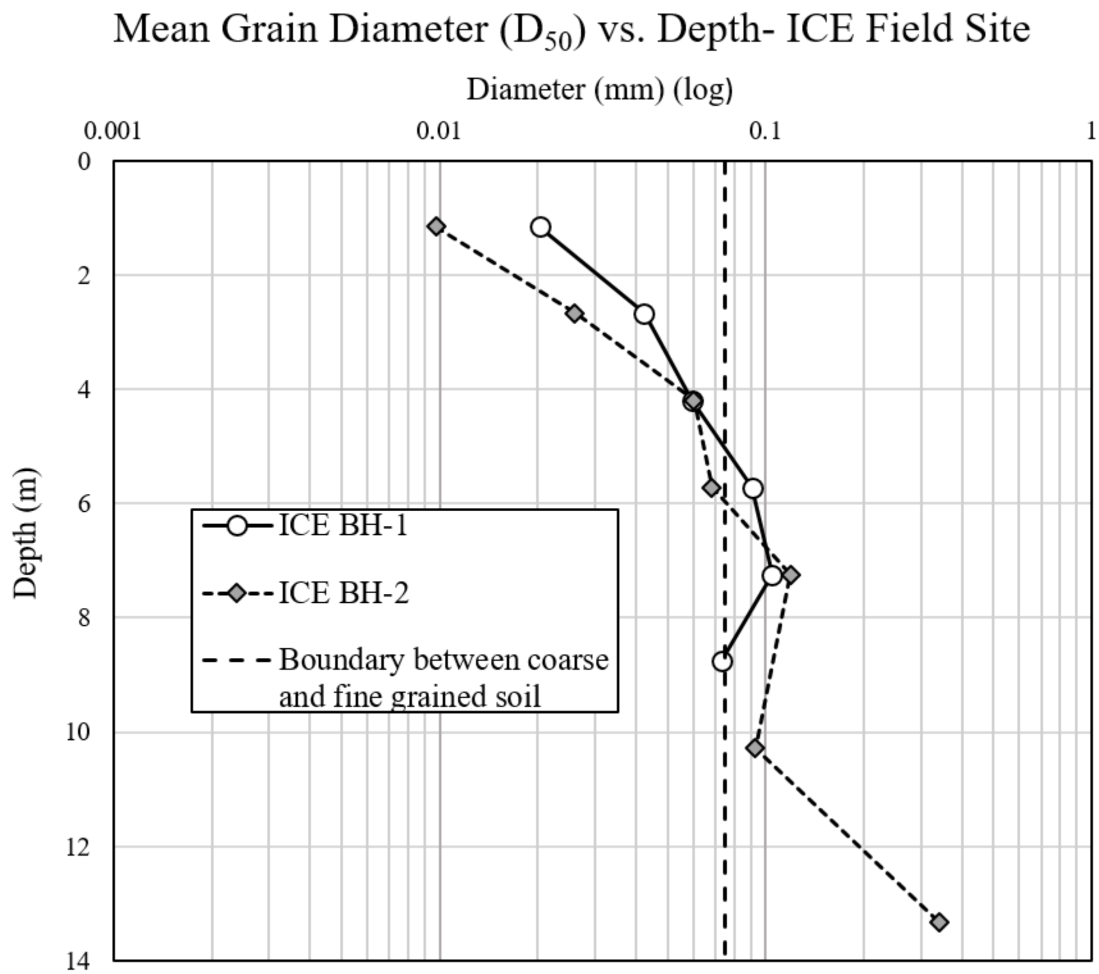


Figure 4-7. Mean grain diameter versus depth for samples collected from ICE field site

4.2.1.3 Pore Water Pressure Measurement and Monitoring

Several aspects were included in the field test program to evaluate the ground water level and behavior of pore water pressure within the soils at the test site. Dissipation tests were conducted during the SCPTu soundings to evaluate the ability of the soil to dissipate excess pore pressures developed from advancing the SCPTu probe. These tests were conducted at depths of 1.35, 3.35, 6.3, and 8.25 m for SCPTu-1, and at depths of 5.3, and 8.6 m for SCPTu-2. These results are presented in Figure 4-8. In general, results indicated excess pore pressures developed from advancing the probe dissipated rapidly within a period of no longer than several minutes. This suggests the soils encountered were relatively free draining at the locations where dissipation tests were conducted.

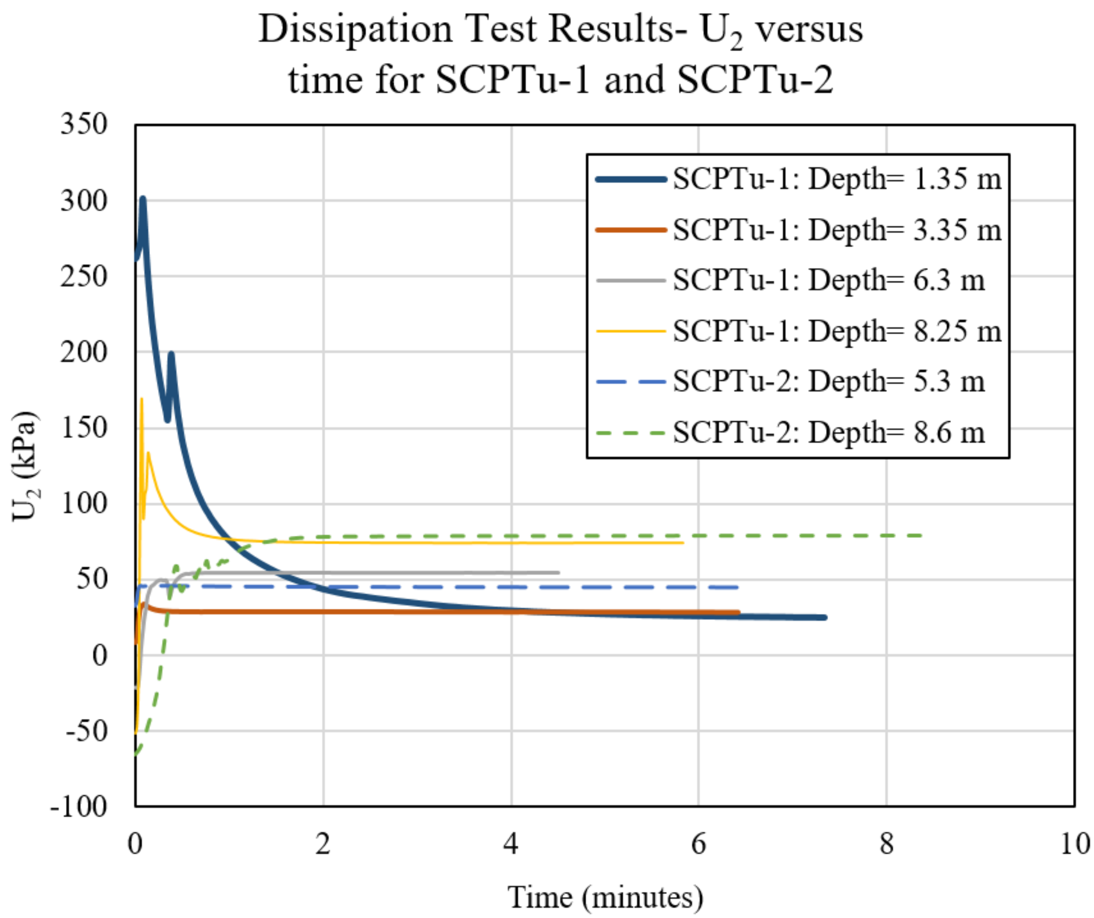


Figure 4-8. Results of dissipation testing at field site

A standpipe as well as piezometers were installed at the site to monitor fluctuations in groundwater around the time of testing as well as seasonal variations. The standpipe consists of a 5.72 cm diameter PVC pipe and was installed to a depth of approximately 5.78 m. The standpipe had slotted perforations along the bottom 3.05 m of its length, an image of the standpipe installation is presented in Figure 4-9.

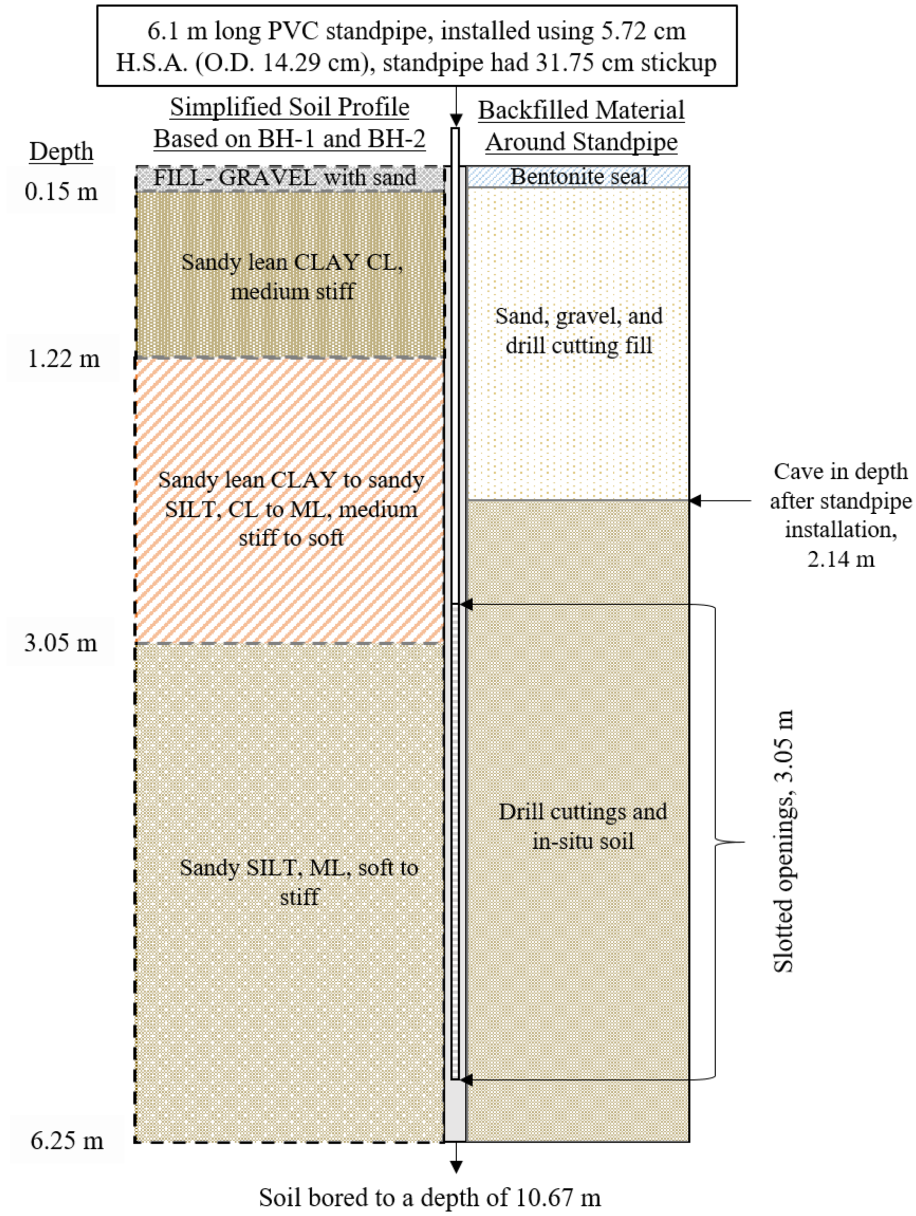


Figure 4-9. Image of standpipe installation at ICE field test site

Piezometers were also installed at the locations of BH-1 and BH-2. The sensors used were vibrating wire pressure transducers obtained from Geokon, model number 4500ALV-70 kPa. Piezometers were installed to a depth of approximately 4.42 m, clean sand was used as backfill 0.15 m above and below the sensors, above this a 0.46 m thick layer of Bentonite was used followed by drill cuttings to within 0.46 m of ground level where another layer of Bentonite was used. These sensors were used to collect data over long periods of ambient conditions at the site for which a reading was taken every ten minutes. Data was also collected for significant events in the project, such as pile load testing. During these significant events, a faster sampling rate was used where a reading was taken every minute. An image of pore water pressure variation measured at the site during the project is presented in Figure 4-10. Measured data indicated that pore water pressure varied by approximately 20 kPa at the field site with values decreasing since the beginning of activity in the field.

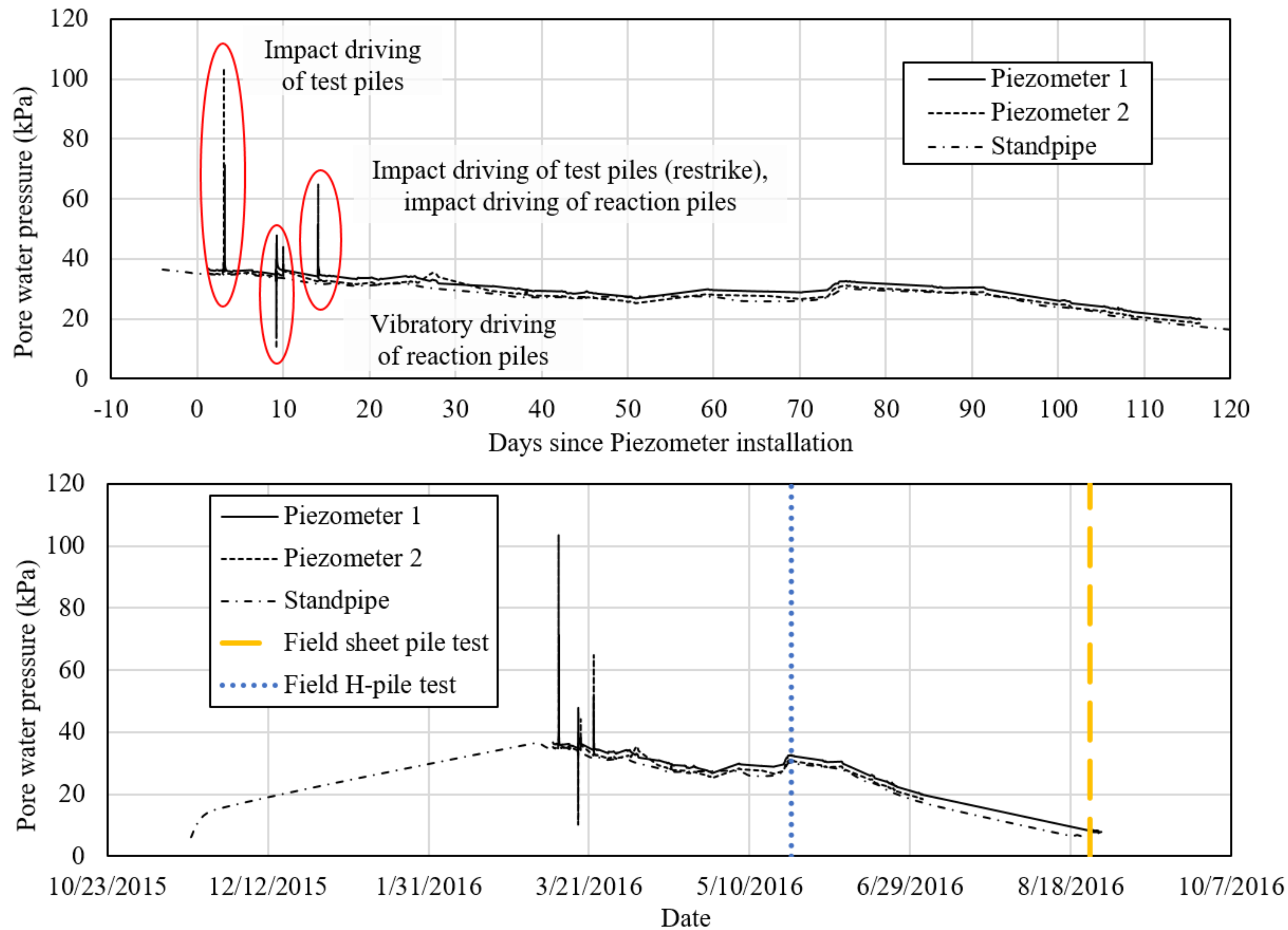


Figure 4-10. Pore water pressure measurement at ICE field site

4.2.2 Test Piles

The test piles include a pair of PZ 27 sheet piles as well as a single HP 12x53 H-pile. Axial load tests were performed on both pile types to facilitate comparison of results. The cross sectional details for these piles are shown in Figure 4-11 and summarized in Table 4-2. Both test piles had total lengths of 6.1 m. Test piles were instrumented along their length with strain gauges installed at eight different levels on the H-pile and sheet piles as indicated in Figure 4-12 a.) and b.) respectively. Instrumentation was protected using a steel angle welded to the test piles. An image of the piles before driving is presented in Figure 4-13. Additional images and details regarding instrumentation are provided in Appendix C.

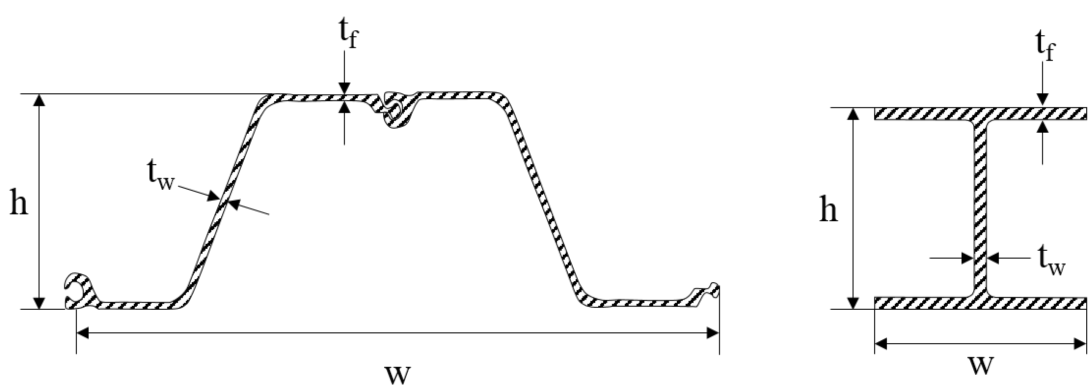


Figure 4-11. Cross section of test piles

Table 4-2. Section dimensions for PZ 27 and HP 12x53 pile sections.

| Test Pile Type | Pile Designation | Width, w (mm) | Depth, h (mm) | Thickness | | Cross Sectional Area ($cm^2$) | Perimeter Surface Area ($m^2/m$) |
|---|---|---|---|---|---|---|---|
| | | | | Flange, $t_f$ (mm) | Wall, $t_w$ (mm) | | |
| Sheet pile | PZ 27 | 914 | 305 | 9.50 | 9.50 | 153.71[1] | 2.74 |
| H-pile | HP 12x53 | 305 | 300 | 11.0 | 11.0 | 100.00 | 1.77 |

Note: (1): Area reported corresponds to the total cross sectional area that includes the pair of PZ 27.

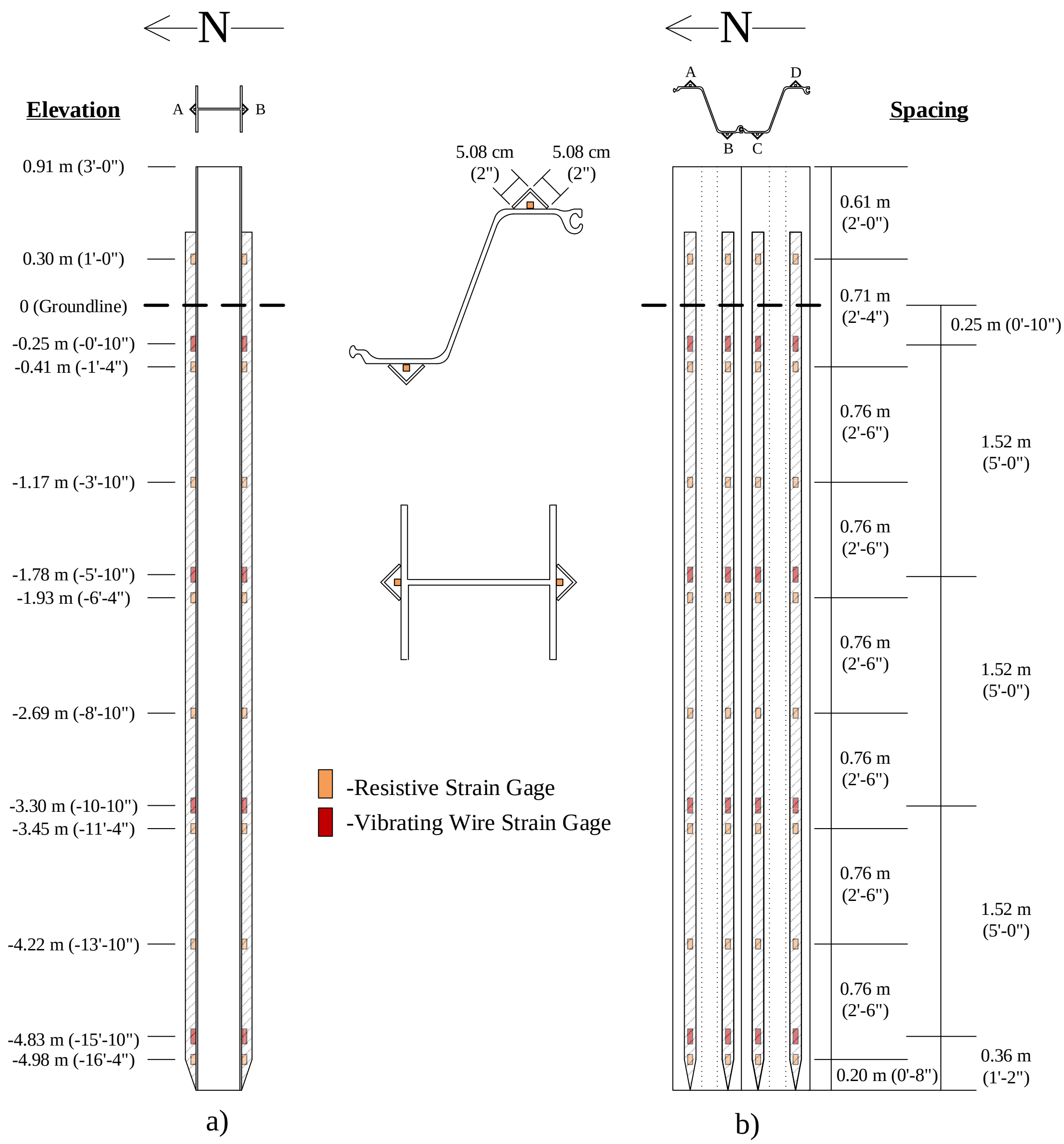


Figure 4-12. Location of instrumentation along length of test piles used for field testing

Figure 4-13. Image of test piles prior to installation

#### 4.2.2.1 Pile Installation

The test piles were installed using both a vibratory and impact hammers. Vibratory driving was performed using an ICE Model 28C hammer with a maximum driving force of up to 1050 kN and impact driving was performed using an ICE Model I-12 single-acting diesel hammer with an energy setting of 23.145 kN-m. Both hammers were used to simulate typical field installation. Figure 4-14 presents an image of both hammers used. The test piles were first installed to an initial embedment depth of 2.44 m using the vibratory hammer and then driven to the end of driving (EOD) depth of 4.88 m using the impact hammer. For the purposes of dynamic testing, a restrike was performed on the piles 11 days after driving and the piles were driven to a final depth after restrike of 5.18 m. Figure 4-15 presents the driving record from pile installation. Figure 4-16 presents an image of pile driving with the vibratory and impact hammers.

a) b)

Figure 4-14. Images of a) vibratory and b) impact hammers used at field test site, hammers provided courtesy of ICE

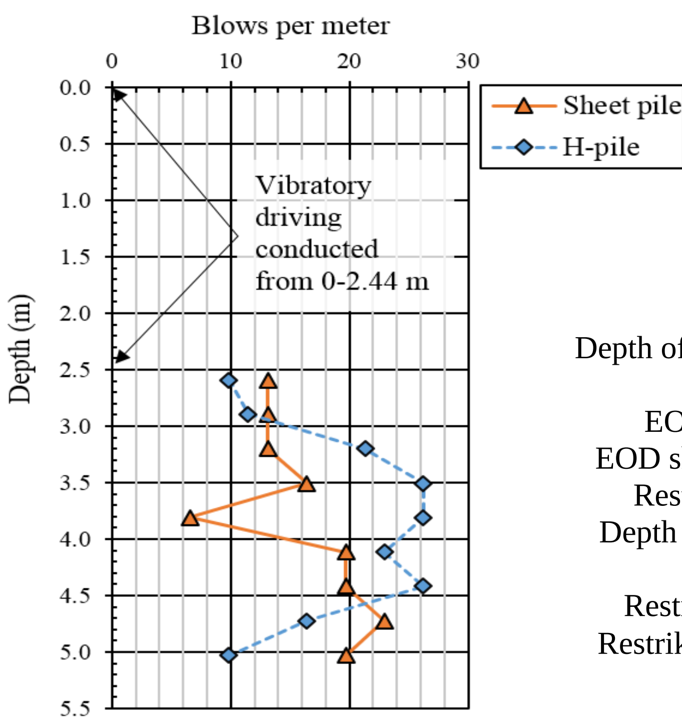


Notes:
Depth of pile tips after end of driving (EOD) = 4.88 m
EOD H-pile = 16 blows/m
EOD sheet pile pair = 23 blows/m
Restrike 11 days after EOD.
Depth of pile tips after Restrike = 5.18 m
Restrike H-pile = 10 blows/m
Restrike sheet piles = 20 blows/m

Figure 4-15. Driving record of field piles

a.) b.)

Figure 4-16. Images of pile driving with a.) vibratory and b.) impact hammers at field test site, driving operations performed courtesy of ICE

#### 4.2.2.2 Dynamic Testing

The test piles were instrumented in order to perform dynamic testing at different stages during the driving process. Accelerometers and strain gages were installed at the pile head approximately 2 effective pile diameters below the top of the piles and were spaced 180 degrees apart. Pile driving analysis (PDA) measurements were obtained during initial impact driving of both piles and again during restrike performed 11 days after driving with the same hammer. The axial pile capacity estimates obtained from the PDA measurements using the Case method damping model with an RX7 damping (Goble et al. 1975) were 196 kN and 40 kN for the sheet pile and H-pile, respectively. PDA records are presented in Figure 4-17 below.

The PDA results present measurements from both the accelerometers and strain gauges versus time in units of L/c where L is the length of the pile and c is wave speed. The plots show interpretation from this analysis which offer insights into the capacities of the piles and the extent to which loads are carried by either shaft or toe bearing. Two vertical black lines, separated by a time of 2L/c indicate the time during the installation process when peak force was measured in the pile to the time when peak velocity was measured. This segment of time represents energy from a hammer blow traveling from the pile head (indicated by a peak in force measurements) to the pile toe and back again (indicated by a peak in velocity measurements). The response is fairly similar for each pile. During this time segment force measurements drop while velocity increases. The separation of force and velocity measurements during this segment is indicated with grey shading. The small area of shading indicates low shaft bearing resistance for both piles.

Accelerometer and strain gauge data from dynamic testing were used to obtain static axial load capacity estimates using the Case method, and information collected during restrike was used to perform CAPWAP analyses. According to CAPWAP, the sheet piles and H-pile have static axial load capacities of 174.4 and 79.2 kN, respectively. The results of CAPWAP also indicate the shaft capacities, as percentages of the total capacities, to be 43.6 percent and 69 percent for the sheet piles and H-pile, respectively. Table 4-3 summarizes these results below.

Table 4-3. Summary of capacity estimates based on PDA

| Method | Capacity Provided | Sheet pile (two PZ-27 sections) | H-pile (one HP 12x53 section) |
|---|---|---|---|
| Case EOD(1) | Total | Not available | Not available |
| Case Restrike(2) | Total | 195.7 kN | 40 kN |
| CAPWAP Restrike(3) | Shaft | 76.1 kN | 54.7 kN |
| | Toe | 98.3 kN | 24.5 kN |
| | Total | 174.4 kN | 79.2 kN |

4.2.2.3 Static Load Test Setup

After test pile installation, preparations were made to perform the static axial load tests. These tests were performed in general accordance with the 'Constant Rate of Penetration Test' procedures presented in ASTM D1143/D1143M, which require that a constant value of pile displacement per unit time be maintained for the duration of the test (ASTM 2013). A reaction frame was constructed around the test piles using driven HP 14x73 for reaction piles. A drawing of the frame is shown in Figure 4-18 and a picture of the reaction frame is presented in Figure 4-19. The reaction frame was designed for a maximum load capacity of 712 kN.

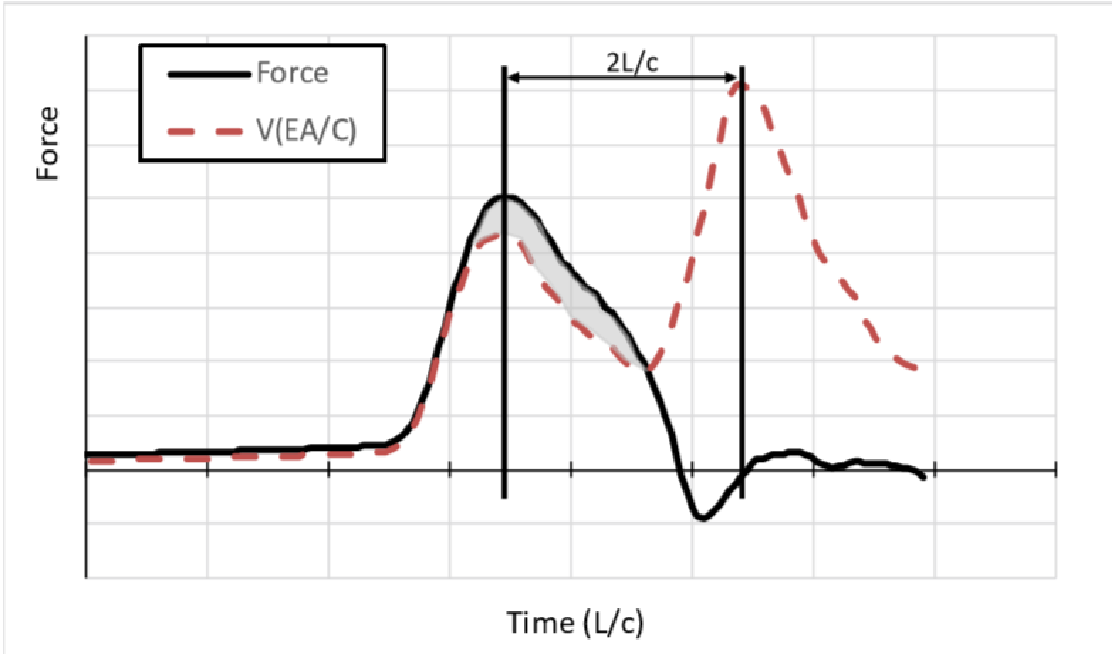


a)

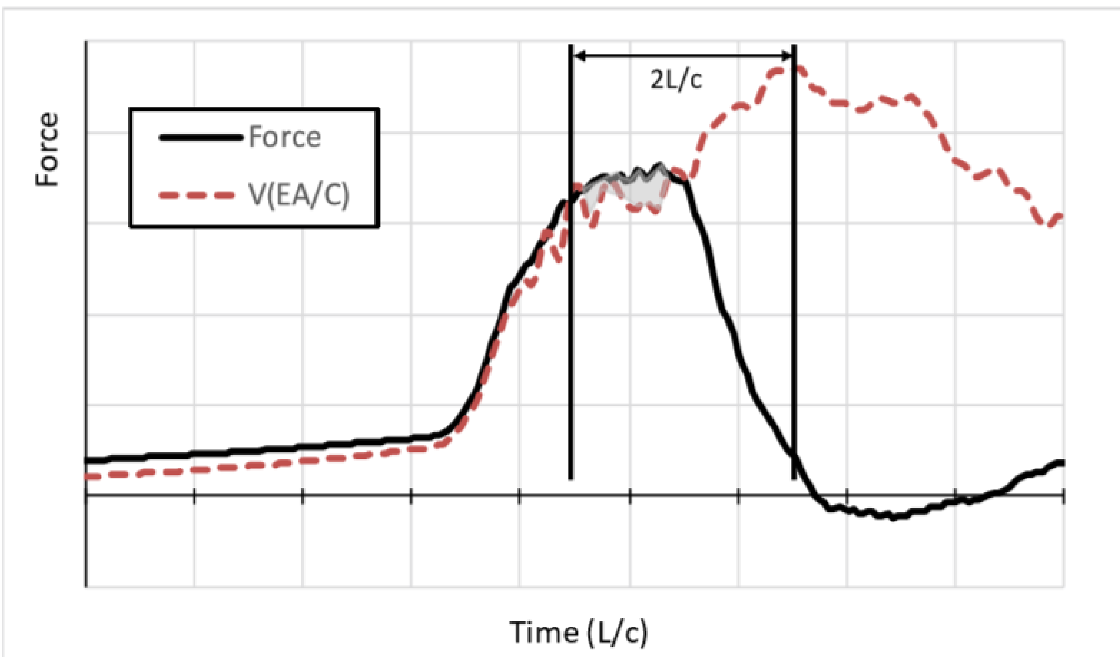


b)

Figure 4-17. Plots of PDA records during restrike for the a) sheet piles and b) H-pile

Loads were applied to the test piles using a hollow plunger type hydraulic jack manufactured by Enerpac, model RCH-603, with 533.8 kN capacity and 7.62 cm stroke. The jack used to advance the piston was an Enerpac hand pump, model number P-80. Vertical displacement of the pile was measured using four digital dial gauges with measurement resolution of 0.002 mm. A model TD175 Industrial Commercial Scales canister load cell with 444.8 kN full-scale range was used to measure the applied axial load at the pile head and was signal conditioned with a 24-bit PXI-4330 bridge input module. The displacement and load measurements were obtained concurrently by a digital data acquisition system. Figure 4-20 presents an image taken during the pile load testing of the H-pile. Appendix C presents additional details and photos pertaining to the field load tests.

## 4.3 Static Axial Load Test Results

Static axial pile load tests were carried out at a constant rate of penetration of 0.13 mm/minute. Figure 4-21 presents the results of head load versus displacement. Results indicate the sheet pile and H-pile to have axial load capacities based on the Davisson’s criteria of 152.5 kN and 100.1 kN, respectively. The corresponding deflection values at the head of the pile for these values are 6.9 and 6.6 mm for the sheet pile and H-pile, respectively. The stiffness in pile axial load response, represented by the slope of the curve of applied load versus displacement at the pile head, indicate comparable values for both test piles, but greater stiffness for the sheet pile pair. For a given displacement of 0.5 mm, the stiffness value for each pile equals 128.9 kN/mm and 116.27 kN/mm for the sheet pile and H-pile, respectively. This would agree with expected behavior given the larger shaft area of the sheet piles as compared to the H-pile

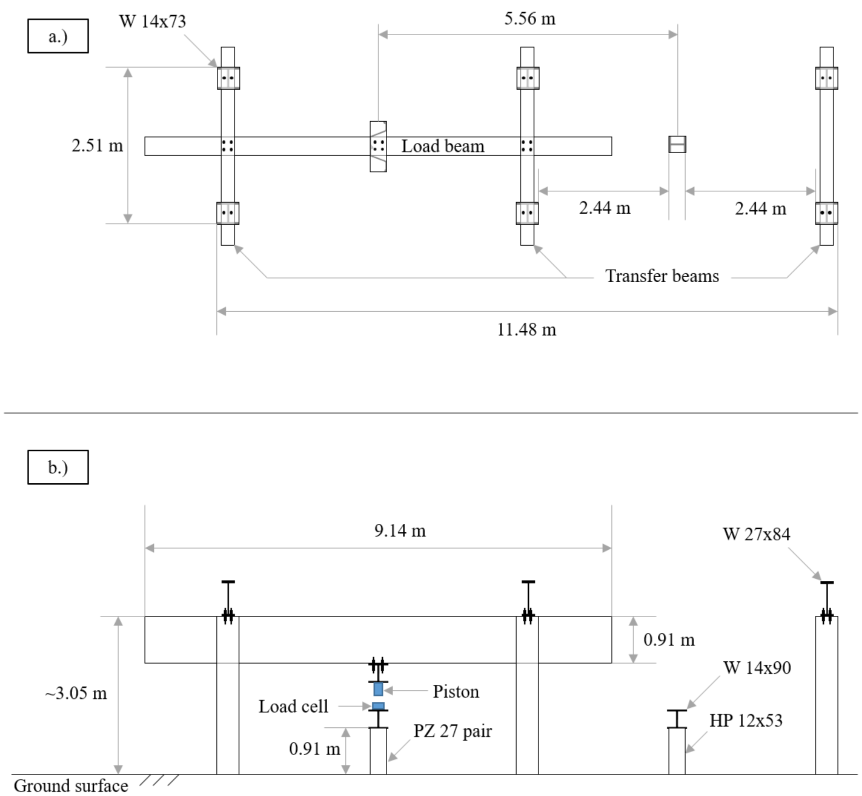


Figure 4-18. Images of a) plan view and b) elevation view of the reaction frame used for static axial load tests at field site


Figure 4-19. Image of reaction frame used for static axial load tests

Figure 4-20. Image of H-pile field load test

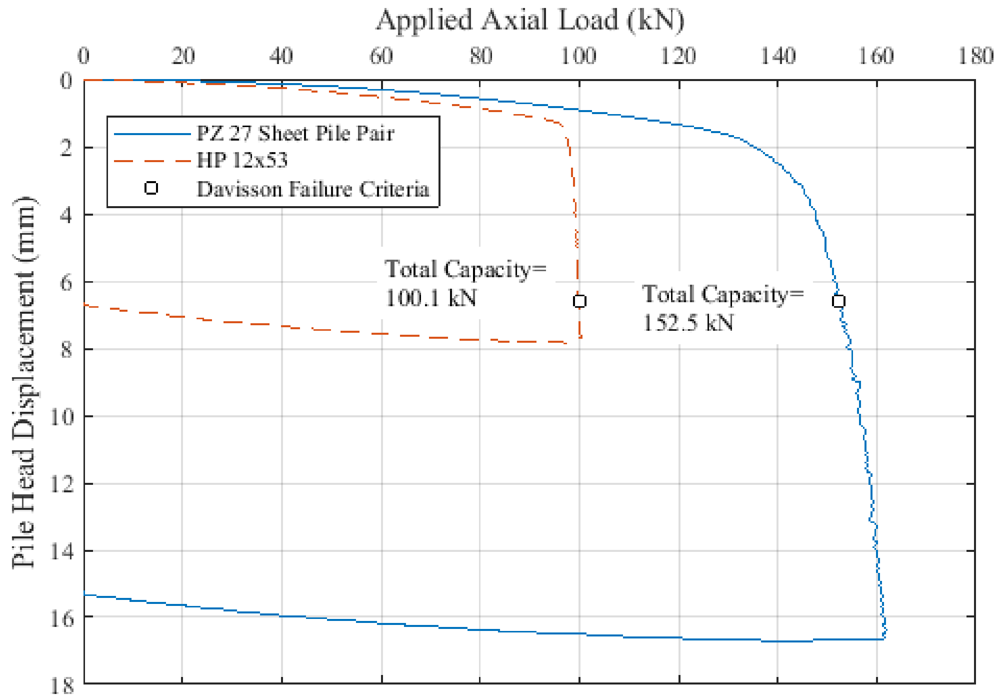


Figure 4-21. Applied axial load versus displacement at the pile head

Figure 4-22 presents measurement of load versus depth for the sheet pile. As shown in the figure, the sheet pile pair carries applied load primarily through shaft resistance, with the majority of the shaft resistance provided within the upper third of the pile length. This response agrees with the in-situ site characterization tests that indicated that the upper 2 m of soil has a higher stiffness compared to the soil along the rest of the pile shaft from 2 to 5.18 m. Based on the failure load of 152.6 kN using Davisson's criteria, the contribution from shaft and toe resistances equal 136.6 (89.5%) and 16 kN (10.5%), respectively.

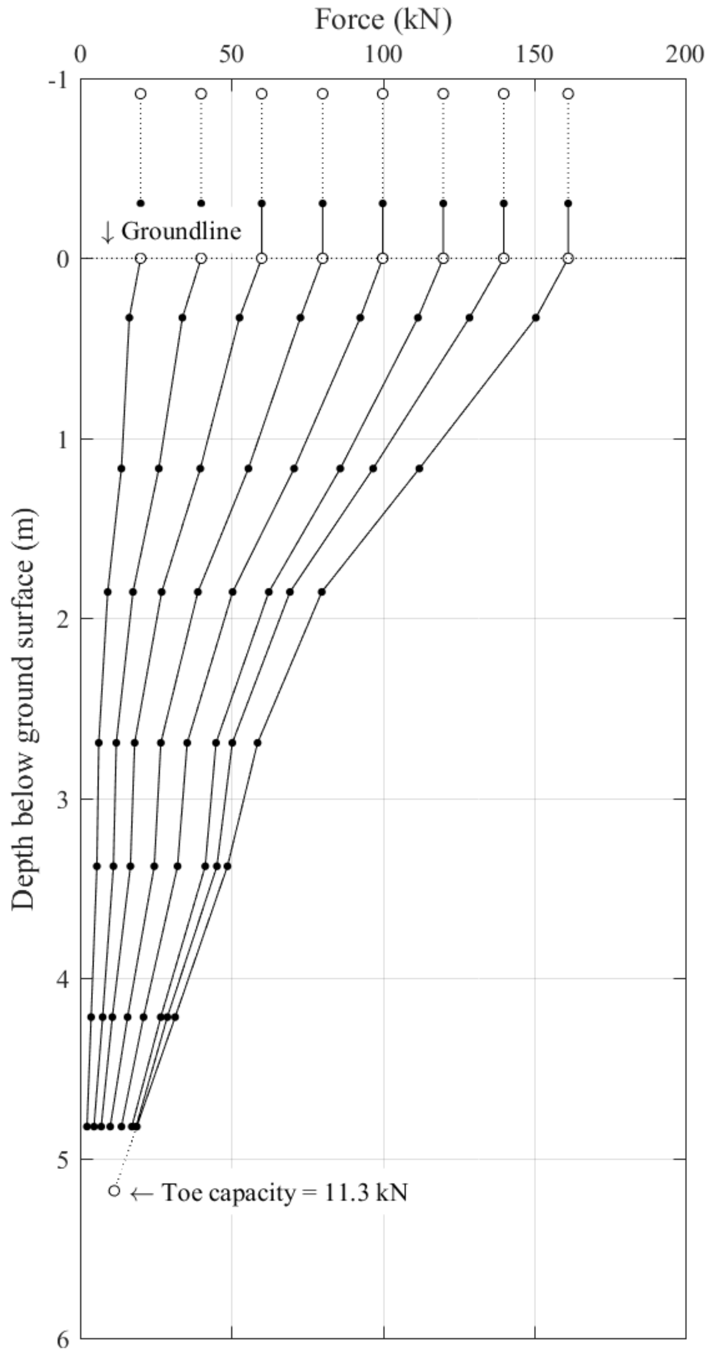


Figure 4-22. Load versus depth measured for sheet pile pair at field test site

In addition to plots of displacement and depth versus load, experimental *T-Z* and *Q-Z* curves can be developed. These plots help demonstrate where the pile obtained capacity in the soil and how load transfer was achieved. *T-Z* curves were generated based on two different layering scenarios. The first layering scenario considers high discretization of layers and provides a separate curve for each region along the pile bound by strain gauges. These curves are presented in Figure 4-23. The figure shows that skin friction generally decreases with depth as expected given the decreasing slope of the force versus depth curves with increasing depth shown in Figure 4-22.

A possibly more useful interpretation involves layering the regions based on the soil profile defined in Figure 4-6. Figure 4-24 presents curves representing this layering scenario. This figure further shows the extent to which shaft loads are carried at shallow depths. The shaft bearing resistance offered by the soil within the upper 1.2 m of soil is nearly 2.5 times greater than the resistance offered in the bottom 3 to 5.18 m layering of soil. This agrees with the expected nature of the encountered soils consisting of low plastic fine grained material with soft to medium stiff consistency. Additionally, peak shaft resistance is reached along the length of the pile at displacements of approximately 3.8 to 12 mm. These values are in good agreement with typical conventional values of relative displacements of 5 to 10 mm required for peak shaft resistance mobilization for piles of any given size or length (Das 2016).

Lastly, developed *Q-Z* curves demonstrate the load bearing behavior at the pile toe. Figure 4-25 presents toe resistance versus displacement for the sheet pile pair. As can be seen, a peak toe resistance value of 16 kN is reached at a displacement of about 2.5 mm. Typical peak end-bearing resistance requires movement at the toe equal to 10 to 25% of the diameter or width of the pile (Das 2016). The observed peak toe resistance of the field sheet pile at a displacement of 2.5 mm suggests that minimal plugging may be occurring. With a fully plugged sheet pile, the effective diameter at the toe of the pile would equal

305 mm (sheet pile depth) and therefore require a toe displacement of 30.5 to 76.25 mm to fully mobilize the toe resistance. For conditions where no plug forms at all, the width of the pile can be taken as the thickness of the steel (9.5 mm) and we would expect toe capacity for this scenario to be fully mobilized at toe displacements of 0.95 to 2.38 mm. As can be seen, the observed values of toe displacement required for development of full toe resistance fall closer to expected displacement values for the scenario where minimal plugging is occurring. This behavior also agrees with measured soil conditions near the pile toe, which indicate soft, saturated, low plasticity and cohesionless soils that would not likely be prone to plugging. It is unexpected to find the required displacement for full toe resistance to be smaller than the displacement required for full shaft resistance. This may be due to the nature of the soil profile and the piles used for testing.

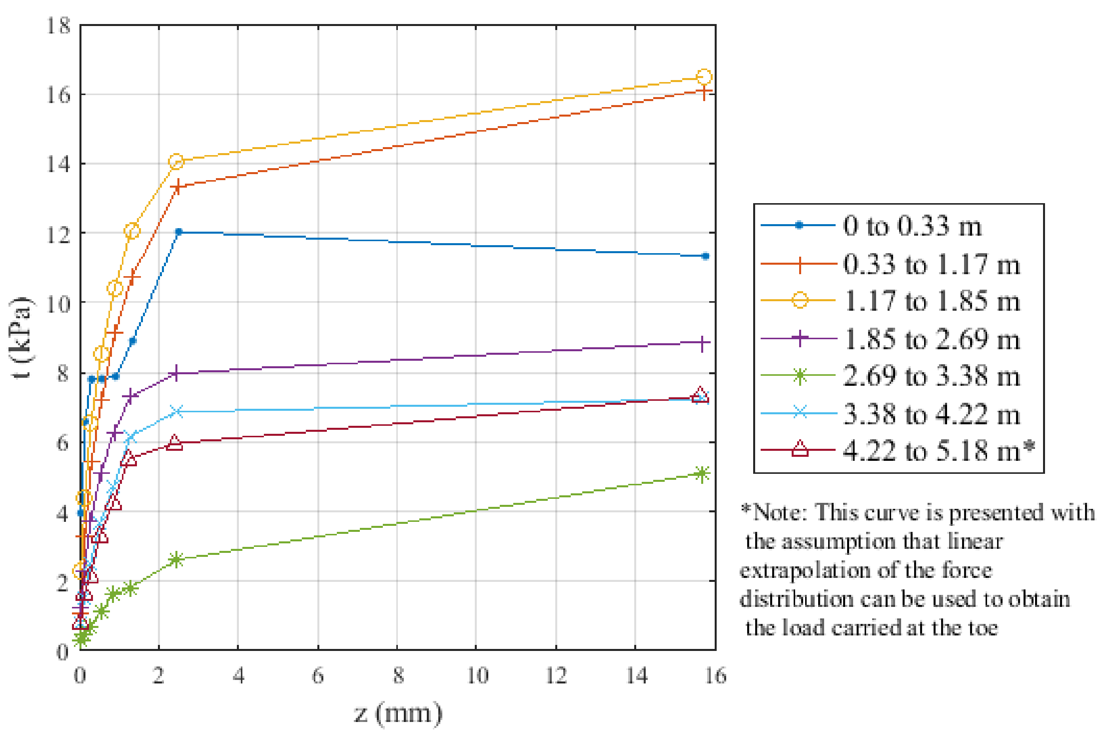


Figure 4-23. Experimental *T-Z* curves for field test on sheet piles using highly discretized layering

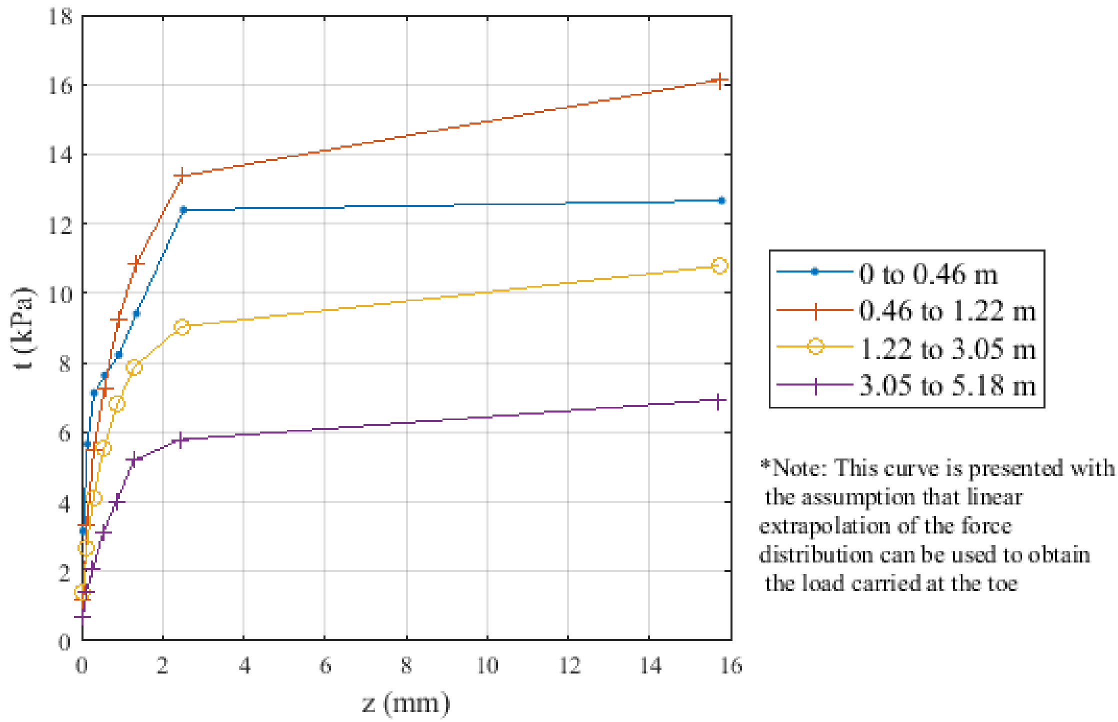


Figure 4-24. Experimental *T-Z* curves for field test on sheet piles using layering based on soil profile

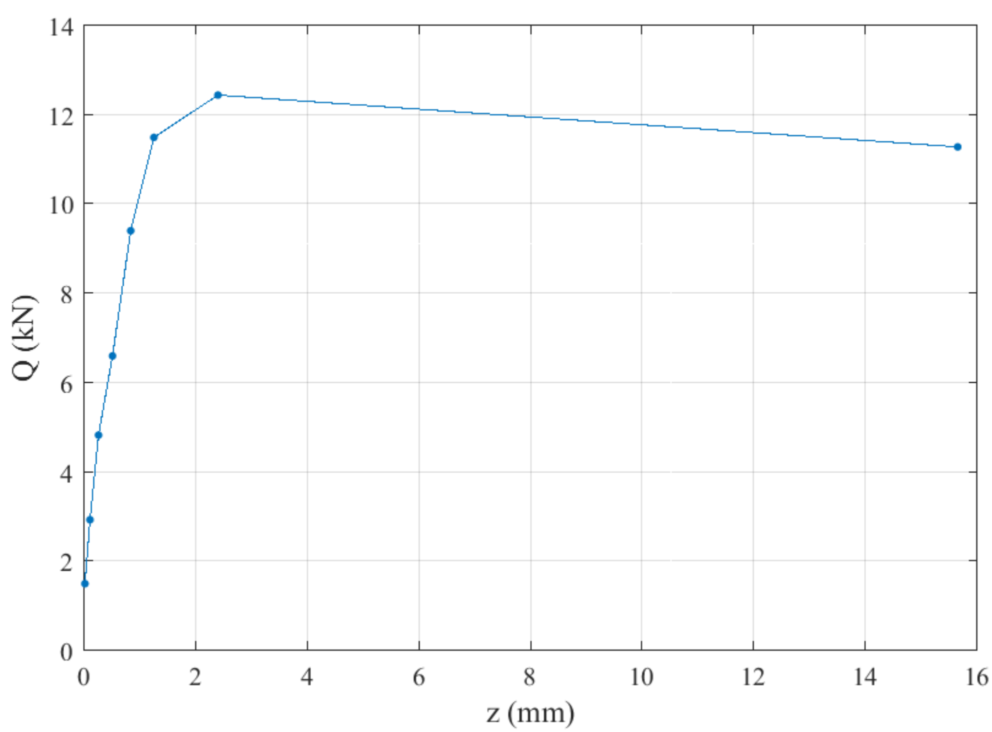


Figure 4-25. Experimental *Q-Z* curves for field test on sheet piles

## 4.4 Summary and Conclusions

In conclusion, field testing of both a sheet pile pair and H-pile section typically used for bridge abutment design in the state of North Carolina was successfully completed at a site located within the Piedmont physiographic province of North Carolina. The test site was relatively flat and the test piles were located approximately 5.5 m apart. The test piles were installed using similar procedures to a final embedment depth of 5.18 m. The geotechnical conditions at the site were characterized through the use of drilling, SPT, SCPTu soundings, and MASW geophysical tests. The soil at the site generally consisted of fine grained residual soils described as low plastic, medium stiff, sandy clays and silts (CL to ML) that extended to a depth of about 6.1 m. Below 6.1 m depth, or below the depth of the toe of the test piles, the residual soils become coarser grained and consist of medium dense to dense silty sand. The groundwater level at the site fluctuated from about 1.43 to 3.78 m depth depending on seasonal climate conditions.

Dynamic testing was performed driving as well as during restrike of the pile, allowing for PDA and CAPWAP analyses of axial capacities. Static axial pile load tests were also performed and strain gauge instrumentation along the length of the piles permitted evaluation of the mobilization of shaft and toe resistance in addition to measurement of the total static axial load capacity. Fair agreement was found between the predicted pile load capacities estimated by CAPWAP based on dynamic testing and the results obtained from static axial load testing. Moderate to poor agreement was observed between load capacities from PDA results based on dynamic testing and the static axial load testing results.

For the static axial load tests, results included pile head load versus pile head displacement as well as depth versus applied load. From these plots, the failure load using the Davisson's criteria were reported. Higher capacities were observed for the sheet pile relative to the H-pile, which suggests ample axial load bearing capacity offered by this type of pile. Depth versus applied load results for the sheet pile showed these piles carried applied load primarily in shaft resistance. The majority of this resistance was provided within the upper few meters of soil, which agrees with the results of the site exploration that indicated stiffer soils within these depths overlying softer soils. The low values observed for toe resistance, as well as the small displacement required to reach peak resistance values, suggest that minimal plugging was occurring. This agrees with expected behavior given the soil profile near the toe of the test piles.

This field test program offers valuable data regarding the axial load bearing behavior of sheet piles, which is especially relevant given the scarcity of reported axial pile load tests on full-scale, well-instrumented, sheet piles. This information helps address one of the identified knowledge gaps highlighted in chapter 2. Results from these experiments demonstrate the load transfer behavior for both a sheet pile pair as well as an H-pile conventionally used for axial load bearing in bridge abutments. The higher load capacity of the sheet piles suggests ample axial load bearing capacity exists for this pile type and strong potential for axial load bearing contribution from sheet piles in bridge abutments.

# CHAPTER 5: NUMERICAL ANALYSES OF AXIALLY LOADED SHEET PILES

## 5.1 Introduction

This chapter presents the numerical analyses performed on the experimental static axial load testing described in Chapters 3 and 4. The chapter is divided into four sections as follows:

1. Description of the methodology (Section 5.2)
2. Analysis of laboratory and field experiments (Section 5.3)
3. Summary and discussion (Section 5.4)

The analyses of the results for both the laboratory experiments (Section 5.3.1) and the field experiments at the ICE facility (Section 5.3.2) are presented in two subsections corresponding to axial capacity estimates and predictions of load-settlement curves, as follows:

- Axial load capacity estimates using static methods, and
- Axial load versus settlement predictions using axial load transfer methods.

The chapter presents the main results, however additional details concerning the different predictions are presented in Appendices D. Appendix D provides additional information associated with the static methods used for predicting static pile load capacity.

## 5.2 Methodology

Two main types of numerical analyses were performed for this research: i) prediction of axial load capacity of the deep foundations tested, and ii) prediction of load-settlement curves of these aforementioned tests. This section describes the general methodologies used for the different types of analyses and predictions.

The two main types of predictions use methodologies that are relatively well established for deep foundations, however the applicability to sheet pile foundations has not been confirmed. Therefore the results presented later in this chapter will be used to assess the suitability of these methods to sheet pile foundation. As mentioned above the description of the methods used will be done by dividing them into the following two groups:

- Static methods that are used for predictions of axial load capacity of deep foundations. This will include estimates of the two main contributing sources of axial load resistance including shaft friction and toe resistance. Where appropriate if the static methods have been updated in the literature to include predictions for sheet piles this will be reported.
- Load-settlement predictions using the load transfer method. This will include description of the methodology and also the different types of load transfer curves commonly used that include empirically- and theoretically-based curves. Later in the chapter a new set of theoretically-based load transfer curves are proposed for load-settlement predictions of sheet piles that were developed as part of this research. These new curves are one of the main contributions of this doctoral study.

These two main methodologies are described in the following sections. As mentioned before, the adequacy of these methods for use with sheet piles has not been well established as this pile type is not commonly used for axial load bearing.

### 5.2.1 Static Methods for Estimating Axial Load Capacity of Deep Foundations

A deep foundation subjected to axial loading, as shown in Figure 5-1, will resist the external applied load by shear stresses generated along the interface of the deep foundation and the surrounding soil and by normal stresses generated at the toe or bottom end of the pile. As shown in Figure 5-1, the shear stresses generated along the pile interface at failure will be a limiting or maximum unit shaft resistance ( $f_{s_{max}}$ ) that when integrated along the shaft surface of the pile ($A_s$) will result in the ultimate shaft resistance ( $R_{s_{max}}$ ) computed as:

$$R_{s_{max}} = \overline{f_{s_{max}}} \cdot A_s \tag{5.1}$$

where,

$\overline{f_{s_{max}}}$ = Average limiting or maximum unit shaft resistance (F/L$^2$), and

$A_s$ = Area of pile shaft that is in contact with soil (i.e. pile-soil interface) (L$^2$).

Similarly, the axial load capacity contribution from the normal stresses developed at the pile bottom end (toe) will be the product of the ultimate unit toe resistance (also referred to as maximum unit toe stress) ( $q_{t_{max}}$ ) times the area of the toe of the pile ($A_t$) as follows:

$$R_{t_{max}} = q_{t_{max}} \cdot A_t \tag{5.2}$$

where,

$q_{t_{max}}$ = Limiting or maximum unit shaft resistance (F/L$^2$), and

$A_t$ = Area engaged in toe bearing (L$^2$).

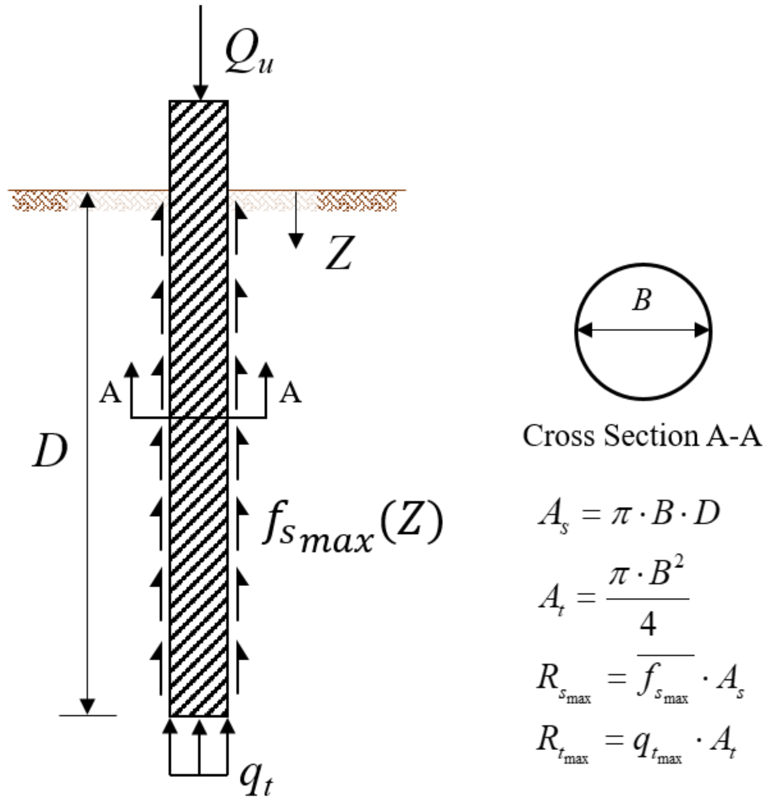


Figure 5-1. Capacity components of an axially loaded pile

Neglecting the self-weight of the pile the ultimate axial compressive load of the pile ($Q_u$) will be the sum of the two components described above, as follows:

$$Q_u = R_{s_{\max}} + R_{t_{\max}} \tag{5.3}$$

where, $Q_u$ , $R_{s_{\max}}$ and $R_{t_{\max}}$ are as defined above.

Static methods are empirical methods commonly used to estimate the ultimate capacity of a single pile or pile group. For this research, focus is given only to the prediction of the capacity of single piles under axial compression. As described above, the axial compression capacity of a single pile is equal to the summation of two main components:

$$Q_u = R_{s_{\max}} + R_{t_{\max}} = \overline{f_{s_{\max}}} A_s + q_{t_{\max}} A_t \tag{5.4}$$

where,

$Q_u$ = Ultimate axial compressive load (F),

$R_{s_{\max}}$ = Total shaft resistance (F),

$R_{t_{\max}}$ = Total toe resistance (F),

$\overline{f_{s_{\max}}}$ = Average maximum unit shaft resistance (F/L$^2$),

$A_s$ = Shaft surface area (L$^2$),

$q_{t_{\max}}$ = Maximum unit toe resistance (F/L$^2$), and

$A_t$ = Toe cross sectional area (L$^2$).

The static methods in essence consist of empirical methods that are used to estimate the values of the maximum unit shaft resistances ( $f_{s_{\max}}$ ) and the maximum unit toe resistance ( $q_{t_{\max}}$ ) based on the geotechnical conditions of the test site, the pile type, the installation procedure, and other factors. Typically static methods are based on field in-situ tests such as the SPT and CPT. The total shaft resistance and total toe resistance are calculated as previously discussed. Table 5-1 provides a summary of commonly used SPT based methods and Table 5-2 provides a summary of CPT based methods that are commonly used in geotechnical practice and used to determine pile capacity as part of this study.

In this research the static methods used to assess the shaft and toe capacity contributions for the different sheet piles tested were:

- SPT-based: Meyerhof (1959), Beta (effective stress method), Nordlund (1963), and Brown (2001)
- CPT-based: LCPC (1982), Nottingham and Schmertmann (1975), De Ruiter and Beringen (1979), and Elsami and Fellenius (1997)

The predicted capacities and levels of accuracy based on comparison with experimental measured values are presented later in this chapter (Section 5.3). Additional information on these commonly used static methods is provided Appendix D.

Table 5-1. Summary table of static methods based on SPT data

| Static methods considered for obtaining axial pile load capacity estimates based on SPT data | | | | | |
|---|---|---|---|---|---|
| Reference | Typical soil behavior used with | Information required for method | Comments on skin friction, $f_s$ | Comments on toe resistance, $q_t$ | General remarks |
| Meyerhof (1959)[1] | Cohesionless | SPT, type of pile (displacement or non-displacement) | Obtained directly from average $(N_1)_{60}$, multiplied by 1 or 2 based on type of pile | Uses $(N_1)_{60}$ of the layer into which pile toe is embedded, limiting value corrected based on silt/sand classification of soil and if weaker layer overlying bearing stratum | Empirical method simple to use and required information is commonly available due to popularity of SPT. Non reproducibility of N values reduce reliability and should limit method to preliminary estimating purposes only |
| Beta[1] (effective stress method) | Cohesionless and cohesive | Soil classification, unit weight, ϕ' | Uses Bjerrum-Burland beta coefficient applied to effective overburden pressure | Uses $N_t$ applied to effective overburden pressure at the pile toe | Semi empirical method, good for design, requires accurate estimates of ϕ' for adequate predictions |
| Nordlund (1963)[1] | Cohesionless | Design charts provided by author, ϕ | Uses design parameters based on ϕ, δ, taper of pile, and geometry and embedment of pile | Uses ϕ, geometry of pile, and effective overburden pressure at the pile toe | Semi-empirical method, popular and good method for design, requires accurate estimates of ϕ for adequate predictions |
| Brown (2001)[1] | Cohesionless | SPT, geometry of pile | Uses $N_{60}$, reduction factor for vibratory driven piles, and empirical coefficients. Recommends using box area for H-piles when calculating $Q_s$ | Directly obtained using $N_{60}$ with a reduction factor applied. Reduction factor selected based on vibratory or impact driving. Recommends using area of steel combined with some fraction of plug area for open ended piles (H and pipe piles) when calculating $Q_t$ | Empirical method, simple to use, based on results from 71 pile load tests encompassing a wide range of soil and pile types, literature recommends use for preliminary estimating purposes only |

Notes:([1]): Method performed as described in report FHWA-NHI-05-042, Design and Construction of Driven Pile Foundations – Volume 1 (2006).

Table 5-2. Summary table of static methods based on CPT data

| Static methods considered for obtaining axial pile load capacity estimates based on CPT data | | | | | |
|---|---|---|---|---|---|
| Reference | Typical soil behavior used with | Information required for method | Comments on skin friction, $f_s$ | Comments on toe resistance, $q_t$ | General remarks |
| LCPC (1982)[2] | Cohesionless and cohesive | CPT, soil classification, type and geometry of pile | Uses $q_c$ divided by $\alpha$ value based on pile and soil classification | Uses $q_{ca}$ multiplied by $k_c$ based on type of pile and soil classification, $q_{ca}$ obtained using averaging procedure applied to $q_c$ readings from area 1.5 b above and below pile toe | Method based on 197 pile load tests for wide range of foundation and soil types |
| Nottingham and Schmertmann (1975)[1] | Cohesionless and cohesive | CPT, material and geometry of pile | Uses $f_s$ for obtaining $Q_s$, uses 'box' area for H-pile when calculating $Q_s$ in cohesionless layers | Uses minimum path rule when obtaining $q_t$, looks at qc values from area 8 b above and 0.7 to 3.75 b below pile toe | Empirical procedure, used in U.S. practice |
| De Ruiter and Beringen (1979)[2] | Cohesionless and cohesive | CPT, Soil classification, unit weight, for clays: $s_u$, OCR | Uses $f_s$ or $q_c$ for sands, uses $s_u$ for clays | Minimum path rule used for 0.7 to 4 b below pile tip and design chart used to obtain limiting value for $q_t$ in sands, uses $s_u$ for clays | Observations made on pile load tests in overconsolidated soil deposits |
| Elsami and Fellenius (1997)[1] | Cohesionless and cohesive | CPTu | Uses coefficient based on soil type applied to $q_E$ (=$q_c$ after correction for pore pressure, not the same as $q_t$) | Uses toe correction coefficient applied to geometric average of $q_E$ applied to depths ranging from 4 b below and up to 8 b above pile toe | Method based on 102 pile load tests with wide ranging soil profiles and embedment depths, uses new soil profiling chart based on CPT data |

Notes:(1): Method performed as described in report FHWA-NHI-05-042, Design and Construction of Driven Pile Foundations – Volume 1 (2006).
(2): Method performed as described in Cone Penetration Testing in Geotechnical Practice by T. Lunne, P.K. Robertson and J.J.M. Powell (1997).

### 5.2.2 Axial Load-Settlement Behavior Evaluated Using Load Transfer Method

The axial load-settlement behavior of single piles depends on several factors, among the most important are soil stratigraphy and properties, pile size, pile axial stiffness, and pile-soil interaction behavior. There are several methods used to evaluate the settlement versus load response of axially loaded pile foundations that can be categorized into four different groups: elastic methods, load transfer methods, modified hyperbolic methods, and stress-strain numerical analyses. In this dissertation, the load transfer method was the approach selected based on its popularity in geotechnical practice and with North American agencies such as the FHWA and US DOT agencies.

The load transfer approach is considered an efficient, practical, analytical, and empirical tool for evaluating the load-settlement behavior of individual piles (Bohn et al. 2016). The method is particularly well suited for incorporating stratified soil conditions as well as soil nonlinearity. In addition to its other advantages, this method may provide a more accessible design approach for members of the industry. This section describes the general procedure used in this methodology. The load transfer method models a single pile as a series of individual masses connected by springs that represent the stiffness of the pile material (Coyle and Reese 1966), as shown in Figure 5-2.

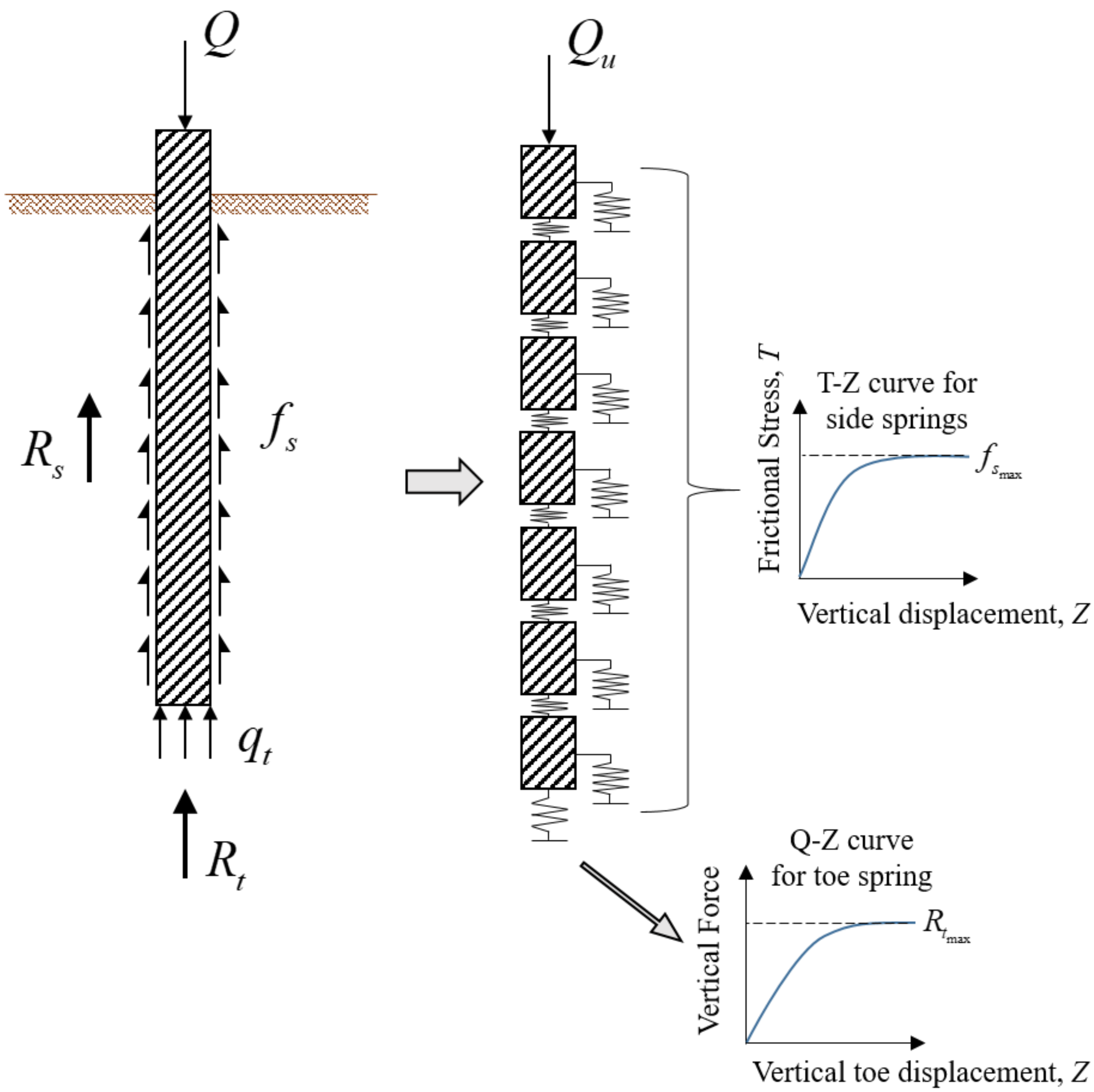


Figure 5-2. *T-Z* load transfer model (adapted from Pando et al. 2006)

As shown in Figure 5-2, the soil interaction with the pile is modeled in the form of discrete nonlinear springs along the length of the pile that act on each discretized pile mass with an additional nonlinear spring at the pile toe. These springs along the length of the pile model the shaft resistance that were discussed before and corresponds to the unit side friction developed along the soil-pile interface. The side springs cumulatively provide the shaft resistance that when it is fully mobilized along the total shaft length becomes the shaft resistance ($R_{s_{max}}$) that was discussed before. Similarly the non-linear spring located at the toe of the pile when its resistance is fully mobilized will develop the pile toe resistance ($R_{t_{max}}$). Therefore, the load transfer model shown in this figure will provide through the nonlinear load transfer springs the shaft and toe resistances that will eventually reach their maximum asymptotic values that will result in the ultimate shaft and toe capacities that in summation provide the total pile load capacity ($Q_u$).

The springs used along the shaft of the pile are typically called *T-Z* springs and they represent the nonlinear relationship between axial pile displacement, *Z* at the location of the spring, and the corresponding mobilized soil shear resistance, *T*. Similarly, the spring used at the pile toe is often referred to as the *Q-Z* or *R*t-*Z* spring. The *R*t-*Z* spring represents the nonlinear relationship between axial pile displacement at the toe of the pile, *Z*, and the corresponding mobilized end-bearing load resistance.

The load transfer curves can be linear or nonlinear. Earlier versions of these curves were linear based on a linear elastic soil typically modeled using an appropriately selected secant soil modulus based on the anticipated strain levels developed in the soil. Present day, the use of nonlinear load transfer curves is considered in routine analyses. The definition of the load transfer curves is an important aspect in these types of analyses. The maximum values of the load transfer curves for the shaft and toe correspond to the same maximum values required for capacity predictions using static methods. Therefore the peak values of the load transfer curves can be selected based on static methods. Additionally the load transfer method requires selection of adequate load transfer curves that will be defined by the initial slope or stiffness and the curve formation that will control the relationship between pile settlement and mobilized resistance. Clearly, the accuracy of load-settlement predictions using the load transfer method will depend on the curves selected and the ultimate capacity is mainly controlled by the asymptotic values assigned to the selected curves.

There are several formulations proposed in the literature that can be used to obtain side and toe load transfer curves. They are usually divided into two main categories, namely empirical and theoretical. They can also be measured during an axial load test of a well-instrumented pile such that you measure the applied load at the head of a pile, the displacement at the head of the pile, and axial strain levels along the depth of the pile. The axial strain measurements can be used to calculate the side load transfer relationship between two consecutive levels of instrumentation that measure axial strain. This approach was used to obtain the experimental load transfer curves for the axial load tests performed at the UNCC Highbay lab and at the field load test located at the ICE facility.

In the absence of experimental load transfer curves, or for estimated load-settlement curves at the design stage, it is common to use load transfer curves from one of the two categories mentioned before, i.e., empirical or theoretical load transfer curves. The next subsections describes the empirical and theoretically-based load transfer curves.

#### 5.2.2.1 Empirically Obtained Load Transfer Curves

Empirically obtained load transfer curves may provide adequate results for areas where soil is well-characterized or load testing has previously been conducted (Guo 1996). Empirical load transfer relationships available in the literature are commonly based on pile load tests performed on conventional axial load bearing pile types, such as H-piles or pipe piles. To the best of our knowledge, no empirically based load transfer curves are based on load tests on sheet piles as no relationships developed specifically for sheet piles were identified through this study.

Past research involving the proposal of empirically based load transfer curves include: exponential curve by Everett (1991), a tri-linear formulation by Kodikara and Johnston (1994), a square and cubic root formulation by Vijayvergiya (1977), the use of Romberg-Osgood functions by O'Neill and Raines (1991), and hyperbolic functions such as those proposed by Hirayama (1990). Because these formulations are based on specific load tests used by the respective authors for formula development they should be used with caution. Typically it is considered that they should work reasonably well for projects involving similar pile types and geotechnical conditions as those used by the authors of the empirical formulation. Thus, a major limitation to these curves is they do not account for project specific design parameters that will affect curve shape. These parameters include but are not limited to: geotechnical conditions, pile type, installation procedure, the Poisson's ratio of the soil ($v$), the shear modulus of the soil ($G$), and the pile slenderness ratio. Table 5-3 presents a summarized description of the empirical load transfer curves proposed by Vijayvergiya (1977) and API (1993), these curves will be used later in this chapter for comparison to experimentally obtained curves and to compare the predicted load-settlement curves with the actual measured load-settlement curves.

Table 5-3. Summary table of empirically obtained load transfer curves

| Reference | *T-Z* Curve Shape Defined By: | | *Q-Z* Curve Shape Defined By: | |
|---|---|---|---|---|
| | Cohesionless Soil | Cohesive Soil | Cohesionless Soil | Cohesive Soil |
| Vijayvergiya (1977) | $f_s = (f_s)_{\max}\left(A\sqrt{\frac{z}{z_c}} - B\frac{z}{z_c}\right)(for\ z \leq z_c)$ See Figure 5-3 | | $q_t = \left(\frac{z}{z_c}\right)^{1/3}(q_t)_{max}$ See Figure 5-4 | |
| API (1993) | See Figure 5-5 | | See Figure 5-6 | |

Notes: $f_s$ = Unit friction mobilized along the pile segment at movement of *z*,

$f_{s_{\max}}$ = Max unit friction,

$z$ = Movement of pile segment,

$z_c$ = Critical movement of pile segment at which $f_{s_{\max}}$ is mobilized (5 to 8 mm for sands and clays) or $q_{t_{\max}}$ is mobilized (0.04 to 0.06·B for sands and clays, values as recommended by Vijayvergiya (1977))

$A$ = Coefficient based on type of soil (2 recommended for clay), and

$B$ = Coefficient based on type of soil (1 recommended for clay).

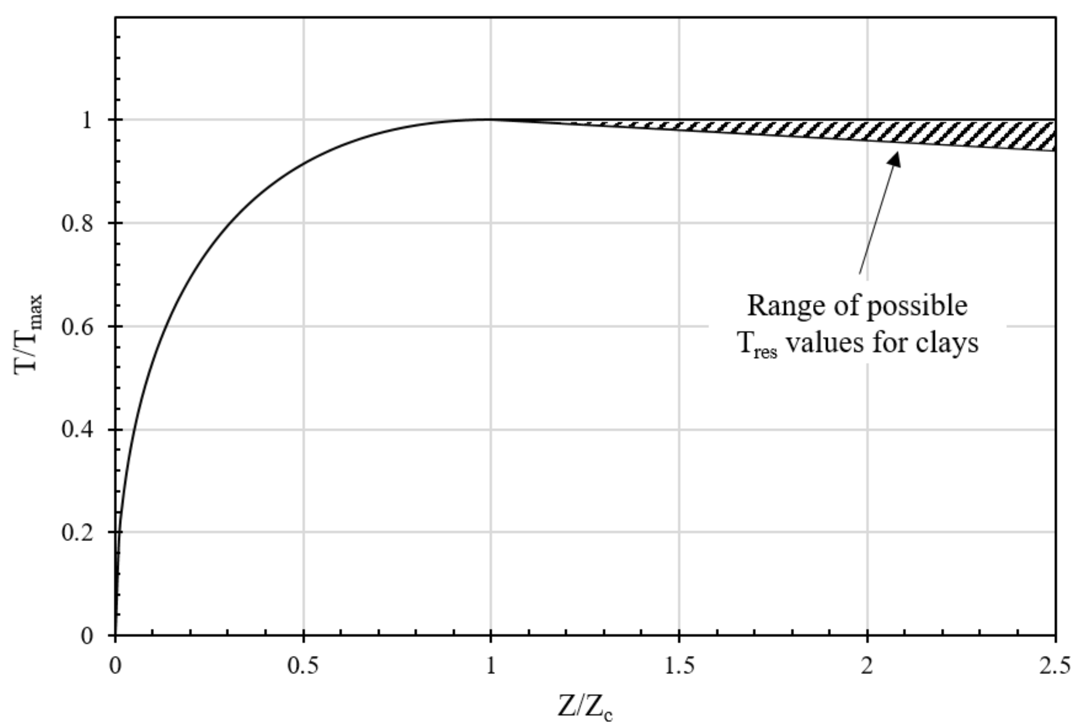


Figure 5-3. Vijayvergiya *T-Z* curves for sand and clay (adapted from Vijayvergiya 1977)

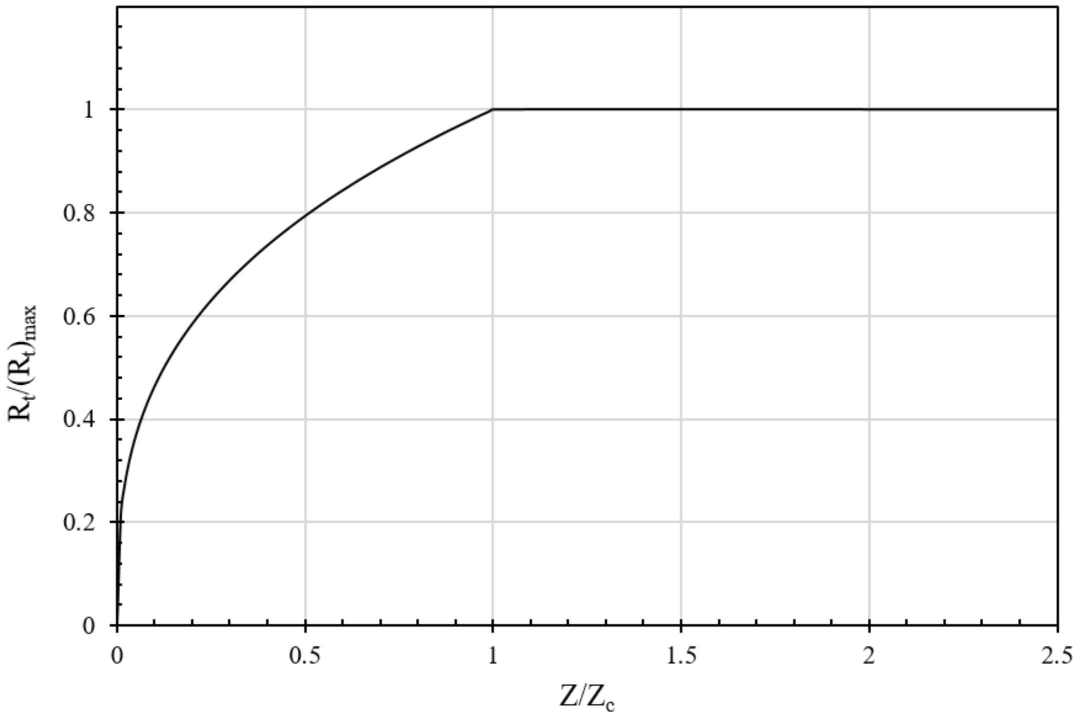


Figure 5-4. Vijayvergiya *R*t-*Z* curves for sand and clay (adapted from Vijayvergiya 1977)

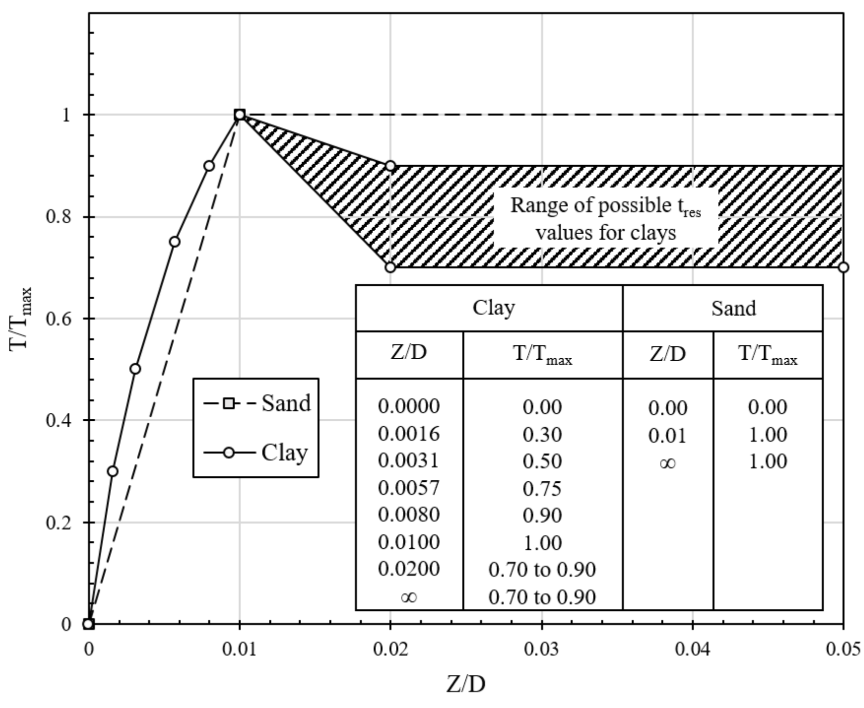


Figure 5-5. API *T*-*Z* curves for sand and clay (adapted from API 1993)

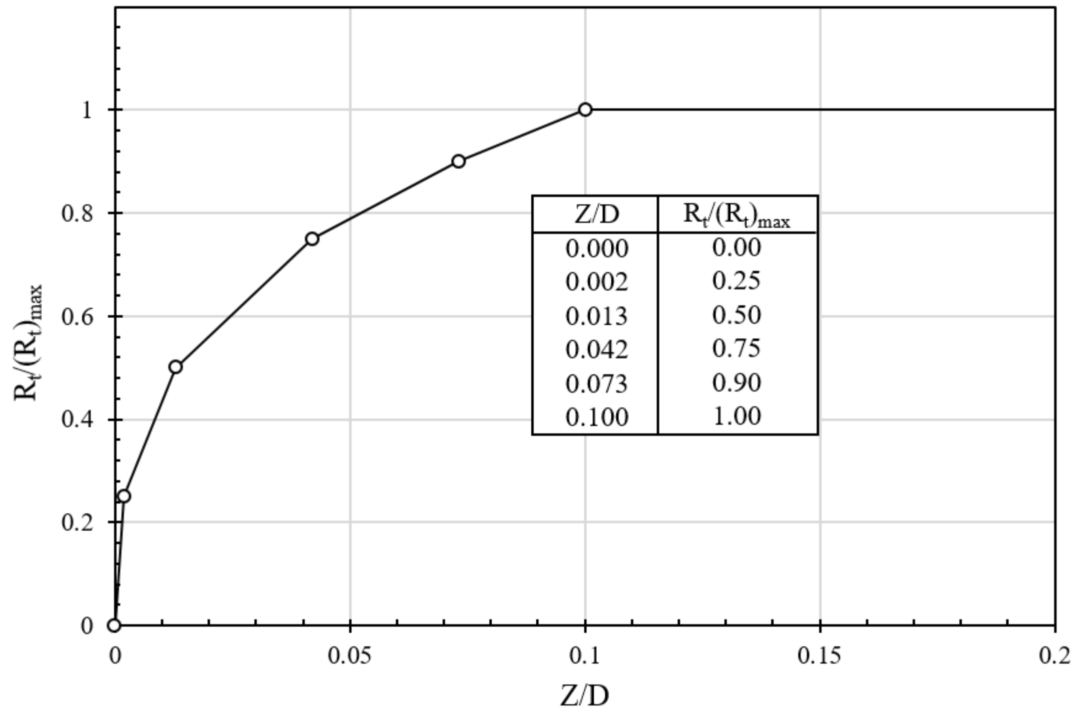


Figure 5-6. API *R*t-*Z* curve for sand and clay (adapted from API 1993)

5.2.2.2 Theoretically Obtained Load Transfer Curves for Cylindrical Piles

This section presents an alternative approach for estimating the load transfer curves needed for load-settlement predictions. In this alternative approach the nonlinear spring models are derived based on elasticity considerations of the problem of an axially loaded pile. Theoretically obtained load transfer curves can be adapted to include site specific geotechnical data and therefore can be used to model a greater diversity of pile types and soil conditions compared to the empirically obtained load transfer curves that as mentioned before are based on specific experimental load test data.

Since most piles are cylindrical, or prismatic with a small cross section compared to their length, the majority of the theoretically-based load transfer curves are based on the well-known concentric cylinder model originally proposed by Randolph and Wroth

(1978). The following sections describe the theoretical load transfer curves for linear elastic and nonlinear soils. Additional details can be found in Chang and Zhu (1998) and Pando et al. (2006).

5.2.2.2.1 Theoretical Load Transfer Curves for Cylindrical Pile in a Linear Elastic Soil

Randolph and Wroth (1978) derived an expression for pile induced deformation in the surrounding soil based on the assumption that the soil surrounding a pile behaves elastically and that soil deformation patterns can be modeled by concentric cylinders interacting in simple shear. Based on derivations performed for an element of soil in this model, the authors present a key conclusion that shear stress decreases with distance such that:

$$\tau = \frac{\tau_0 r_0}{r} \tag{5.5}$$

where,

$\tau$ = Shear stress due to pile loading at radial distance *r*,

$r$ = Radial distance from the centerline of the pile,

$\tau_0$ = Shear stress at the soil-pile interface, and

$r_0$ = Radius of the pile.

The authors use Equation (5.5) to develop the following equation for the total settlement of the pile, based on the assumption that the soil behaves elastically and that soil only deforms vertically due to the pile loads with little to no lateral displacement:

$$w_s \approx \int_{r_0}^{r_m} \left( \frac{\tau(r)}{G} \right) dr = \int_{r_0}^{r_m} \frac{\tau_0 r_0}{G} \left( \frac{dr}{r} \right) = \frac{\tau_0 r_0}{G} \ln\left( \frac{r_m}{r_0} \right) \tag{5.6}$$

where,

$w_s$ = Total settlement of the pile,

$G$ = Shear modulus of the soil, and

$r_m$ = Distance at which shear stress becomes negligible.

The simplifying assumptions used to develop the linear elastic *T-Z* curve based on the concentric cylinder model by Randolph and Wroth (1978) include:

- Treating the soil as a linear elastic material,
- The soil is considered homogeneous as layering effects on the pattern of deformations (i.e., concentric cylinder model) are not discussed or considered,
- the process of pile installation does not influence the relevant soil properties around the pile,
- deformations and stresses in the soil due to the axially loaded pile are taken to be primarily vertical,
- The distance $r_m$ along the pile is based on a simple equation based on the average shear modulus and Poisson's ratio of the soil as well as the embedment depth of the pile.

The above derivation is simple and useful if used with an appropriate secant value of G. However, it is common practice to extend the above formulation to capture the nonlinear behavior of soils. The following section presents a summary of theoretical load transfer curves based on the concentric cylinder model that is extended to capture soil nonlinearity using a modified hyperbolic model.

5.2.2.2.2 Theoretical Load Transfer Curves for a Cylindrical Pile in a Nonlinear Soil

The presentation below includes load transfer curves for the side friction (*T-Z* curves) and for the toe resistance (*Q-Z* curves).

*T-Z* Curves:

The concentric model approach by Randolph and Wroth (1978) can be extended to capture soil nonlinearity by adopting a suitable constitutive model for the soil (Chow 1986; Kraft Jr. et al. 1981). Past researchers have used the conventional hyperbolic stress-strain model by Kondner (1963) to model nonlinear soil behavior (Duncan and Chang 1970; Kondner and Zelasko 1963). The use of the hyperbolic model requires the use of an initial shear modulus from a resonant column or other similar geotechnical test. If the initial shear modulus is based on the $G_{max}$ value that corresponds to very small strain levels (typically from shear wave velocity measurements), then it has been recommended to use the modified hyperbolic model by Fahey and Carter (1993). This modified hyperbolic model allows starting with $G_{max}$ as the initial soil shear stiffness and the model captures the typical soil modulus degradation rate and nonlinearity. The modified curves allow for a flexible curve shape to capture the complicated degradation behavior for different soils while only adding a few additional parameters. Combining the modified hyperbolic expression with the concentric cylinder model proposed by Randolph and Wroth (1978) results in the following equation (Chang and Zhu 1998; Pando et al. 2006):

$$w_s = \frac{\tau_0 r_0}{G_0 g} \ln\left( \frac{\left(\frac{r_m}{r_0}\right)^g - f\left(\frac{\tau_0}{\tau_{max}}\right)^g}{1 - f\left(\frac{\tau_0}{\tau_{max}}\right)^g} \right) \tag{5.7}$$

where,

$f$, $g$ = Empirical curve fitting parameters based on the type of soil encountered, and

$\tau_{\max}$ = Shear stress at failure.

For comparison purposes, Figure 5-7 presents normalized *T-Z* curves based on the linear elastic and modified hyperbolic soil models. The curvature of the *T-Z* curve based on the modified hyperbolic curve depends on the selection of $f$ and $g$ parameters which are related to the nature of the soil encountered. For the *T-Z* curve presented in Figure 5-7, values of 0.98 and 0.25 were assumed for $f$ and $g$, respectively. As can be seen in the figure, the degradation of shear stress for these chosen curve fitting parameters occurs over a much larger pile displacement for the modified hyperbolic curve. The initial curvature of the modified hyperbolic *T-Z* curve will match the other curve as this initial slope only depends upon $G_0$, $\tau_0$, $r_0$, and $r_m$. The expression in Equation (5.5) yields a linear *T-Z* curve as shown with the dash-dot line in Figure 5-7. The asymptotic value of this curve is $f_{s_{\max}}$ that can be selected from the static method of choice.

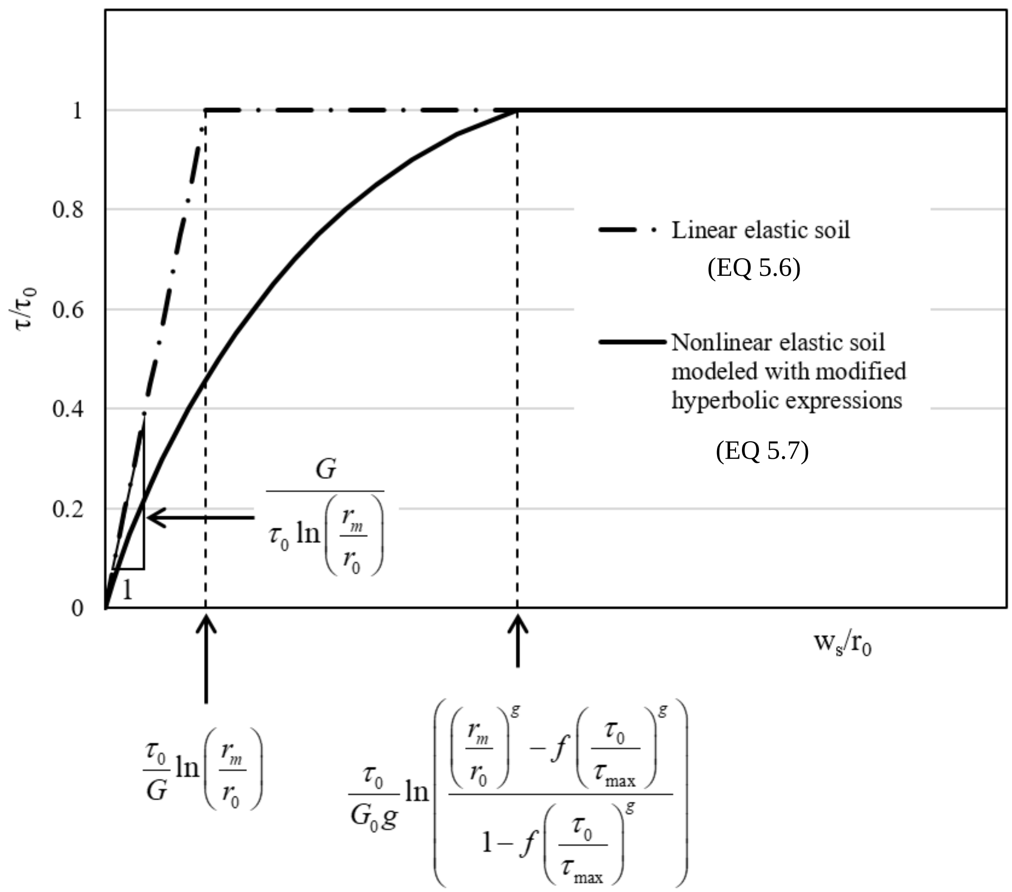


Figure 5-7. Normalized *T-Z* curve based on linear, hyperbolic, and modified hyperbolic soil shear behavior for the concentric cylinder model

It is important to note that the concentric cylinder model and the *T-Z* curves presented are for prismatic or cylindrical piles that have a small cross-section compared to the embedded length of the pile. Later in this chapter (Section 5.3.3) a modified *T-Z* curve is derived for a plate type deep foundation that better captures the geometry of sheet piles.

Derivation of *Q-Z* Curves:

*Q-Z* (or $R_t$-*Z*) curves have also been developed to reflect the soil nonlinearity in a similar fashion as for *T-Z* curves. However, creating *Q-Z* curves to capture nonlinear soil behavior presents a greater challenge relative to the previous *T-Z* development. An approach outlined by Chow (1986) can be summarized as follows:

$$\frac{R_t}{(R_t)_{\max}} = \left(\frac{Z_b}{r_0}\right)\cdot\left(\frac{4Gr_0^{\,2}}{(R_t)_{\max}(1-\nu)}\right)\cdot\left[1-f\cdot\left(\frac{R_t}{(R_t)_{\max}}\right)^g\right] \tag{5.8}$$

Figure 5-8 presents normalized *Q-Z* curves based on the linear, hyperbolic, and modified hyperbolic soil models. Similar to the presented *T-Z* curves, the modified hyperbolic soil model in this figure assumes values for *f* and *g* of 0.98 and 0.25, respectively.

.

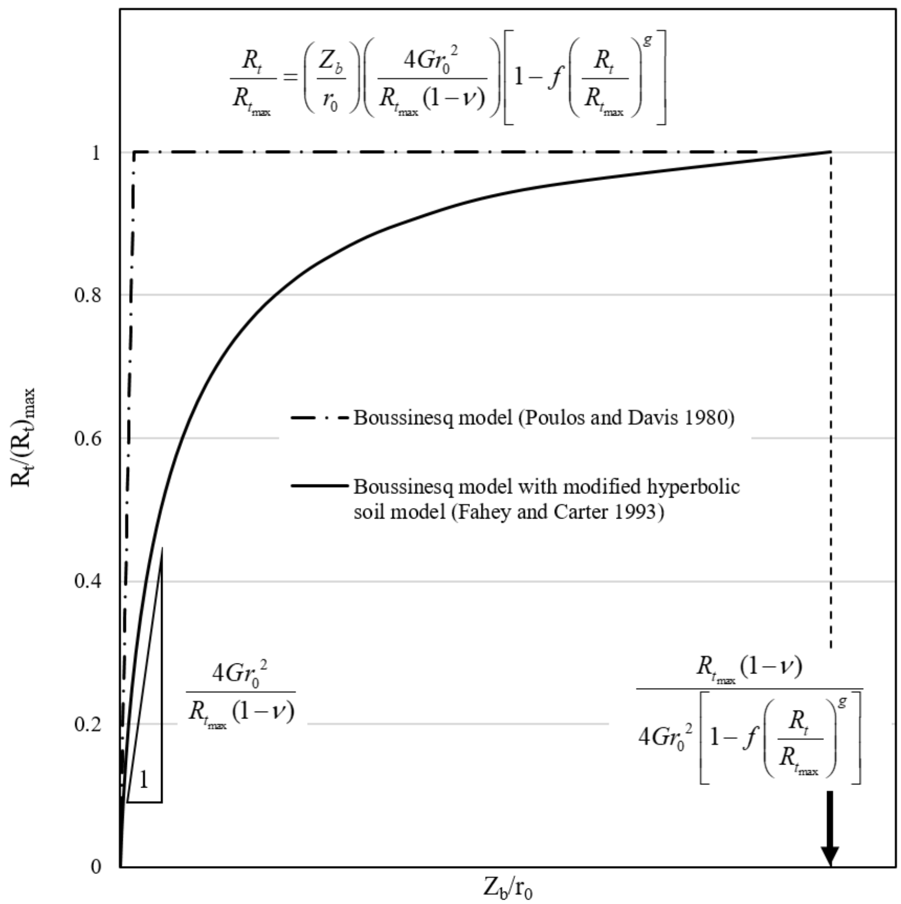


Figure 5-8. Normalized *Q-Z* curve based on linear, hyperbolic, and modified hyperbolic soil shear behavior for concentric cylinder model

As shown in the figure, the modified hyperbolic *Q-Z* curve shows greater displacement is required to mobilize maximum toe capacity and similar to the *T-Z* curves, both *Q-Z* curves have the same initial slope. The large initial slope of the linear curve demonstrates how the assumption of a constant maximum shear modulus value for the soil can lead to a very stiff response requiring minimal toe displacement for maximum toe resistance. Selecting the secant shear modulus is recommended in cases where a constant value for shear modulus is used.

### 5.2.3 Derivation of Load Transfer Curves for an Axially Loaded Plate

A review of commonly used empirical and theoretically-based load transfer curves was presented in Section 5.2.2. The empirical curves are based on pile load tests involving conventional piles with prismatic geometries that have large length to width ratios. Similarly, the theoretically-based load transfer curves are primarily based on the concentric cylinders model proposed by Randolph and Wroth (1978). As shown in Figure 5-9 (a) the concentric cylinders model involves a cylindrical pile and it has been approximated with reasonable success to other prismatic pile cross sections such as squares and rectangles. It has also been applied to H-piles. However, the concentric cylinders model does not reflect the geometric differences of a sheet pile or the flat approximation of a long plate as the one shown in Figure 5-9 (b). As shown in this figure, the long plate geometry will not result in soil deformation patterns near the axially loaded plate that are similar to the concentric cylinders. Therefore, this section presents the derivations of new load transfer curves (shaft resistance *T-Z* and toe resistance *Q-Z*) for a plate geometry that are a closer approximation to a sheet pile compared to the cylindrical pile model.

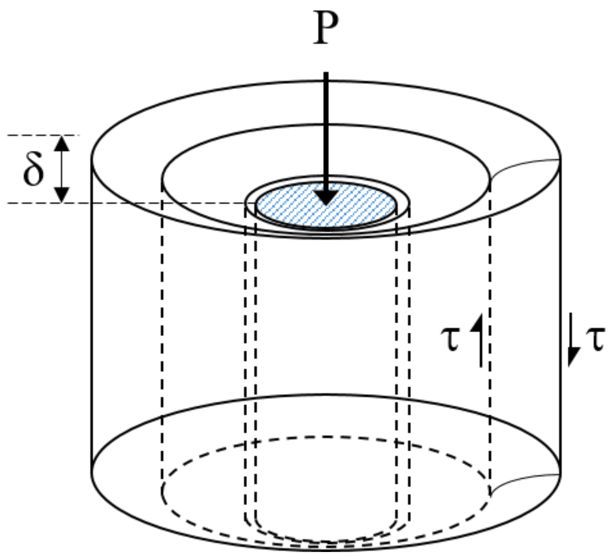


(a)

Note: Shaded areas correspond to pile.

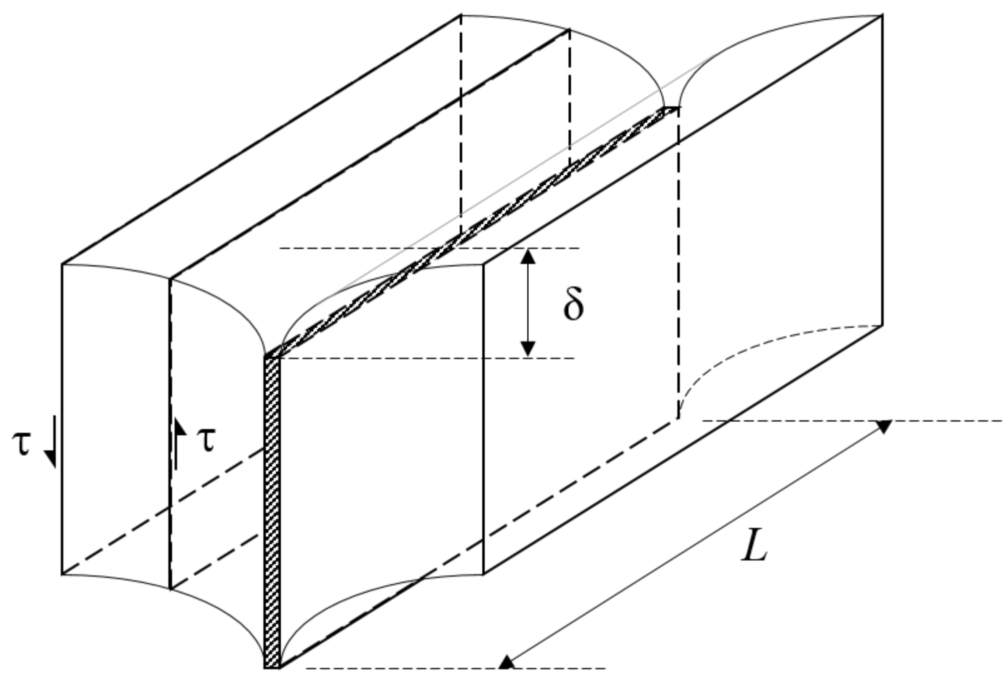


(b)

Figure 5-9. Deformation patterns considered for development of theoretical load transfer curves for piles: (a) model based on conventional pile geometry, and (b) model based on a plate geometry to approximate a sheet pile

5.2.3.1 Development of *T-Z* Load Transfer Curve

This section presents a mathematical analysis performed for an axially loaded plate wall foundation. Figure 5-10 presents a plan view of the geometry considered in this derivation. In this figure the shaded area corresponds to the foundation plate with thickness $2 \cdot r_0$ and length $L+2 \cdot r_0$. The cross section considered includes semicircles of radius $r_0$ at both ends of the plate.

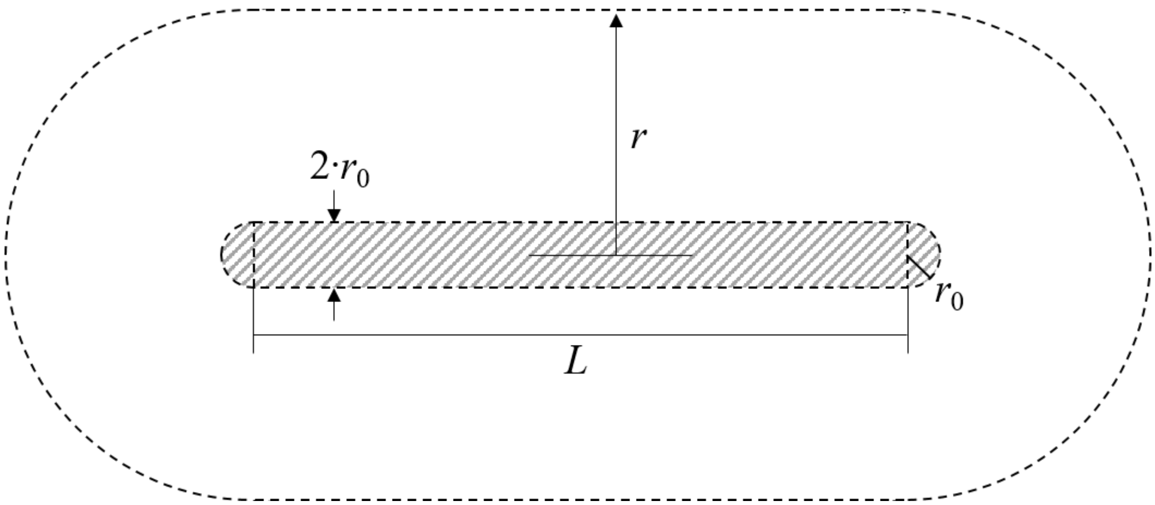


Figure 5-10. Image of plate geometry used for mathematical derivations

For this geometry, Equation (5.9) provides the plate cross sectional area and Equation (5.10) provides the perimeter:

$$A_{wall} = (2 \cdot L \cdot r_0) + (\pi \cdot r_0{}^2) \tag{5.9}$$

$$P_{wall} = 2 \cdot (L + \pi \cdot r_0) \tag{5.10}$$

where,

$A_{wall}$= Cross sectional area of wall,

$P_{wall}$= Perimeter of wall,

$r_0$= Half the wall thickness, and

$L+2\cdot r_0$= Length of the foundation wall.

When this plate foundation is vertically loaded, the interface with the soil will be mobilizing a shear stress, $\tau_0$. Considering vertical equilibrium we obtain:

$$V = \tau_0 \cdot P_{wall} \cdot \Delta z = \tau_0 \cdot \left(2 \cdot (L + \pi \cdot r_0)\right) \cdot \Delta z \tag{5.11}$$

where,

$V$= Applied vertical compression load,

$\tau_0$ = Vertical shear stress at the plate to soil interface, and

$\Delta z$ = Depth of pile resisting applied load.

Similarly, considering a surface at some distance ($r$) away from the centerline of the pile wall, with the perimeter corresponds to the dashed line shown in Figure 5-10 yields the following expression for $V$:

$$V = \tau \cdot P_{wall} \cdot \Delta z = \tau \cdot \left(2 \cdot (L + \pi \cdot r)\right) \cdot \Delta z \tag{5.12}$$

where,

$r$ = Distance away from the centerline of the pile wall, and

$\tau$ = Vertical shear stress at distance $r$.

To satisfy vertical force equilibrium the expression for $V$ in Equations (5.11) and (5.12), must be equal and lead to:

$$\tau = \tau_0 \cdot \frac{\left(L + \pi \cdot r_0\right)}{\left(L + \pi \cdot r\right)} \tag{5.13}$$

The rate of decay of the shear stress depends on $L$ and $r_0$ as shown in Figure 5-10. In this derivation it is assumed that the decrease in shear stress due to the loaded pile with distance from the pile is due applied loads acting over a larger area with radial distance, $r$.

Any other possible sources of shear stress decay with radial distance are neglected in this derivation. The above expression shows the variation of the vertical shear stress with radial distance of the plate pile. It is worth noting that when *L* becomes zero the expression in Equation (5.13) becomes:

$$\tau = \left(\tau_0 \cdot r_0\right) / r \qquad (5.14)$$

Equation (5.14) is the equation used in the concentric cylinder model by Randolph and Wroth (1978). Using a similar approach to the concentric cylinder model, Equation (5.13) can be used to develop the following equation for the total settlement of the pile, based on the assumptions that the soil behaves elastically, as follows:

$$w_s = \frac{\tau_0 (L + \pi \cdot r_0)}{G \cdot \pi} \cdot \ln\left(\frac{L + \pi \cdot r_m}{L + \pi \cdot r_0}\right) \qquad (5.15)$$

where, as before for the concentric cylinder model,

$w_s$ = Total settlement of the pile,

$G$ = Shear modulus of the soil, and

$r_m$ = Distance at which shear stress becomes negligible.

Figure 5-11 presents the developed *T-Z* curves from Equation (5.15). For comparison purposes this figure also presents the *T-Z* curve corresponding to the cylindrical pile. Both *T-Z* curves correspond to a linear elastic soil behavior. As can be seen, the stiffness of the *T-Z* curve corresponding to the concentric cylinder model is greater than that of the newly derived curve for a plate geometry foundation wall. This difference in observed stiffness is explained by the different geometries of the volume of strained soil involved and the differences in rate of decay of the shear stress levels. The shear stresses induced in the surrounding soil due to loading of the wall act over a larger shaft area with increasing radial distance from the pile as compared to the change of area for the cylindrical pile. This results in a lower rate of shear stress decay with radial distance. The lower rate of decay requires additional settlement for the wall to reach the same unit shaft resistance as compared to a cylindrical pile. Additionally, the volume of soil affected by pile loading is larger for the wall geometry as compared to the cylinder, resulting in larger required values for settlement to fully engage and reach peak unit shaft resistance.

Similar to the theoretical curves developed by Randolph and Wroth (1978), several assumptions are made when developing the equation for the *T-Z* curve for linear elastic soil for the plate pile. Similar to the assumptions stated in Section 5.2.2.2.1 these include:

- Treating the soil as a linear elastic material,
- The soil is considered homogeneous as layering effects on the pattern of deformations (i.e., concentric cylinder model) are not discussed or considered,
- the process of pile installation does not influence the relevant soil properties around the pile,
- deformations and stresses in the soil due to the axially loaded pile are taken to be primarily vertical,
- The distance $r_m$ along the pile is based on a simple equation based on the average shear modulus and Poisson's ratio of the soil as well as the embedment depth of the pile.

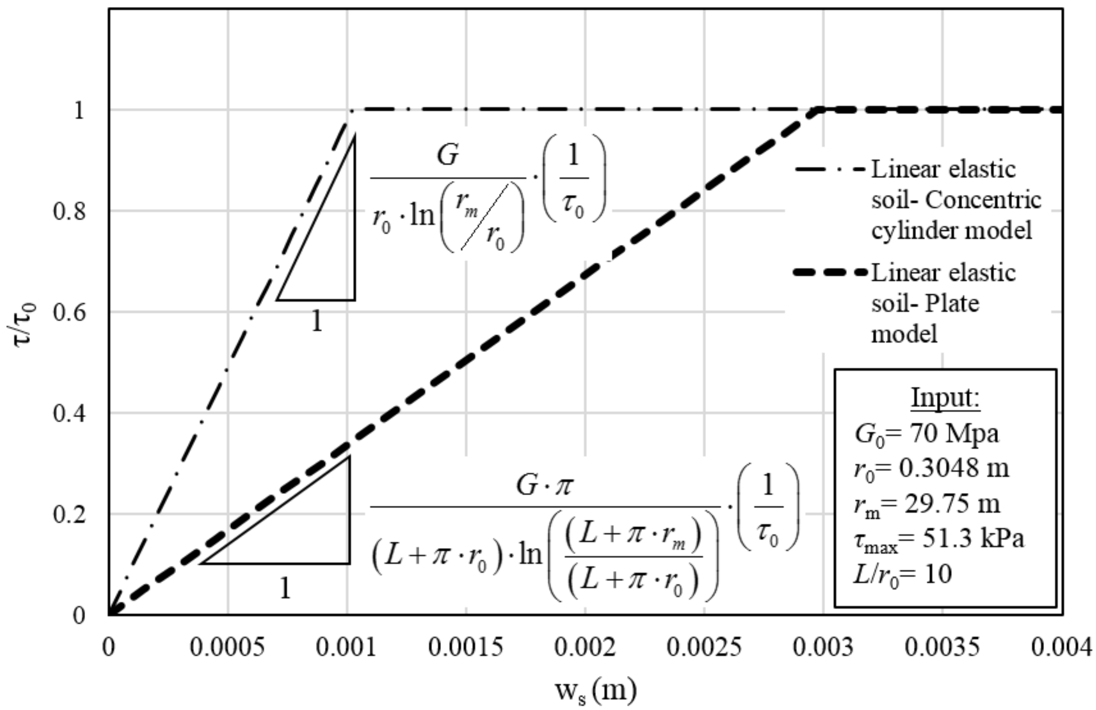


Figure 5-11. Comparison of linear elastic soil *T-Z* curves for cylindrical and plate piles

If a length of zero is entered into Equation (5.15) the *T-Z* expression reduces to:

$$w_s = \frac{\tau_0 r_0}{G} \ln\left(\frac{r_m}{r_0}\right) \tag{5.16}$$

The above equation is the same expression for the *T-Z* curve obtained using the concentric cylinder model.

The modified hyperbolic soil model can be applied in these derivations to evaluate the effect of nonlinear shear stress-shear strain response of the soil on the *T-Z* curve. Equation (5.17) presents the equation for total settlement of the plate pile assuming a modified hyperbolic soil model.

$$w_s = \frac{\tau_0 (L + \pi \cdot r_0)}{G_0 \cdot \pi \cdot g} \cdot \ln\left( \frac{\left(\frac{L + \pi \cdot r_m}{L + \pi \cdot r_0}\right)^g - f\left(\tau_0 / \tau_{\max}\right)^g}{1 - f\left(\tau_0 / \tau_{\max}\right)^g} \right) \tag{5.17}$$

where, as before,

$f, g$ = Empirical curve fitting parameters for the modified hyperbolic soil model, and

$\tau_{\max}$ = Shear stress at failure.

The *T-Z* curve obtained from Equation (5.17) is shown in Figure 5-12. For comparison purposes this figure also shows the *T-Z* curve for a plate deep foundation for the linear elastic soil model.

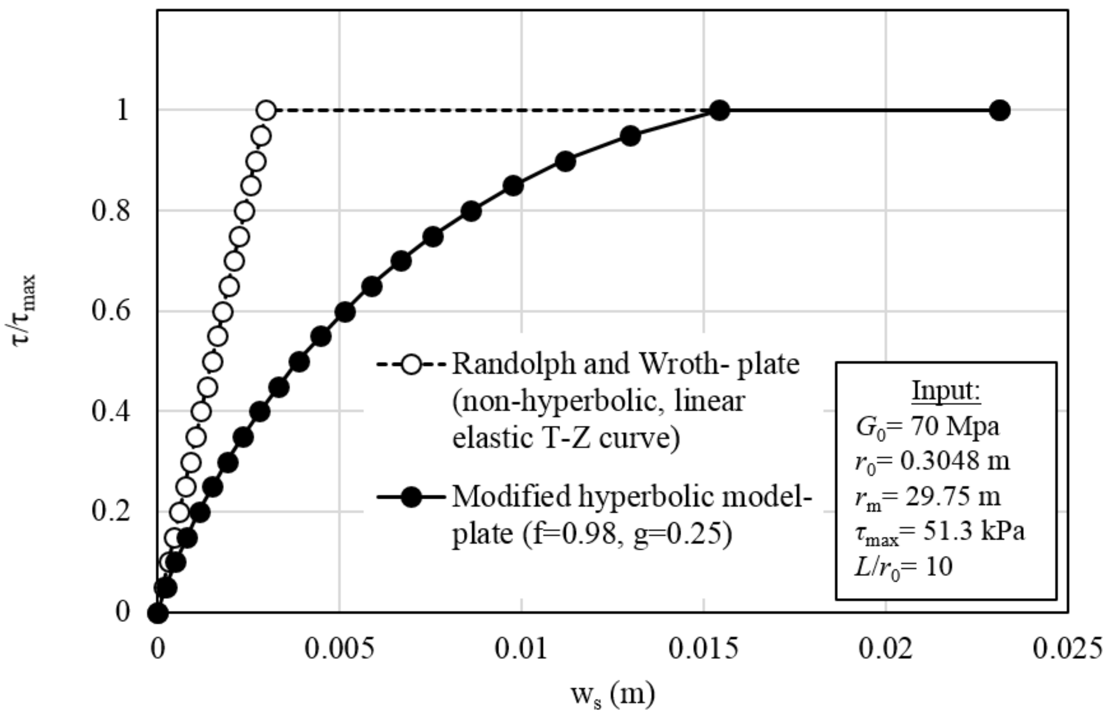


Figure 5-12. Normalized *T-Z* curves for linear and modified hyperbolic soil models based on the derived *T-Z* curves for the foundation plate wall

Equation (5.17) becomes Equation (5.15) when *f*= 0 and *g*= 1 that corresponds to the case of a linear elastic soil, and is as expected as *f*=0 in the modified hyperbola corresponds to the linear elastic model.

Additionally, the resulting expression for total settlement based on the modified hyperbolic soil model provided by Equation (5.17) reverts to the concentric cylinder model case when a value of *L*=0 is used, as follows:

$$w_s = \frac{\tau_0 r_0}{G_0 g} \ln\left( \frac{\left(\frac{r_m}{r_0}\right)^g - f\left(\frac{\tau_0}{\tau_{\max}}\right)^g}{1 - f\left(\frac{\tau_0}{\tau_{\max}}\right)^g} \right) \tag{5.18}$$

5.2.3.2 Development of *Q-Z* Load Transfer Curve

A similar approach for *Q-Z* curve development as was used for the concentric cylinder model is used for the plate pile. The derivation of the *Q-Z* curve for the plate geometry considered a rigid, long, rectangular footing on an elastic half space. The equation for elastic settlement for a rectangular footing, as presented by Holtz et al. (2011)is as follows:

$$Z_b = \frac{R_t \cdot B}{A_{wall} \cdot E}(1-\upsilon^2) I_s \tag{5.19}$$

Where,

$R_t$= The applied load at the pile toe,

$B$= The characteristic dimension of the loaded area,

$A_{wall} = (2 \cdot L \cdot r_0) + (\pi \cdot r_0^{\,2})$ = The area being loaded,

$E$ = Young's modulus of the soil,

$\upsilon$ = Poisson's ratio of the soil, and

$I_s$ = A rigidity and shape factor

For long plates where $L/B \cong 10$, the shape factor *I*s is equal to 2. Additionally, the value for *B* can be given by 2·$r_0$, defining $A_{wall}$ in terms of $r_0$, and using the relation $E = 2G(1+\upsilon)$ (Landau and Lifshitz 1970) the above equation reduces to:

$$Z_b = \frac{R_t(1-\upsilon)}{Gr_0\left(20+\pi/2\right)} \tag{5.20}$$

The above expression corresponds to a linear *Q-Z* (or $R_t$-*Z*) relationship. Therefore an appropriate secant value for shear modulus must be used for the the stiffness of the *Q-Z* spring, as follows:

$$K_0^{base} = \frac{R_t}{Z_b} = \frac{G_{sec} r_0\left(20+\pi/2\right)}{(1-\upsilon)} \tag{5.21}$$

This linear *Q-Z* curve can be extended to capture soil nonlinearity using a hyperbolic relationship in a similar approach as done previously, as follows:

$$K_{sec}^{base} = K_0^{base}\left[1 - f\left(\frac{R_t}{R_{t_{max}}}\right)^g\right] \tag{5.22}$$

Combining Equations (5.21) and (5.22) yields:

$$K_{sec}^{base} = \left(\frac{G_{sec} r_0\left(20+\pi/2\right)}{(1-\upsilon)}\right)\left[1 - f\left(\frac{R_t}{R_{t_{max}}}\right)^g\right] \tag{5.23}$$

this simplifies to the final expression as follows:

$$Z_b = \frac{R_t}{K_{\sec}^{base}} = \frac{R_t(1-\upsilon)}{\left(G_{\sec} r_0 \left(20 + \pi/2\right)\right)\left[1 - f\left(\frac{R_t}{R_{t_{\max}}}\right)^g\right]} \tag{5.24}$$

The above equation can be used to generate a non-linear *Q-Z* curve based on a modified hyperbolic soil model. Figure 5-13 presents the normalized *Q-Z* curves for linear elastic soil and the modified hyperbolic soil model (with *f* and *g* as 0.98 and 0.25, respectively). As can be seen, similar to the *Q-Z* curves presented for the concentric cylinder derivation, the linear elastic model results in peak toe resistance mobilized at very small values of displacement while the modified hyperbolic model predicts large deformation required to fully mobilize toe resistance. The initial slope for both curves is equal, and similar to previous recommendations, if a single value of *G* is assumed for the soil a secant value should be used.

The equation for settlement used in this derivation treats the loading as a shallow foundation. Applying this equation to the pile wall geometry is an approximation as the behavior at the wall base is located at a certain depth within the half space elastic medium. However, this is a reasonable assumption based on the work of Randolph and Wroth (1978) and the assumptions made to reach the previous steps.

For non-linear elastic soil modeled with modified hyperbolic expressions:

$$\frac{R_t}{R_{t_{max}}} = \left(\frac{Z_b}{r_0}\right) \cdot \left( \frac{G_{sec} \cdot r_0^{\,2} \left(20 + \pi/2\right) \left[1 - f\left(\frac{R_t}{R_{t_{max}}}\right)^g\right]}{R_{t_{max}}(1-\nu)} \right)$$

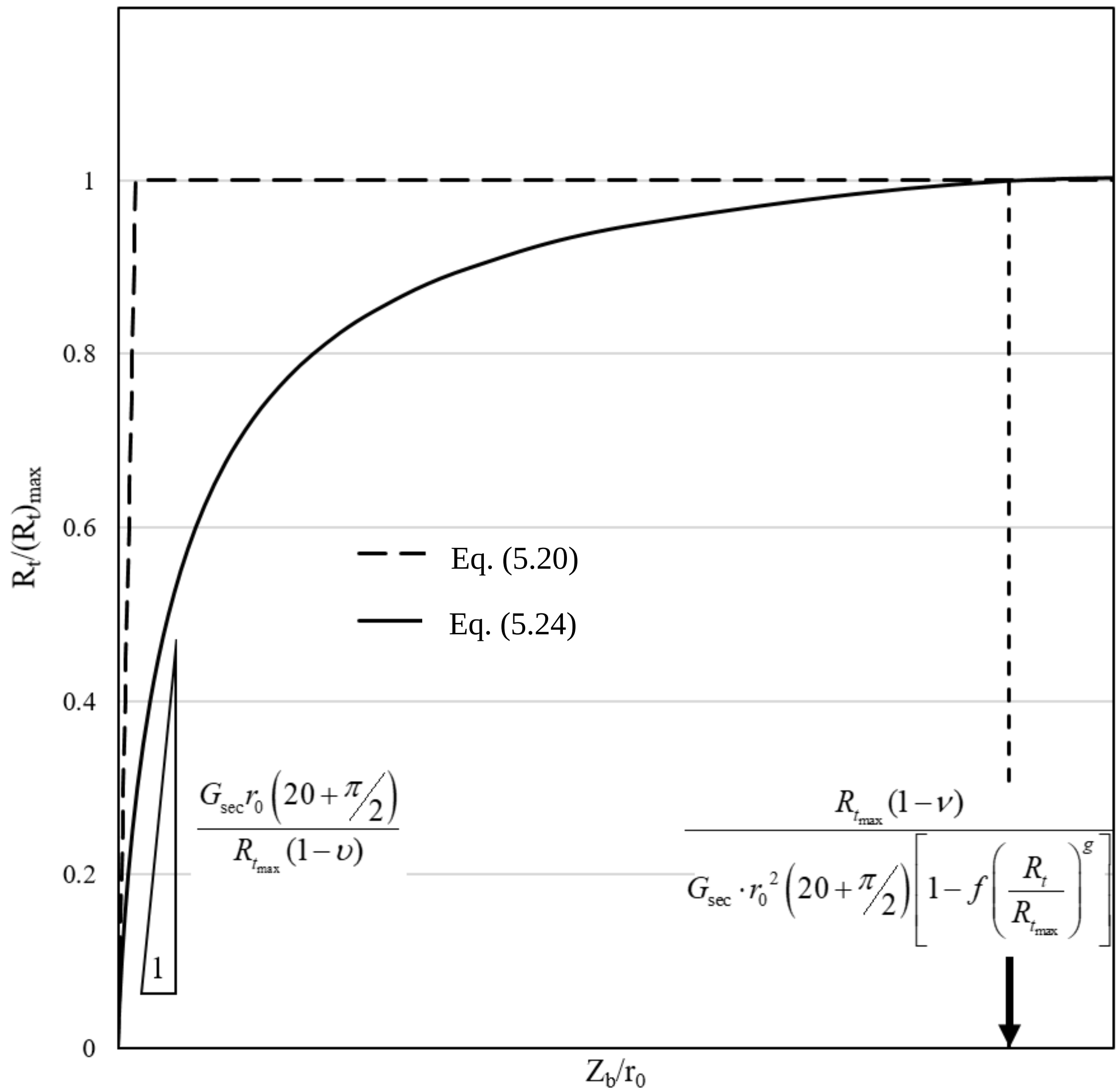


Figure 5-13. *Q*-*Z* curves for a plate deep foundation

## 5.3 Numerical Evaluation of Experimental Results

This section presents and discusses the results obtained from conventional static methods used to predict axial pile capacity. Additionally, this section compares load-settlement predictions obtained from *T-Z* analyses using conventional load transfer curves with pile load test measurements obtained in the Highbay lab and field site. The results obtained from Highbay laboratory and the field test site are presented separately.

### 5.3.1 Numerical Evaluation of Highbay Tests

#### 5.3.1.1 Axial Capacity Estimates Using Static Methods

Shaft and toe resistances are considered separately in order to determine how appropriate the different static methods were for evaluating both sources of pile capacity. Figure 5-14 presents a summary of the result of the comparison between total measured axial capacity and predicted values. A dashed line in this figure indicates the total measured capacity as determined using the Davisson’s failure criteria. Similarly, Figure 5-15 and Figure 5-16 present summaries of the results of a similar comparison for shaft and toe capacities, respectively. Table 5-4 presents a summary of predicted versus measured values for these capacities. Predicted capacity values are dependent on unit resistances as well as the areas over which these resistances act. Due to the large influence of plugging on the area used to calculate capacity from the shaft and toe, the above mention figures present both unplugged (dash marker) and fully plugged (square marker) conditions used in calculations. Figure 5-17 presents an image showing the assumed area of the plug for fully plugged calculations.

All methods considered under predict total pile capacity for the unplugged condition, with predicted values ranging from 196.0 to 643.0 kN (vs. total measured capacity of 1219 kN). In contrast, all methods, except LCPC, over predict the axial load capacity measured in the pile load test. Based on these results, it is not possible to determine whether a full plug condition occurred because the degree of under and over prediction for the no plugging and full plugging assumptions are similar. However, given the fact that measured total capacity fell within the middle of the range of calculated total capacity values for unplugged and plugged conditions suggests that partial plugging likely developed.

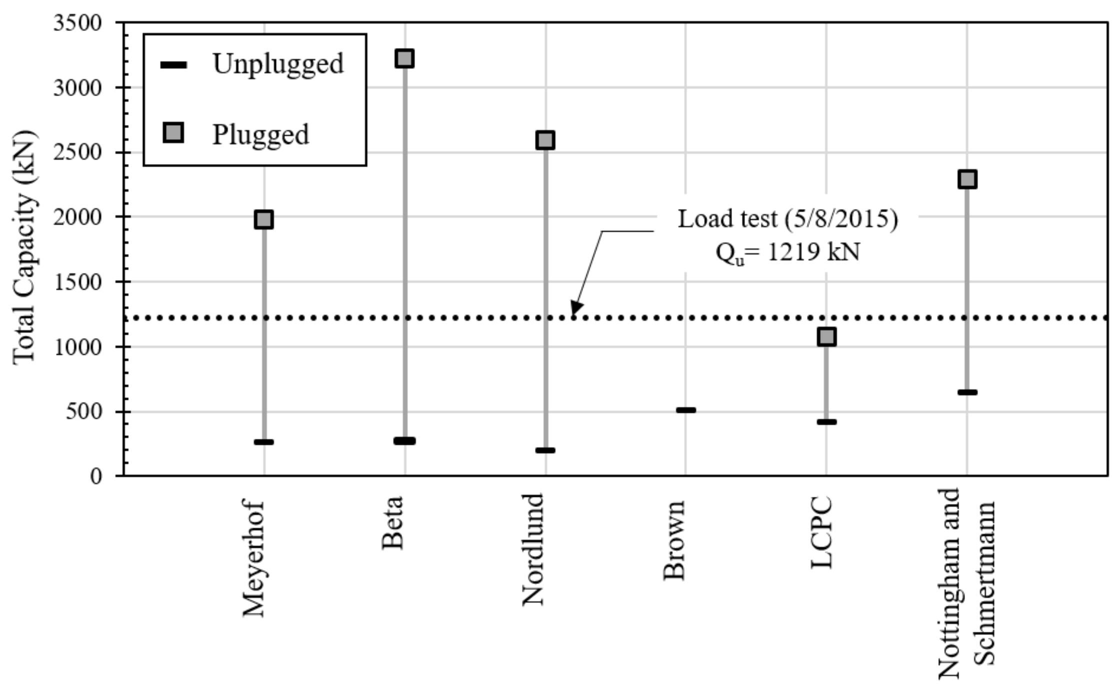


Figure 5-14. Summary of predicted pile load capacity for plugged and unplugged conditions compared to measured axial capacity for laboratory test

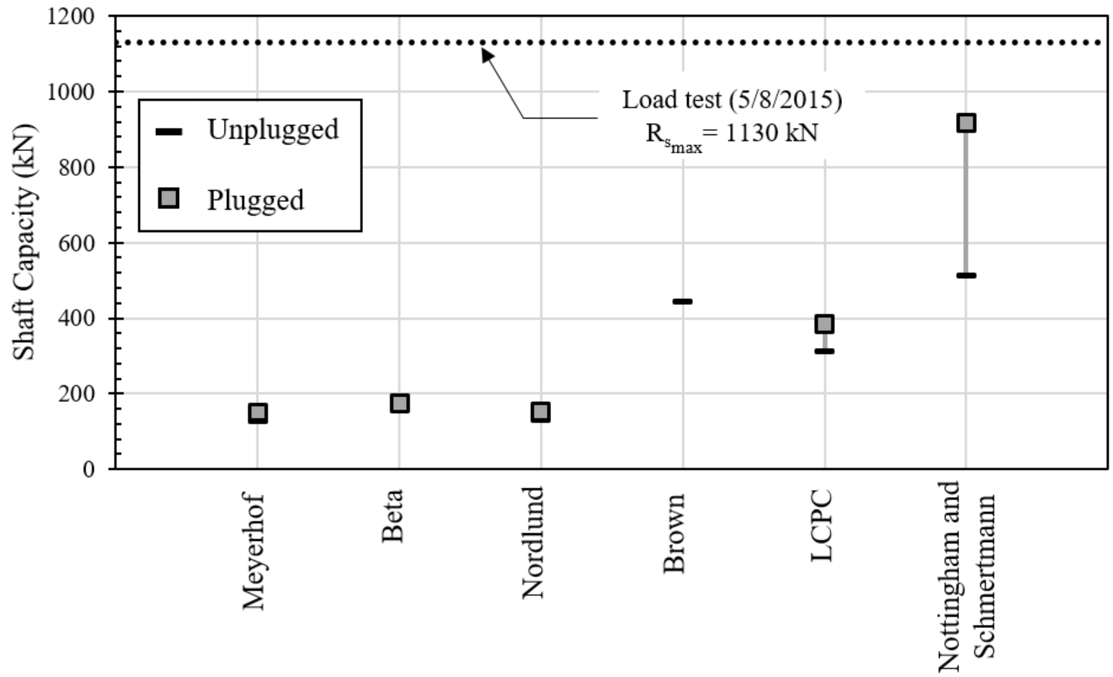


Figure 5-15. Summary of predicted shaft capacity for plugged and unplugged conditions compared to measured shaft capacity for laboratory test

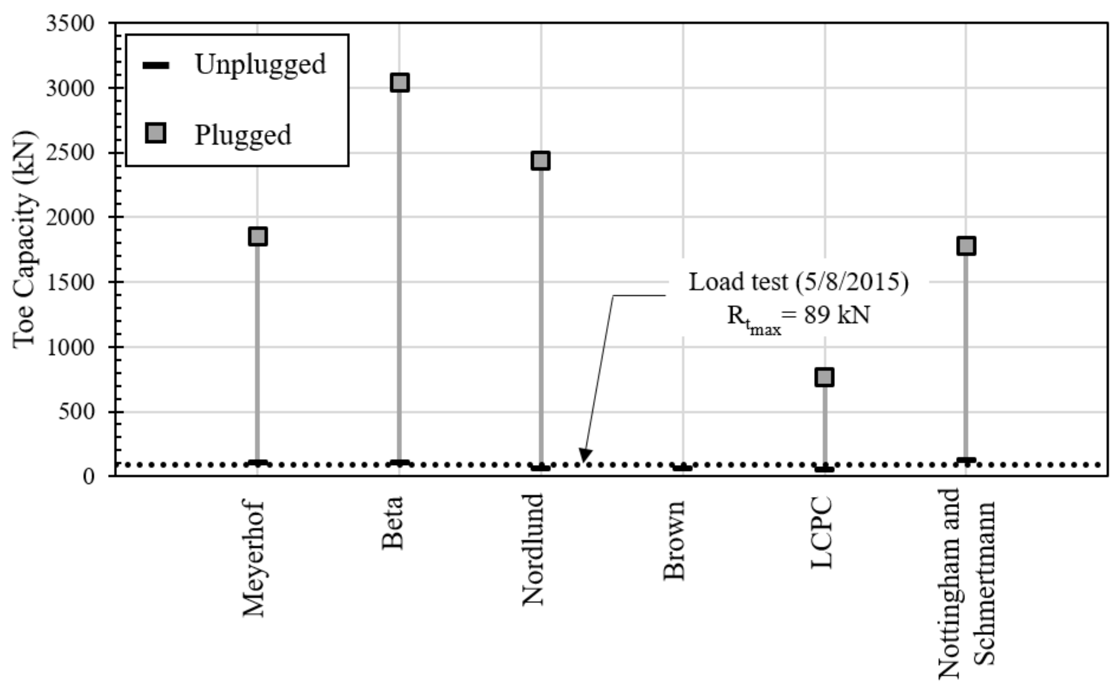


Figure 5-16. Summary of predicted toe capacity for plugged and unplugged conditions compared to measured toe capacity for laboratory test

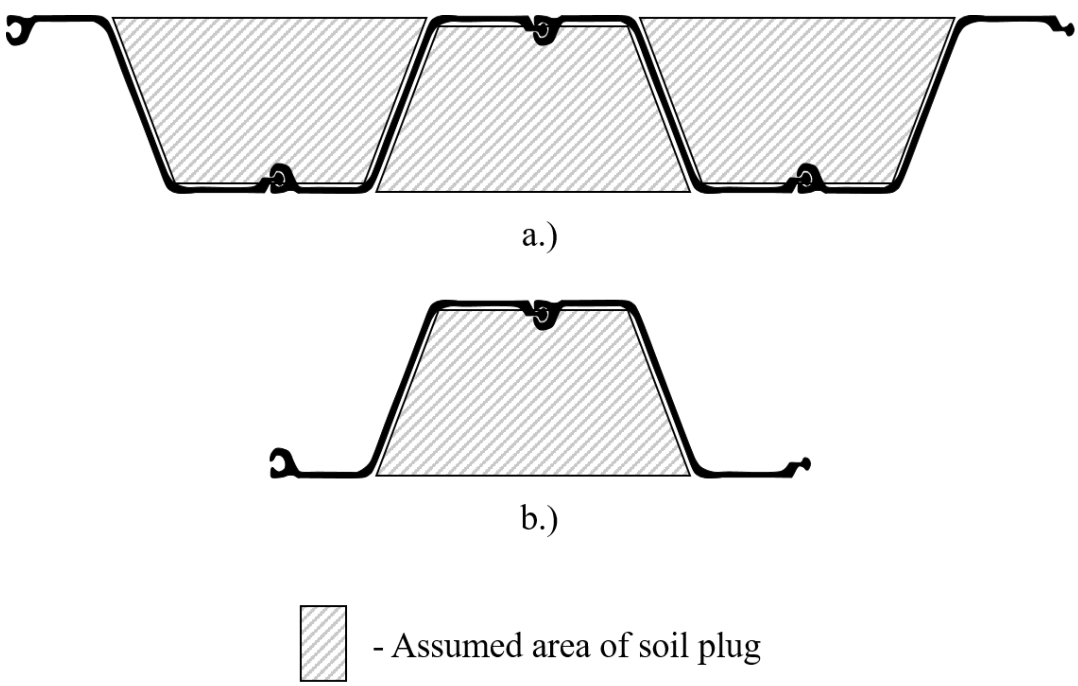


Figure 5-17. Assumed area of the plug for static capacity estimates for the fully plugged condition for both a.) laboratory test piles, and b.) field piles

Table 5-4. Predicted versus measured axial capacities for laboratory testing of sheet piles

| Prediction Method | | Total Capacity | | Shaft Capacity | | Toe Capacity | |
|---|---|---|---|---|---|---|---|
| | | $Q_c$ (kN) | $Q_c/Q_m$ | $Q_c$ (kN) | $Q_c/Q_m$ | $Q_c$ (kN) | $Q_c/Q_m$ |
| Meyerhof | Unplugged | 259.8 | 0.21 | 149.4 | 0.13 | 110.3 | 1.25 |
| | Plugged | 1979.3 | 1.62 | 127.6 | 0.11 | 1851.6 | 20.90 |
| Beta | Unplugged | 267.5 | 0.22 | 160.1 | 0.14 | 107.4 | 1.21 |
| | Plugged | 3218.1 | 2.64 | 174.9 | 0.15 | 3043.2 | 34.35 |
| Nordlund | Unplugged | 196.0 | 0.16 | 131.0 | 0.12 | 65.1 | 0.73 |
| | Plugged | 2588.4 | 2.12 | 153.8 | 0.14 | 2434.6 | 27.48 |
| Brown | Unplugged | 508.0 | 0.42 | 443.1 | 0.39 | 64.8 | 0.73 |
| LCPC | Unplugged | 415.9 | 0.34 | 383.1 | 0.34 | 50.6 | 0.57 |
| | Plugged | 1077.0 | 0.88 | 313.8 | 0.28 | 763.2 | 8.62 |
| Nottingham & Schmertmann | Unplugged | 643.0 | 0.53 | 514.4 | 0.46 | 128.6 | 1.45 |
| | Plugged | 2294.5 | 1.88 | 915.5 | 0.81 | 1780.1 | 20.10 |

Note: $Q_c$= Calculated capacity using static methods, $Q_m$= measured value corresponding to Davisson's failure criterion (total= 1218.9 kN, shaft= 1130.3 kN, toe= 88.6 kN). $Q_c/Q_m$= the ratio of calculated to measured capacity

Based on the results of predictions made for the laboratory test pile, it can be seen that predicted values produced ratio values of calculated capacity to measured capacity ranging from 0.16 to 0.53 assuming unplugged conditions, and values ranging from 0.88 to 2.64 assuming plugged conditions. This suggests predictions obtained assuming unplugged conditions consistently under predict the pile capacity by approximately 50 to 75%, while predictions made assuming plugged conditions under and over predict the pile capacity by values up to 12 to 164%, respectively. The degree of agreement between predicted and measured capacity values are reasonable when compared to capacity estimates for conventional deep foundations where factors of safety can be equal to values of 3.0 or greater. A major design consideration which must be accounted for when using these predictive methods is the plugging behavior of the pile. Determining this behavior is difficult and the formation of a plug will have a large influence over calculated capacities, especially for toe capacity. Based on observations made from testing and these predictions, plugging over a certain length of the pile above the toe appears to have occurred. The behavior at the toe of the pile appears to be governed by unplugged conditions where only the cross sectional area of steel of the pile is acting. Therefore, the plugging behavior of sheet piles can be thought to occur as a range of possible plug geometries existing between the extremes of full or no plug development. A conservative approach to design may be warranted to account for uncertainties regarding this behavior in sheet piles, where selection of the minimum values for toe and shaft capacities from calculations assuming full or no plugging may be most appropriate.

Based on the predictions presented, the most accurate method for predicting the pile capacities was the Nottingham & Schmertmann method assuming unplugged behavior for the toe capacity (128.6 kN) and plugged behavior for the shaft capacity

(915.5 kN) which resulted in a total predicted pile capacity of 1044.1 kN which is within 20% of the measured capacity of 1218.9 kN.

#### 5.3.1.2 Evaluation of Lab Study Results Through Load Transfer Analyses

The laboratory pile load tests were evaluated using load transfer methodology and the results are presented in this section. Load-settlement as well as load transfer curves were generated based on the results of pile load testing, and these curves are compared with empirical curves provided by API (1993) and Vijayvergiya (1977). Peak resistance values were obtained from the LCPC and Meyerhof methods, two of the most accurate methods used to predict pile ultimate capacity based on CPT and SPT, respectively.

Based on the empirical load transfer curves, load-settlement curves were developed. These were prepared for both a plugged and unplugged condition, similar to the approach used with the static method predictions. Figure 5-18 summarized the results from these tests. In general, poor agreement exists between predicted and measured curves. The best predicted load-settlement curve is provided with Meyerhof obtained maximum unit resistances and the Vijayvergiya (1977) method using a plugged condition assumption. The level of agreement between predicted and measured load-settlement curves can be further explained by comparing the predicted and measured *T-Z* and *Q-Z* curves.

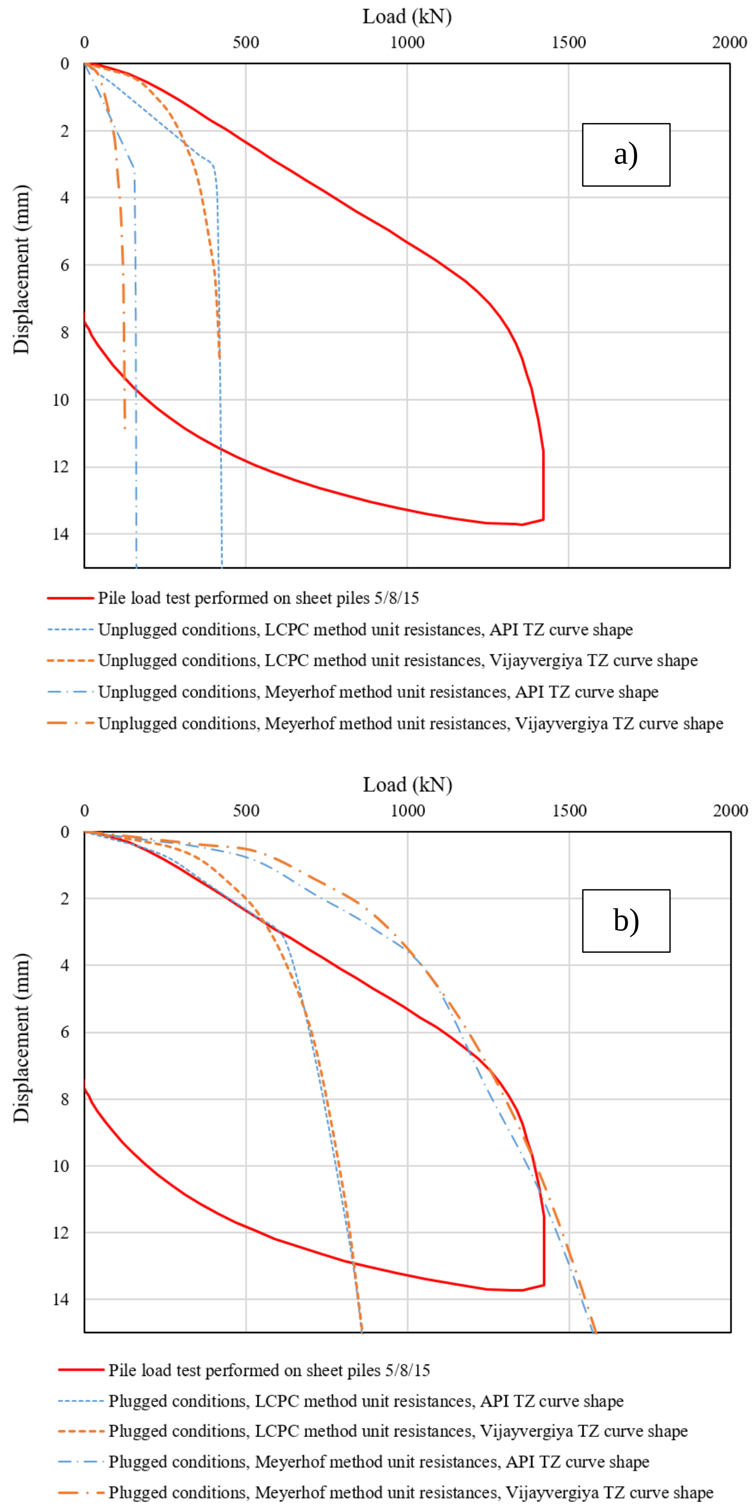


Figure 5-18. Predicted and measured load-settlement curves for a) unplugged and b) plugged conditions for laboratory pile load testing

Figure 5-19 presents the results of comparing the measured *T-Z* curves with empirically obtained curves generated with the maximum shaft resistance provided by the LCPC method averaged over the length of pile embedment. The agreement between both types of curves is poor, with empirically obtained curves under predicting capacity by a large margin up to a factor of approximately four. The initial slope of the empirical curve provided by Vijayvergiya (1977) shows the best agreement with measured data and provides a reasonable prediction of curve shape in this figure. It should be noted that for the *T-Z* curve representing the lowest elevations along the pile, extrapolation was used to obtain forces at the toe of the pile when performing calculations to obtain this curve, similar to the procedure used for generating the toe capacities for the load distribution curves. The *Q-Z* curve development uses the same information obtained from this extrapolation. The load transfer analysis for the field test uses the same extrapolation procedures for *T-Z* and *Q-Z* curve development presented in later sections. Figure 5-20 presents the results of the comparison between empirically and experimentally obtained normalized *T-Z* load transfer curves, where unit resistance is normalized using the maximum measured values and displacement is normalized using pile width. The initial slope of the measured curves appears to match well with the API obtained curve. However, the agreement between measured and empirical normalized curve shapes past this initial portion is of poor quality. Measured curves show a lesser slope of normalized shaft resistance versus normalized displacement compared to that of both empirical curves.

Figure 5-21 presents the results of the comparison of experimentally measured and empirical *Q-Z* load transfer curves utilizing peak resistance from the LCPC method.

Here we can see the agreement between empirical and experimental results is better than that was observed for the *T-Z* curves, however the empirically obtained curves under predict measured values by a factor of approximately two. Figure 5-22 presents the results of the comparison of measured and empirical normalized *Q-Z* load transfer curves. This comparison shows the peak measured resistance value is mobilized at a displacement that is captured reasonably well by the empirical curves. The curve shape provided by Vijayvergiya (1977) provides the best match with experimental results with good agreement existing between predicted displacement required for development of peak resistance values.

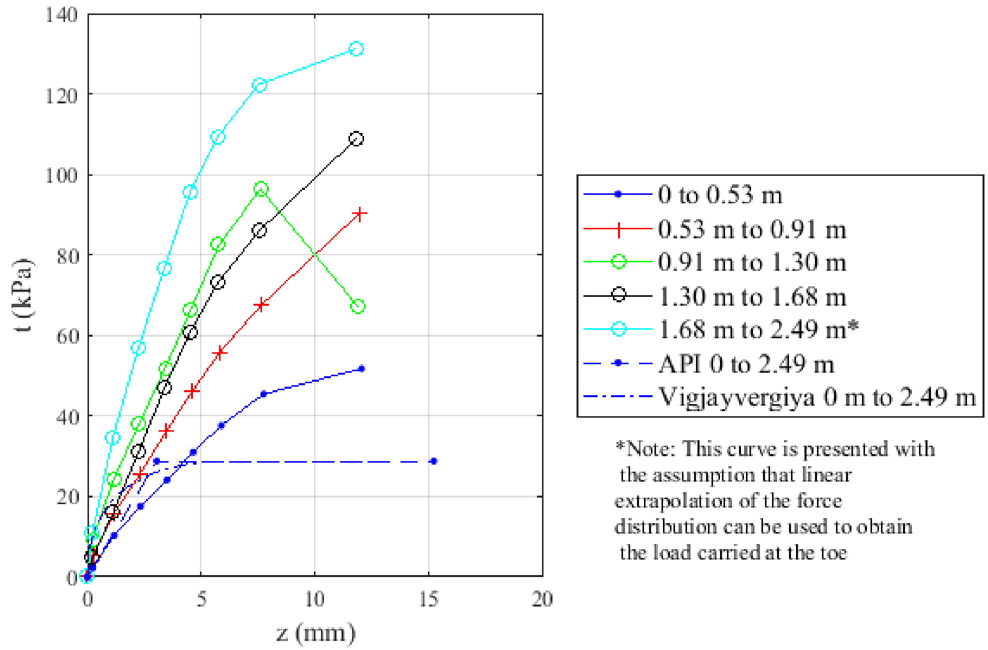


Figure 5-19. Comparison of experimentally measured and empirical *T-Z* load transfer curves utilizing peak resistance values from the LCPC method for sheet piles at the lab

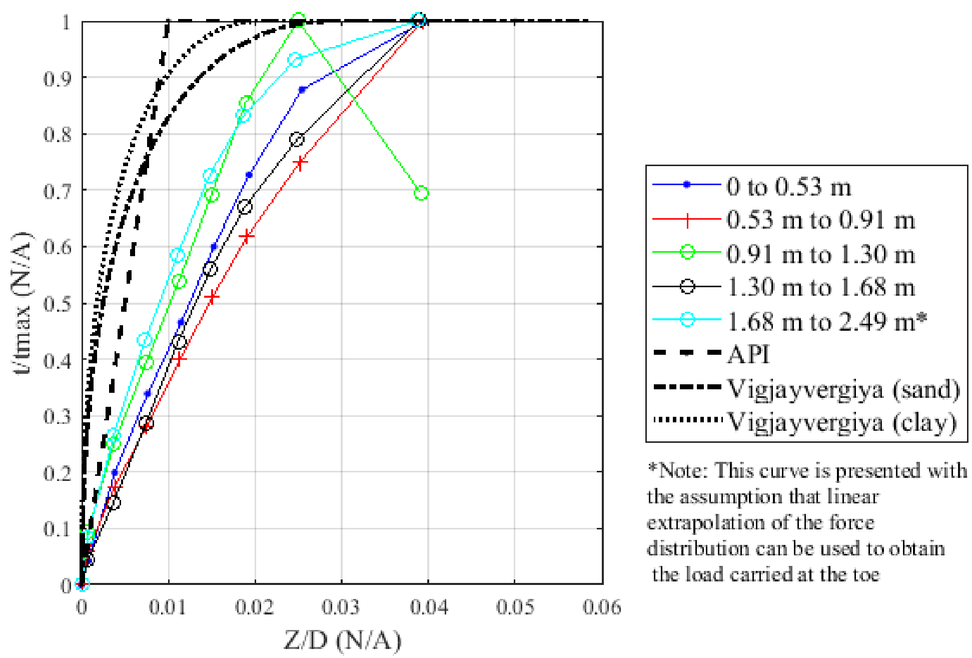


Figure 5-20. Comparison of normalized experimentally measured and empirical *T-Z* load transfer curves for sheet piles at the lab

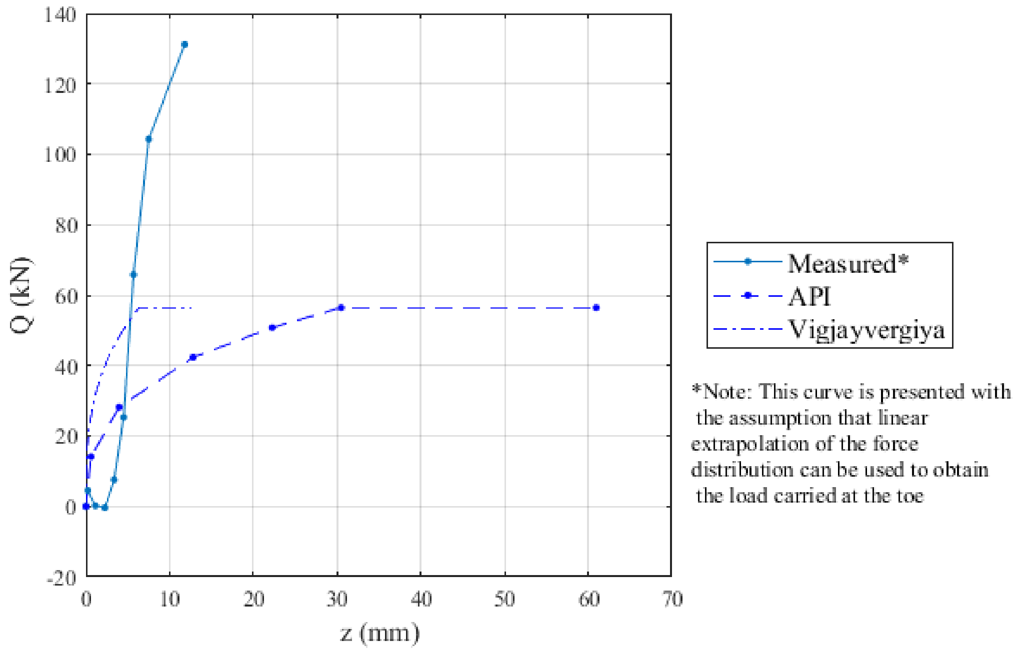


Figure 5-21. Comparison of experimentally measured and empirical *Q-Z* load transfer curves utilizing peak resistance values from the LCPC method for sheet piles at the lab

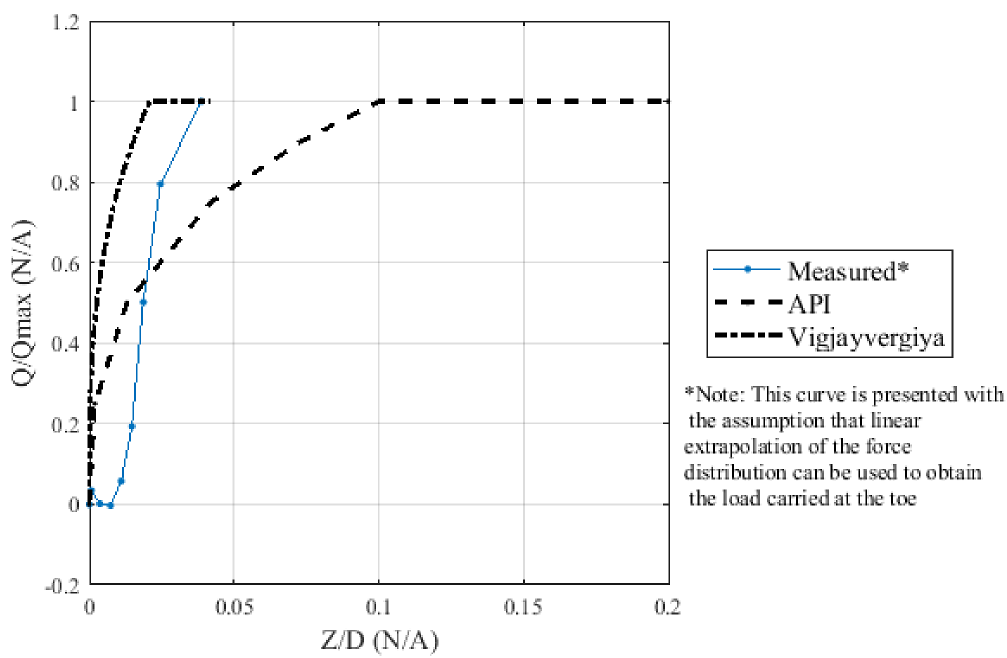


Figure 5-22. Comparison of normalized experimentally measured and empirical *Q-Z* load transfer curves for the sheet piles at the lab

Figure 5-23 presents the comparison between measured *T-Z* curves and empirical curves based on maximum resistance values provided by the Meyerhof method. The agreement between measured and empirical curves is poor, with empirical results under predicting measured values by a very large margin up to a factor of approximately twelve. The agreement between the two sets of curves is worse than the agreement presented in Figure 5-19. This agrees with the results presented earlier indicating that the peak shaft resistance values provided by the Meyerhof method provide a worse prediction of shaft capacity as compared to the LCPC method. Figure 5-24 presents the *Q-Z* load transfer curves obtained from empirical methods and experimental measurements. The agreement between peak predicted toe resistance and measured values is excellent with measured peak resistance values exceeding predicted values by a factor of approximately 0.08 or less than 10%. Due to the same assumed layering, toe resistance, and toe displacements used for generating all experimental *T-Z* and *Q-Z* curves, the same normalized plots are obtained for both sets of comparisons. The normalized curve shapes presented in Figure 5-20 and Figure 5-22 can be referenced for ascertaining the degree of fit between predicted and measured curves.

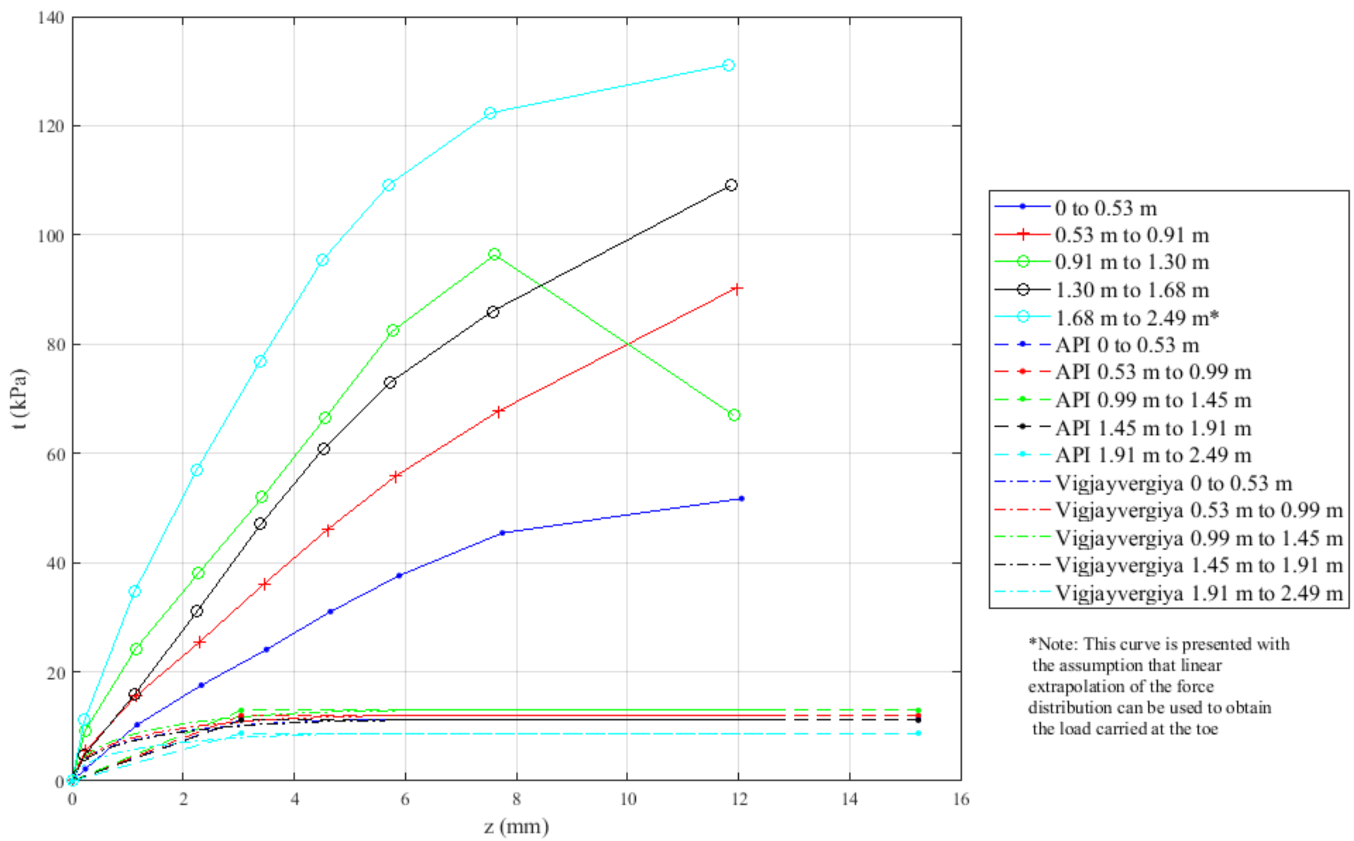


Figure 5-23. Comparison of experimentally measured and empirical T-Z load transfer curves utilizing peak resistance values from the Meyerhof method for sheet piles at the lab

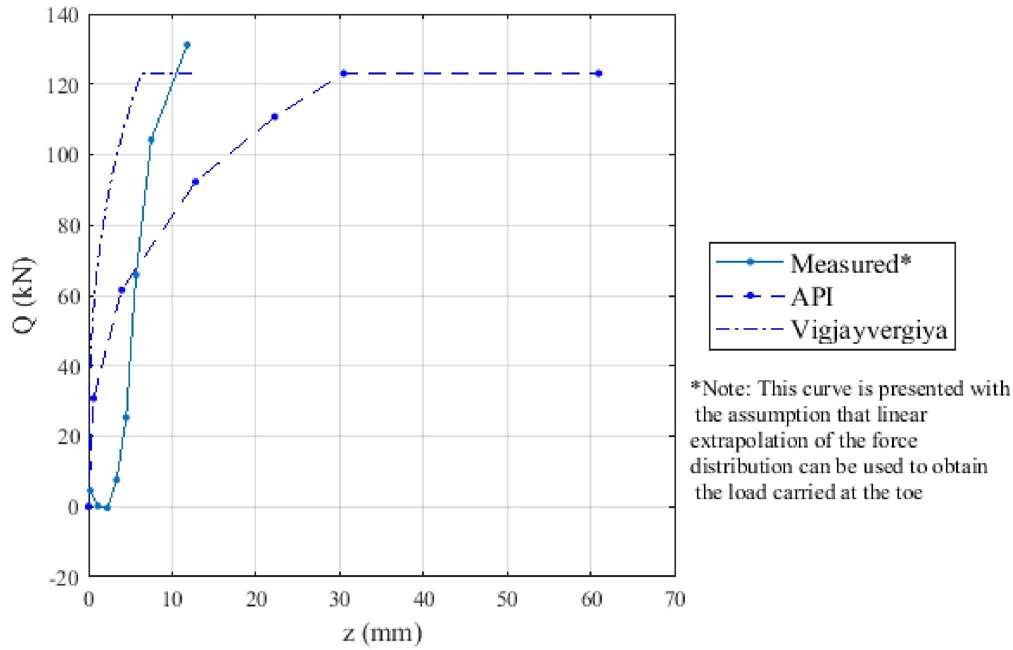


Figure 5-24. Comparison of experimentally measured and empirical *Q-Z* load transfer curves utilizing peak resistance values from the Meyerhof method for sheet piles at the lab

Overall, the empirically obtained load transfer curves were generally not able to capture the experimentally obtained results. The comparison presented considers the curve shapes provided by API (1993) and Vijayvergiya (1977) used in combination with maximum resistance values obtained from the Meyerhof and LCPC methods. The poor agreement between max resistance values presented for the empirically obtained curves and measured *T-Z* and *Q-Z* values is due in part to the difficulty in predicting shaft and toe resistances for the laboratory tests using static methods. In addition to the poor agreement between maximum resistance values, poor agreement exists between both curve shapes. The poor agreement between normalized curve shapes provided by the empirical methods and experimentally measured curves may be explained by the failure of the test to fully mobilize the test piles. It is not clear if shaft and toe resistance were fully mobilized due to the slope measured in the load transfer curves at large displacement values. In other words, the measured load transfer curves may not have reached the characteristic plateau usually observed when peak shaft and toe resistance values are reached. However, despite the generally poor agreement between both sets of curves, the load transfer curves for the *Q-Z* behavior did indicate fair to good agreement with the curve shape proposed by Vijayvergiya (1977) . Furthermore, the maximum resistance values predicted using the Meyerhof method provided excellent predictions of the maximum load bearing resistance at the pile toe.

### 5.3.2 Numerical Evaluation of Field Tests

#### 5.3.2.1 Axial Capacity Estimates Using Static Methods

Axial load capacity predictions based on static methods for the field sheet piles and H-pile tested at the ICE facility are presented in this section. The results of the predictions made with the different static methods are compared in summary plots. Each summary plot includes a horizontal dashed line that corresponds to the measured value at the failure load predicted using the Davisson failure criterion.

Figure 5-25 and Figure 5-26 present the summary plots for the total capacity predictions for the sheet piles and H-pile, respectively. As seen in these figures, all methods considered over predict the total capacities for both pile types. The figures indicate predicted capacities have a similar degree of accuracy for both pile types for any given method. Figure 5-27 and Figure 5-28 present the results of the total capacity predictions for the sheet piles and H-pile, respectively. Again, these prediction results show calculated values over predict the measured shaft capacity for both the sheet piles and H-pile, and a similar degree of accuracy was observed between the sheet pile and H-pile values for any given method. Predicted capacity values assuming plugging were most accurate for both pile types, and the CPT methods resulted in the highest degree of over prediction for this set of estimates. Figure 5-29 and Figure 5-30 present the results of the toe capacity predictions for the sheet piles and H-pile, respectively. These figures indicate predicted toe capacity values for the no plugging condition produced the most accurate values when compared to measured toe capacities for both the sheet piles and H-pile. In general, the methods considered had a higher degree of accuracy for the H-pile as compared to the sheet pile. Table 5-5 and Table 5-6 provide summaries of the results presented in the above referenced figures for the sheet pile and H-pile results, respectively.

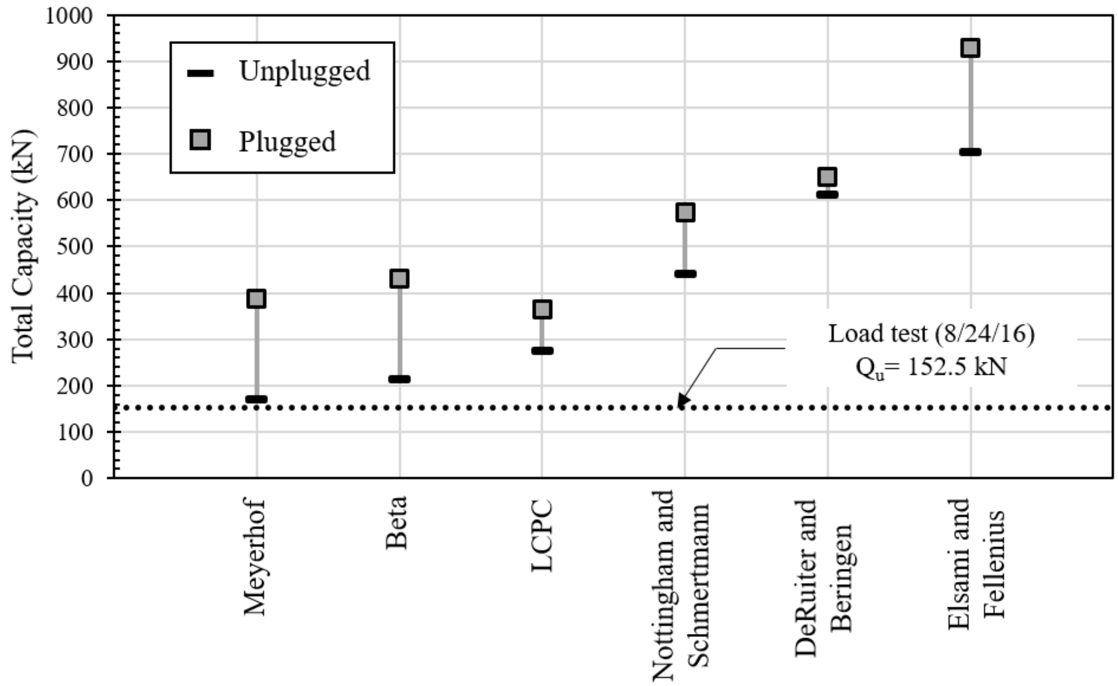


Figure 5-25. Summary of predicted pile load capacity for plugged and unplugged conditions compared to measured axial capacity for field test on sheet piles

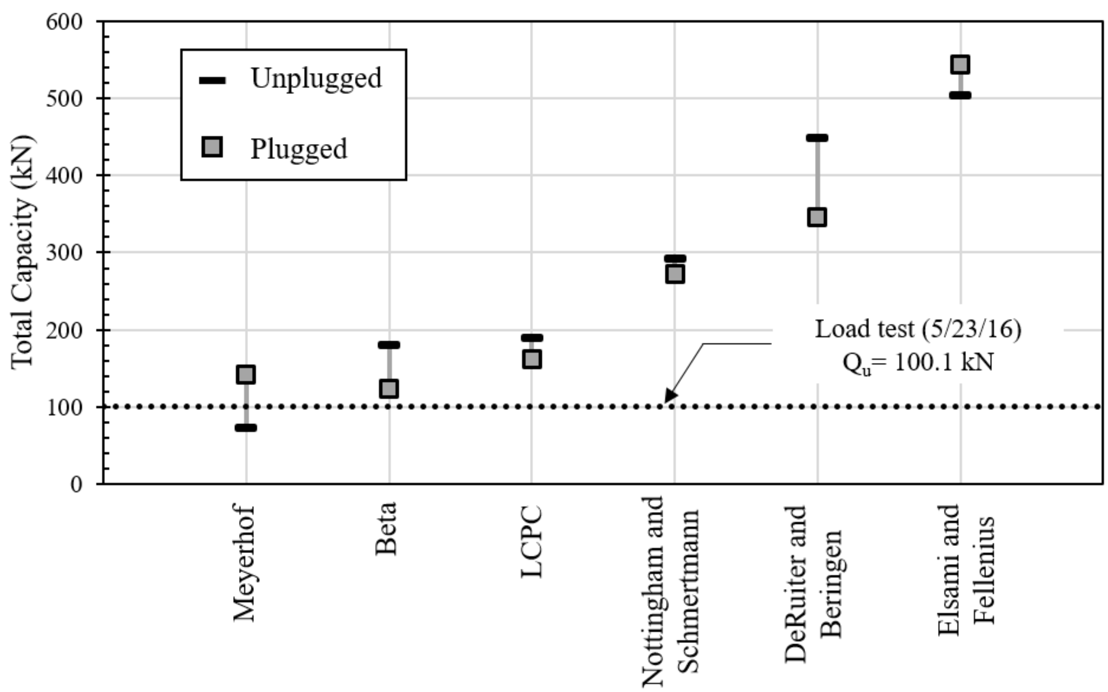


Figure 5-26. Summary of predicted pile load capacity for plugged and unplugged conditions compared to measured axial capacity for field test on H-pile

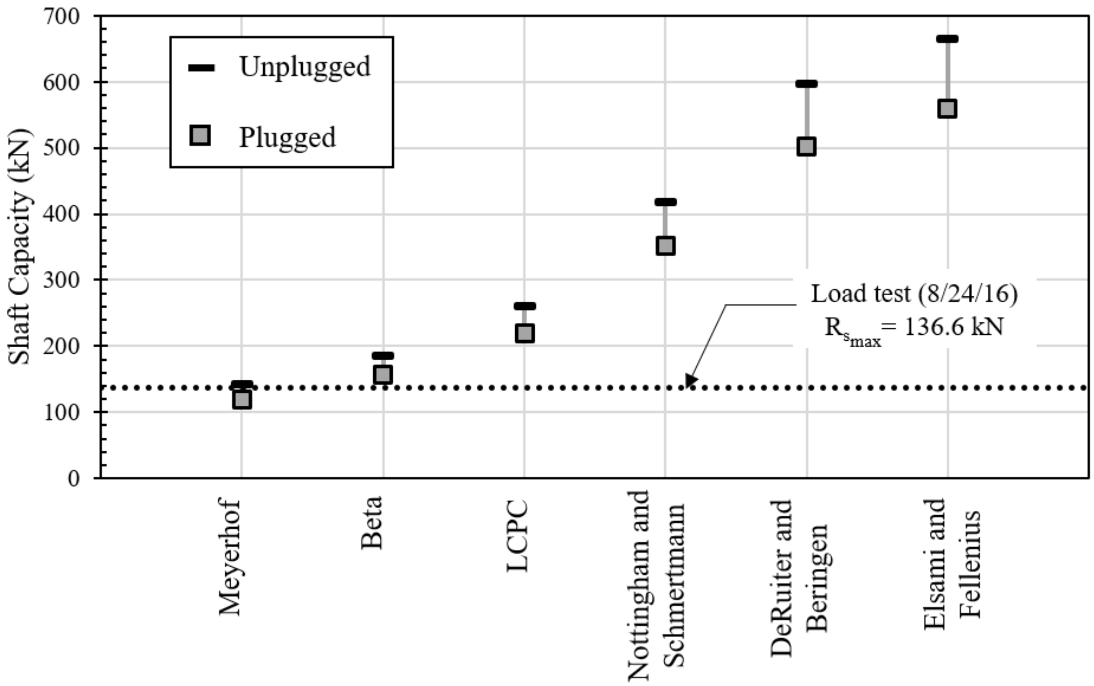


Figure 5-27. Summary of predicted shaft capacity for plugged and unplugged conditions compared to measured shaft capacity for field test on sheet piles

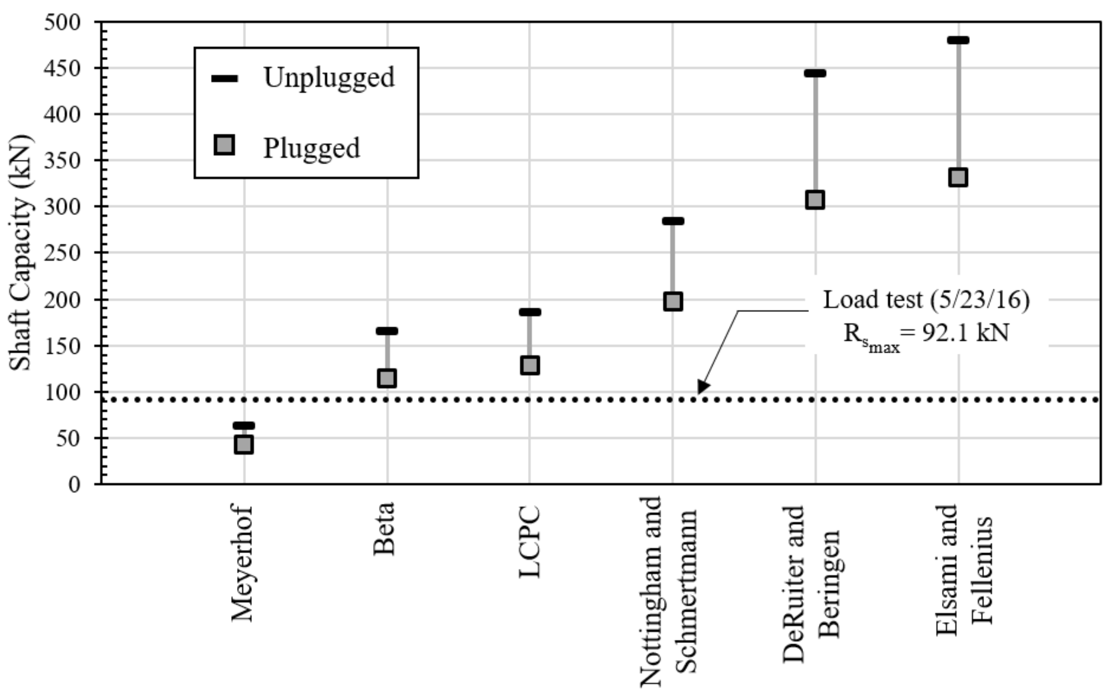


Figure 5-28. Summary of predicted shaft capacity for plugged and unplugged conditions compared to measured shaft capacity for field test on H-pile

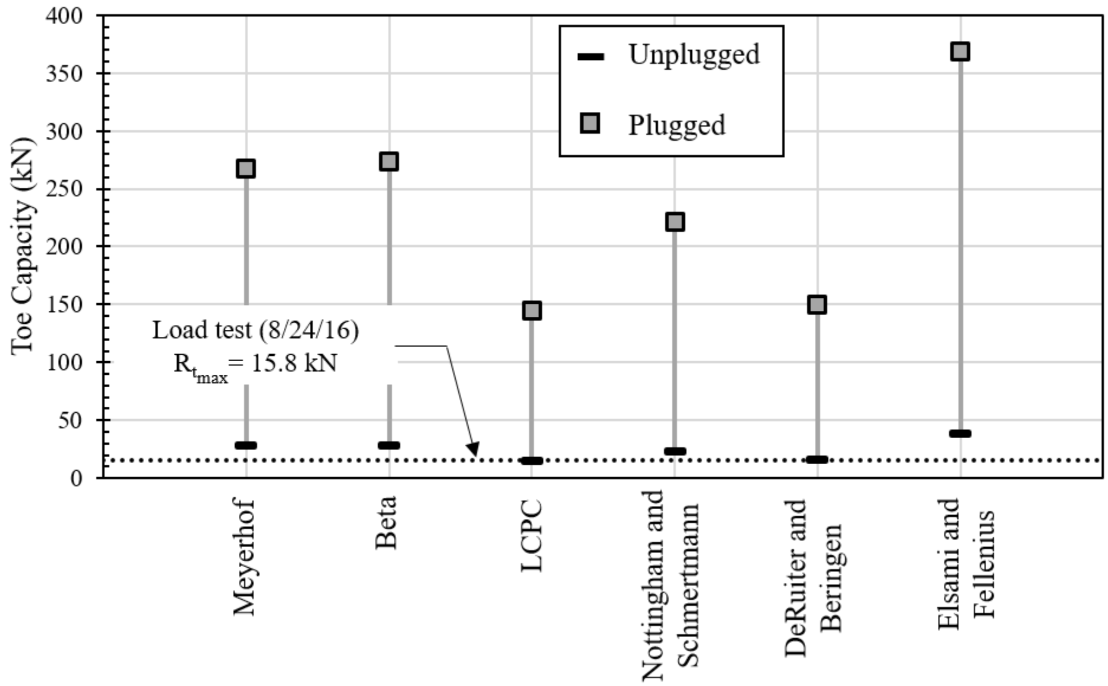


Figure 5-29. Summary of predicted toe capacity for plugged and unplugged conditions compared to measured toe capacity for field test on sheet piles

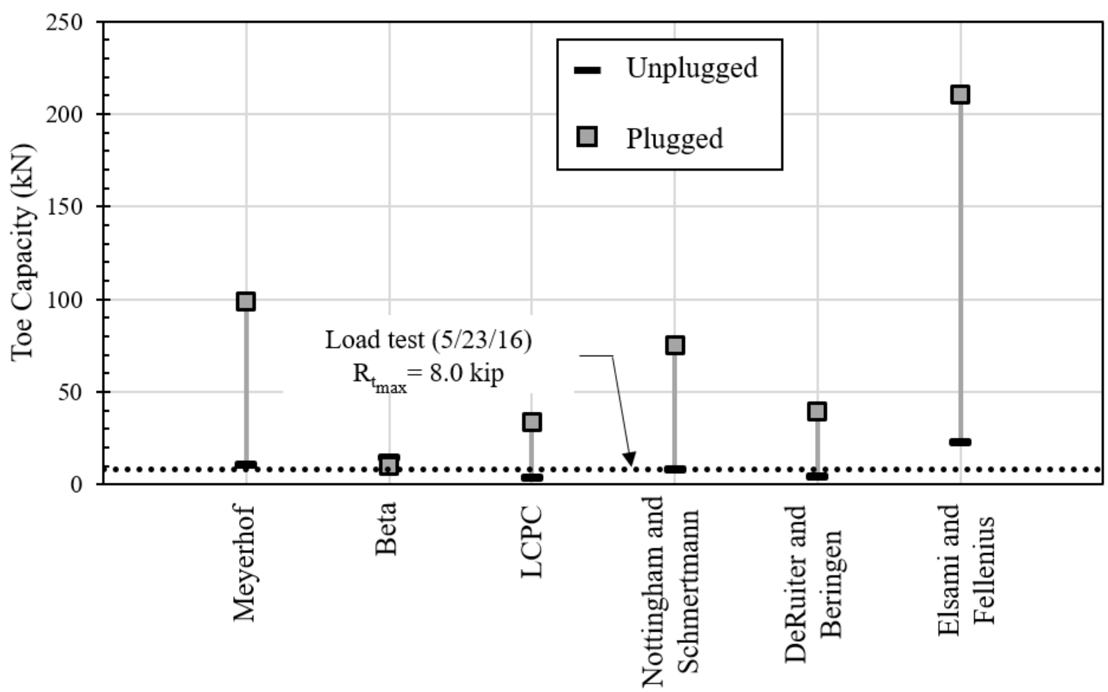


Figure 5-30. Summary of predicted toe capacity for plugged and unplugged conditions compared to measured toe capacity for field test on H-pile

Table 5-5. Predicted versus measured axial capacities for field testing of sheet piles

| Prediction Method | | Total Capacity | | Shaft Capacity | | Toe Capacity | |
|---|---|---|---|---|---|---|---|
| | | $Q_c$ (kN) | $Q_c/Q_m$ | $Q_c$ (kN) | $Q_c/Q_m$ | $Q_c$ (kN) | $Q_c/Q_m$ |
| Meyerhof | Unplugged | 170.7 | 1.1 | 142.7 | 1.0 | 28.0 | 1.7 |
| | Plugged | 387.9 | 2.5 | 120.1 | 0.9 | 267.8 | 16.7 |
| Beta | Unplugged | 214.0 | 1.4 | 185.3 | 1.4 | 28.7 | 1.8 |
| | Plugged | 430.0 | 2.8 | 156.0 | 1.1 | 273.9 | 17.1 |
| LCPC | Unplugged | 275.2 | 1.8 | 260.1 | 1.9 | 15.1 | 0.9 |
| | Plugged | 363.7 | 2.4 | 218.9 | 1.6 | 144.8 | 9.0 |
| Nottingham & Schmertmann | Unplugged | 451.3 | 3.0 | 428.1 | 3.1 | 23.2 | 1.4 |
| | Plugged | 589.4 | 3.9 | 367.6 | 2.7 | 221.8 | 13.8 |
| DeRuiter & Beringen | Unplugged | 611.6 | 4.0 | 595.9 | 4.4 | 15.7 | 1.0 |
| | Plugged | 651.7 | 4.3 | 501.6 | 3.7 | 150.1 | 9.4 |
| Elsami & Fellenius | Unplugged | 703.6 | 4.6 | 665.0 | 4.9 | 38.5 | 2.4 |
| | Plugged | 543.1 | 3.6 | 332.2 | 2.4 | 210.8 | 13.2 |

Note: $Q_c$= Calculated capacity using static methods, $Q_m$= measured value corresponding to Davisson's failure criterion (total= 152.6 kN, shaft= 136.6 kN, toe= 16.0 kN). $Q_c/Q_m$= the ratio of calculated to measured capacity

Table 5-6. Predicted versus measured axial capacities for field testing of H-pile

| Prediction Method | | Total Capacity | | Shaft Capacity | | Toe Capacity | |
|---|---|---|---|---|---|---|---|
| | | $Q_c$ (kN) | $Q_c/Q_m$ | $Q_c$ (kN) | $Q_c/Q_m$ | $Q_c$ (kN) | $Q_c/Q_m$ |
| Meyerhof | Unplugged | 73.7 | 0.7 | 62.9 | 0.7 | 10.8 | 1.4 |
| | Plugged | 142.5 | 1.4 | 43.5 | 0.5 | 99.0 | 12.4 |
| Beta | Unplugged | 179.8 | 1.8 | 165.5 | 1.8 | 14.3 | 1.8 |
| | Plugged | 124.4 | 1.2 | 114.5 | 1.2 | 9.9 | 1.2 |
| LCPC | Unplugged | 190.0 | 1.9 | 186.3 | 2.0 | 3.7 | 0.5 |
| | Plugged | 162.3 | 1.6 | 128.9 | 1.4 | 33.4 | 4.2 |
| Nottingham & Schmertmann | Unplugged | 308.0 | 3.1 | 299.8 | 3.3 | 8.2 | 1.0 |
| | Plugged | 287.4 | 2.9 | 212.3 | 2.3 | 75.1 | 9.4 |
| DeRuiter & Beringen | Unplugged | 448.4 | 4.5 | 444.1 | 4.8 | 4.3 | 0.5 |
| | Plugged | 346.4 | 3.5 | 307.3 | 3.3 | 39.1 | 4.9 |
| Elsami & Fellenius | Unplugged | 503.2 | 5.0 | 480.2 | 5.2 | 23.1 | 2.9 |
| | Plugged | 543.1 | 5.4 | 332.2 | 3.6 | 210.8 | 26.3 |

Note: $Q_c$= Calculated capacity using static methods, $Q_m$= measured value corresponding to Davisson's failure criterion (total= 100.1 kN, shaft= 92.1 kN, toe= 8.0 kN). $Q_c/Q_m$= the ratio of calculated to measured capacity

The methods considered produced ratios of calculated to total capacity ($Q_c/Q_m$) values for the sheet piles ranging from 1.11 to 4.61 for the unplugged condition and 2.38 to 4.27 for the plugged condition. Values determined for $Q_c/Q_m$ for toe capacity for the sheet pile were much closer to unity for unplugged conditions as compared to plugged conditions.

Values determined for $Q_c/Q_m$ for the shaft capacity for the sheet piles obtained from SPT methods ranged from 1.04 to 1.36 and 0.88 to 1.14 for the unplugged and plugged assumptions, respectively. Values determined for $Q_c/Q_m$ for the shaft capacity for the sheet pile obtained from CPT methods ranged from 2.0 to 5.2 and 1.4 to 3.6 for the unplugged and plugged assumptions, respectively. A similar trend is observed for the H-pile. These results indicate SPT based capacity estimates to have a higher degree of accuracy for the sheet piles. Ratio values are closer to unity for plugged capacity estimates as compared to unplugged capacity values, suggesting plugging may have occurred along the shaft of the test piles.

Values determined for $Q_c/Q_m$ for the toe capacity for the sheet piles obtained from all methods ranged from 0.95 to 2.41 and 9.04 to 17.11 for the unplugged and plugged assumptions, respectively. A similar trend was observed for the H-pile, where predictions assuming no plugging yielded values with higher accuracy as compared to the measured toe capacities. This would suggest that plugging at the toe was not encountered for both test piles. Furthermore, based on measured SCPTu tip resistances near the toe soils encountered were a soft, low plastic sandy silt that is not likely to promote plug formation.

Based on the results of these comparisons, it is not possibly to definitively state if plugging occurred or not. Results suggest that plugging at the toe did not occur but some degree of plugging may have occurred along the pile shaft. The static methods considered produced similar degrees of accuracy for both the sheet piles and H-pile. Similar to findings from the laboratory capacity values, it is recommended to use the lowest capacity values computed based on the assumed behavior of full or no plug formation. For the both test piles it was observed that shaft capacity estimates assuming full plugging produced the lowest values, while toe capacity estimates assuming no plugging produce the lowest values. A fully plugged condition at the pile toe should only be assumed when there is reasonable assurance based on field evidence from a project specific load test that a soil plug will form. Using this criteria when determining shaft and toe capacity estimates will lead to a lower probability of over predicting total pile axial load capacity.

5.3.2.2 Evaluation of Field Study Results Through Load Transfer Analyses

The load transfer curve shapes from API (1993) and Vijayvergiya (1977) utilizing peak resistance values from the Meyerhof and LCPC methods are compared with measured results and presented in this section, similar to the analyses performed for the laboratory test. Empirical load transfer curves are used to develop load-settlement curves and these were prepared for both a plugged and unplugged condition, similar to the approach used with the static method predictions. Figure 5-31 summarized the results from these tests.

The agreement between predicted and measured curves varies. The best predicted load-settlement curve is provided with Meyerhof obtained maximum unit shaft resistances and the Vijayvergiya (1977) method using an unplugged condition assumption. The agreement between this predicted curve and measured values is good. The level of agreement between predicted and measured load-settlement curves can be further explained by comparing the predicted and measured *T-Z* and *Q-Z* curves.

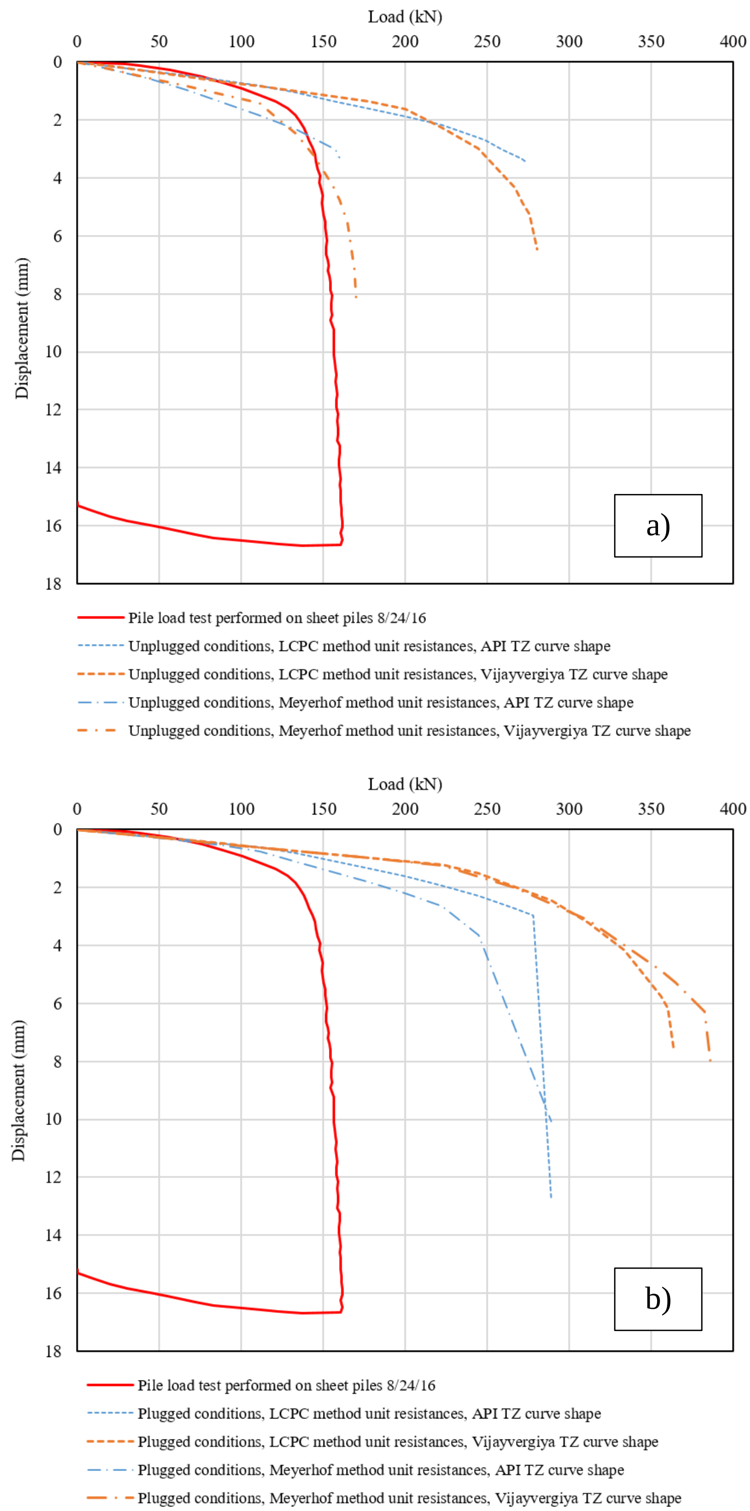


Figure 5-31. Predicted and measured load-settlement curves for a) unplugged and b) plugged conditions for field pile load testing

Figure 5-32 presents a comparison between the measured *T-Z* curves from the field test and predicted *T-Z* curves using maximum resistance values obtained from the LCPC method. For this comparison, separate *T-Z* curves are generated for each layer of soil based on measurements from the CPT and soil stratigraphy. As can be seen in the load transfer figure, the empirical curves provide a fair to poor prediction of peak unit resistance compared with experimentally measured values, with empirically obtained curves over predicting capacity by a factor of up to approximately two to three. However, the empirical curves do have aspects that compare well with the experimental curves such as the displacement required to reach peak resistance values. Figure 5-33 presents a comparison between the normalized measured *T-Z* curves from the field test and predicted *T-Z* curves, where unit resistance is normalized using the maximum measured values and displacement is normalized using pile width. The measured curves presented represent the soil layering based on CPT and soil stratigraphy. The empirical methods provide reasonable comparisons to the measured *T-Z* curve shape, and in general the curve shape presented by Vijayvergiya (1977) for clay provides the best match with measured values. Figure 5-34 and Figure 5-35 present a similar comparison for the *Q-Z* load transfer curve. The agreement between the empirical and measured curves is fair, where empirical curves over predict measured capacity by a factor of approximately 1.25, and again Vijayvergiya (1977) provides the best agreement in terms of curve shape.

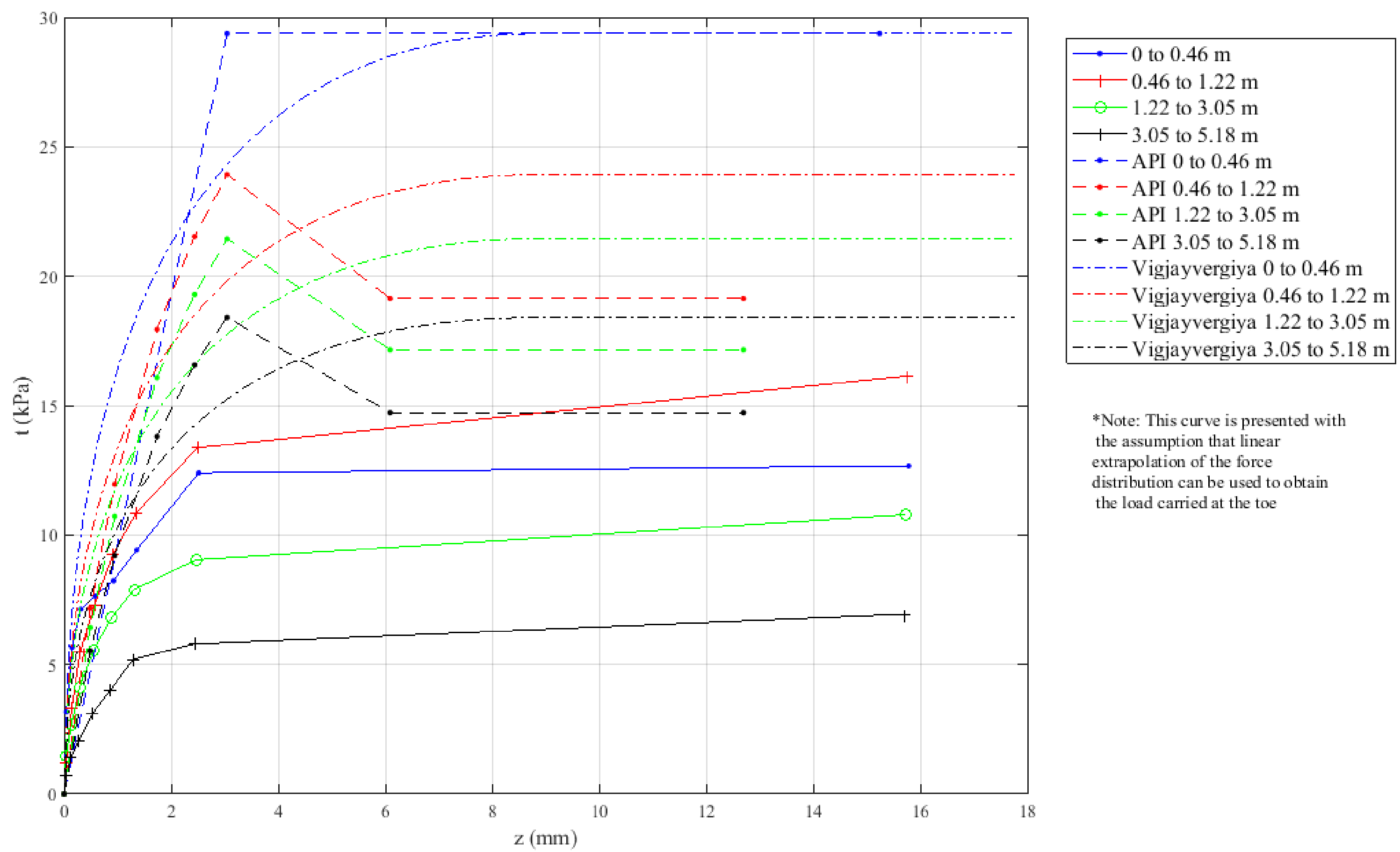


Figure 5-32. Comparison of experimentally measured and empirical T-Z load transfer curves utilizing peak resistance values from the LCPC method for sheet piles at the field site

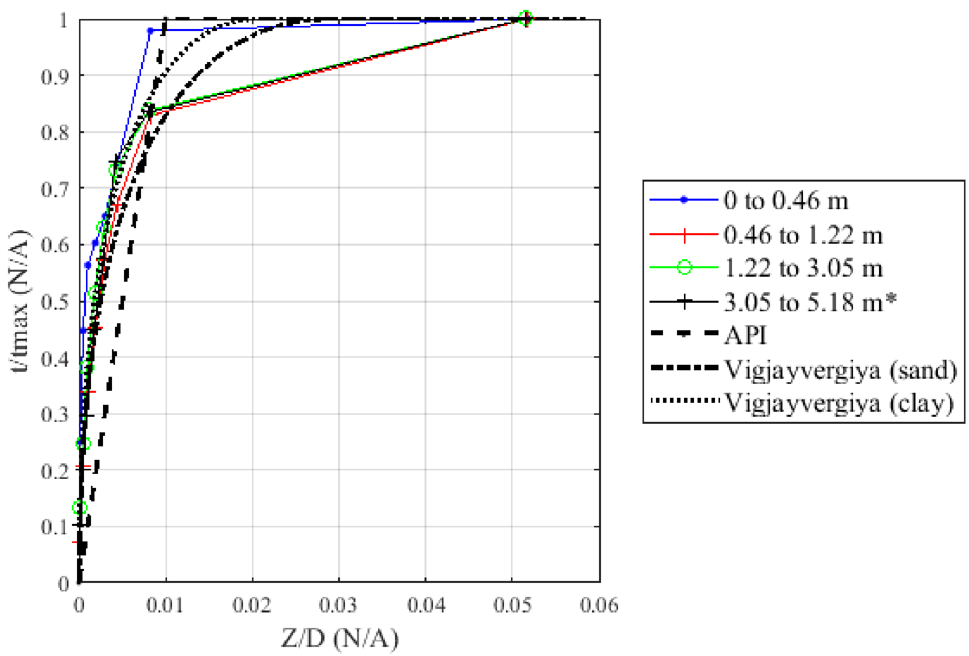


Figure 5-33. Comparison of normalized experimentally measured and empirical *T-Z* load transfer curves utilizing peak resistance values from the LCPC method for sheet piles at the field site

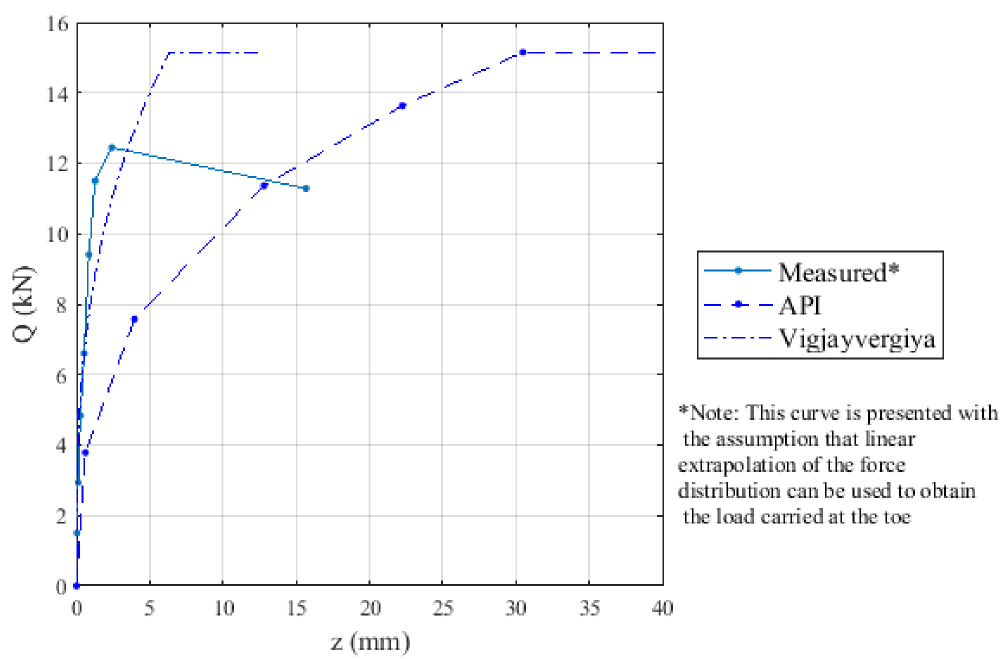


Figure 5-34. Comparison of experimentally measured and empirical *Q-Z* load transfer curves utilizing peak resistance values from the LCPC method for sheet piles at the field site

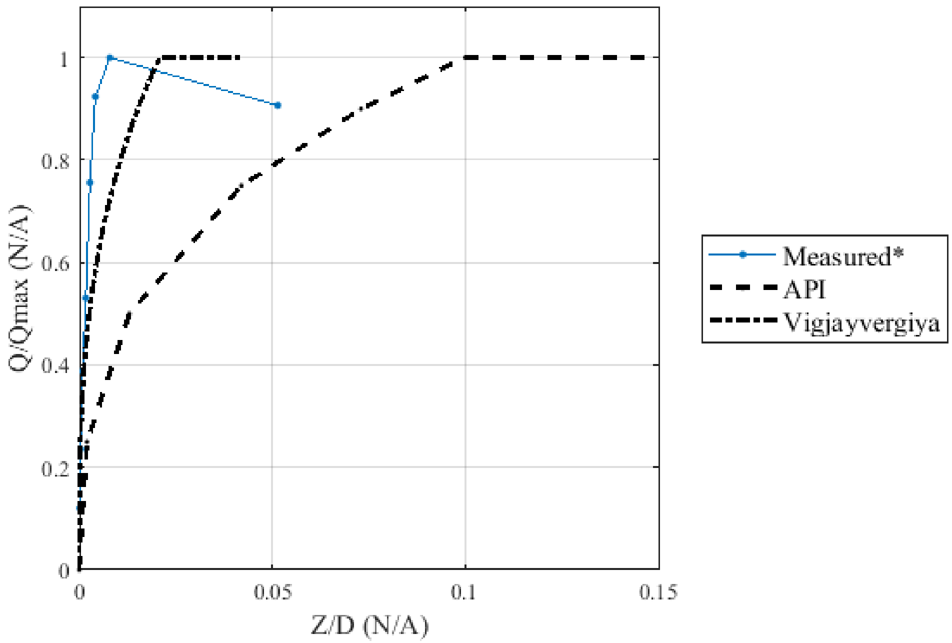


Figure 5-35. Comparison of normalized experimentally measured and empirical *Q-Z* load transfer curves for the sheet piles at the field site

Figure 5-36 presents the comparison between measured *T-Z* curves and empirical curves based on maximum resistance values provided by the Meyerhof method. The layering used in this comparison corresponded to the location of SPT data. As shown in the figure, fair to good agreement exists between the empirical curves and experimentally measured *T-Z* values, both in terms of curve shape and magnitude of peak unit resistance values. Figure 5-37 presents normalized *T-Z* curves from empirical calculations and experimental measurements, where unit resistance is normalized using maximum measured resistance values and displacement is normalized using pile diameter. The agreement between both curve shapes is good. Similar to the curves presented in Figure 5-33, the best agreement with the experimental curves is provided by the curve shape presented by Vijayvergiya (1977) for clay. Lastly, Figure 5-38 presents the *Q-Z* load transfer curves from empirical calculations and experimental measurements. The agreement between the two sets of curves is poor with empirically obtained curves over predicting measured values by a factor greater than approximately two. Due to the same toe resistance and displacement values used for *Q-Z* load transfer curve development, the same observations made regarding the normalized curves in Figure 5-35 apply for this analysis.

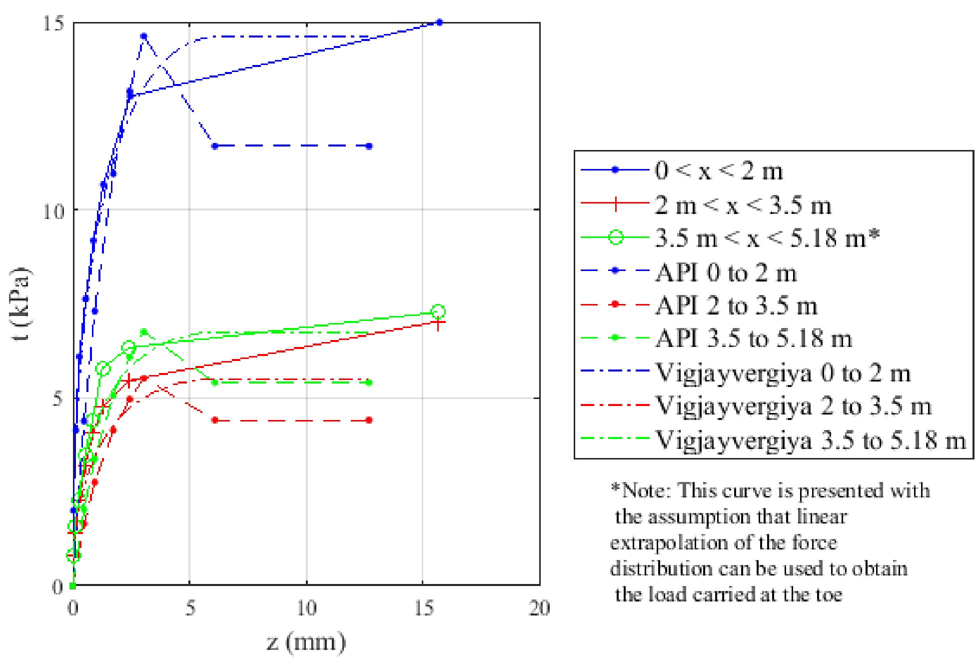


Figure 5-36. Comparison of experimentally measured and empirical *T-Z* load transfer curves utilizing peak resistance values from the Meyerhof method for sheet piles at the field site

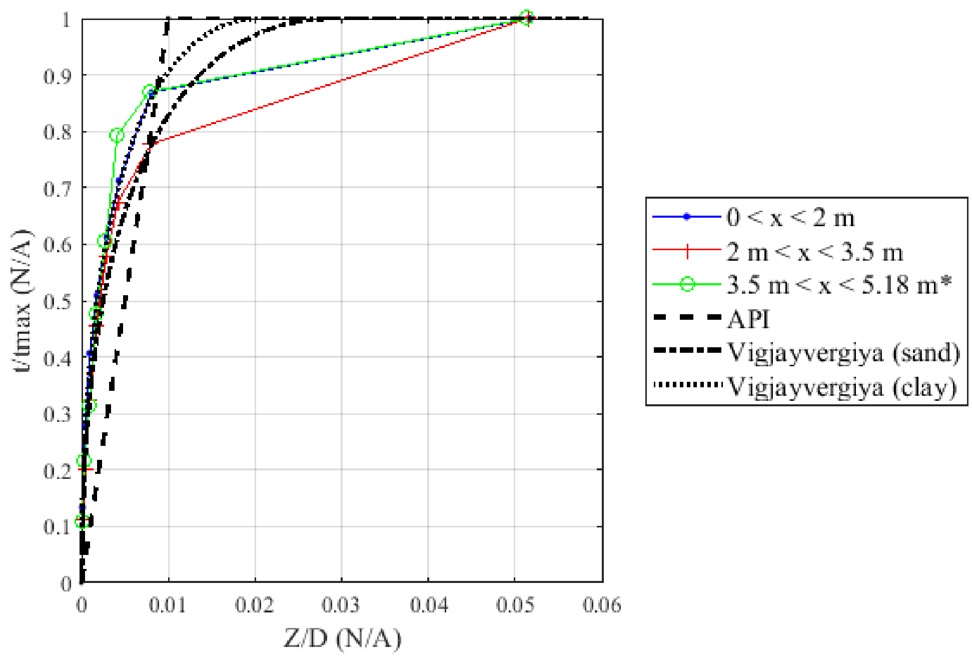


Figure 5-37. Comparison of normalized empirical and experimentally measured *T-Z* load transfer curves based on the defined layers used to compare to results from the Meyerhof method for sheet piles at the field site.

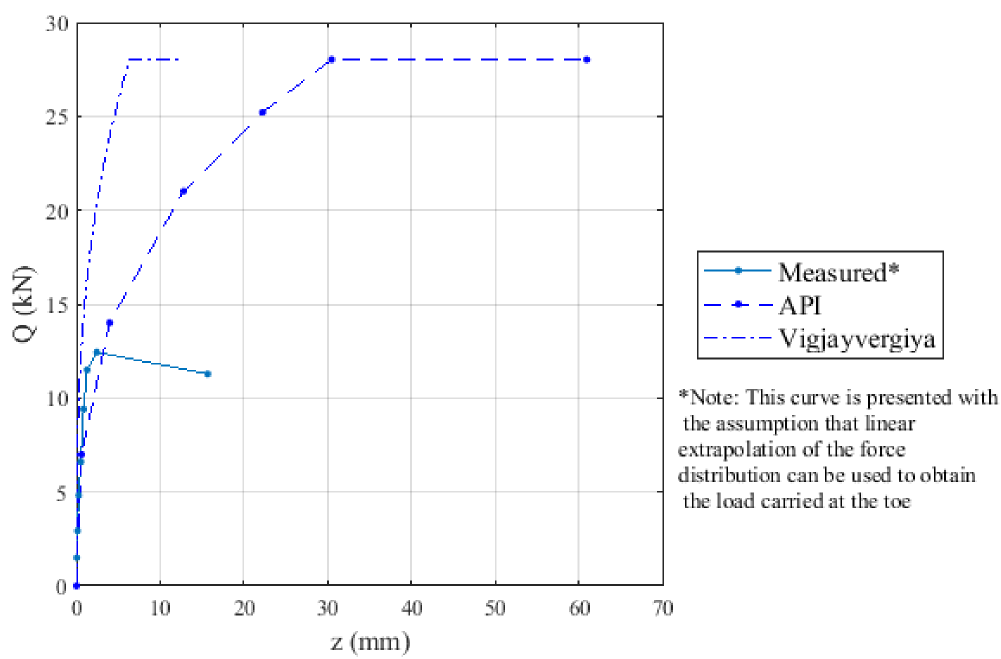


Figure 5-38. Comparison of experimentally measured and empirical *Q-Z* load transfer curves utilizing peak resistance values from the Meyerhof method for sheet piles at the field site

Overall, the empirically obtained load transfer curves were able to capture experimentally obtained results reasonably well. Curve shape and maximum resistance values define these curves. The curve shapes provided by API (1993) and Vijayvergiya (1977) were considered in this comparison. Two of the most accurate static methods of predicting ultimate capacity utilizing SPT and CPT data were considered in order to obtain maximum unit resistance values, these were the Meyerhof and LCPC methods, respectively. Based on the comparison with LCPC derived unit resistance values, poor agreement was found between empirical and experimental *T-Z* curves. Unit resistance values obtained using LCPC were found to over predict measured values by a wide margin. In contrast, toe resistance values predicted from LCPC was found to have good agreement with measured values. The empirical *T-Z* curves obtained with Meyerhof based resistance values had good to excellent agreement with experimental values. The empirical *Q-Z* curve created with Meyerhof based resistance values was found to have poor agreement with measured values, and empirical values over predicted measured values by a wide margin. This comparison indicates the LCPC method is able to provide reasonably accurate toe resistance values while the Meyerhof method provides reasonably accurate shaft resistance values. These findings reinforce the comparisons found in section 5.3.2.1 and the curve shapes developed by Vijayvergiya (1977) for clay provided reasonably accurate predictions compared with the measured curves.

### 5.3.3 Predicted Load Transfer Behavior Using Derived Load Transfer Curves

The derived load transfer curves previously presented for a plate pile are evaluated using results from the pile load tests performed at the field site. This section also compares the predicted *T-Z* load transfer curve shape obtained using the plate pile model and the concentric cylinder model with measured *T-Z* load transfer curves. *T-Z* and *Q-Z* curves are presented separately to facilitate the direct comparison between measured and calculated values for both curve types. A summary table of the analyses performed in this section using the theoretical *T-Z* and *Q-Z* curves is provided in Table 5-7. For this analysis, the field sheet piles were modeled as a pipe pile with an equivalent perimeter and cross sectional area using a commercially available software.

#### 5.3.3.1 Predicting Load-Settlement Curves With Load Transfer *T-Z* Curves

In order to develop *T-Z* curves, a maximum unit shaft resistance value and curve shape are required. The static methods considered in this study are used to provide this value with depth. Figure 5-39 presents the maximum unit shaft resistance, $f_{s_{\max}}$, obtained from all static methods considered in this study plotted versus depth. Additionally, calculated resistance values were averaged and bounds one standard deviation above and below were calculated and plotted. These curves were compared with measured values (red line). The majority of the methods considered over predict measured values, and the line calculated from the average maximum unit shaft resistance minus one standard deviation as well as values from the Meyerhof method provide the best agreement with measured values.

Table 5-7. Summary of models used to verify derived load transfer curves for plate pile

| Case No. | Source of $f_{s_{max}}$ | Source of $q_{t_{max}}$ | $r_0$ used for load transfer curve shapes (cm) | $r_m$ used for load transfer curve shapes (m) | Modified hyperbolic curve fitting parameters | | Equivalent pipe pile dimensions | | Notes |
|---|---|---|---|---|---|---|---|---|---|
| | | | | | $g$ value *TZ* (*QZ*) | $f$ value *TZ* (*QZ*) | Diameter (cm) | Thickness (cm) | |
| 1 | Avg. calculated | Measured | 15.24 | 51.23 | 0.3 | 1.0 | 90.72 | 0.54 | Considering $f_s$ only. Looking at two sets of values from static methods for predicting $f_s$. |
| 2 | Lower bound calculated | Measured | 15.24 | 51.23 | 0.3 | 1.0 | 90.72 | 0.54 | |
| 3 | Lower bound calculated | Calculated ($r_0$= 0.48 cm) | 15.24 | 51.23 | 0.3 | 1.0 | 90.72 | 0.54 | Considering $f_s$ and $q_t$. Looking at comparing concentric cylinder and plate pile models |
| 4 | Lower bound calculated | Calculated ($r_0$= 0.48 cm) | 15.24 | 17.71 | 0.3 | 1.0 | 90.72 | 0.54 | |

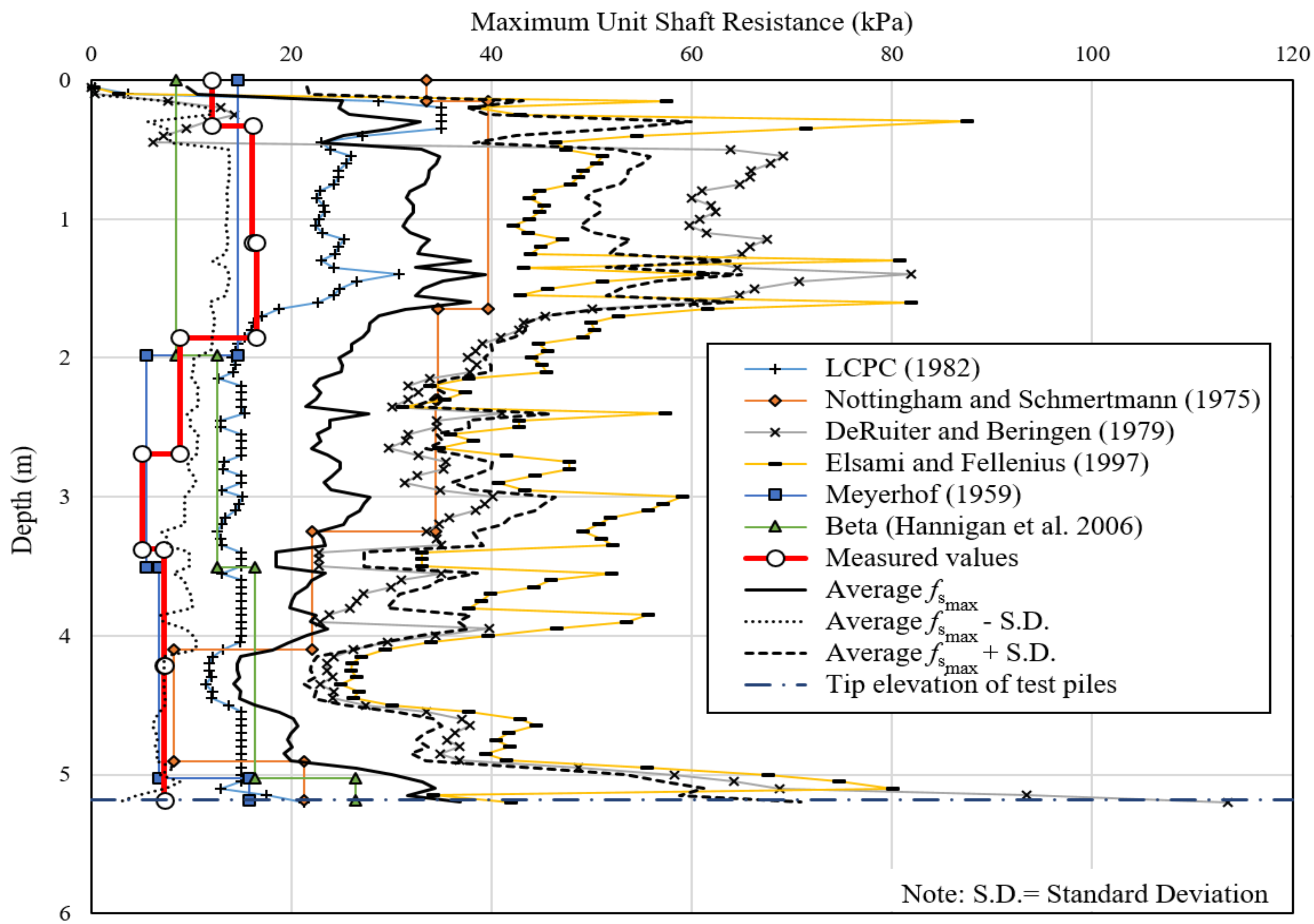


Figure 5-39. Calculated and measured maximum unit resistance values for field site

A final profile for shear wave velocity, $V_s$, was developed primarily based on direct field measurements of the field soil, although results from index testing were also considered in the development of this profile. The final layering consists of four layers with boundaries at 0.46, 1.22, 3.05, and 5.18 m. Weighted averaging is used to develop final $V_s$ and unit weight, $\gamma_t$, values for these layers. Unit weight values are obtained from measurements made on Shelby tube samples obtained through field testing. Figure 5-40 presents this profile. Values obtained from this profile are used to determine required $G_0$ values for developing the theoretical *T-Z* and *Q-Z* curves.

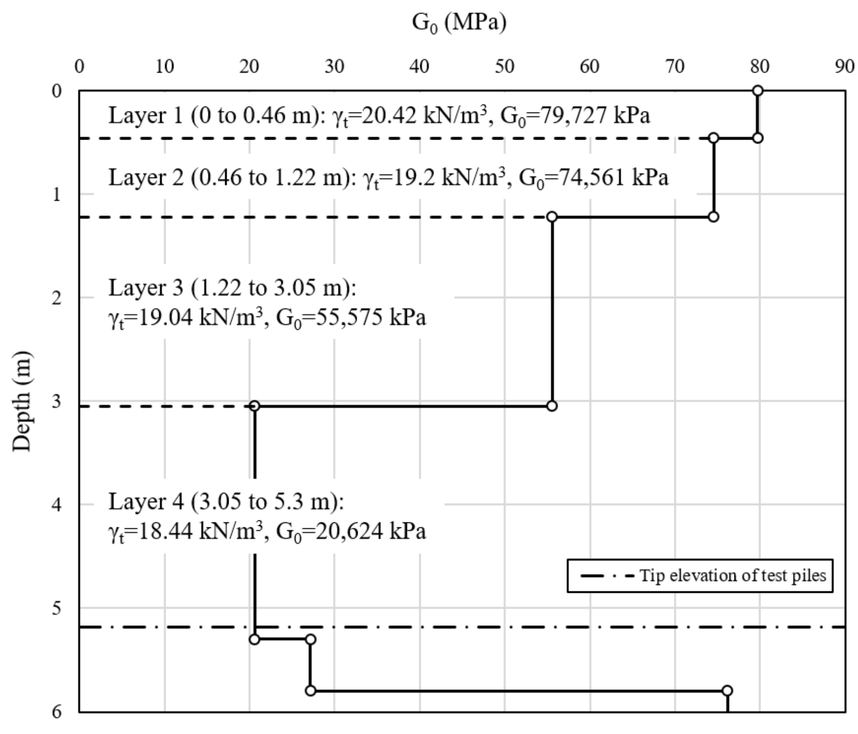


Figure 5-40. Maximum shear modulus versus depth and properties of selected layers for ICE field site

Based on the calculated $f_{s_{max}}$ with depth, the lower bound values and average values are considered for further analyses. For the selected predicted $f_{s_{max}}$ profiles, averaged values taken across each layer were used for *T-Z* curve development. Figure 5-41 presents these final $f_{s_{max}}$ values for *T-Z* curve development, together with the selected predicted $f_{s_{max}}$ profiles used to generate these values.

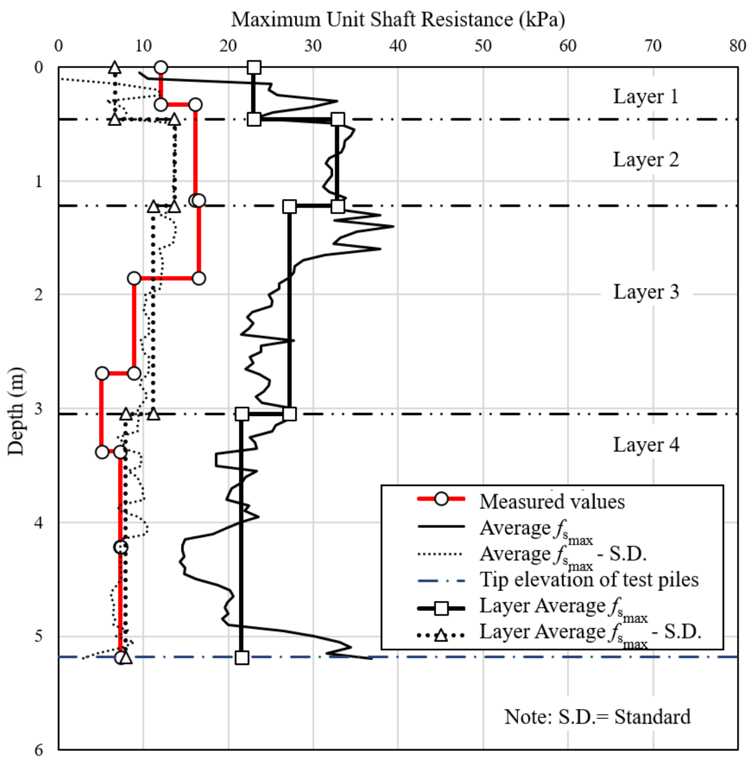


Figure 5-41. Calculated and measured maximum unit resistance values for field site with selected layers

Using the maximum unit shaft resistance values defined above, Figure 5-42 presents the developed *T-Z* curves, where curves are presented for theoretically obtained and measured values. These curves represent the *T-Z* curves developed using the lower bound maximum unit shaft resistances. The agreement between theoretically obtained and measured curves is fair. The curve shapes of the theoretically derived curves are in generally good agreement with measured values. It should be noted values of *f* and *g* of 1.0 and 0.3 were selected for the modified hyperbolic method used to develop the theoretical curves. These values were selected based previously reported curve fitting parameter values for Piedmont residual soils at a test site located at Atlanta, Georgia (Mayne 1995).

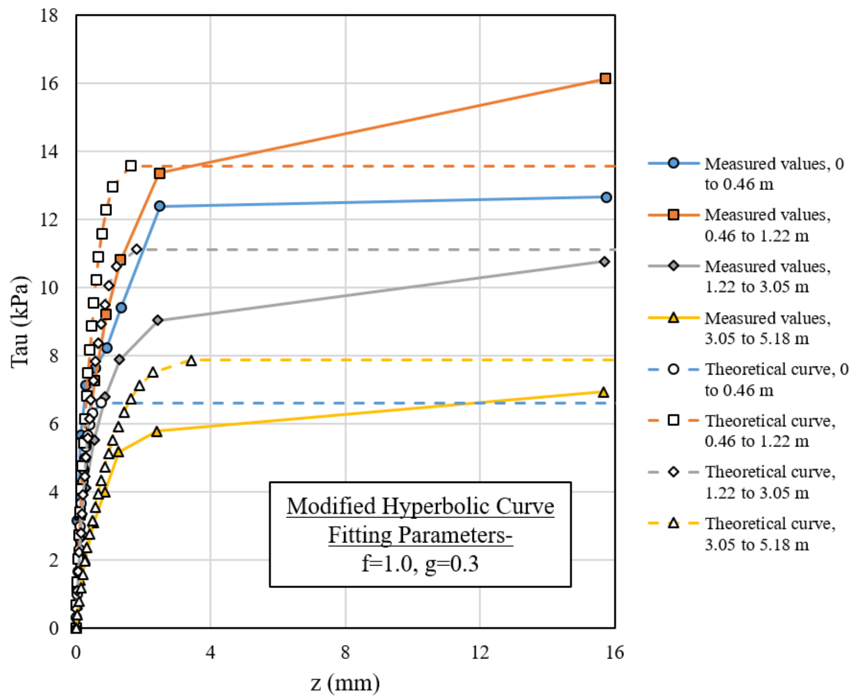


Figure 5-42. Comparison of measured and theoretically derived *T-Z* curves for field site using lower bound $f_{s_{\max}}$ values and layering presented in Figure 5-42

Predicted load-settlement behavior was evaluated. The toe behavior for all models in this analysis equals the measured *Q-Z* response at the field site. This facilitates the direct comparison of any deviations in the load-settlement response to the difference between theoretical and measured *T-Z* curves. Figure 5-43 presents the load-settlement results from this analysis. These results agree with the findings of Figure 5-39. Based on these results, the chosen values for maximum shaft resistance have a very large impact on predicting load-settlement behavior in sheet piles. The results of the theoretical derivations appear to capture well the shape of the load transfer curves. These results suggest the theoretical curves can accurately predict the load-settlement curves measured for the field site in this study when appropriate maximum unit shaft resistance values are used.

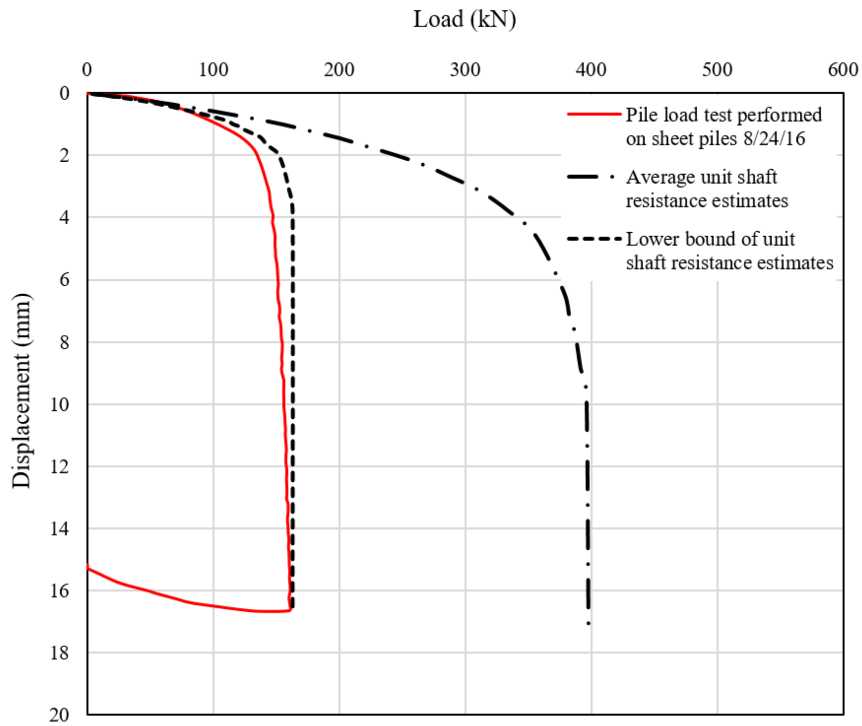

Figure 5-43. Measured versus calculated load-settlement curve for field site

5.3.3.2 Development of *Q-Z* Curves

This section considers the *Q-Z* curves developed based on the theoretical approach outlined in previous sections. Similar to *T-Z* curves, in order to develop *Q-Z* curves a maximum unit toe resistance value and curve shape are required. Normalized toe resistance values are considered in this section in order to avoid introduction of possible error in the comparison due to plugging. Figure 5-44 presents normalized *Q-Z* plots for the Boussinesq model for linear elastic soil, the modified hyperbolic soil model, and values measured from the field. Values for *f* and *g* equal 1.0 and 0.3, respectively, based on the Piedmont residual soils encountered at the site. The modified hyperbolic model provides a much better prediction over the linear elastic model. The measured curve shape shows reasonable agreement with the modified hyperbolic curve. Pile toe displacement required to reach maximum toe resistance equal 2.41 and 1.76 mm for measured values and predicted values from the modified hyperbolic curve, respectively. This represents a difference of 26.9%, a contributing factor to this large number is the small displacement values for measured and calculated displacement. Also, the modified hyperbolic provides a much more accurate prediction of the load-settlement behavior at the toe as compared to the linear elastic model.

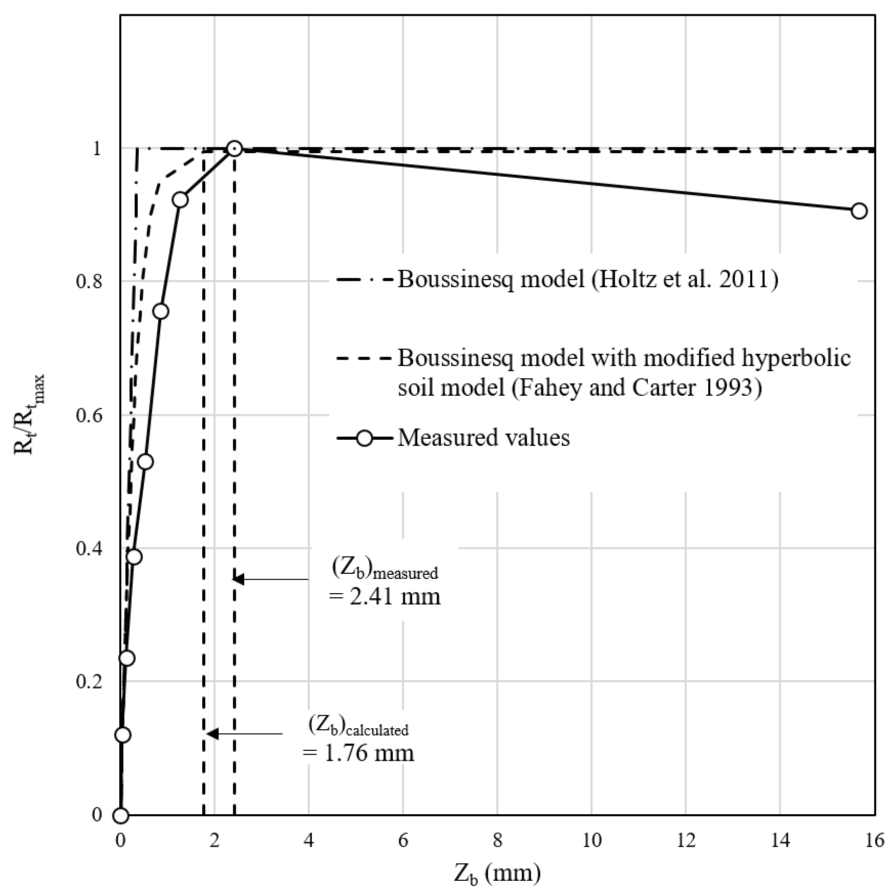


Figure 5-44. Normalized *Q-Z* curves for plate pile compared with measured values from ICE field testing

5.3.3.3 Comparison Between *T-Z* Curves for Cylindrical and Plate Pile Models

This section compares predicted load transfer *T*-Z curve shape, as well as predicted load-settlement curves, for the concentric cylinder and newly developed plate pile models. Predicted load transfer curves from these two models are compared with measured load transfer curves provided by the field data. For these comparisons the load transfer curve shape is the key consideration, adequate $f_{s_{\max}}$ values are determined separately by an appropriate method with no impact on the adequacy of the predicted curvature from the chosen model. Therefore, for this comparison, measured $f_{s_{\max}}$ values are used to generate the load transfer curves to help compare predicted and measured values and best assess which method provides the most adequate load transfer curve shape. Values of $f_{s_{\max}}$ are taken at 5 cm of displacement for theoretical load transfer curve development.

Additionally, the effect of curve fitting parameters, *f* and *g*, on the load transfer curves are considered. These values depend on the encountered soil. Upper and lower bound values are defined based on the literature and compared for both models. Since increasing *g* values are representative of a stiffer soil and increasing *f* values represent a weaker soil (Zhu and Chang 2002), upper and lower bounds for *f* and *g* are chosen to be *g*= 0.4, *f*= 0.6 representing a stiffer soil and *g*= 0.1, *f*= 1.0 for a weaker soil. Figure 5-45 presents the results of this comparison for each of the defined soil layers.

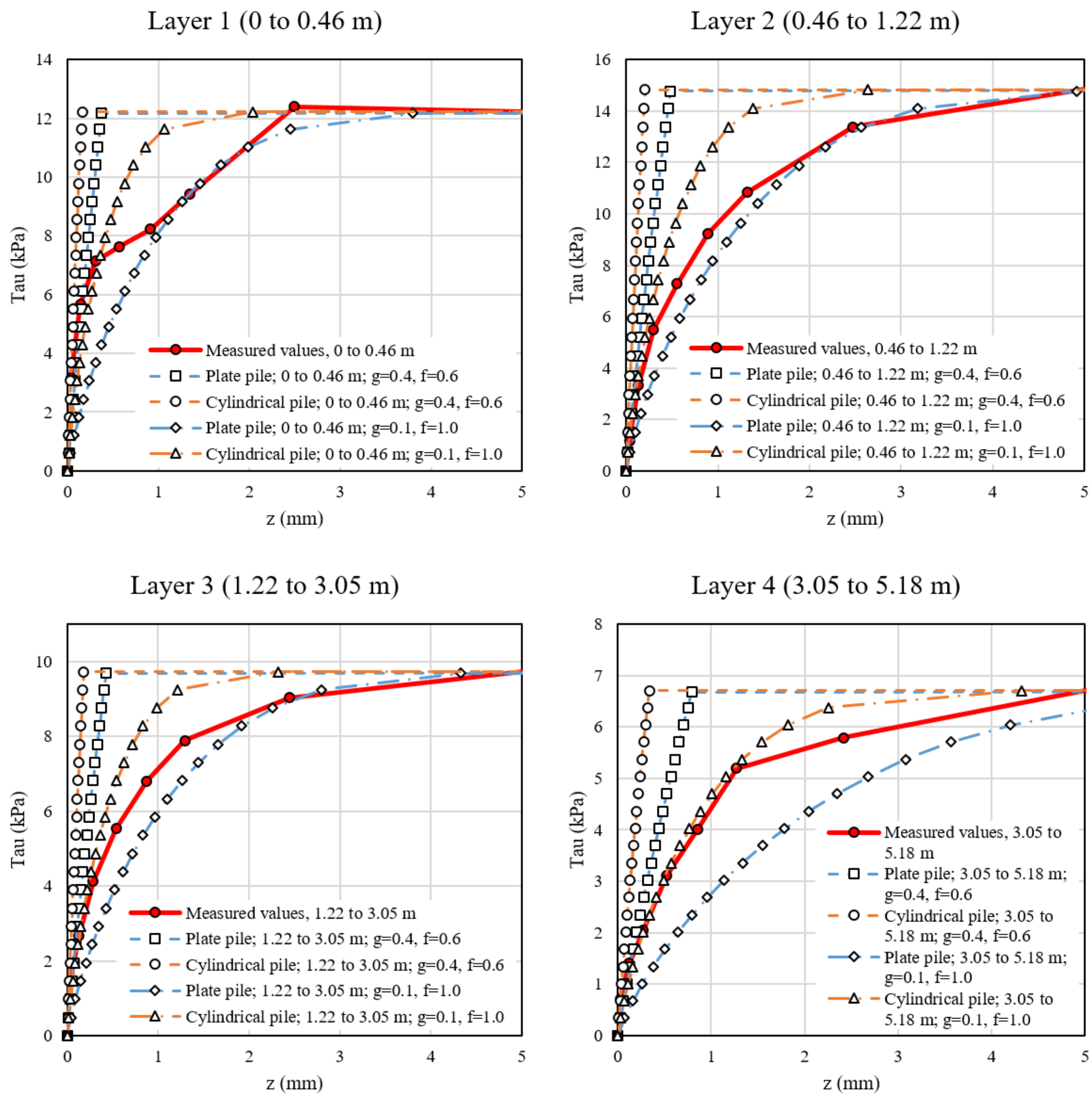


Figure 5-45. Results of theoretical and measured *T-Z* curve comparison for plate and cylindrical pile models

Based on the results of the comparison, the theoretical *T-Z* curve presented in this dissertation based on a plate geometry captures the measured results to a much better degree as compared to the concentric cylinder model. Increased accuracy of predicted curve shapes can be achieved by modifying chosen *f* and *g* values. The previous sections have considered *T-Z* and *Q-Z* curve development separately in order to isolate the potential for bias when combining these two curve types in predicting load-settlement response. With both curve shapes now defined, combining these two curve types is possible and can be used to compare how well load-settlement behavior is captured by the concentric cylinder and newly developed plate pile models for the field test piles.

Load-settlement predictions are made using the concentric cylinder and plate pile models. As discussed previously, values of 1.0 and 0.3 are used for *f* and *g*, respectively. Additionally, the theoretical *Q-Z* curve presented earlier is used to model behavior at the toe. In order to aid this comparison, the final predicted load values are normalized for all load values using the recorded load at approximately 2 mm of displacement. Figure 5-46 presents the results of this comparison.

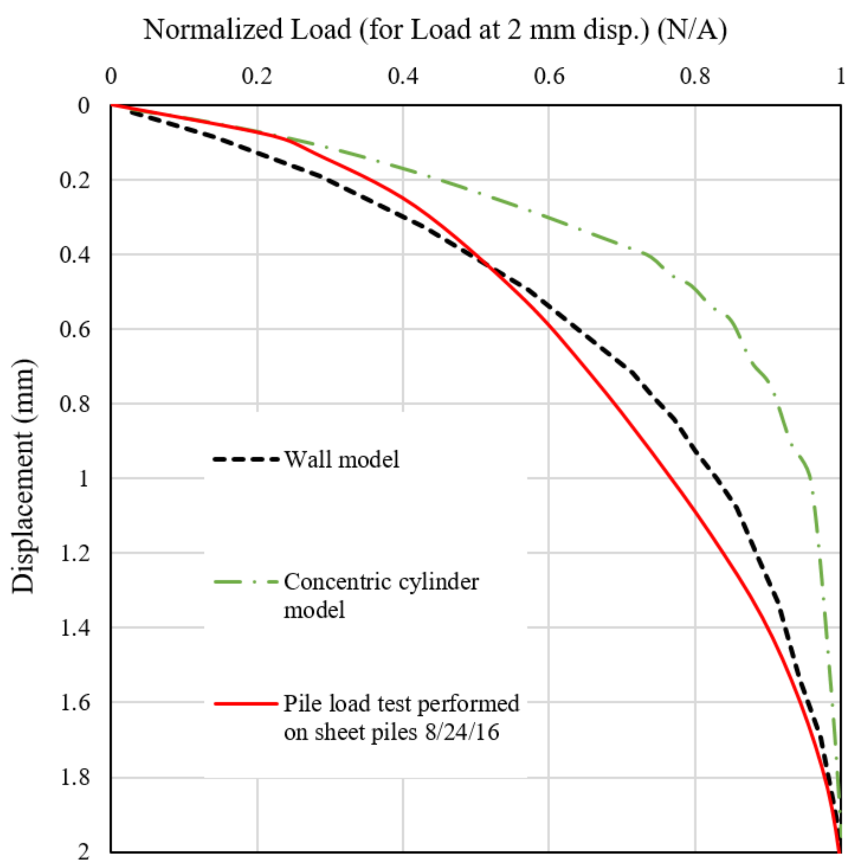


Figure 5-46. Measured versus calculated load-settlement curve for field site using theoretical *T-Z* and *Q-Z* curves

Based on the results of this comparison, it is clearly shown the wall model provide a better prediction of the load-settlement behavior measured at the field site. The concentric cylinder model predicts a much stiffer load-settlement response. This result agrees with findings obtained from Figure 5-45 that indicated the concentric cylinder model has a tendency to over predict the stiffness of the load transfer behavior related to shaft resistance.

### 5.3.4 Recommended Design Procedure Based on Theoretical Development

This section presents a general set of design procedures for determining the load transfer behavior of sheet piles based on the results of the theoretical development presented in this chapter:

1. Characterize the soils at the test site. Obtain measurements of $V_s$ to a minimum depth equal to future pile embedment. Direct in-situ measurements provide the most reliable and robust values, however values obtained through correlations with other in-situ tests or laboratory obtained values can also be used. Based on the information collected from field testing, a $V_s$ based soil profile should be created. Use $\gamma_t$ values obtained from samples or correlations with in-situ test results with $V_s$ values to obtain values for the maximum shear modulus, $G_0$.
2. Using results of in-situ testing, determine maximum unit shaft resistance values with depth. Multiple methods should be employed, however the best predictions may be provided by the Meyerhof, Beta, and LCPC methods. If multiple methods are considered, lower bound values for resistance equal to one standard deviation below the mean resistance value should provide a conservative value for resistance. This

may be most appropriate if there is large scatter in measured resistance values or uncertainty regarding engineering behavior of soils of the region.

3. Using values obtained from in-situ testing, determine the maximum unit toe resistance value at the depth of pile toe embedment. The most reliable predicted values obtained in this study for the field tests were provided by LCPC and other CPT based methods.
4. Determine *T-Z* curves using the theoretical methods outlined in this chapter. When determining hyperbolic model curve shapes, *f* and *g* values of 1.0 and 0.3 were found to be appropriate for the residual Piedmont soils encountered in the field tests as part of this study.
5. Determine *Q-Z* curves using the theoretical methods outlined in this chapter. Again, *f* and *g* values of 1.0 and 0.3 were found to be appropriate for the residual Piedmont soils encountered in the field tests as part of this study.

## 5.4 Summary and Conclusions

This chapter presents in greater detail the results of the pile load tests in the laboratory and field. Results from the tests are compared with conventional static methods for calculating pile capacity. The calculations involving the static methods considered geometries both for unplugged and fully plugged behavior. Both calculations are performed in order to capture the measured behavior and provide insights into the nature of the plugging behavior for the test piles. Results from this comparison indicate that formation of a partial plug was likely for the piles tested under laboratory conditions. It was found that the most accurate method for predicting the pile capacities was the Nottingham & Schmertmann method, assuming that there was unplugged behavior for the toe capacity (128.6 kN) and plugged behavior for the shaft capacity (915.5 kN). The resulting ultimate capacity of 1044.1 kN is within twenty percent of the measured capacity equal to 1218.9 kN.

For the field piles, predictive methods generally overestimated both shaft and toe capacities for the sheet piles and H-pile. Predicted values assuming unplugged conditions were most accurate for the sheet piles, and values assuming plugged conditions were most accurate for the H-pile. For both piles, predictions indicated plugging at the toe was not likely. This finding is further supported by the presence of soft silt soil at the installation depth of both piles. In contrast to the toe, predictive methods indicate plugging along the shaft possibly occurred. All predicted methods using CPT methods were found to have the largest margin of error with regards to over predicting capacity values. The most accurate methods for predicting ultimate capacity for the sheet piles and H-pile were the SPT based methods, and the most accurate of these was the Meyerhof method.

In general, due to uncertainties regarding plugged behavior, the smallest capacity values for shaft and toe resistance determined through assuming no plugging or full plugging should be used. A fully plugged condition at the pile toe should only be assumed when there is observable evidence based on field experience or from a project's specific load test. This conservative approach to design decreases the likelihood of over predicting the resistance provided from the shaft and toe. For both the field and lab, results from this component of the analysis indicate that conventional methods used to predict pile capacity have comparable accuracy when used for sheet piles as compared to conventional axial load bearing piles.

This chapter interprets results using load transfer methodology. Two key aspects of these curves were discussed prior to comparisons with popular empirically based load transfer curves and select static methods. These two key aspects include the maximum resistance values and the curvature and shape of the load transfer curves. Accurate data for these two components allow for a well-defined prediction of the load transfer curve. API (1993) and Vijayvergiya (1977) provided the two methods considered for predicting curve shape, and Meyerhof and LCPC provide the methods for finding the maximum unit resistance values for shaft and toe.

For laboratory testing, results from the comparison indicate poor agreement in general between empirical and experimental curves in terms of peak resistance values and curve shapes. Peak resistance values show a level of agreement between measured and empirical values that is similar to the agreement obtained through static capacity estimates. The poor agreement between normalized curve shapes provided by the empirical methods and experimentally measured curves may be explained by the failure of the test to fully mobilize the test piles. Despite the generally poor match between these two sets of curves, the load transfer curves for the *Q-Z* behavior indicate fair to good agreement with the curve shape proposed by Vijayvergiya (1977). Furthermore, the maximum resistance values predicted using the Meyerhof method provide excellent predictions of the maximum load bearing resistance at the pile toe.

For field-testing, results from the comparison indicate good agreement in general between empirical and experimental curves. Results from the comparison indicate that the curve shape provided from Vijayvergiya (1977) produced the best agreement with normalized curve shapes measured for *T-Z* and *Q-Z* curves. The LCPC method was found to provide poor predictions of peak shaft resistance; however, fair agreement was observed between the predicted and measured peak toe resistance values. The Meyerhof method was found to provide good to excellent predictions of peak shaft resistance values while predicted toe resistance values were found to be poor.

Finally, this chapter investigates the theoretical development of load transfer curves for sheet piles. A new analytically derived equation for pile settlement is presented for axially loaded piles with a plate geometry. The new theoretical load transfer curves are used to generate load-settlement curves and are compared with measured results. This comparison demonstrates that accurate values for maximum unit shaft resistance are essential for accurate predictions of load-settlement behavior using these theoretical load transfer *T-Z* curves. A theoretical *Q-Z* curve based on the plate pile geometry is compared with measured values and the predicted curve shape produces good agreement with measured results.

A comparison is also made with the equations developed for the concentric cylinder model proposed by Randolph and Wroth (1978). A direct comparison is made between theoretical load transfer *T-Z* curves developed using the cylindrical and plate pile equations. These results are compared to field measurements and consider two sets of values for the modified hyperbolic curve fitting parameters, $f$ and $g$. Results indicate the equations developed for the plate pile provide more accurate predictions of the *T-Z* curve shape as compared to the cylindrical pile model. Additionally, normalized load-settlement curves generated using theoretical load transfer curves for both geometries are compared with measured results and this comparison indicates the plate pile model to provide a better estimate of the stiffness and curve shape of the normalized load-settlement curve. In general, the concentric cylinder model over predicts the stiffness and curve shape of the measured load transfer curves. The predicted curves provided by the newly developed plate pile model were in better agreement with the measured results. Lastly, generalized recommendations for applying these findings to the prediction of load-settlement behavior of axially loaded sheet piles was presented.

# CHAPTER 6: SUMMARY, CONCLUSIONS, AND RECOMMENDATIONS FOR FUTURE WORK

## 6.1 Summary

Steel sheet piles represent a potential axial load bearing foundation element for bridge abutments, underutilized in typical U.S. design practice. Many regions of the U.S. treat sheet piles as lateral retaining elements and scour protection elements only, contributing no axial load to the design of the abutment. This has been demonstrated to be a conservative design practice based on numerous successful bridge projects across Europe and the U.K. which have used sheet piles as the only axial load bearing elements for over fifty years. Numerous benefits can be realized by incorporating this foundation type for axial load bearing. Savings, in terms of building materials and construction time, are possible due to shorter and fewer piles required for design.

This study examines the axial load bearing capacity of sheet piles through two large scale, well-instrumented pile load tests. Tests were performed in a laboratory and a field setting. Both sites were well-characterized through in-situ and laboratory testing. Predictive methods used to determine static axial load capacity for piles were considered and applied to the test piles. Additionally, this study also looks at the load transfer mechanism involved with axially loaded sheet piles. Conventional methods used to predict load transfer were considered and compared to the test results. This behavior in sheet piles was further evaluated using analytical methods in order to develop a new set of equations to describe how load transfer is achieved for this type of pile.

Laboratory testing of a sheet pile wall consisting of four PZ 27 sheet piles resulted in pile capacity values that exceeded many conventional predictive methods used to determine axial load bearing. These methods included PDA, CAPWAP, and other conventional static methods based on SPT and CPT testing. Despite poor agreement between ultimate capacity and the static methods considered, the level of accuracy of the static methods for sheet piles was similar compared to the typical accuracy of these methods when applied to conventional axial load bearing piles. The level of instrumentation used allowed for assessment of shaft and toe resistance. Results indicated that the sheet pile carried load primarily through shaft resistance. While it is difficult to determine the exact plugging behavior during these tests, observed results indicate that the formation of at least a partial plug near the toe of the pile and along the shaft was likely.

Field testing was performed on a PZ 27 sheet pile pair as well as an HP 12x53 H-pile, both typical sizes used for short span bridge construction in North Carolina. The field site was located within the Piedmont physiographic province of North Carolina and the soil profile at the field site consisted primarily of residual soils classified according to USCS as sandy lean clay, sandy silt, and silty sand. The sheet piles were found to have greater axial load bearing capacity than the H-pile, suggesting a strong potential for incorporating the axial load bearing capacity provided by this foundation type for bridge abutments. Predictive static methods had similar degrees of accuracy for both piles and generally over predicted ultimate pile capacity. Fair agreement was obtained from CAPWAP based capacity estimates, while PDA resulted in fair to poor predictions of pile load capacity. Based on results from instrumentation along the length of the sheet piles, it was determined that the piles carried load primarily through shaft resistance. Results of the pile load tests and field-testing indicated that minimal plugging likely occurred at the toe of the pile, and partial plugging along the shaft was possible. Based on the agreement between predictive static methods and the favorable performance of the sheet piles as compared to the H-pile, these results suggest that ample axial load bearing capacity exists for sheet piles under axial loading and that their behavior is similar to steel driven piles used for axial load bearing with geometries that are more conventional.

Load transfer analysis was used to describe in detail how sheet piles transfer applied axial loads to the surrounding soil. Experimental and empirical load transfer curves were obtained for both full-scale tests. The quality of agreement between both curve types varied. In general, the laboratory tests showed poor agreement between empirical and experimental curves while the field tests showed good agreement between these curves. The empirical curves shape proposed by Vijayvergiya (1977) for *T-Z* and *Q-Z* curves produced the best agreement in general. The comparison with laboratory testing indicated the empirical *Q-Z* curve proposed by Vijayvergiya (1977) had fair agreement with measured curve shape, and peak toe resistance values provided by the Meyerhof method produced excellent agreement with measured values. The comparison with field tests yielded good agreement with the curve shapes proposed by Vijayvergiya (1977), and comparison with peak resistance values indicates that the LCPC method is able to provide reasonably accurate toe resistance values while the Meyerhof method provides reasonably accurate shaft resistance values for the soils encountered at the field site.

Finally, an analytical approach was used to develop new load transfer curves for an axially loaded plate pile. A new equation for settlement of a plate pile is presented, as well as new *Q-Z* load transfer curves. These equations incorporate non-linear soil behavior based on the modified hyperbolic soil model. Predicted load transfer curves for a plate geometry are compared with predicted load transfer curves from the concentric cylinder model and measured results from field testing. Results indicate the importance of accurate maximum unit shaft resistance values for predicting load-settlement behavior. Based on comparisons with measured results, the predicted *T-Z* curves using the new plate pile model are able to capture the measured load transfer curve shapes and provide improved predictions compared to the cylindrical pile model. Additionally, the predicted normalized load-settlement response based on the plate pile model provides a better prediction of load-settlement curve shape as compared to the concentric cylinder model that over predicts the stiffness of the load-settlement behavior. Some recommendations regarding design procedures based on this theoretical development are presented.

## 6.2 Conclusions

Based on the results of this study, below are a few design recommendations associated with the axial load bearing behavior of sheet piles:

- Plugging is a key behavior associated with axially loaded sheet piles and will strongly influence axial load bearing behavior. Plugging should be thought of as occurring within a range of possible behaviors for sheet piles. Plugging can occur at either the toe, along the shaft, or both. Additionally, the geometry of a plug can occur between the two extreme cases of no plugging or full plugging. The location and geometry of a soil plug is a function of several characteristics including soil conditions, pile attributes, pile geometry, and the installation process used to place the piles(Jeong et al. 2015). Characterizing this behavior accurately for design is difficult. Due to uncertainties regarding this behavior and the large effect it can have when determining design resistance values, it is recommended that an unplugged and fully plugged geometry be considered when calculating shaft and toe resistance and that the lower of the two values be used for both shaft and toe resistance. This approach is consistent with design practice used for other steel pile geometries such as H-piles and pipe piles where plugging occurs and is reported as a complex and difficult behavior to predict. If field experience is available, assigning more appropriate area values for the plug geometry is possible.

- Axially loaded sheet piles provide load capacity primarily through shaft bearing due to the piles having large shaft area as compared to their cross sectional area. This may not necessarily be true for soil profiles consisting of a dense/firm layer underlying a loose/soft layer and where the elevation of the pile toe is installed into the dense/firm layer or for cases where certain plug geometries are occurring. However, characterizing sheet piles as a frictional load bearing foundations is consistent with identified design guidance in the literature and the results of the full-scale load tests conducted as part of this study that found the piles to carry load primarily through frictional load bearing.
- When predicting static axial load capacity, predictive methods used for evaluating steel driven piles can be expected to have a similar degree of accuracy when applied to steel sheet piles. For steel piles driven into residual soils of the Piedmont with soil profiles resembling the soils encountered at the field site for this study, the SPT based Meyerhof method can be considered for providing the most appropriate values for peak shaft resistance, and the CPT based LCPC method can be considered for providing the most appropriate values for peak toe resistance.

- When estimating load transfer behavior, theoretically derived load transfer curves presented in this study can be considered. These curves are developed based on the modified hyperbolic soil model. Measured load transfer curves were found to have a reasonable match with theoretically derived values, the comparison emphasizes the need for accurate predictions of maximum unit shaft and unit toe resistances. The values for shaft resistance are especially important as sheet piles will tend to act as friction bearing foundation elements.

## 6.3 Recommendations for Future Work

Based on the results of the literature review and the findings of this study, recommendations for future work are provided below:

- Additional study of the load transfer behavior at the head of sheet piles and definition of adequate structural design details to ensure proper connection of the sheet pile walls to the bridge abutments is required. For the pile load tests conducted in this study, steel beams and connections were used to ensure uniform load transfer to the pile heads. However, sheet piles are typically capped with concrete for bridge abutment design within the U.S. A better understanding of what is needed for the size and location of reinforcing rebar when sheet piles are capped with concrete will be required before using this type of configuration for axial load bearing.
- The force distribution along a cross section of steel piles may require further research. An individual sheet pile or sheet pile pair under axial loads will behave in a different manner compared to sheet piles installed as part of a sheet pile wall. This is due to a more complicated load bearing behavior as compared to individual piles. This difference in behavior is similar to how individual piles will behave differently as

compared to group piles. The effects of interlock friction between sheets can be the source of considerable changes to the distribution of load stresses due to vertically applied loads and may affect design.

- The design and construction community needs to establish design guidelines for the incorporation of axial load bearing capacity of sheet piles for U.S. design practice. This may require additional reports of well-documented bridge case histories and field load tests, both static and dynamic.
- Long term monitoring of axially loaded sheet piles should be conducted in order to better understand how these piles behave during the design life of structures. This understanding will help address performance and durability factors that are unknown. Factors such as corrosion and lateral movement of the sheet piles may lead to changes in performance that should be understood before utilizing this foundation type as axially load bearing members in bridge abutments.
- Development of design guidance regarding the formation of a possible gap within the active side of the sheet pile wall is required. A gap may result from the effects of cyclic expansion and contraction of the bridge superstructure and could be a significant design consideration, especially for integral bridge abutments.
- The performance of sheet piles exposed to axial, lateral, and bending moments and the performance of sheet piles during monotonic and dynamic loading conditions should be better understood. This study mainly addresses the performance of sheet piles under static axial loads.

**REFERENCES**

Abbondanza, D. (2009). "Steel innovation: Changing the economics of below grade foundations." *International Foundation Congress and Equipment Expo*, ASCE, Orlando, Florida, 57-64.

AISC (2011). *Steel Construction Manual*, Chicago, IL.

API (1993). *Recommended Practice for Planning, Designing and Constructing Fixed Offshore Platforms-Load and Resistance Factor Design*, American Petroleum Institute, Washington, DC.

ArcelorMittal (2008). *Piling Handbook*, West Midlands, United Kingdom.

ArcelorMittal (2009). "Successful Load Bearing Test of AZ-700 Steel Sheet Piles in Poland." *Foundation Solutions for Projects: Commercial RPS*, 1-2.

ASTM (2007). "D422: Standard test method for particle-size analysis of soils."100 Barr Harbor Drive, PO Box C700, West Connshohocken, PA 19428-2959, 1-8.

ASTM (2010). "D4318: Standard test methods for liquid limit, plastic limit, and plasticity index of soils."100 Barr Harbor Drive, PO Box C700, West Connshohocken, PA 19428-2959, 1-16.

ASTM (2011). "D1586: Standard test method for standard penetration test (SPT) and split-barrel sampling of soils."100 Barr Harbor Drive, PO Box C700, West Connshohocken, PA 19428-2959, 1-9.

ASTM (2011). "D2487: Standard practice for classification of soils for engineering purposes (Unified Soil Classification System)."100 Barr Harbor Drive, PO Box C700, West Connshohocken, PA 19428-2959, 1-12.

ASTM (2011). "D3080: Direct shear test of soils under consolidated drained conditions."100 Barr Harbor Drive, PO Box C700, West Connshohocken, PA 19428-2959, 1-9.

ASTM (2011). "D5777: Standard guide for using the seismic refraction method for subsurface investigation."100 Barr Harbor Drive, PO Box C700, West Connshohocken, PA 19428-2959, 1-14.

ASTM (2012). "D698: Standard test methods for laboratory compaction characteristic of soil using standard effort (12400 ft-lbf/ft$^3$ (600 kN-m/m$^3$))."100 Barr Harbor Drive, PO Box C700, West Connshohocken, PA 19428-2959, 1-13.

ASTM (2012). "D5778: Standard test method for electronic friction cone and piezocone penetration testing of soils."100 Barr Harbor Drive, PO Box C700, West Connshohocken, PA 19428-2959, 1-20.

ASTM (2013). "D1143/D1143M: Standard test methods for deep foundations under static axial compressive load."100 Barr Harbor Drive, PO Box C700, West Connshohocken, PA 19428-2959, 1-15.

ASTM (2014). "D854: Standard test methods for specific gravity of soil solids by water pycnometer."100 Barr Harbor Drive, PO Box C700, West Connshohocken, PA 19428-2959, 1-8.

ASTM (2014). "D4428: Standard test methods for crosshole seismic testing."100 Barr Harbor Drive, PO Box C700, West Connshohocken, PA 19428-2959, 1-7.

ASTM (2014). "D7400: Standard test methods for downhole seismic testing."100 Barr Harbor Drive, PO Box C700, West Connshohocken, PA 19428-2959, 1-10.

ASTM (2015). "D1195/D1195M: Standard test method for repetitive static plate load tests of soils and flexible pavement components, for use in evaluation and design of airport and highway pavements."100 Barr Harbor Drive, PO Box C700, West Connshohocken, PA 19428-2959, 1-3.

ASTM (2015). "D1556/D1556M: Standard test method for density and unit weight of soil in place by sand-cone method."100 Barr Harbor Drive, PO Box C700, West Connshohocken, PA 19428-2959, 1-8.

ASTM (2015). "D2850: Standard test method for unconsolidated-undrained triaxial compression test on cohesive soils."100 Barr Harbor Drive, PO Box C700, West Connshohocken, PA 19428-2959, 1-7.

ASTM (2015). "D6635: Standard test methods for performing the flat plate dilatometer."100 Barr Harbor Drive, PO Box C700, West Connshohocken, PA 19428-2959, 1-16.

ASTM (2017). "D2937: Standard test method for density of soil in place by the drive-cylinder method."100 Barr Harbor Drive, PO Box C700, West Connshohocken, PA 19428-2959, 1-8.

ASTM (2017). "D6938: Standard test methods for in-place density and water content of soil and soilaggregate by nuclear methods (shallow depth)."100 Barr Harbor Drive, PO Box C700, West Connshohocken, PA 19428-2959, 1-10.

Biddle, A. R. (1997). *Steel Bearing Piles Guide*, The Steel Construction Institute, Silwood Park, Ascot, SL5 7QN, United Kingdom.

Bohn, C., Lopes dos Santos, A., and Frank, R. (2016). "Development of axial pile load transfer curves based on instrumented load tests." *ASCE Journal of Geotechnical and Geoenvironmental Engineering*, 143(1), 1-15.

Borel, S., Bustamante, M. G., and Gianeselli, L. "Two comparative field studies of the bearing capacity of vibratory and impact driven sheet piles." *Proc., International Conference on Vibratory Pile Driving and Deep Soil Compaction*, 167-174.

Brown, D. A., O Neill, M. W., Hoit, M., McVay, M., El Naggar, M. H., and Chakraborty, S. (2001). "Static and dynamic lateral loading of pile groups." Transportation Research Board - National Research Council, Washington, DC, 1-60.

Bustamante, M. G., and Gianeselli, L. (1982). "Pile bearing capacity prediction by means of static penetrometer CPT." *Proc., 2nd European Symposium on Penetration Testing*, 493-500.

Bustamante, M. G., and Gianeselli, L. (1991). "Predicting the bearing capacity of sheet piles under veritical load." *4th International Conference on Piling and Deep Foundations*, Deep Foundations Institute, Stresa, Italy, 1-8.

Carle, R., and Whitaker, S. (1989). "Sheet piling bridge abutments." *Deep Foundations Institute Annual Meeting*, Baltimore, Maryland, 1-16.

Chang, M. F., and Zhu, H. "A *t-z* curve with consideration of modulus degradation for pile analaysis." *Proc., 13th Southeast Asian Geotechnical Conference, SEAGS*, 461-466.

Chew, V. C. (1993). "Underfoot: a geologic guide to the Appalacian Trail." Appalacian Trail Conference, Harpers Ferry, West Virginia, 1-237.

Chow, Y. K. (1986). "Analysis of vertically loaded pile groups." *International Journal for Numerical and Analytical Methods in Geomechanics*, 10(1), 59-72.

Coyle, H. M., and Reese, L. C. (1966). "Load transfer for axially loaded piles in clay." *Journal of the Soil Mechanics and Foundations Division*, 92(2), 1-26.

Das, B. M. (2016). *Principles of Foundation Engineering*, Cengage Learning, 20 Channel Center Street, Boston, MA, 02210.

De Ruiter, J., and Beringen, F. (1979). "Pile foundations for large North Sea structures." *Marine Georesources & Geotechnology*, 3(3), 267-314.

Duncan, J. M., and Chang, C.-Y. (1970). "Nonlinear analysis of stress and strain in soils." *ASCE Journal of Soil Mechanics & Foundations Division*, 96(SM5), 1629-1653.

Eslami, A., and Fellenius, B. H. (1997). "Pile capacity by direct CPT and CPTu methods applied to 102 case histories." *Canadian Geotechnical Journal*, 34(6), 886-904.

European Committee for Standardization (2004). "Eurocode 7: Geotechnical Design - Part 1: General Rules." *EN 1997-1*, BSI, London, 1-159.

European Committee for Standardization (2005). "Eurocode 3: Design of Steel Structures- Part 1: General Rules and Rules for Buildings." *EN 1993-1*, BSI, London, 1-91.

European Committee for Standardization (2007). "Eurocode 3: Design of Steel Structures - Part 5: Piling." *EN 1993-5*, BSI, London, 1-94.

Evans, R., White, D., and Klaiber, W. (2012). "Modified Steel Pile Abutments for Low-Volume Road Bridges." *IHRB Project TR-568*, Iowa Department of Transportation, Ames, Iowa, 1-294.

Everett, J. P. (1991). "Load transfer functions and pile performance modelling." *Geotechnics in the African environment. Regional conference for Africa on soil mechanics and foundation engineering*, Balkema, A.A., 229-234.

Fahey, M., and Carter, J. P. (1993). "A finite element study of the pressuremeter test in sand using a nonlinear elastic plastic model." *Canadian Geotechnical Journal*, 30(2), 348-362.

Goble, G. G., Likins, G. E., and Rausche, F. (1975). "Bearing Capacity of Piles from Dynamic Measurements." Case Western Reserve University, Cleveland, Ohio, 1-76.

Guo, W. D. (1996). "Analytical and Numerical Solutions for Pile Foundations." Ph.D. Dissertation, The University of Western Australia.

Hannigan, P. J., Goble, G. G., Likins, G. E., and Rausche, F. (2006). "Design and Construction of Driven Pile Foundations, Reference Manual." U.S. Department of Transportation, Washington, D.C. , 1-968.

Hickman, R. C. (2011). "Plans for Lone Star Canal at Double Bayou Aqueduct Replacement Project." *Project P00644 Aqueduct Replacement*, LEAP Engineering, Beaumont, Texas, 1-18.

Hirayama, H. (1990). "Load-settlement analysis for bored piles using hyperbolic transfer functions." *Soils and Foundations*, 30(1), 55-64.

Holtz, R. D., Kovacs, W. D., and Sheahan, T. C. (2011). *An Introduction to Geotechnical Engineering*, Pearson Education, Inc., Upper Saddle River, NJ.

Jeong, S., Ko, J., Won, J., and Lee, K. (2015). "Bearing capacity analysis of open-ended piles considering the degree of soil plugging." *Soils and Foundations*, 55(5), 1001-1014.

Kodikara, J., and Johnston, I. (1994). "Analysis of compressible axially loaded piles in rock." *International Journal for Numerical and Analytical Methods in Geomechanics*, 18(6), 427-437.

Kondner, R. L. (1963). "Hyperbolic stress-strain response: cohesive soils." *ASCE Journal of the Soil Mechanics and Foundations Division*, 89(1), 115-143.

Kondner, R. L., and Zelasko, J. S. (1963). "A hyperbolic stress-strain formulation for sands." *Proc. 2nd Pan-American Conf. on SMFE*, 289-324.

Kraft Jr., L. M., Ray, R. P., and Kagawa, T. (1981). "Theoretical tz curves." *ASCE Journal of Geotechnical and Geoenvironmental Engineering*, 107(ASCE 16653), 1543-1561.

Landau, L. D., and Lifshitz, E. M. (1970). *Theory of Elasticity* Pergamon Press, Oxford.

Lunne, T., Robertson, P. K., and Powell, J. J. M. (1997). *Cone Penetration Testing in Geotechnical Practice*, Blackie Academic and Professional, London.

Mayne, P. W. (1995). "Evaluation of foundation response by $G/G_{max}$ degradation relationships in soils." *U.S.-Taiwan Geotechnical Engineering Collaboration Workshop*, National Science Foundation, 136-148.

Mayne, P. W., and Brown, D. A. (2003). "Site characterization of Piedmont residuum of North America." *Characterization and Engineering Properties of Natural Soils*, Vol. 2, 1323-1339.

McShane, G. "Steel sheet piling used in the combined role of bearing piles and earth retaining members." *Proc., 4th International Conference on Piling and Deep Foungations*, Deep Foundations Institute, 1-6.

Meyerhof, G. G. (1959). "Compaction of sands and bearing capacity of piles." *ASCE Journal of the Soil Mechanics and Foundations Division*, 85(SM6), 1-29.

Mosher, R. L. (1987). "Comparison of Axial Capacity of Vibratory-Drive Piles to Impact-Driven Piles." U.S. Army Corps of Engineers, Vicksburg, MS.

Nippon Steel & Sumitomo Metal Corporation (2012). "Construction Products: Steel Sheet Piles."Tokyo, Japan.

Nordlund, R. L. (1963). "Bearing capacity of piles in cohesionless soils." *ASCE, Journal of the Soil Mechanics and Foundations Division*, SM3, 1-35.

Nottingham, L. C. (1975). "Use of quasi-static friction cone penetrometer data: To predict load capacity of displacement piles." Ph.D. Dissertation, University of Florida.

O'Neill, M. W., and Raines, R. D. (1991). "Load transfer for pipe piles in highly pressured dense sand." *Journal of Geotechnical Engineering*, 117(8), 1208-1226.

Pando, M. A., Ealy, C. D., Filz, G. M., Lesko, J. J., and Hoppe, E. J. (2006). "A Laboratory and Field Study of Composite Piles for Bridge Substructures." No. FHWA-HRT-04-043, 1-384.

Randolph, M. F., and Wroth, C. P. (1978). "Analysis of deformation of vertically loaded piles." *ASCE Journal of Geotechnical and Geoenvironmental Engineering*, 104(ASCE 14262), 14262-11488.

Rice, C. D., Pando, M. A., Whelan, M. J., and Ogunro, V. O. (2014). "Vertical load capacity of steel sheet piles for bridge abutments- preliminary assessment for sand conditions." *9th International Conference on Short and Medium Span Bridges*, Calgary, Alberta, Canada, 1-10.

Rybak, J., and Zyrek, T. (2013). "Experimental validation of sheet pile and combined pile axial capacity computation." *Vplyv Vody na Geotechnicke Konstruckcie*, Bratislava, 1-8.

SACILOR "Steel Sheet Piling in Inland Structures." Hayange, France, 1-53.

Skyline Steel LLC (2009). "Roads and bridge abutments in sheet piles." Skyline Steel LLC, 1-8.

Sowers, G. F., and Richardson, T. L. (1983). "Residual soils of piedmont and Blue Ridge." *Transportation Research Record*, (919), 10-16.

Sylvain, M. B., Pando, M. A., Whelan, M. J., Rice, C. D., Ogunro, V. O., Park, Y., and Koch, T. (2017). "Case history of a full scale axial load test of sheet piles." *Geotechnical Frontiers 2017*, ASCE, Orlando, Florida, 335-365.

Taenaka, S., Otani, J., Tatsuta, M., and Nishiumi, K. (2006). "Vertical bearing capacity of steel sheet piles." *Proc., 6$^{th}$ International Conference on Physical Modelling in Geotechnics-Physical Modelling in Geotechnics-6$^{th}$ ICPMG'06*, 1-6.

Underwood, C. A., and Greenlee, R. M. (2010). "Steel sheet pile used as permanent foundation and retention systems-design and construction." *Proc., 2010 Earth Retention Conference (Earth Retention Conference 3)*, ASCE, Bellvue, Washington, 129-136.

Vijayvergiya, V. N. (1977). "Load-movement characteristics of piles." *Proc., Ports'77. 4$^{th}$ annual symposium of the American Society of Civil Engineers, Waterway, Port, Coastal and Ocean Division*, Vol. 2, Long Beach, California, 269-284.

Vinson, J. L., and Brown, D. A. (1997). "Site characterization of the Spring Villa geotechnical test site and a comparison of strength and stiffness parameters for a Piedmont residual soil." *Harbert Engineering Center, Auburn University, Auburn, Alabama*, 1-385.

Yandzio, E. (1998). "Design Guide for Steel Sheet Pile Bridge Abutments." The Steel Construction Institute, Silwood Park, Ascot, Berkshire SL5 7QN, United Kingdom, 1-146.

Zhu, H., and Chang, M.-F. (2002). "Load transfer curves along bored piles considering modulus degradation." *ASCE Journal of Geotechnical and Geoenvironmental Engineering*, 128(9), 764-774.

# APPENDIX A. SUPPLEMENTAL LITERATURE REVIEW

Supplemental material identified in the literature review regarding the design of sheet piles is presented in this appendix. The majority of this material was obtained from the literature review presented in the NCDOT report FHWA/NC/2014-08-1 titled 'Literature Review of State of Practice for Sheet Pile Bridge Abutments' as part of NCDOT Project No. 2014-08. Table A-1 presents additional information regarding the sheet pile sections identified in the literature. Table A-2 presents additional information regarding the European bridges identified in the literature. Table A-3 presents additional information regarding the U.S. bridges identified in the literature. The European sheet pile abutment designs identified in the literature commonly used sheet piles combined with boxed sheet piles to support both lateral load demand from the abutment fill and axial loading from the superstructure. Figure A-1 presents different pile configurations used in the identified European bridges and load tests.

Table A-1. Sheet pile details obtained from literature review

| Sheet Pile Section | Type | Dimensions[1] | | | | Cross Sectional Area ($cm^2/m$) | Moment of Inertia ($cm^4/m$) | Rigidity[6], EI ($kN*cm^2/m$) |
|---|---|---|---|---|---|---|---|---|
| | | Width, $w$ (cm) | Height, $h$ (cm) | Flange Thickness, $t_f$ (cm) | Web Thickness, $t_w$ (cm) | | | |
| LP IIn[2] | U | 40 | 27 | 0.95 | 0.95 | 156 | 14898.57 | 2.98E+08 |
| LP IIn Box | U-Box | 40 | 27 | 0.95 | 0.95 | 312 | 29797.14 | 5.96E+08 |
| LP IIs | U | 50 | 34 | 1.23 | 1.23 | 176.95 | 27202.53 | 5.44E+08 |
| LP IIs Box | U-Box | 50 | 34 | 1.23 | 1.23 | 353.91 | 54405.05 | 1.09E+09 |
| LP IIIn | U | 40 | 29 | 1.3 | 0.9 | * | 23201.35 | 4.64E+08 |
| LP IIIn Box | U-Box | 40 | 29 | 1.3 | 0.9 | * | 46402.7 | 9.28E+08 |
| LP IIIs | U | 50 | 40 | 1.41 | 1 | * | 40011.75 | 8.00E+08 |
| LP IIIs Box | U-Box | 50 | 40 | 1.41 | 1 | * | 80023.5 | 1.60E+09 |
| LP IVn | U | 40 | 36 | 1.48 | 1.05 | * | 39588.42 | 7.92E+08 |
| LP IVn Box | U-Box | 40 | 36 | 1.48 | 1.05 | * | 79176.83 | 1.58E+09 |
| LP IVs | U | 50 | 44 | 1.55 | 1 | * | 55005.91 | 1.10E+09 |
| LP IVs Box | U-Box | 50 | 44 | 1.55 | 1 | * | 110011.82 | 2.20E+09 |
| LP 20W | U | 52.5 | 40 | 1.7 | 1.05 | 252.73 | 73004.37 | 1.46E+09 |

Notes:
(*): Denotes official information could not be found in company catalogs or literature
(1): Please refer to Figure 2-1
(2): LP = Larssen pile
(3): F = Frodingham pile
(4): AZ = Arbed pile
(5): PZ = Ball and socket interlock pile
(6): Assuming E = 199.95 GPa, this rigidity is per unit width of sheet pile abutment wall

Table A-1. (continued)

| Sheet Pile Section | Type | Dimensions[1] | | | | Cross Sectional Area ($cm^2/m$) | Moment of Inertia ($cm^4/m$) | Rigidity[6], EI ($kN*cm^2/m$) |
|---|---|---|---|---|---|---|---|---|
| | | Width, $w$ (cm) | Height, $h$ (cm) | Flange Thickness, $t_f$ (cm) | Web Thickness, $t_w$ (cm) | | | |
| LP 32W | U | 52.5 | 45.39 | 1.13 | 0.94 | 187.96 | 34030.47 | 6.80E+08 |
| LP SL 3,4,5 | U | * | * | * | * | * | * | - |
| F 3N[3] | U | 48.31 | 28.3 | 1.17 | 0.89 | 175.05 | 23884.15 | 4.78E+08 |
| F 4N | U | 48.31 | 32.99 | 1.4 | 1.04 | 218.02 | 39834.22 | 7.96E+08 |
| AZ 13[4] | Z | 67 | 30.3 | 0.95 | 0.95 | 136.95 | 19705.44 | 3.94E+08 |
| AZ 25 | Z | 63 | 42.6 | 1.2 | 1.12 | 185 | 52247.42 | 1.05E+08 |
| AZ 36 | Z | 63 | 46 | 1.8 | 1.4 | 247.02 | 82795.64 | 1.66E+09 |
| AZ 14-770 | Z | 77 | 34.44 | 0.95 | 0.95 | 131.45 | 23296.94 | 4.66E+08 |
| AZ 37-700 | Z | 70 | 49.91 | 1.7 | 1.22 | 226.06 | 92395.73 | 1.87E+09 |
| PZ 22[5] | Z | 55.88 | 22.86 | 0.95 | 0.95 | 136.95 | 11525.57 | 2.30E+08 |
| PZ 27 | Z | 45.72 | 30.48 | 0.95 | 0.95 | 168.06 | 25154.14 | 5.03E+08 |
| PZ 27 Box[7] | Z-Box | 91.44 | 60.96 | 0.95 | 0.95 | 336.13 | 128378.99 | 2.57E+09 |

Notes:
(*): Denotes official information could not be found in company catalogs or literature
(1): Please refer to Figure 2-1
(2): LP = Larssen pile
(3): F = Frodingham pile
(4): AZ = Arbed pile
(5): PZ = Ball and socket interlock pile
(6): Assuming E = 199.95 GPa, this rigidity is per unit width of sheet pile abutment wall
(7): Not found in case studies, for comparison purposes only

Table A-2. Relevant information for European bridge case histories

| Structure Identifier | No. of Spans | Span Length (m) | Abutment Width (m) | Sheet Pile Type | Vertical Length of Sheet Piles (m) | Lateral Support[1] | General Soil Condition |
|---|---|---|---|---|---|---|---|
| Pont de Chambiere | 1 | 25 | 3.05 | LP IV | 14.02 | Tie rod anchor | Sand/Gravel to Stiff Marl Clay |
| A8 | 1 | 26.39 | 16 | LP SL3 box column | 9.5 | Bridge deck | N/A[2] |
| Somme River | 1 | 10.21 | N/A | LP IIn | 10.41 | Bridge deck | N/A |
| | | | | LP IIIn Box | 17.98 | | |
| A31 | 1 | N/A | N/A | LP IIIs | N/A | Tie rods | N/A |
| | | | | LP IIs box | | | |
| Moselle Canal | 1 | 44.5 | 12.24 | LP IV | 12.19 | N/A | Gravel |
| | | | | LP IIIn box | 14.05 | | |
| Brenne River | 1 | 6.4 | N/A | LP IIIs | 6 | N/A | Silt Clay |
| Seurre Et Ecuelles | 3 | 42.06 | 7.01 | AZ 14-770 | N/A | N/A | N/A |
| Croisé Laroche overpass | 1 | 12.42 | NA | LP SL 5 | 10 | Overpass deck | Silty Sand |
| | | | | LP SL 5 box | | | |
| St. Genes tunnel | 1 | 8.6 | 264 | LP IIn | 8 | Overpass deck | N/A |
| | | | | LP IIn box | | | |
| Pont de Pierre overpass | 1 | N/A | N/A | LP IIs | 14 | Prestressed tie rods | N/A |
| | | | | LP IIs box | | | |
| Winston Churchill overpass | 1 | 6.95 | 47 | LP SL 4 | 6.8 | Overpass deck | N/A |
| Humber Road | 1 | 36 | N/A | LP 20W | N/A | N/A | N/A |
| | | | | LP 30W | | | |
| Canal | 1 | N/A | N/A | F 3N | N/A | N/A | N/A |
| | | | | F 4N | | | |
| Chapel St. Mary A12 Underpass | 1 | 10 | N/A | N/A | N/A | N/A | N/A[2] |
| Stockman's Lane | 1 | N/A | N/A | LP IV box | N/A | Concrete Anchor | N/A |
| S8 Express Road Bridge | 1 | 15 | N/A | AZ 37-070 | 14.1 | Bridge Deck | Medium Dense Sand |

Notes: Please refer to Table A-1 for sheet pile dimensions.
(1): Lateral support is defined here as the support provided to the pile in the abutment to resist horizontal loads along the longitudinal axis of the bridge
(2): Literature does not specify this information, therefore, not available

Table A-3. Relevant information for U.S. bridge case histories

| Structure Identifier | No. of Spans | Span Length (m) | Abutment Width (m) | Sheet Pile Type | Vertical Length of Sheet Piles (m) | Lateral Support[1] | General Soil Condition |
|---|---|---|---|---|---|---|---|
| Taghkanic Creek | 1 | 12.8 | N/A | PZ 22 | 4.88 | N/A | Compact Silty Gravely Sand |
| Banks Road | 1 | 19.79” | N/A | N/A | 13.72 | Cabled Anchors | Clay |
| Small Creek | 1 | 24.18 | N/A | PZ 27 | 8.84 | Bridge Deck | N/A[2] |
| Bryan Road | 1 | 11.68 | 33’-0” | PZ 22 | 10.06 | Concrete Deadman | Sand and Clay |
| Lone Star Canal | 1 | 24.38 | 13.03 | AZ 14-770 | 13.63 | N/A | Clay |
| Route 4 | 1 | 14.63 | 63.7 | AZ 36 | N/A | Sheet Pile Deadman | Sand, Silt, Clayey Silt, Gravel, Rock |

Notes: Please refer to Table A-1 for sheet pile dimensions.
(1): Lateral support is defined here as the support provided to the pile in the abutment to resist horizontal loads along the longitudinal axis of the bridge
(2): Literature does not specify this information, therefore, not available

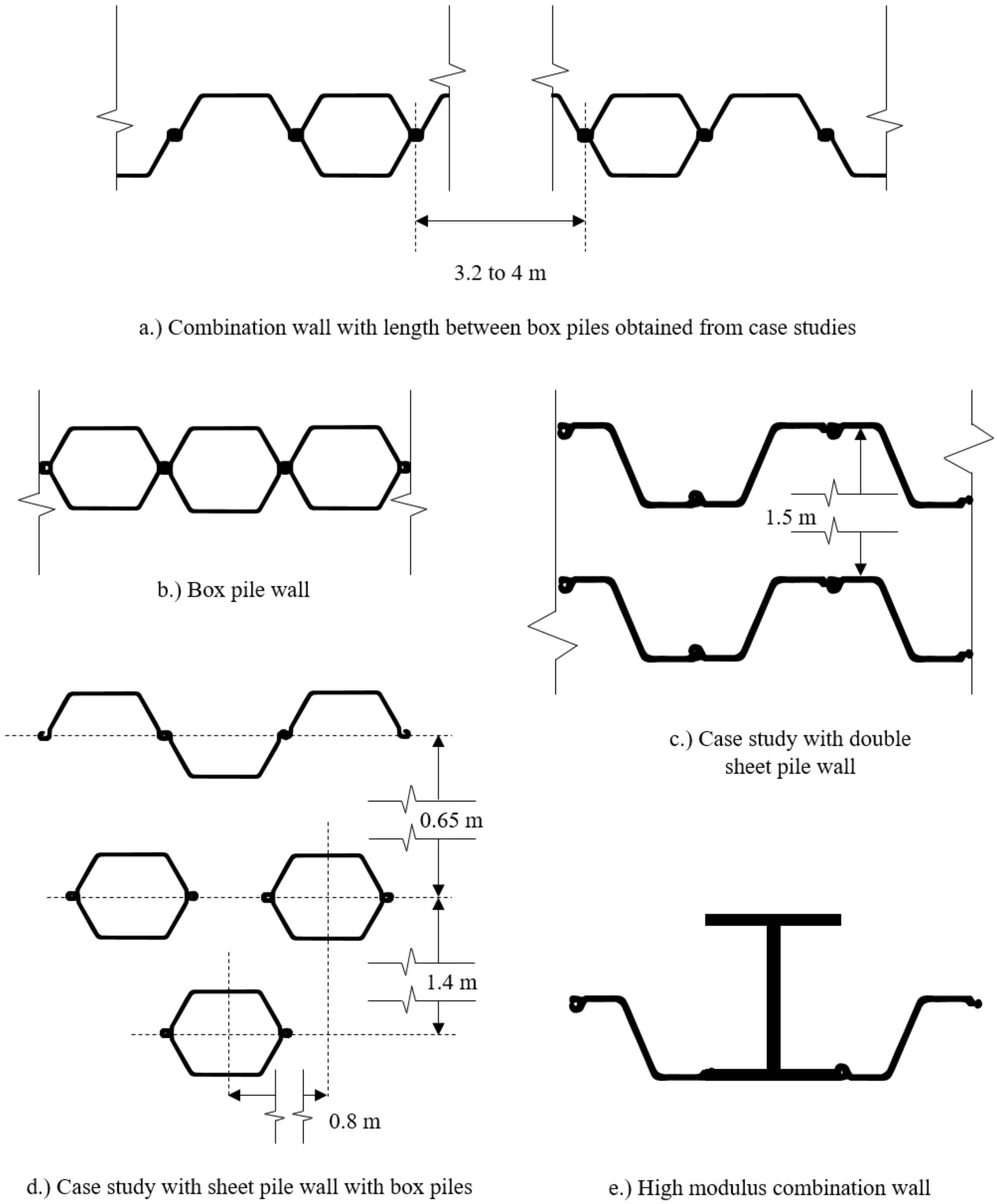


Figure A-1. Pile configurations used in European bridge case histories and pile load tests: a.) Sheet pile configuration for Somme River, Croisé Laroche overpass, St. Genes tunnel, and Pont de Pierre overpass, b.) Sheet pile configuration for A8 and Winston Churchill overpass, c.) Sheet pile configuration for S8 Express Road, d.) Sheet pile configuration for Moselle Canal bridge, and e.) Sheet pile configuration for A12 bridge

The following sections present summaries of the European and U.S. case studies. Examples of projects involving sheet pile abutments for both locations are also presented.

### A.1.1. European Case Studies

Several countries in Europe have used sheet piles as the only load bearing elements in a bridge abutment. Most case histories were reported in France, the United Kingdom, and Poland. A total of twelve bridges have been identified in Europe, seven of which are located in France, four in the United Kingdom, and one in Poland. Most of the European case histories involved sheet piles that were Larssen, Frodingham, or Arbed sections. Figure A-2 presents an example bridge from the European case histories, the Humber Road bridge in Immingham, England, which consists of a 35.9 m long span and 7.9 m high abutments.

a.) Image of Humber road bridge

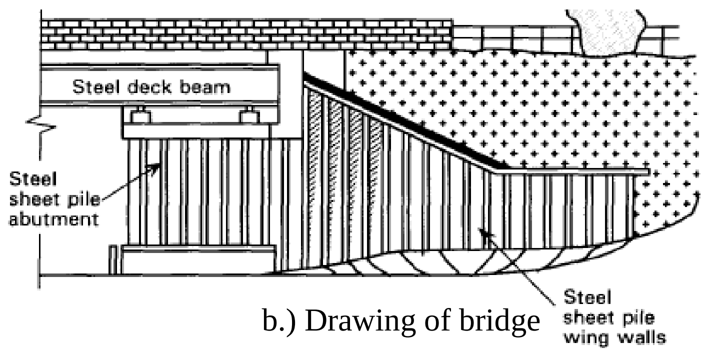


b.) Drawing of bridge

Figure A-2. Image (a) and drawing (b) of Humber Road bridge, Immingham, England (Yandzio 1998)

### A.1.2. U.S. Case Studies

A total of six bridges are identified in the U.S., two in New York and one in New Jersey, Iowa, Texas, and Alaska (Carle and Whitaker 1989; Evans et al. 2012; Hickman 2011; Skyline Steel LLC 2009). Several different designs were utilized for the U.S. bridges. Bridge abutments were constructed of PZ or AZ sections. Section size varied, however all of the piles used were Z type. Bridge span lengths ranged from 11.68 to 24.38 m with an average of 17.91 m. Sheet piles were driven to an average depth of 9.13 m. Designs typically included considerations for lateral load support, which consisted of cabled anchors, the bridge or overpass deck, or a concrete or sheet pile deadman. Sheet piles were driven to bedrock in many cases.

### A.1.3. Demonstration Project in Black Hawk County, Iowa

A successful demonstration project was reported by Evans et al. (2012) located in Black Hawk County, Iowa, involving instrumented sheet piles used for axial load bearing capacity. This bridge has a finished span length of 11.89 m, and is a two lane single-span beam-in-slab bridge, an elevation view of the bridge is shown in Figure A-3. Sheet piles were the sole foundation element used, the abutment consisted of a 10.06 m wide row of Skyline PZ 22 steel sheet piles driven to bedrock and the abutment construction is shown in more detail in Figure A-4.

Piles were instrumented with vibrating wire strain gages down the length of the pile to monitor short term and long term performance of the sheet pile abutments. Data was collected to evaluate the axial and lateral load bearing characteristics of the sheet pile abutment. The findings indicate, for the shallow bedrock conditions existing at this bridge site, that sheet piles provide adequate capacity and are a feasible alternative for bridge abutment construction. The authors of the study provide recommendations regarding the use of sheet piles abutments, mentioning the need for additional research in order to optimize the design.

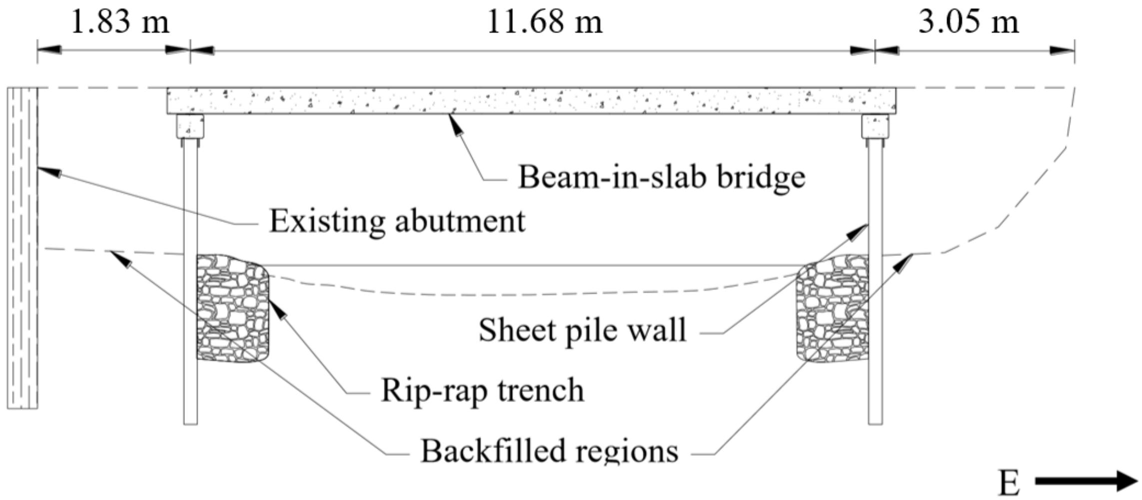


Figure A-3. Elevation view of bridge construction for demonstration project in Iowa (Evans et al. 2012)

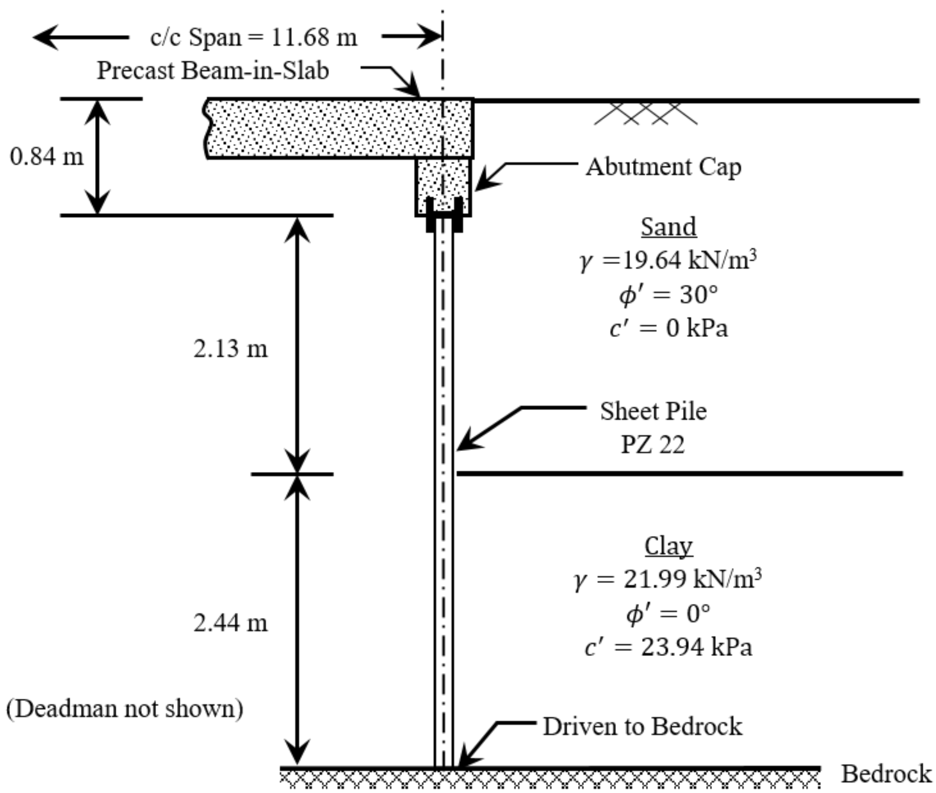


Figure A-4. Elevation view of abutment construction for demonstration project in Iowa (adapted from Evans 2010)

The identified literature provides numerous design recommendations and commentary on design considerations. A summary for the most important information identified is provided. The most comprehensive design guidance was found in the publications by Yandzio (1998) , the ‘Piling Handbook’ by ArcelorMittal (2008) , the ‘Steel Bearing Piles Guide’ by Biddle and the Steel Construction Institute (1997), and Eurocode 7 (2004). Common design considerations identified in these publications are outlined and summarized below. These sections are not meant to provide comprehensive design guidance for use of sheet pile elements for axial load bearing in sheet pile abutments. However, this summary is meant to provide a relevant review of existing design guidance and important design considerations which should be considered in the formulation of recommendations for this type of design practice in the U.S.

#### A.1.4. Geotechnical Design Guidance

Eurocode 7 (European Committee for Standardization 2004) provides information regarding the relevant geotechnical design considerations required when assessing design aspects such as pertinent limit states, obtaining design values for pile load capacity, as well as other general recommendations such as when to perform pile load tests to assess pile load response. The design requirements outlined in Eurocode 7 are based on a combination of limit states relevant to the particular project and design situations. Design situations refer to a range of considerations that pertain to the project site and are deemed significant to the foundation design. It is recommended that the limit states and design situations considered be based on the site conditions pertaining to overall stability and ground movements, function and size of structure, neighboring structures, ground conditions, ground-water conditions, regional seismicity, and influence of the environment.

Limits states can be exceeded in the ground, the structure, or both. Ground is defined as the soil and rock present at the site prior to construction. Eurocode 7 requires that limit states be verified by the use of calculations, the adoption of prescriptive measures, experimental models and load tests, or observational methods. Experience will typically be used to evaluate which limit states are relevant to a project. For geotechnical design requirements, the use of geotechnical categories are used. These categories are defined based on structure complexity, risk factors associated with the site, and any unique ground conditions:

<u>Geotechnical Category 1.</u> Applies to only small and simple structures. Category includes areas where there is low risk to overall stability or ground movements and excavations are kept above the water table.

<u>Geotechnical Category 2.</u> Applies to conventional types of structures and foundations. Category includes areas where there is no exceptional risk or difficult/unique loading or ground conditions.

<u>Geotechnical Category 3.</u> Applies to large or unusual structures outside of categories 1 and 2. Category includes areas where there is high risk or high seismicity.

The Eurocode defines the following limit states to consider based on the project:

- The loss of equilibrium either of the ground or structure, where the resistances provided by the structural material and ground are insufficient (EQU),

- Internal failure or excessive deformation of structural components that are significant to providing resistance (STR),
- Failure of the soil or rock where the resistance provided by the ground is significant to providing resistance (GEO),
- The loss of equilibrium of the structure or ground due to uplift forces by water pressure, such as buoyancy or other vertical action (UPL),
- Failure caused by hydraulic gradients such as hydraulic heave, internal erosion, and piping in the ground (HYD).

### A.1.5. Serviceability Considerations

For foundation design, limiting values must be determined for foundation movements. For all movements, differential settlement must be minimized in order to satisfy serviceability limit states in the supported structure. Deformations must account for the following factors:

- The expected accuracy of the calculated movement,
- The occurrence and rate of ground movement,
- Type of structure,
- Construction materials used,
- Type of foundation,
- Type of ground,
- Mode of deformation,
- Use of the structure,
- The need to ensure that there are not problems with the services entering the structure.

- and for differential settlement, the following factors should be considered:
- The occurrence and rate of settlement and ground movements,
- Variations in the properties of the ground,
- Load distributions,
- Construction methods (and sequence of loading), and
- The stiffness of the structure after construction.

For cases where limiting deformation values cannot be obtained for the supported structure, structural deformation and foundation movement can be obtained in Annex H.

### A.1.6. Design Strength of Limit States

For axially loaded piles, the Eurocode specifies that the design procedure must demonstrate a low probability of exceeding the following limit states:

- Ultimate limit states of compressive or tensile resistance failure of a single pile,
- Ultimate limit states of compressive or tensile resistance failure of the pile foundation as a whole,
- Ultimate limit states associated with damage to supported structure due to foundation settlement, and
- Serviceability limit states in supported structure caused by displacement of piles.

The design procedure must also account for the overall stability of the structure. Overall stability introduces several additional limit states such as:

- Loss of overall stability of the ground and associated structures,
- Excessive movements in the ground due to shear deformation, settlement, vibration, or heave,

- Damage or loss of serviceability in neighboring structures, roads or services due to movements in the ground.

A.1.7. Compressive Ground Resistance

Performance of the pile system is evaluated both for limit states associated with compressive and tensile action. The piles and pile foundation must demonstrate the capacity to safely resist these forces to avoid compressive and tensile failure for all limit states. Compressive ground resistance is evaluated through the following inequality:

| (Eurocode) | (LRFD Equivalent) | |
|---|---|---|
| $F_{c;d} \le R_{c;d}$ | $P_u \le \phi P_n$ | (A.1) |

Where,

$F_{c;d}$ = the design axial compression load on a pile or a group of piles, and

$R_{c;d}$ = the design value of $R_c$, the compressive resistance of the ground against a pile, at the ultimate limit state.

For the case of pile groups, two failure mechanisms are considered: individual piles failing in compression and the pile group failing in compression as a block. Piles failing as a group can be evaluated by treating the group as a single equivalent pile of large diameter. The stiffness of the supported structure should also be accounted for in the design resistance. A very stiff structure will lead to a more uniform pile stress distribution and, consequently, the failure mode involving individual piles can be neglected. Conversely, if the structure is flexible, the compressive resistance of the weakest pile will develop as the controlling limit state. In particular, edge piles should be evaluated for failure, as eccentric loading from the structure may lead to failure in these piles. The soil strata must be considered in the resistance of the piles in compression.

Particular attention should be given to the soil above and below the end of the pile within a zone that extends for several pile diameters both above and below the pile base. The effects of a weak soil strata must be considered when calculating the compressive resistance of the foundation, as a weak soil layer under the base of the pile will have a large influence over the pile compressive resistance. Punching failure should be considered when weak soil is encountered at a depth less than 4 times the pile diameter below the base. For the case of open ended piles, such as pipe or box piles, with openings of more than 500 mm in any direction, the effects of plugging must be considered. If there are no special devices to induce plugging, the base resistance will be obtained from the smallest of the shearing resistance between the soil plug and the inside face of the pile and the base resistance obtained using the gross cross-sectional area of the base.

Static load tests are highly recommended by Eurocode 7 both for design purposes and verification of calculation models. Guidance is provided for evaluating the compressive resistance of piles through static load testing. If trial piles are used, they must be installed using the same method and must be in a similar soil strata existing at the site of the pile foundation. If the test piles and working piles have different diameters, requirements in Eurocode 7 must be met. For open ended piles, the use of smaller test piles is not ideal as it leads to differences in the mobilization of the compressive resistance of a soil plug in the pile. In some cases, piles will experience negative skin friction caused by the downward movement of soil (referred to as downdrag). When downdrag is expected, the applied load and pile resistance at failure must be corrected in order to compensate.

The compressive resistance of the pile is supplied from a base resistance value and a shaft resistance value. The equation below provides for the characteristic pile resistance:

$$R_{c;k} = R_{b;k} + R_{s;k} \tag{A.2}$$

Where,

$R_{c;k}$ = the characteristic compressive resistance of the ground,

$R_{b;k}$ = the characteristic value of the base resistance of a pile, and

$R_{s;k}$ = the characteristic value of the shaft resistance of a pile.

The value of these components can be obtained through static load testing, or estimated based on ground test results or dynamic load tests. The design compressive resistance of the pile or pile group is developed from the nominal compressive resistance of the pile through the application of partial factors. The specific partial factors used are determined by the installation method and depend on short or long term conditions, Table A-4 presents information given in Annex A of Eurocode 7 which provide values for partial factors. The following equations can be used to obtain the design resistance of the pile:

$$R_{c;d} = {R_{c;k}}/{\gamma_t} = {R_{b;k}}/{\gamma_b} + {R_{s;k}}/{\gamma_s} \tag{A.3}$$

Where,

$R_{c;d}$ = the design value of the compressive resistance of the ground against a pile, at the ultimate limit state,

$\gamma_t$ = the partial factor for total resistance of a pile,

$\gamma_b$ = the partial factor for the base resistance of a pile, and

$\gamma_s$ = is the partial factor for shaft resistance of a pile.

Table A-4. Partial resistance factors ( $\gamma_R$ ) for driven piles

| Resistance | Symbol | Set | | | |
|---|---|---|---|---|---|
| | | R1 | R2 | R3 | R4 |
| Base | $\gamma_b$ | 1.0 | 1.1 | 1.0 | 1.3 |
| Shaft (compression) | $\gamma_s$ | 1.0 | 1.1 | 1.0 | 1.3 |
| Total/combined (compression) | $\gamma_t$ | 1.0 | 1.1 | 1.0 | 1.3 |
| Shaft in tension | $\gamma_{s;t}$ | 1.25 | 1.15 | 1.1 | 1.6 |

Evaluation of the compressive resistance of pile can be used for design, but must be based on ground test results verified through pile load tests from comparable experience. Comparable experience consists of documented or clearly established results obtained for similar soil and rock conditions, and involving similar structures. A model factor may be included that accounts for the range of uncertainty in the results and account for systematic errors associated with the method of analysis. Model factors are used where a high factor of safety is desired. The above equations are used to evaluate the compressive resistance of the pile, however values obtained from ground testing are used to obtain values for $R_{b;k}$ and $R_{s;k}$ .The following equation may be used to obtain the characteristic values:

$$\begin{aligned} R_{c;k} &= R_{b;k} + R_{s;k} = \left( \frac{R_{b;cal} + R_{s;cal}}{\xi} \right) = \frac{R_{c;cal}}{\xi} \\ &= Min\left\{ \frac{(R_{c;cal})_{mean}}{\xi_3} ; \frac{(R_{c;cal})_{min}}{\xi_4} \right\} \end{aligned} \tag{A.4}$$

Where,

$R_{b;cal}$ = the pile base resistance, calculated from ground test results, at the ultimate limit state,

$R_{s;cal}$ = the ultimate shaft friction, calculated from ground parameters from test results,

$\xi$ = the correlation factor depending on the number of piles tested or of profiles of tests,

$R_{s;cal}$ = the calculated value of compressive resistance of ground against pile, at the ultimate limit state, and

$\xi_3$ and $\xi_4$ = the correlation factors depending on the number of profiles of tests, *n*.

Thus, for multiple tests:

$$(R_{s;cal})_{mean} = \left(R_{b;cal} + R_{s;cal}\right)_{mean} = \left(R_{b;cal}\right)_{mean} + \left(R_{s;cal}\right)_{mean} \tag{A.5}$$

and

$$(R_{s;cal})_{min} = \left(R_{b;cal} + R_{s;cal}\right)_{min} \tag{A.6}$$

As an alternative to Equations (A.5) and (A.6), $R_{b;k}$ and $R_{s;k}$ may be evaluated through the following equations:

$$R_{b;k} = A_b + q_{b;k} \tag{A.7}$$

and

$$R_{s;k} = \sum_i A_{s;i} + q_{s;i;k} \tag{A.8}$$

Where,

$q_{b;k}$ and $q_{s;i;k}$ = characteristic values of base resistance and shaft friction in the various strata, obtained from values of ground parameters,

$A_b$ = the base area under pile, and

$A_{s;i}$ = the pile shaft surface area in layer $i$.

For Equation (A.3), the values used for partial factors $\gamma_b$ and $\gamma_s$ may need to be corrected by a model factor larger than 1.0.

The applicability of a model developed from ground test results should consider several factors, as recommended by Eurocode 7:

- Soil type used, grading, angularity, mineralogy, density, pre-consolidation, compressibility, and permeability
- Methods used to install the piles, method of boring or driving should be included,
- Pile dimensions such as length, diameter, material, and shape of pile at base, and
- Method of ground testing.

The ultimate compressive resistance of the pile can be evaluated using other methods such as dynamic impact tests, the use of driving formulae, and wave equation analysis. These methods must first be verified through the use of static load tests for similar piles driven using similar methods into a similar soil as for the pile foundation site.

### A.1.8. Ground Tensile Resistance

In cases where the pile foundation may experience tensile loading, such as heave loading or excessive pore water pressure, the foundation must be designed accordingly.

To ensure safe design against failure in tension, the following inequality must be satisfied:

$$F_{t;d} \leq R_{t;d} \tag{A.9}$$

Where,

$F_{t;d}$ = the design axial tensile load on a tensile pile or a group of tensile piles, and

$R_{t;d}$ = the design value of the tensile resistance of a pile or group of piles, or of the structural tensile resistance of an anchorage.

For tension piles, two failure mechanisms are considered: the pull out of a pile from the ground mass and the uplift of the block of ground containing the piles. Piles load tests as well as ground test results can be used to evaluate the ultimate tensile resistance of an isolated pile, which is given in the following equation:

$$R_{t;d} = {R_{t;k}}/{\gamma_{s;t}} \tag{A.10}$$

Where,

$R_{t;d}$ = the design value of the tensile resistance of a pile or of a group of piles, or of the structural tensile resistance of an anchorage,

$R_{t;k}$ = the characteristic value of the shaft resistance of a pile, and

$\gamma_{s;t}$ = the partial factor for total resistance of a pile.

### A.1.9. Load Testing of Piles

Eurocode 7 provides recommendations for when pile tests should be used in the design process and how such tests should be conducted. Pile load tests include both static load and dynamic load tests and can be conducted on trial or working piles. In general, pile tests should be conducted where there is little prior knowledge associated with the driving methods or site conditions, when there are concerns based on the lack of theory or experience with the applied loading, or if there observations during installation of any deviations from the expected behavior of the pile that cannot be explained by additional ground investigations. Pile load testing can be used to verify the suitability of the construction method, assess how the pile and surrounding soil will respond to loading, and provide evidence to evaluate the suitability of the foundation design. Several considerations are provided by Eurocode 7 concerning the pile load test. Pile tests should be conducted at critical locations where the most adverse ground conditions exist and adequate time should be allowed between driving and testing such that pore water pressures are allowed to reach their initial values. Pore water pressure may be recorded to help determine when to start the load test in cases where it is difficult to determine the dissipation of these pressures.

The loading of test piles for static load tests must be carried out such that conclusions can be made concerning deformation behavior, creep, and rebound of the pile foundation. Trial piles have the additional requirement that they be loaded until they reach the ultimate failure load. For tests used to evaluate the tensile and compressive behavior of the pile, the direction of loading must be applied along the longitudinal axis of the piles. Devices used to measure the applied loads, stress or strain, and displacements of the piles must be calibrated prior to testing.

For trial piles, the selection of the number of piles to test in order to verify the design depends on several factors. The soil conditions at the site should be well-documented and any soil layer that will influence the response of the pile should be investigated. The geotechnical classifications of the soils, how they vary across the site, and the performance of piles installed in similar ground conditions must be considered. The number of piles required for the foundation design should also be considered and the method used to install the piles should be fully documented. For working piles, the number of pile tests is determined by observations made during installation of the piles. Test loading of working piles should be equal to or greater than the design load.

### A.1.10. Structural Design Guidance

Structural design guidance provided in the Eurocode related to sheet pile elements is summarized below. Note that the Standard Specifications (2012) section 1084-2 states that steel sheet piles for permanent applications should be hot rolled and meet ASTM A690 specifications. Thus, in this section steel grade A690 will be considered when interpreting the design guidance relative to what a standard sheet pile section used in the U.S. would equate to within the Eurocode.

### A.1.11. Required Strength Analysis

Within the ultimate limit state criteria, the Eurocode considers structural failure due to bending and/or axial forces, failure due to overall flexural buckling, local buckling due to overall bending, local failure at points of load application, and fatigue. The Eurocode also considers the combination of failure regarding both soil and structural failure. It is important to note that the provisions of the Eurocode (BSI 2007) do not cover special requirements due to seismic design but do contain corrosion effects on the durability of steel piling as well as overall design considerations governed by the ultimate limit state criteria and serviceability limit state criteria.

The Eurocode classifies sheet pile sections for the limit state analysis and prescribes certain analysis methods that are dependent on this classification system, as shown in Table A-5.

Table A-5. Classification of sheet piles for analysis.

| Class No. | Description |
|---|---|
| 1 | Plastic analysis involving moment redistribution can be utilized and full plastic resistance can be utilized, provided that sufficient rotation capacity exist |
| 2 | Elastic global analysis, but plastic resistance of cross-section can be utilized |
| 3 | Elastic global analysis, but analysis is limited to the elastic resistance of the cross-section |
| 4 | Cross-sections for which local buckling affects the cross-sectional resistance is to be used |

The classification of the sheet piles depends on the width-thickness ratios of elements in the cross-section, as shown in Table A-6, where:

$b$ = the width of the flat portion of the flange, measured between the corner radii, provided that the ratio $r/t_f$ is not greater than 5.0; otherwise a more precise approach should be used,

$t_f$ = the thickness of the flange or flanges with constant thickness,

$r$ = the midline radius of the corners between the webs and the flanges,

$f_y$ = yield strength

It is important to note that this criteria is similar to AISC compactness criteria (AISC 2011) for sections, however, AISC does not provide criteria for sheet pile sections.

Table A-6. Classification of cross-sections (modified from EN 1993-5:2007)

<table>
<tr><td>Classification</td><td colspan="7">Z-profile</td></tr>
<tr><td>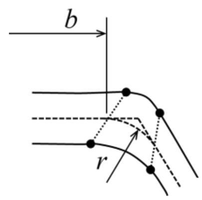
</td><td colspan="7">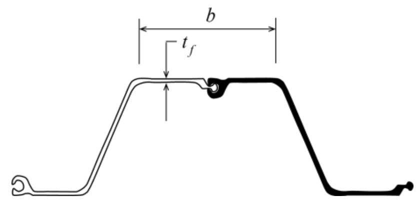
</td></tr>
<tr><td>Class 1</td><td colspan="7">Same boundaries as for Class 2 apply<br>A rotation check has to be carried through</td></tr>
<tr><td>Class 2</td><td colspan="7">$\frac{b/t_f}{\varepsilon} \leq 45$</td></tr>
<tr><td>Class 3</td><td colspan="7">$\frac{b/t_f}{\varepsilon} \leq 66$</td></tr>
<tr><td rowspan="2">$\varepsilon = \sqrt{\frac{235}{f_y}}$</td><td>$f_y\ (N/mm^2)$</td><td>240</td><td>270</td><td>320</td><td>355</td><td>390</td><td>430</td></tr>
<tr><td>$\varepsilon$</td><td>0.99</td><td>0.93</td><td>0.86</td><td>0.81</td><td>0.78</td><td>0.74</td></tr>
<tr><td colspan="8">Note: For Class 1 cross-sections it should be verified that the plastic rotation provided by the cross-section is not less than the plastic rotation required in the actual design case. Guidance for this verification (rotation check) is given in Annex C.</td></tr>
</table>

Determining whether a cross-section can be analyzed as a Class 1 section (incorporate full plastic analysis and plastic resistance of the cross-section) “requires verifying that the plastic rotation provided by the cross-section is not less than the plastic rotation required in the actual design case.” Guidance for this determination can be found in Annex C of the standard. The plastic rotation provided by the cross-section can be estimated for Z sections through the plot provided inFigure A-5. The plastic rotation in the required strength analysis of the actual design case can be determined either by:

1) a plastic hinge model (where $\phi_{Cd}$ is taken as the maximum rotation angle in any plastic hinge),
2) a plastic hinge and plastic zone model, or
3) a plastic hinge and plastic zone model where the rotations are computed from the displacements.

These analysis options are depicted in Figure A-6. The Annex C of the EN 1993-5 Standard provides simplified equations for estimating the design rotation angles for cases 2 and 3.

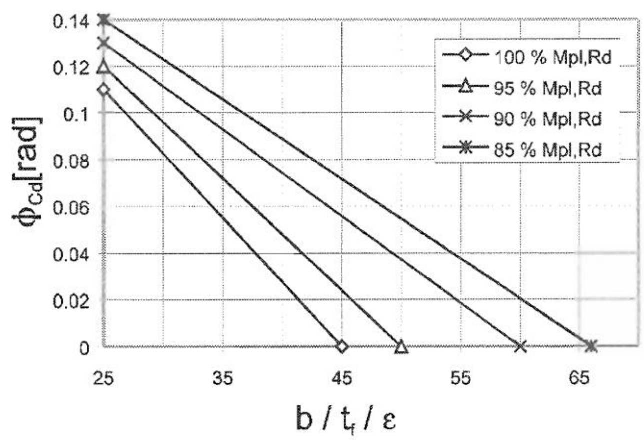


Figure A-5. Design plastic rotation angle provide by the cross-section as a function of the design plastic moment resistance (from EN 1993-5:2007).

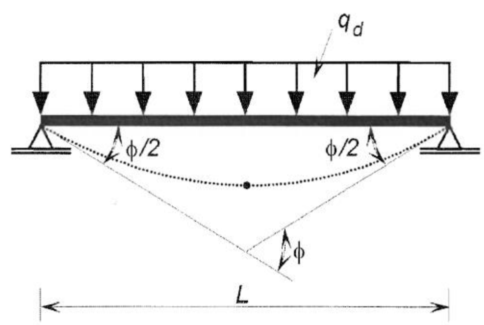


a) Plastic Hinge Model

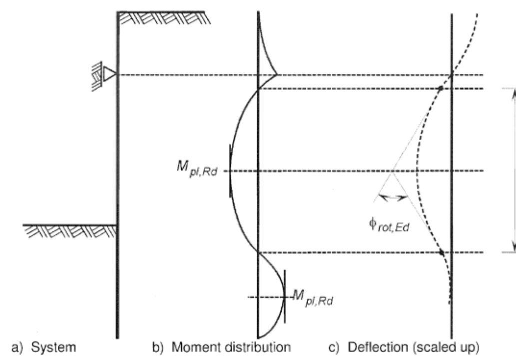


b) Plastic Hinge/ Plastic Zone Model

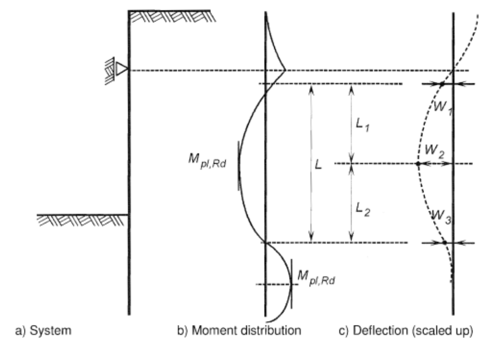


c) Plastic Hinge/ Plastic Zone Model with Rotations Determined from

Figure A-6. Permitted methods for determining the design rotation angle for the actual design case (from EN 1993-5:2007).

A.1.12. Serviceability Considerations

Within the serviceability limit state criteria, the Eurocode places limits on vertical and/or horizontal displacements as necessary to suit the supported structure and places vibration limits necessary to suit structures directly connected to or near the bearing piles. According to the Eurocode, the allowable vertical movement of the foundation should be evaluated and checked against limiting values based on serviceability limit states of the structure and limiting values based on site conditions such as ground conditions, type of structure, and load distribution. Differential settlement must be minimized to avoid exceeding a limit state in the supported structure, guidance is provided concerning the parameters which must be considered in this analysis. Due to the uncertainties in ground conditions, calculations of settlement are treated as only approximations

The serviceability limit states due to settlement must be checked under condition that account for downdrag, when it is expected to occur. Piles must be evaluated individually and as a group for settlement.  For piles whose base is resting on rock or very stiff stratum, the partial factors for the ultimate limit state conditions are considered sufficient to satisfy serviceability limit state conditions. For cases where upward displacements are expected to occur, similar considerations as for downward settlements must be covered in design.

A.1.13. Design Strength of Limit States

The following sections summarize the Eurocode limit state analysis applicable for sheet pile elements with an effort made to translate the nomenclature, verbiage, and equations to an equivalent form of U.S./AISC specification.

Considering the flexural strength of the cross section, design bending moment for sheet pile cross-section is governed by the design equation:

| | (Eurocode) | (AISC Equivalent) | |
|---|---|---|---|
| | $M_{Ed} \leq M_{c,Rd}$ | $M_u \leq \phi M_n$ | (A.11) |

Where the design resistance of the cross-section is determined by:

| | (Eurocode) | (AISC Equivalent) | | |
|---|---|---|---|---|
| Class 1 or 2: | $M_{c,Rd} = \beta_B W_{pl} f_y / \gamma_{M0}$ | $\phi M_n = \phi F_y Z_x$ | (F2-1) | (A.12) |
| Class 3: | $M_{c,Rd} = \beta_B W_{el} f_y / \gamma_{M0}$ | $\phi M_n = \phi F_y S_x$ | (F4-1) | (A.13) |

Where:

$M_{c,Rd}$ = design moment resistance of the cross-section,

$\beta_B$ = a factor that takes in account of possible lack of shear force transmission in the interlocks,

$W_{pl}$ = plastic section modulus determined for a continuous wall, and

$W_{el}$ = elastic section modulus determined for a continuous wall

As indicated in the AISC equivalent design equations, the Class 1 or 2 limit state is governed by plastic moment yielding of the cross-section, while the Class 3 limit state is governed by compression flange yielding due to the non-compact section classification. Note that for Z-shaped piles, the shear force transmission factor, $\beta_B$, is taken as 1.0, so the equations reduce almost identically to the AISC limit state equations. However, the partial factors applied to the yield limit state are 1.0 in the Eurocode, while the AISC associated resistance factors for these limit states are 0.9 so the Eurocode approach is slightly less conservative (assuming comparable load factors in the computation of the required flexural strength). Class 4 sections require a more in-depth analysis covered in Annex A of the EN 1993-5 Standard that considers local buckling of the cross-section. However, these should not be a concern for PZ 27 cross-sections currently used in NCDOT designs.

Considering the shear strength of the cross section, the Eurocode specifies the design strength of the cross-section for the limit state of shear yielding of the web of the sheet pile as:

(Eurocode) (AISC Equivalent)

$$V_{pl,Rd} = \frac{A_v f_y}{\sqrt{3}\gamma_{M0}} = \frac{0.5774 A_v f_y}{\gamma_{M0}} \qquad \phi V_n = \phi 0.6 F_y A_w C_v \quad \text{(G2-1)} \tag{A.14}$$

Where,

$A_v$ = the projected shear area, shown in Figure A-7, for each web, acting in the same directions as the design shear force and is defined as $A_v = t_w\left(h - t_f\right)$,

$t_w$ = web thickness shown in Figure A-7

$h$= section height shown in Figure A-7

$t_f$ = flange thickness shown in Figure A-7

The shear buckling resistance of the cross-section is also required to be evaluated if:

$$\frac{c}{t_w} > 72\varepsilon \tag{A.15}$$

Where:

$$c = \frac{h - t_f}{sin\alpha} \tag{A.16}$$

and $\alpha$ is the inclination of web shown in Figure A-7.

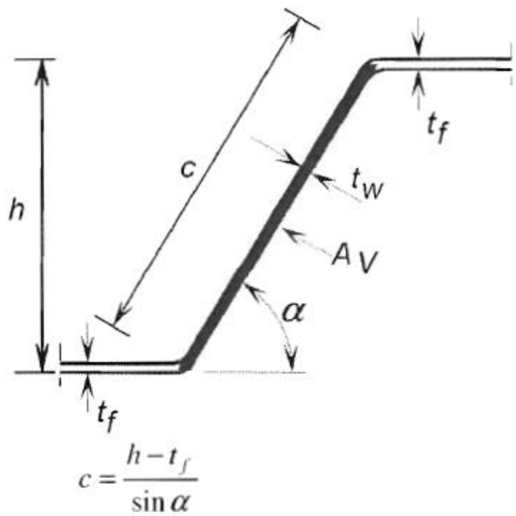


Figure A-7. Definition of shear area for Z-profile sheet piles in the Eurocode (EN 1993-5:2007).

For the PZ 27 cross-section, $c = 13.3$, so the classification of PZ 27 cross-sections by steel grade is given in Table A-7.

Table A-7. Classifications of PZ 27 cross section by steel grade.

| Grade | $F_y\ (MPa)$ | $\varepsilon$ | $c/t_f$ | $72\varepsilon$ | Classification |
|---|---|---|---|---|---|
| A328 | 268.9 | 0.935 | 35.5 | 67.3 | No Shear Buckling Consideration |
| A572 Gr. 50<br>A588<br>A690 | 344.7 | 0.825 | 35.5 | 59.4 | No Shear Buckling Consideration |
| A572 Gr. 60 | 413.7 | 0.754 | 35.5 | 54.3 | No Shear Buckling Consideration |

Since the PZ 27 cross-section is not subject to shear buckling considerations for any of the grades of material that it is available in, this document will forego further discussion of the shear buckling strength analysis provided by the Eurocode. The relevant equations for shear buckling strength can be found in Section 5.2.2 of the EN 1993-5 Standard.

The Eurocode standard provides consideration for the interaction of flexural and shear limit states in the analysis of sheet piles. Two cases are provided as summarized below:

1) If the $V_{Ed} \leq 0.5V_{pl,Rd}$ (Equivalent AISC: $V_u \leq 0.5\phi V_n$ for shear yielding of web limit state), then there is no reduction of the design plastic moment strength of the cross-section.

2) If $V_{Ed} \leq 0.5V_{pl,Rd}$ then the design plastic moment strength of the cross-section is reduced to:

(Eurocode) (AISC Equivalent)

$$M_{V,Rd} = \left[\beta_B W_{pl} - \frac{\rho A_v^2}{4t_w sin\alpha}\right] f_y \qquad \phi M_n = \phi\left[Z_x - \frac{\rho A_w^2}{4t_w sin\alpha}\right] F_y \tag{A.17}$$

where:

$$\rho = \left(\frac{2V_{Ed}}{V_{pl,Rd}} - 1\right)^2 \tag{A.18}$$

The interaction diagram for combined shear and flexure according to the Eurocode standard is calculated for the PZ 27 sheet pile using geometric properties provided by the Skyline Steel technical data. The interaction diagram exhibits a mild reduction in the flexural capacity of the cross-section when the required shear strength approaches the design shear strength of the cross-section. Note that the interaction diagram is independent of the grade of steel used.

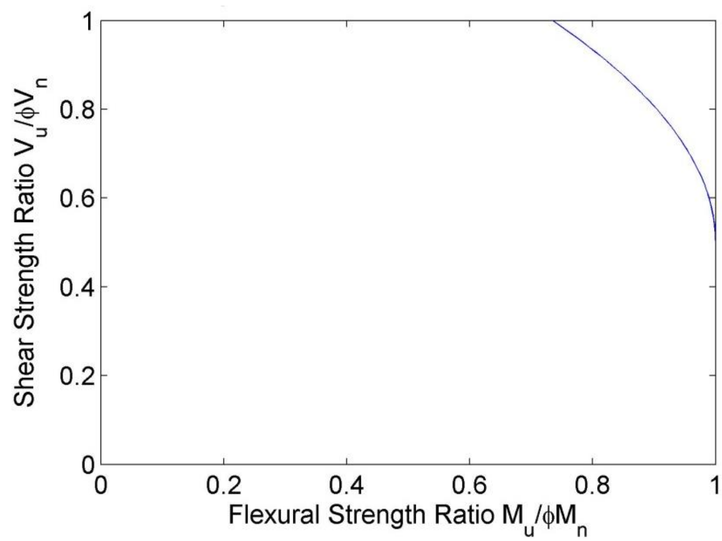


Figure A-8. Developed interaction diagram for PZ 27 under combined flexure and shear according to EN 1993-1-1:2005.

Guidance is provided for combined flexure and axial loading. The criteria established for considering the influence of member buckling under cases of combined bending and compression is:

(Eurocode)

$$\frac{N_{Ed}}{N_{cr}} \leq 0.04$$

(AISC Equivalent)

$$\frac{P_u}{\phi P_n} \leq 0.04 \qquad \text{(A.19)}$$

Where $N_{cr} (= P_{cr})$ is the elastic critical buckling load of the sheet pile.

According to the EN 1993-5 Standard, the elastic critical buckling load may be calculated:

1) With an appropriate soil model, such as *T-Z* / *Q-Z* analysis involving soil springs at shear and bearing locations
2) Using the simplified Euler buckling equation:

$$N_{cr} = \frac{EI\beta_D\pi^2}{l^2} \tag{A.20}$$

Where,

$l$= the buckling length (see Figure A-9), and

$\beta_D$= a reduction factor that accounts for incomplete shear transfer at the interlock between adjacent sheet piles.

This reduction yields an effective flexural rigidity that accounts for incomplete shear transfer at the interlock, but for most Z-profile constructions, the interlock is located far from the centroid of the bending axis, so this reduction factor should be close to 1.0.

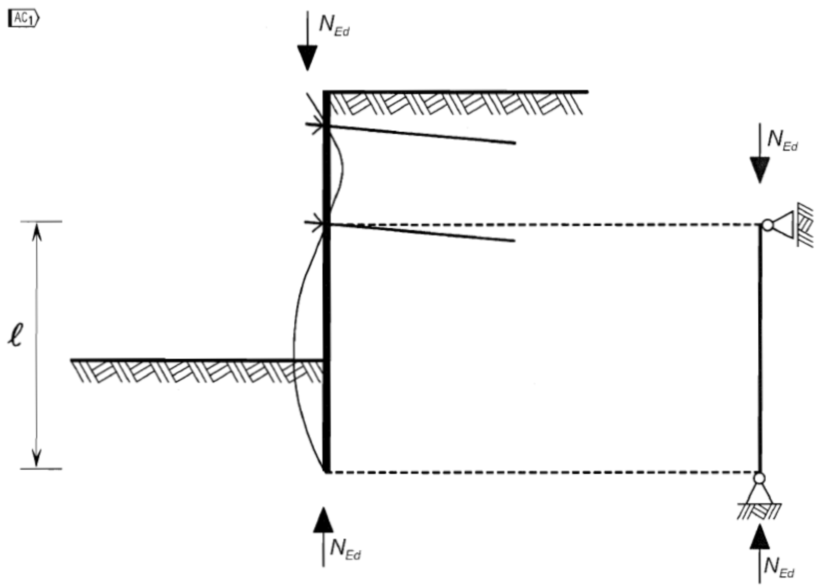


Figure A-9. Determination of effective buckling length for use in simplified Euler critical load equation (from EN 1993-5:2007).

If $\frac{N_{Ed}}{N_{cr}} > 0.04 \left( \text{or} \frac{P_u}{\phi P_n} > 0.04 \right)$, then the buckling resistance needs to be verified.

For the case of a cantilever wall (no deadman or anchor), considering the interaction of flexural and axial effects, if the horizontal displacement due to a support load of $\frac{N_{Ed}}{100}$ is less than $\frac{l}{500}$ then the support is assumed to provide enough restraint that the analysis can be considered for non-sway behavior. In all other cases, the buckling mode is a sway mode and a detailed buckling investigation is required based on the methods in Eurocode 3(EN 1993-1-:2005).

If boundary conditions are provided by elements (defined as anchor, earth support, capping beam, etc.) that give positional restraint corresponding to a non-sway buckling mode, then the following interaction equation must be satisfied:

$$\frac{N_{Ed}}{\chi \mathrm{N}_{\mathrm{pl,Rd}}\left(\frac{\gamma_{M0}}{\gamma_{M1}}\right)}+1.15\frac{M_{Ed}}{M_{c,Rd}\left(\frac{\gamma_{M0}}{\gamma_{M1}}\right)}\leq 1.0 \tag{A.21}$$

Which reduces to:

$$\frac{0.909N_{Ed}}{\chi A_g F_y}+1.046\frac{M_{Ed}}{M_{c,Rd}}\leq 1.0 \tag{A.22}$$

The flexural buckling resistance of the cross-section is determined using a buckling coefficient, $\chi$, obtained from curve $d$ in Figure A-10 below using a non-dimensional slenderness1 given by:

$$\bar{\lambda}=\sqrt{\frac{Af_y}{N_{cr}}} \tag{A.23}$$

1 *Note that this non-dimensional slenderness is equivalent to the old* $\lambda_c=\frac{KL}{\pi r}\sqrt{\frac{F_y}{E}}$ *that AISC used to use before replacing it (during the change to the 13th edition manual) with the now more familiar KL/r.*

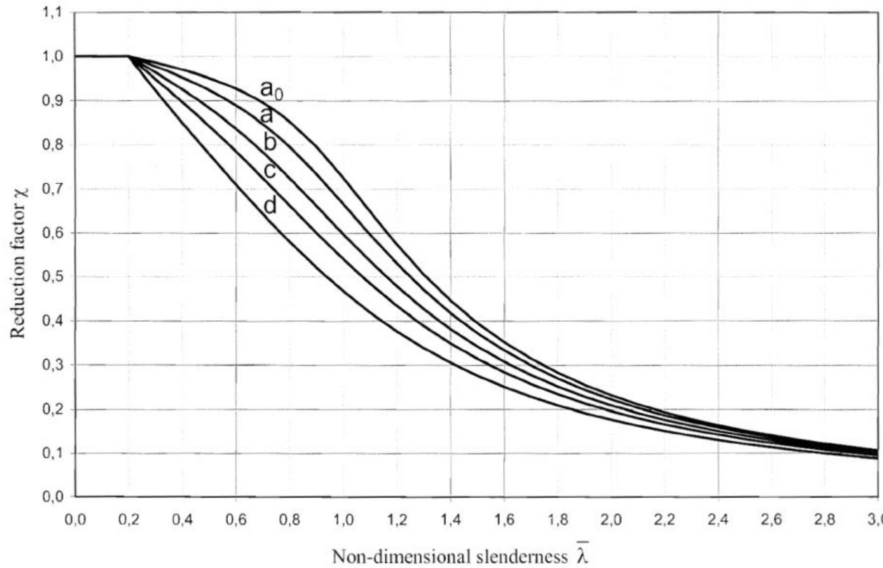


Figure A-10. Buckling coefficient for flexural buckling resistance calculation (from EN 1993-1-1:2005).

According to BSI (2005), the appropriate buckling curve prescribed for use with sheet piles (curve $d$) takes the analytical form:

$$\chi = \frac{1}{\Phi + \sqrt{\Phi^2 - \bar{\lambda}^2}} \leq 1.0 \tag{A.24}$$

where:

$$\Phi = 0.5\left[1 + 0.76\left(\bar{\lambda} - 0.2\right) + \bar{\lambda}^2\right] \tag{A.25}$$

Since we have the analytical form, we can compare the buckling resistance as a fraction of yield stress per the Eurocode and AISC reductions for residual stresses and imperfections. The plot provided in Figure A-11 was generated to make this comparison and reveals that application of the AISC equations for the flexural buckling limit state may severely over-predict the strength of steel sheet piles compared to the Eurocode buckling estimates. Incorporating guidance from AISC Section E7 (2007) “Members with Slender Elements” would likely improve the correlation, if the elements in the sheet pile cross-section are classified as slender. Examining the limiting width-thickness ratios in Table B4.1 of the AISC (2007) specification, the limiting width thickness ratio for slender webs of Z-profile sheet piles would most likely come from case 14 (uniform compression in all other stiffened elements), which provides:

$$\lambda_r = 1.49\sqrt{\frac{E}{F_y}} \tag{A.26}$$

Approximating the width thickness ratio for the PZ 27 section as $\approx 37$ using available dimensions, it appears that A328 (Fy=39ksi) sheet piles are non-slender, but sheet piles with nominal yield stress of 50ksi or 60ksi would just qualify as containing slender stiffened elements.

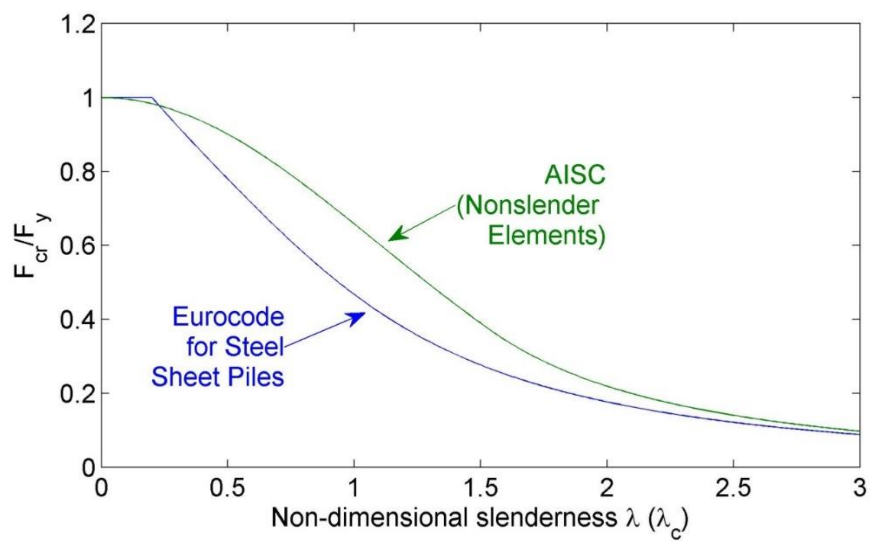


Figure A-11. Comparison between AISC flexural buckling curve versus Eurocode.

In computing the elastic critical load for non-sway conditions, the Eurocode provides simplified approaches for free earth and fixed earth (Figure A-12) restraint conditions. In order for a design to provide sufficient restraint for the free earth condition, the Eurocode recommends that the passive earth pressure and friction be able to resist the horizontal force:

$$F_{Q,Ed} = \pi N_{Ed} \left( \frac{d}{l} + 0.01 \right) \tag{A.27}$$

Where $d$ is the maximum relative deflection occurring between supports determined by elastic analysis. The free-body diagram associated with this criterion is provided in Figure A-13.

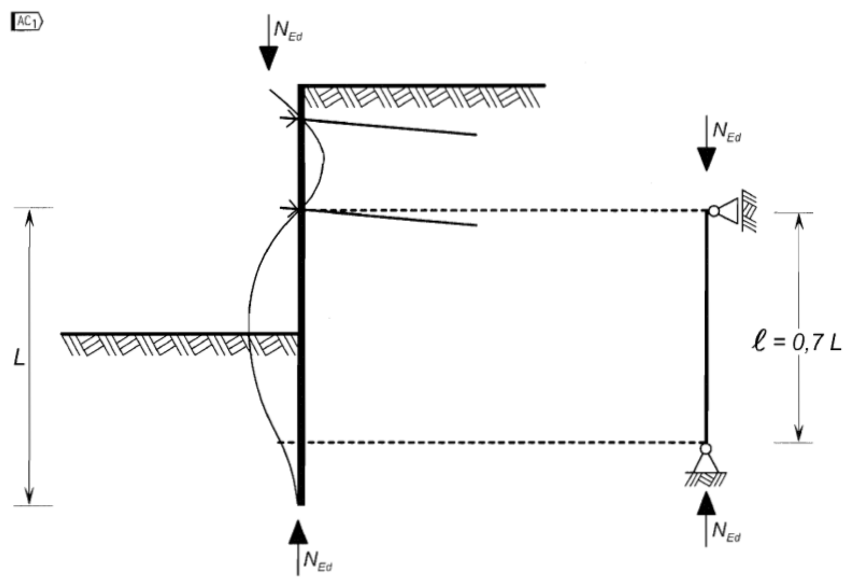


Figure A-12. Fixed earth support simplified buckling length determination (from EN 1993-5:2007).

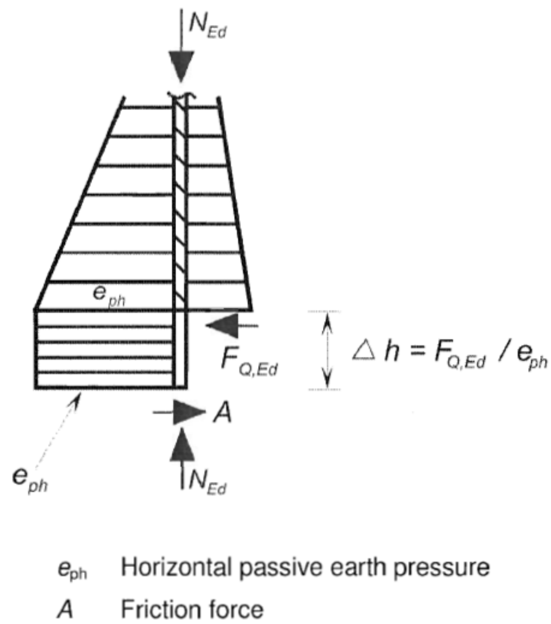


Figure A-13. Determining horizontal force at toe for free earth condition (from EN 1993-5:2007).

For Z-profiles, the following interaction equation are provided by the Eurocode for combined loads including flexure, axial, and shear loads:

*If the required shear strength <u>does not</u> exceed 50% of the design shear strength:*

For $\frac{N_{Ed}}{N_{pl,Rd}} \leq 0.1$:

$$\frac{M_{Ed}}{M_{c,Rd}} \leq 1.0 \tag{A.28}$$

For $\frac{N_{Ed}}{N_{pl,Rd}} > 0.1$:

$$M_{N,Rd} = 1.11 M_{c,Rd}\left(1 - \frac{N_{Ed}}{N_{pl,Rd}}\right); \quad M_{N,Rd} \le M_{c,Rd} \tag{A.29}$$

Which can be rearranged to produce:

$$\frac{N_{Ed}}{N_{pl,Rd}} + \frac{9}{10}\frac{M_{Ed}}{M_{c,Rd}} \le 1.0 \tag{A.30}$$

While the form of these equations are different from those presented in Chapter H of the AISC (2007) specification, after plotting the interaction curves (Figure A-14) for combined flexure and compression, it can be seen that both interaction diagrams are essentially the same.

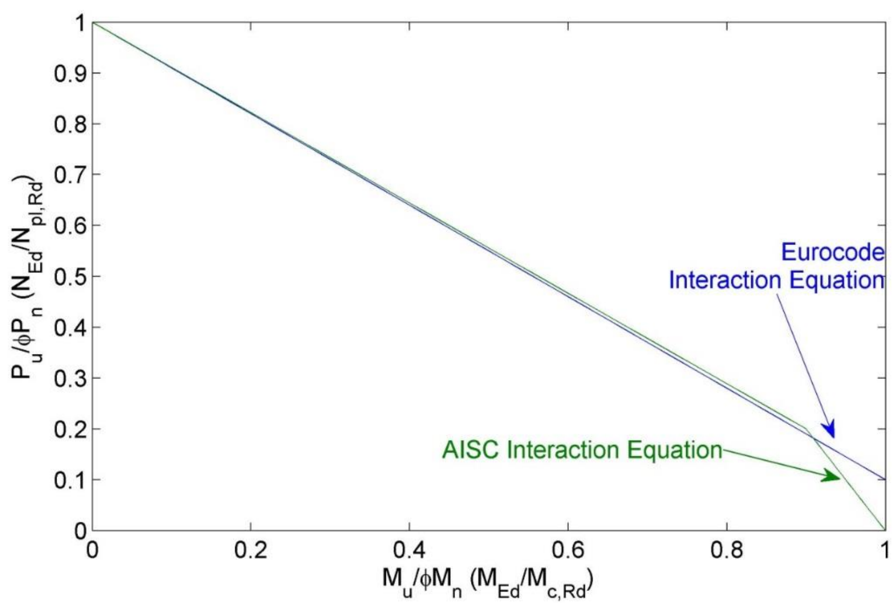


Figure A-14. Comparison of Eurocode and AISC interaction equations for combined flexure and compression.

*If the required shear strength <u>does</u> exceed 50% of the design shear strength:*

The reduced yield strength is $f_{y,red} = (1-\rho)\, f_y$ for the shear area, where

$\rho = \left( \frac{2V_{Ed}}{V_{pl,Rd}} - 1 \right)^2$, should be used to calculate the cross-sectional design resistance in combined loading.

### A.1.14. Additional Considerations and Limit States Provided in the Eurocode

In addition to what has been previously described in this section, the Eurocode gives consideration as to the durability of the steel sections in regards to long-term corrosion loses, differential water pressure considerations to local plate bending, anchoring limit states and serviceability guidance. All of which are important to the design of the sheet pile but may be currently out of the scope of this report.

### A.1.15. Structural Design Guidance Provided from 'Design Guide for Steel Sheet Pile Bridge Abutments' from E. Yandzio

This section considers design guidance provided by the publication 'Design Guide for Steel Sheet Pile Bridge Abutments' developed by E. Yandzio and The Steel Construction Institute. As mentioned, this document provides discussion, design guidance, and references to code (UK construction legislation, DETR Highways Agency Specifications, UK Codes of Practice, and European Standards) and further reading regarding a wide array of topics pertaining to the design and construction of sheet pile retaining walls for bridge abutments. The use of sheet piles as the foundation elements bridge abutments is a soil-structure interaction problem and relevant information regarding the structural design guidance for this type of construction is summarized below.

It is recognized in the publication that the use of steel sheet piles alone may not provide adequate axial load bearing or the required flexural rigidity for all projects. In these scenarios, it is possible to increase the capacity of sheet pile walls through the use of boxed sheet piles, or incorporating steel piles with higher rigidity behind and welded to the sheet pile wall acting in conjunction which is referred to as high modulus piles. Boxed sheet piles and high modulus pile walls can be constructed in different configurations as noted previously, the examples provided by the author are presented in Figure A-15 below.

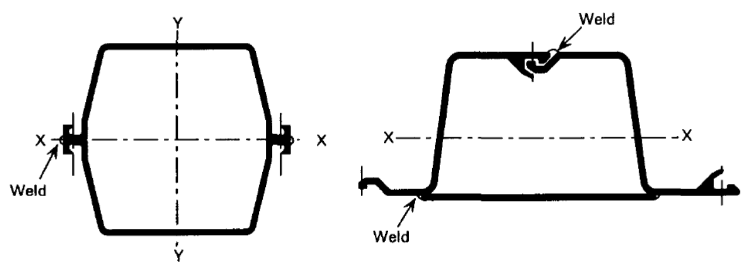


A.

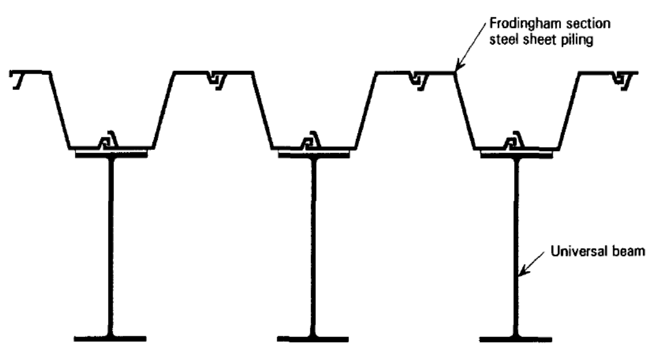


B.

Figure A-15. Configurations of A.) Boxed sheet piles, and B.) high modulus piles as presented by Yandzio (1998)

Lateral loading due to thermal expansion and contraction of the bridge is mentioned as an important design consideration in sheet pile abutment construction. The lateral movement and associated loads and rotations associated with the interaction of the bridge superstructure and abutment fill all need to be considered when designing for this aspect. It is noted that due to the lateral movement associated with thermal expansion and contraction, the anticipated shaft capacity along the sheet pile wall in contact with retained soil should be neglected due to possible separation between steel and soil. While this is an important design consideration for the construction of sheet pile bridge abutments, these specific loading conditions associated with thermal expansion and contraction were not part of the current study which focuses on axial load capacity of sheet piles.

Design guidelines must comply with applicable bridge design standards. Yandzio (1998) refers to several standards including:

- BS 8002- The national standard for small to medium sized retaining walls (up to 8 m). Recommends limit equilibrium methods for design and uses theoretical limiting earth pressures. This document provides a simplistic approach and can’t uniquely define limit states to be used for design, 8002 refers to BS 8110, BS 5400, BS 5950, and BS 449: Part 2 for partial factors based on limit state codes. The code treats forces acting on the wall at the serviceability limit state to be greater than those at ultimate limit state and uses the worst credible soil and ground parameters to develop a margin of safety. A mobilized soil strength is to be used at the serviceability limit state only.

- BS 8004- Covers design and construction of foundations. It uses the working stress approach that utilizes lumped factors of safety and moderately conservative soil parameters, loads, and geometries.
- CP2- This code is superseded by BS 8002, but provides useful guidance regarding a total stress design approach applicable to cohesive soils and is still in use.
- Eurocodes- Eurocode 7 Geotechnical design (issued by BSI as DD-ENV 1997-1) and Euocode 3: Part 5 Design of steel structures- piling (prENV 1993-5) use limit state design and partial factors. Partial factors are provided for actions and ground properties.
- Highway Agency standards- Provides governing design regulations for bridges in the UK through standards (BDs) which are mandatory and Advice Notes (BAs) which are not mandatory.
    - BD 42 Design of embedded retaining walls and bridge abutments specifies limit state design principles are to be applied to both the ultimate and serviceability states. The document permits design approach using limit equilibrium or soil-structure interaction.
    - Design guidance for evaluating the vertical bearing capacity of retaining walls is given in BD 32 Piled Foundations, and BA 25 provide guidance for its use.

Similar to the Eurocode, a limit state design method is recommended, where serviceability limit states (SLS), and ultimate limit states (ULS) are considered (provided by BD 42). The SLS is reached when serviceability criteria no longer met and ULS occurs at the point when collapse or other failure occurs. The main ULS failure modes considered in standard sheet pile design are used in canals and retention project. A summary of the limit states considered by the author are presented in Figure A-16. Load considerations include: soil weight, soil lateral earth pressures, ground water and seepage forces, surcharge loads, interaction with bridge superstructure (dead loads, live loads, temperature, etc.).

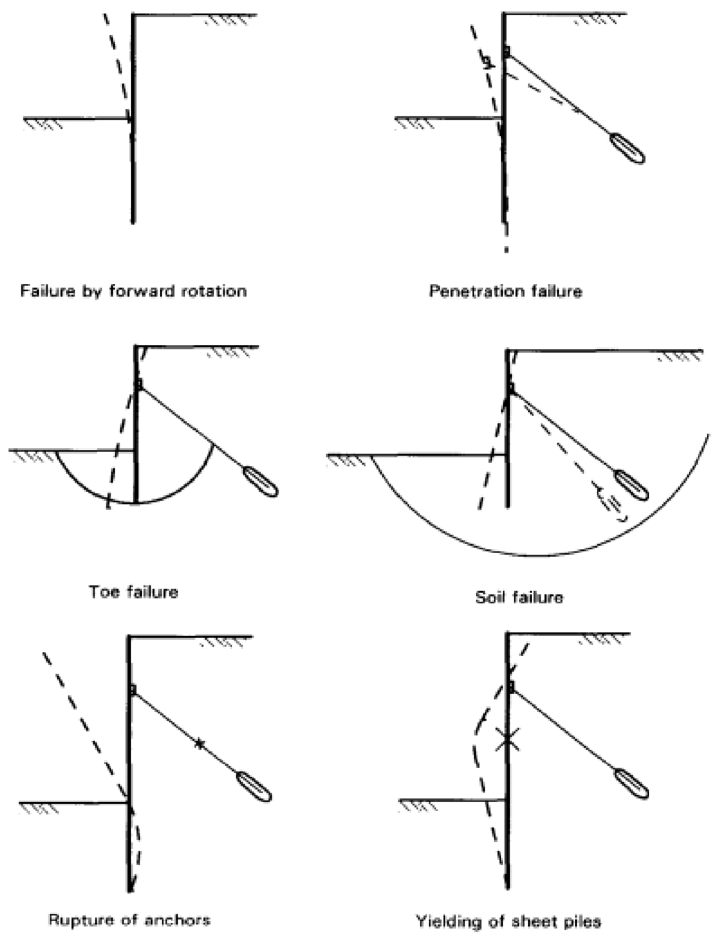


Figure A-16. Modes of failure at the ultimate limit states as presented by Yandzio (1998)

A.1.16. Corrosion

Several of the publications make reference to the effects of corrosion on the performance of steel sheet piles. Effects of corrosion can have significant implications for load bearing piles as if the section properties are changed, a piles ability to withstand design loads can be diminished (Yandzio 1998). When piles are fully embedded, the rate of corrosion has been observed to be negligible, however in instances where the piles are exposed rates of corrosion are much greater. This is especially relevant for steel sheet piles which can have exposed facing in bridge abutments and marine construction. Additionally, different environments will lead to different rates of corrosion, with marine and industrial sites having the highest rates. This section summarizes some of the design recommendations provided by the literature review

ArcelorMittal (2008) report values for corrosion for unprotected steel piles based on information in Eurocode 3: Part 5 for various environments. For non-saline water, values for loss of pile thickness for a period of 25 years range from 0.3 mm (0.012 inch) to 2 mm (0.079 inch) for undisturbed natural soils and non-compacted aggressive fills respectively. For sea water values for loss of pile thickness for a period of 25 years range from 0.9 mm (0.035 inch) to 1.9 mm (0.075 inch). For marine environments, corrosion rates depend on the exposure zone of the steel and several different zones are defined, with the greatest rates of corrosion occurring within the zone where air and water meet.

Based on design values of corrosion, it can be determined if corrosion will be significant based on the design life of the project and whether or not preventative measures should be taken. Different methods exist to improve the survivability of the piles in these scenarios. ArcelorMittal (2008) recommend the following:

- Use of a heavier section (go with larger, thicker pile in design or add plating to existing structures).
- Use of a high yield steel at mild steel stress levels
- Application of a protective organic coating or concrete encasement
- Applying cathodic protection

Yandzio (1998) outlines a number of standards which address long term performance of steel sheet pile structures which must be considered to avoid high costs associated with durability problems and maintenance. The design code BS 5400 used in U.K. practice requires an end of design life of 120 years for piles. Based on the environment of the pile, additional 'sacrificial' thickness must be added to the pile based on BD 42. These values range from 2 mm (0.079 inch) to 9 mm (0.354 inch) for piles exposed to natural soil and piles exposed to splash or alternating wet and dry conditions, respectively. While adding sacrificial thickness to the piles is noted to likely be the most cost effective solution, other options for dealing with corrosion include application of protective coatings, cathodic protection (for below water conditions in marine environments), and concrete encasement.

Biddle (1997) mentions that for steel piles completely embedded into undisturbed natural soils, corrosion is negligible and its effects on load bearing resistance can be neglected. Corrosion of steel piles in soil is noted to be electrochemical in nature, requiring the presence of water and oxygen. Unless a soil has a high acidity (pH <4), corrosion will not occur due to low levels of oxygen just a few feet below the ground surface. The design code BS 6349 is referenced which recommends that working stresses be based on the thickness of wall section remaining at the end of the design life and should not exceed maximum permissible working stresses given in BS 8002. Based on the design guidance referenced, it is recommended to assume a corrosion rate of 0.015 mm/year/side. Steel piles with exposed facing can experience corrosion rates many times greater than that experienced by fully embedded piles. Piles exposed to the atmosphere may be expected to corrode at rates of 0.035 mm/year/side as per BS 8002. Still higher rates can be expected for piles exposed to water, piles immersed in sea water can experience corrosion at a rate of 0.035 mm/year/side, while the zone near the water level at low tide with little marine growth (barnacles and sea weed) has a rate of 0.075 mm/year/side. Zones near tidal fluctuations usually experience increased rates of marine growth which reduce oxygen exposure and have an average rate of corrosion of 0.035 mm/year/side. Zones which are exposed to the splashing of wave action face the greatest corrosion rates of 0.075 to 0.125 mm/year/side. Fills and industrial soils can also lead to the highest rates of pile corrosion based on the pH and resistivity of the soil. Methods of increasing the effective life of the pile include:

- Use of a heavier section than structurally required
- Use of a pile with a higher yield stress than required
- Apply a protective coating
- Use of concrete encasement
- Use of cathodic protection (not effective in marine splash or atmospheric zones)

The most economical option is noted to be increasing the yield stress of the steel being used, this typically increases the life of the pile by 30% while only increasing the cost by 7%. It should be noted that protective coatings should be applied primarily where a pile is vulnerable to corrosion, and that damage to the coating can result from transit, the nature of the soil, and driving methods used.

In summary, depending on the level of exposure, corrosion will occur at different rates for steel piles. Corrosion leads to reductions in the cross sectional area of a pile and can potential lead to lower load capacities due to the change in area. In the literature presented, it was recommended that the final design incorporate this reduced cross section based on the exposure level of the pile and the design life of the pile. Methods to mitigate corrosion were presented, the most cost effective among them include increase the thickness of the steel section and increasing the yield stress of the steel being used. Corrosion may be an issue for sheet piles used in bridge abutments due to increased exposure to water and should be considered when designing this type of structure.

# APPENDIX B. SUPPLEMENTAL INFORMATION- HIGHBAY LAB

## B.1. Soil Characterization for Highbay Laboratory Testing

This appendix presents supplementary information regarding testing performed at the UNCC EPIC Highbay laboratory. During backfilling of the geotechnical test pit, compaction control was achieved using Nuclear gauge, Sand-cone, and Drive-Cylinder methods. Nuclear gauge and Drive-Cylinder testing were performed by SUMMIT Engineering. Results of testing were used to evaluate compaction procedures through measurement of relative compaction as well as dry unit weight and water content. As mentioned previously, the backfill was placed in layers and compacted using vibratory plate compactor and had tampers.

Several tests were performed after backfilling to characterize the soil. These included SPT, SCPTu, DMT, and geophysical tests including MASW. These tests were performed with assistance provided by the Charlotte office of S&ME. In addition to dynamic measurements provided by the SCPTu and MASW tests, crosshole testing (CHT) was conducted using a system developed in-house.

Additional images are provided of the test piles, installation of instrumentation on the piles, and driving of the sheet piles. Images of equipment and results from direct shear testing are also presented. Lastly, procedures used for the data analysis of the pile load testing conducted at the UNCC Highbay are presented.

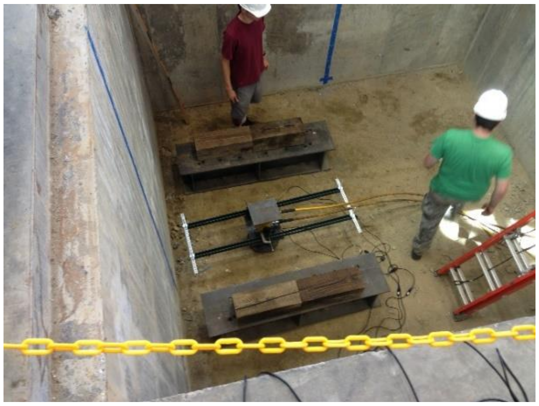

(a) Setup for plate load test

(b) Dial gauges for plate load test

(c) Close up of plate load test setup

Figure B-1. Images taken from plate load testing at base of UNCC Highbay test pit

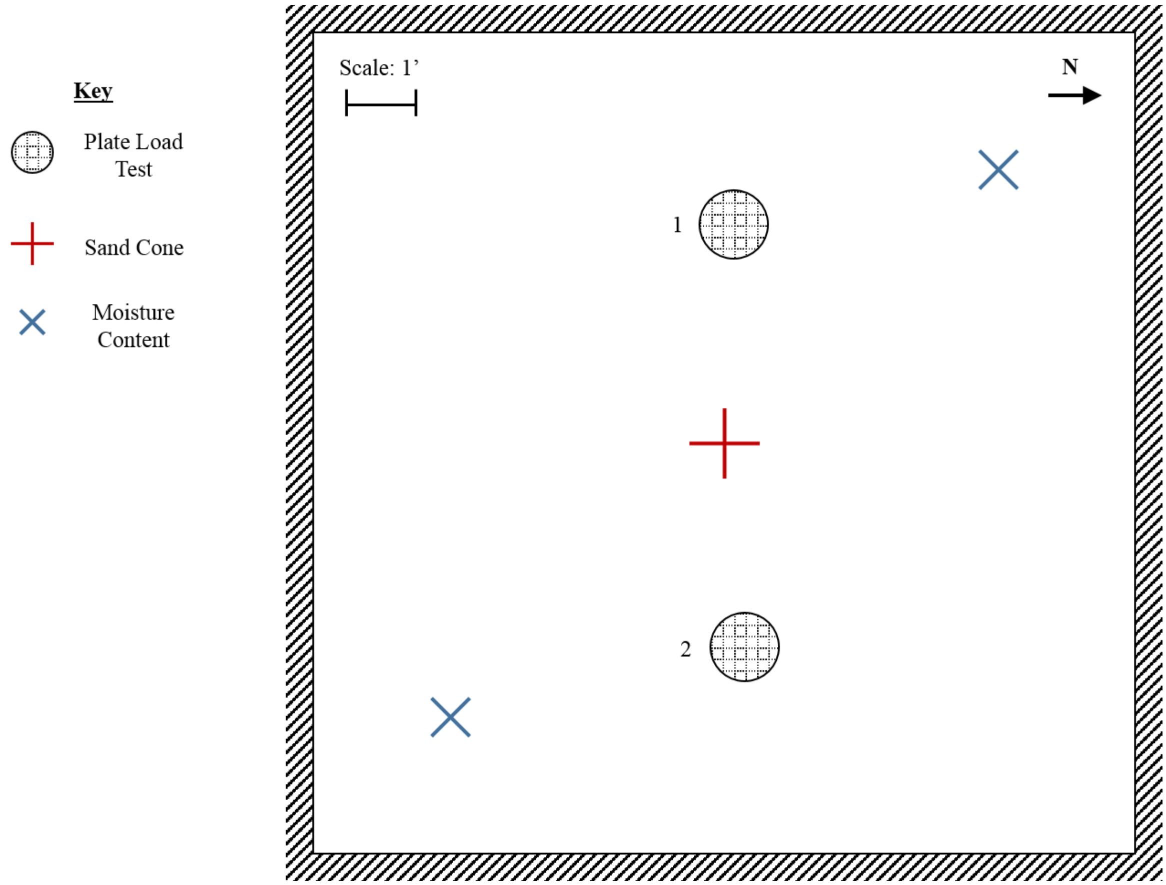


Figure B-2. Images of location of plate load tests at base of UNCC Highbay test pit.

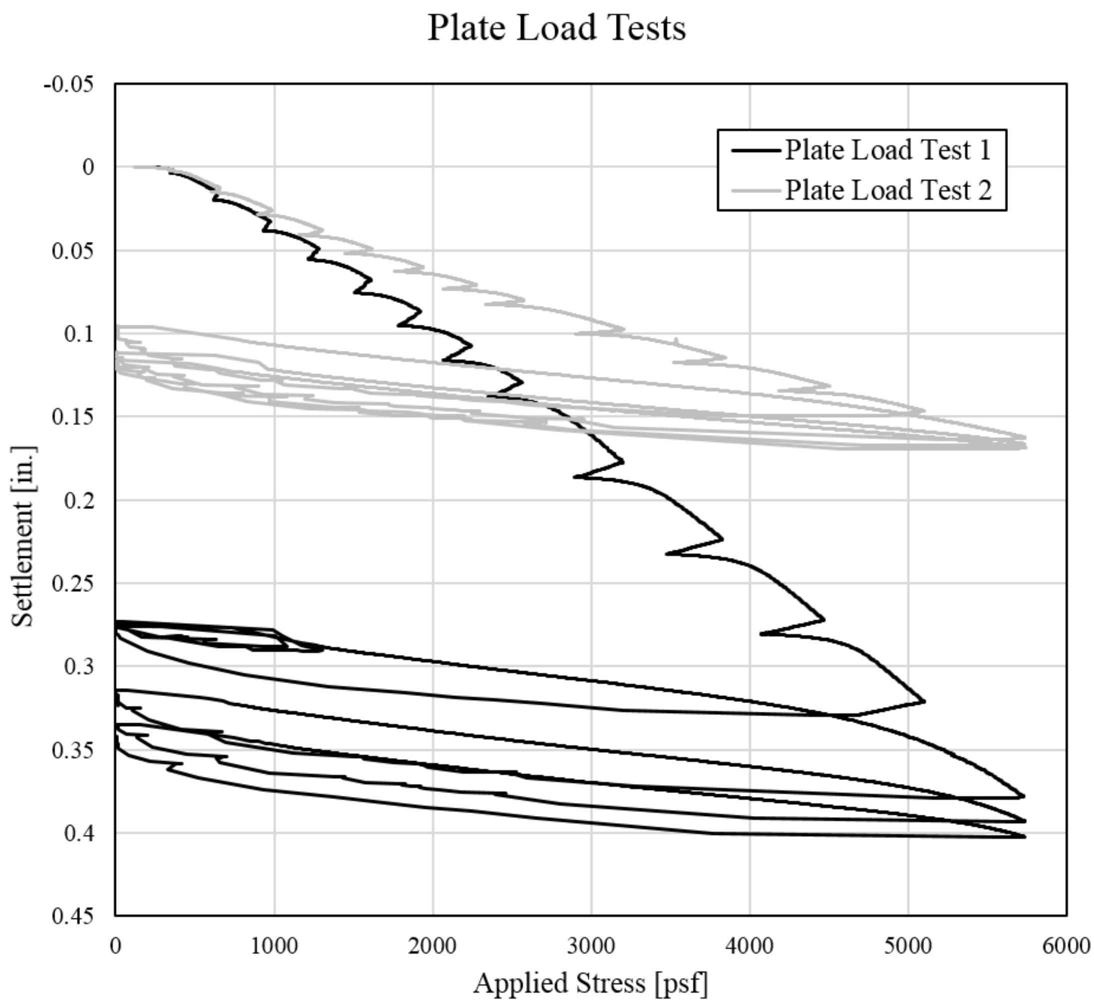


Figure B-3. Plot of results from plate load tests at base of Highbay test pit.

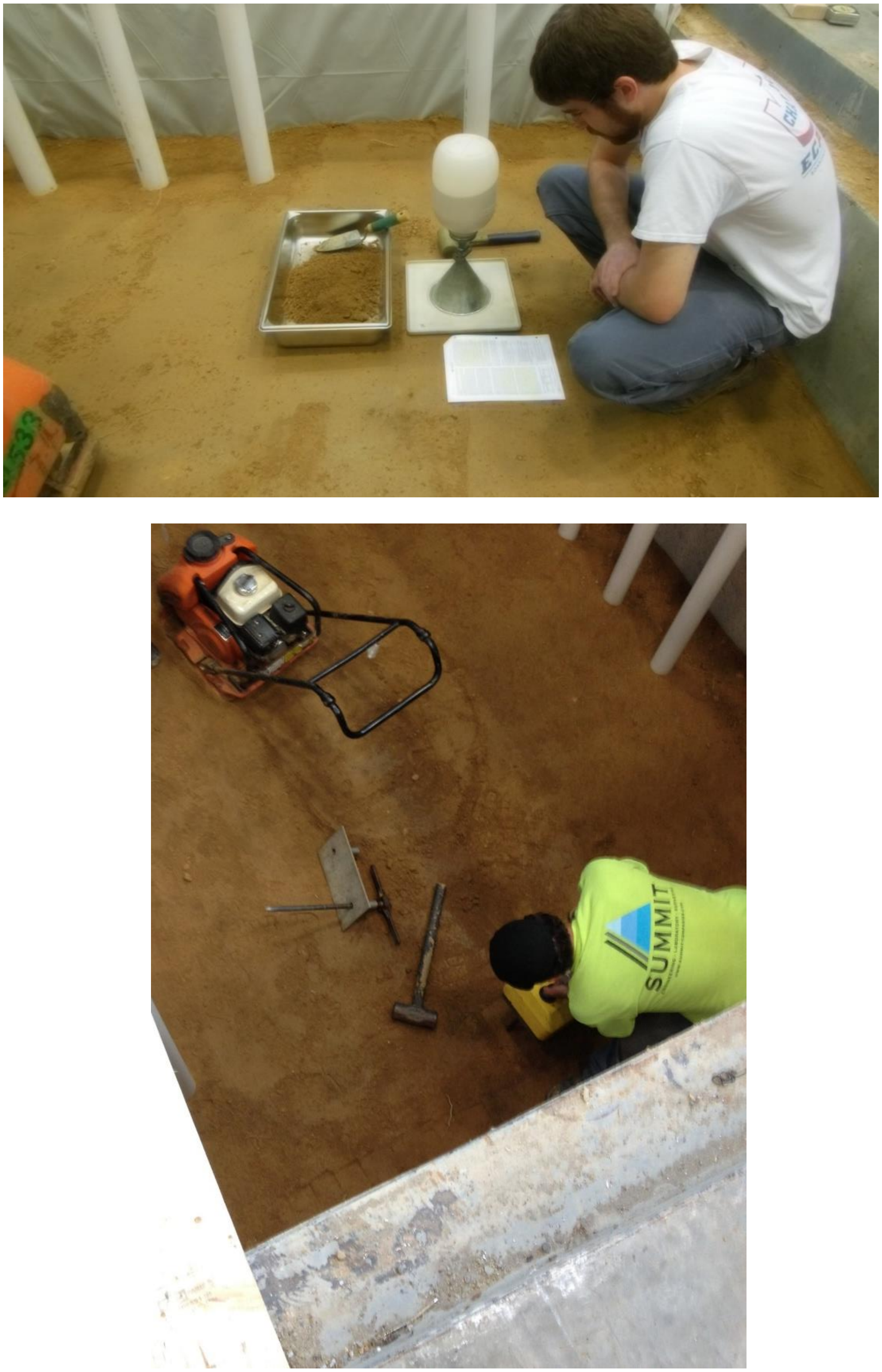


Figure B-4. In-situ density testing performed to characterize placement of backfill, sand cone testing (top), and nuclear density testing (bottom)

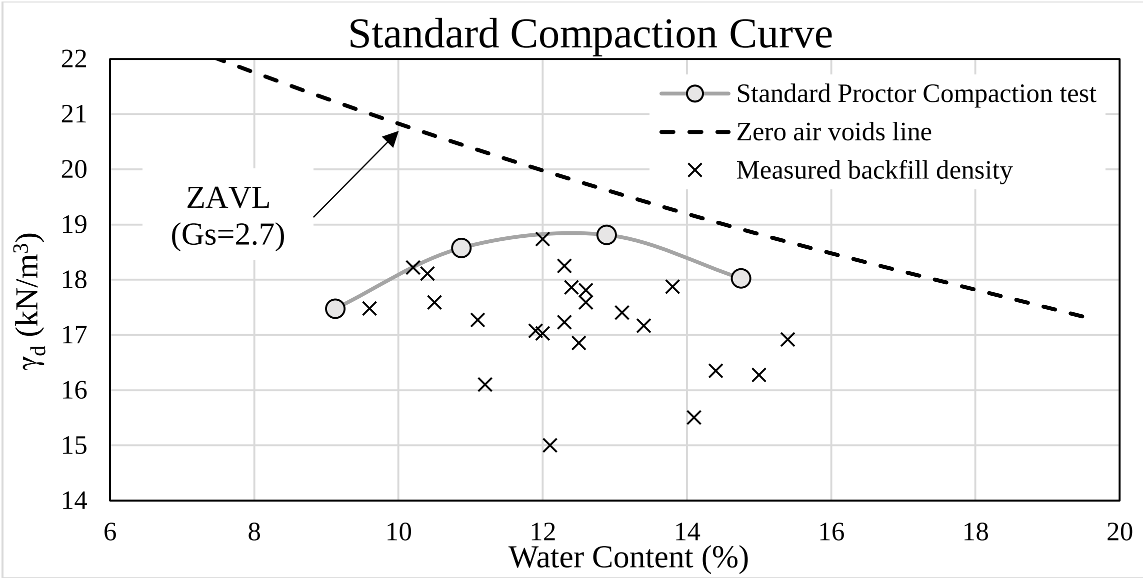


Figure B-5. As compacted dry unit weight and moisture content values measured for the SW-SC backfill during backfilling of the Highbay geotechnical test pit


Figure B-6. Images taken during SPT testing at the UNCC Highbay geotechnical test pit

Figure B-7. Images of test setup used for SCPTu testing of EPIC geotechnical test pit performed by S&ME (Charleston, SC, office)

Figure B-8. Image of DMT testing at EPIC geotechnical test pit prior to sheet pile installation

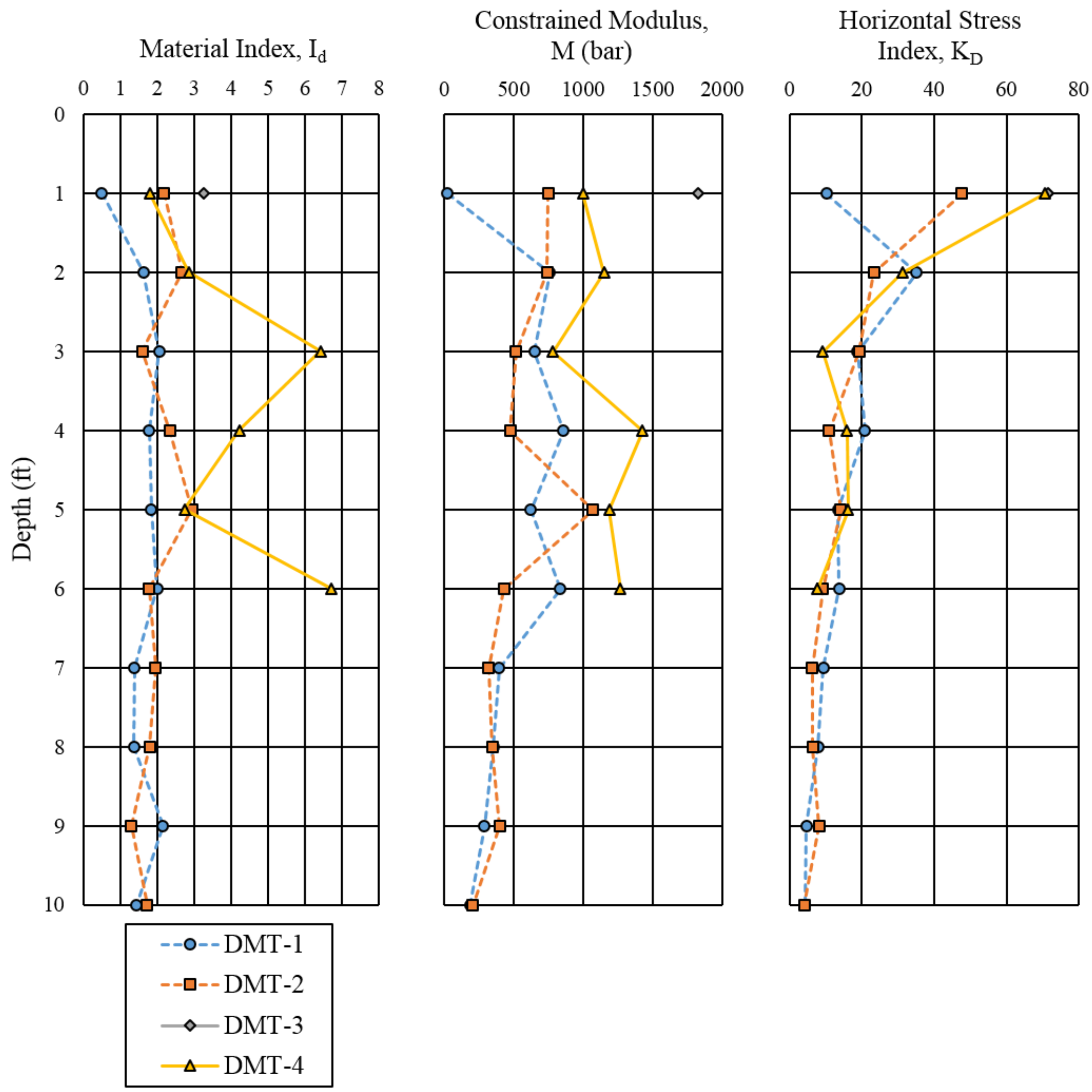


Figure B-9. Summary plot of DMT Material Index results from four DMT soundings.

a.) Hammers used for MASW

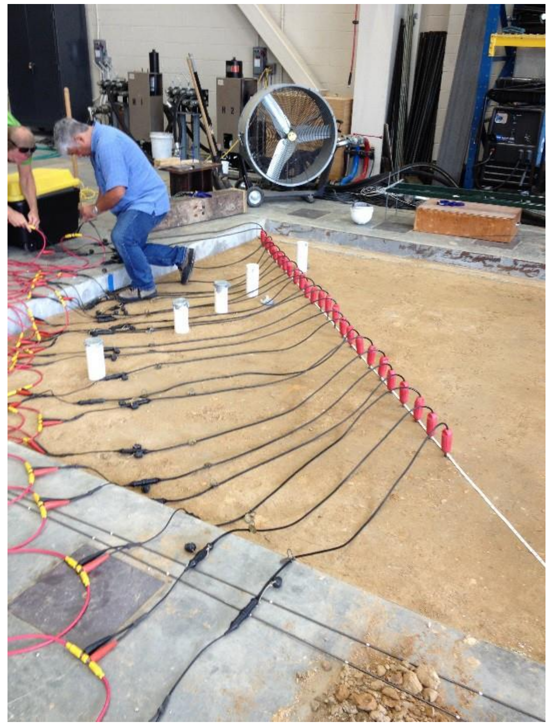

b.) MASW testing


c.) 14 Hz geophone array

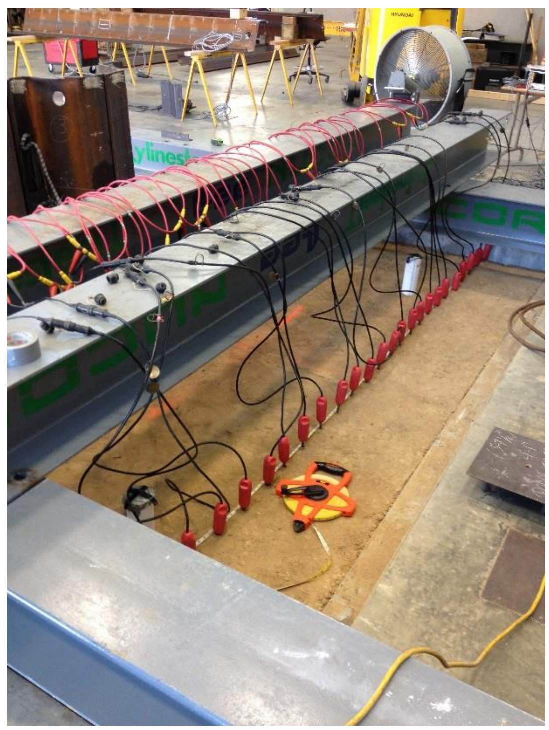

d.) 100 Hz geophone array

Figure B-10. Images of MASW testing at UNCC Highbay

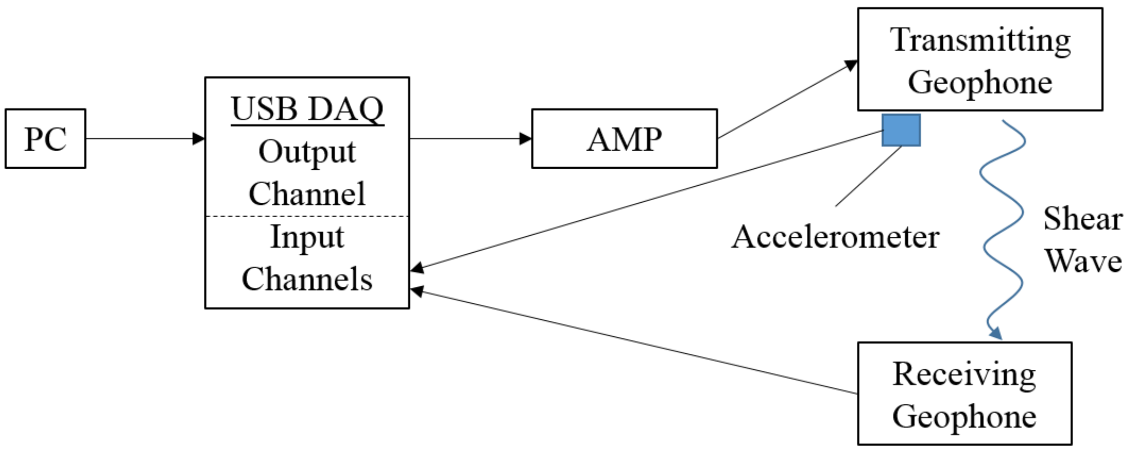


a.) Layout of system components for crosshole testing

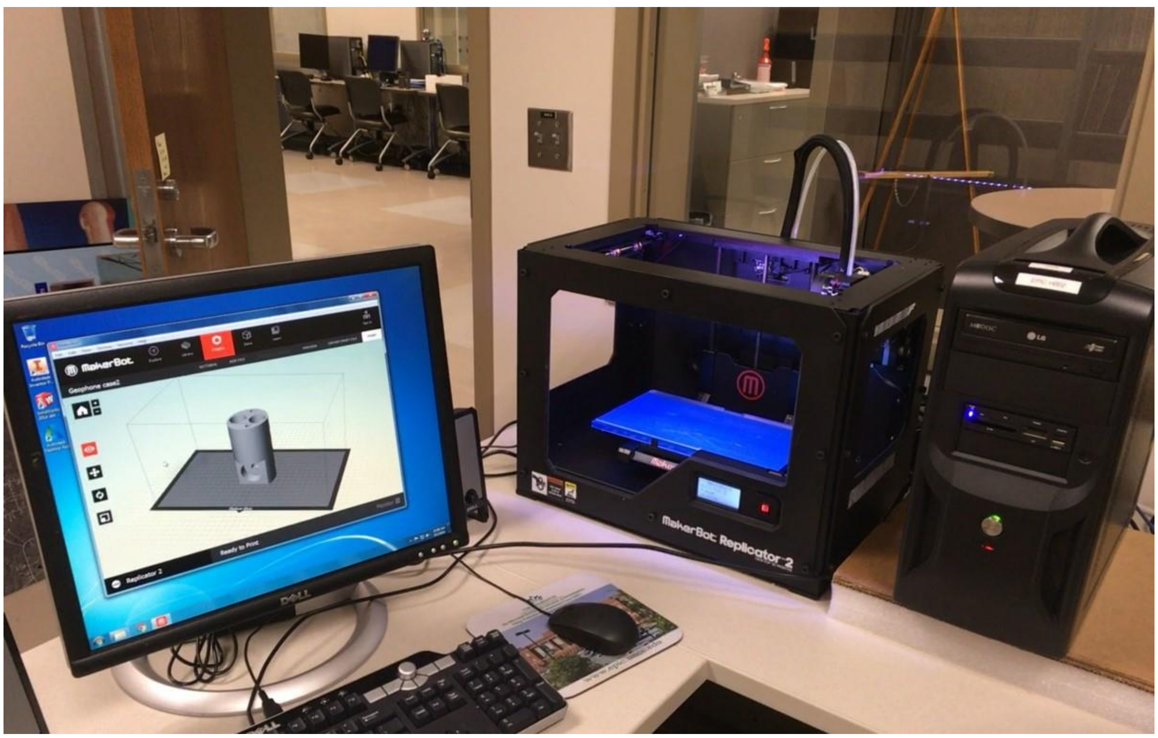

b.) 3D printing for geophone casing for crosshole test

Figure B-11. Crosshole test system in-house development at UNCC

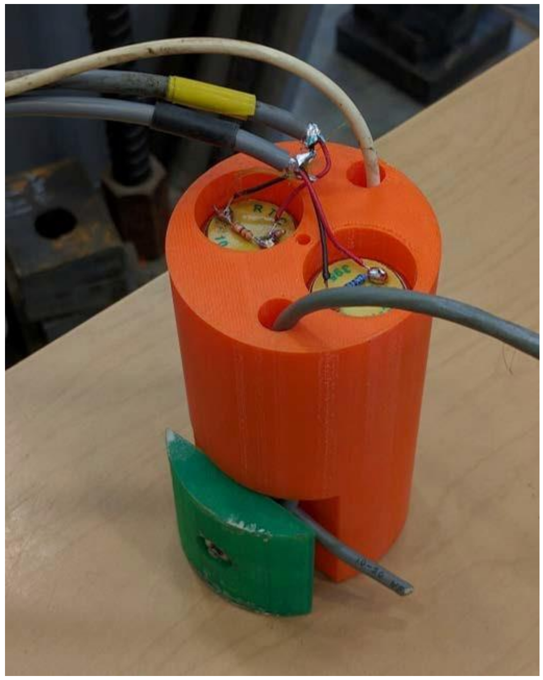

a.) 3D printed sensor casing for crosshole test

b.) Observing crosshole data and modifying computer program

c.) Collecting crosshole data

Figure B-12. Photos of equipment and crosshole testing at UNCC Highbay

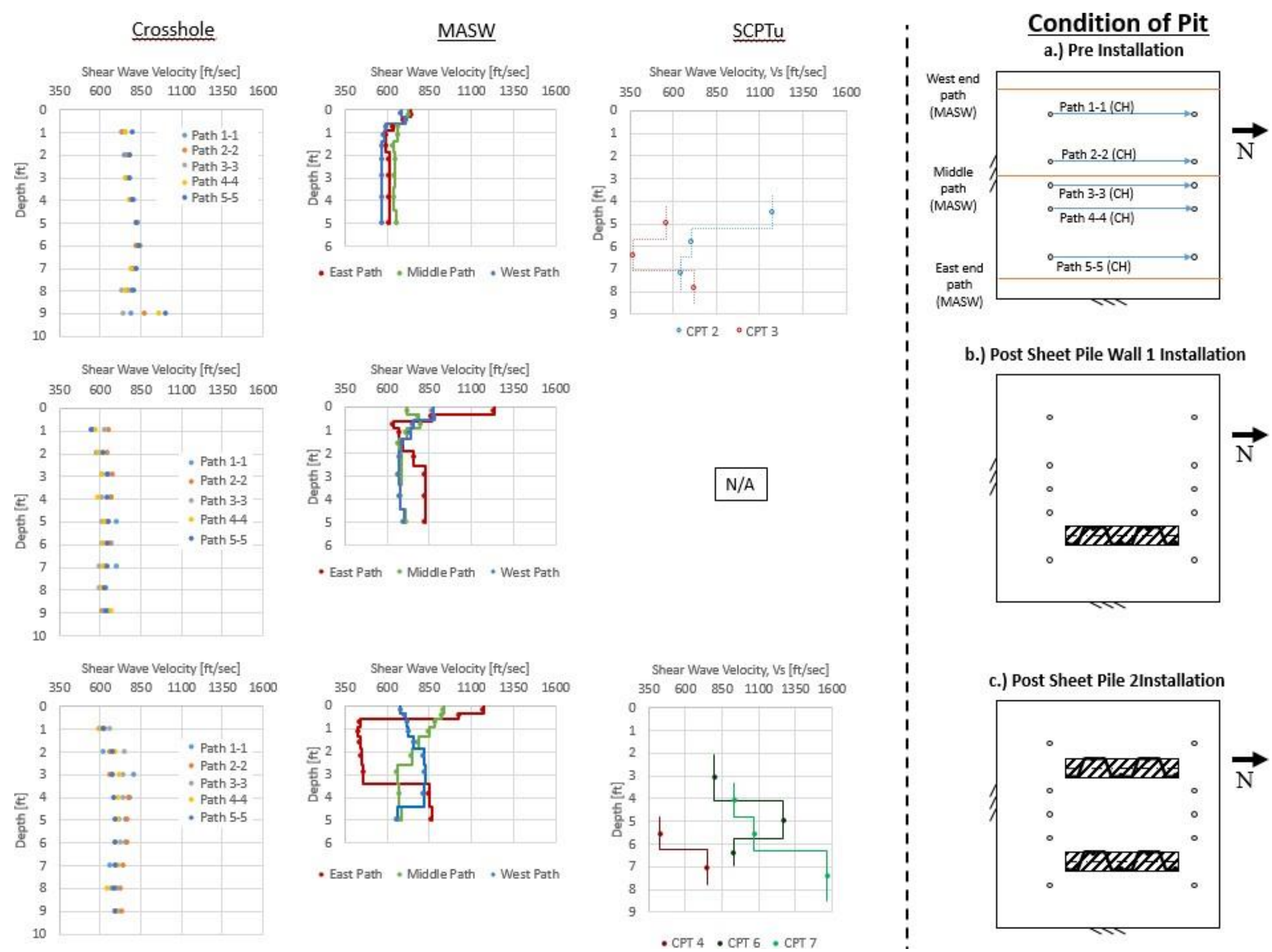


Figure B-13. Comparison of shear wave velocity measurement of compacted backfill at UNCC Highbay.

a.) Test sheet piles

b.) Instrumenting sheet piles

c.) Welded coverplate used to protect sensors

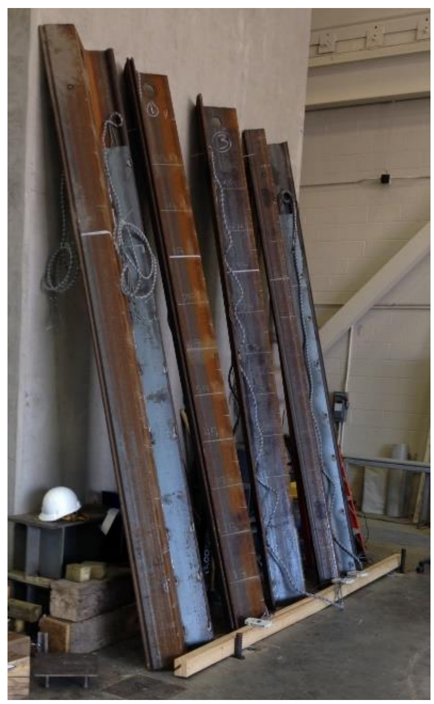

d.) Instrumented sheet piles

Figure B-14. Images of UNCC Highbay test piles


Figure B-15. Image of ICE 6E vibratory hammer used at UNCC Highbay

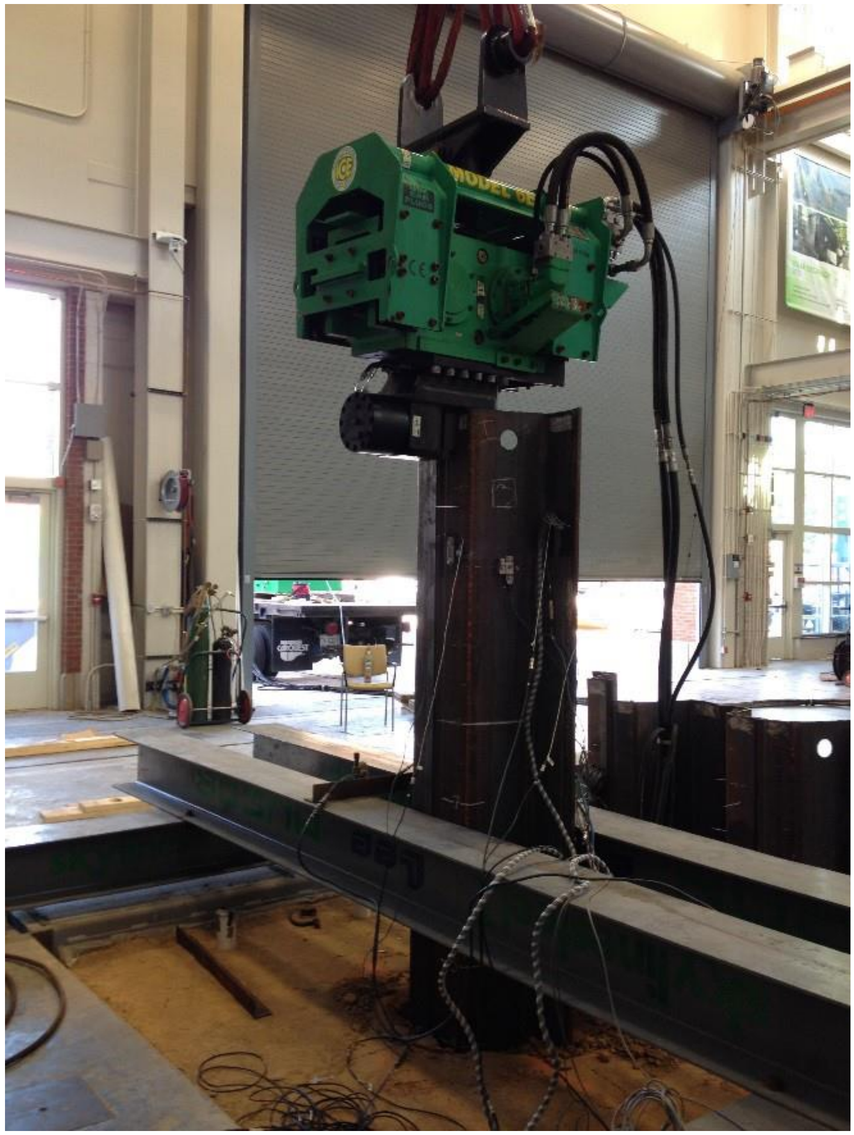


Figure B-16. Driving sheet pile with ICE Model 6E vibratory hammer

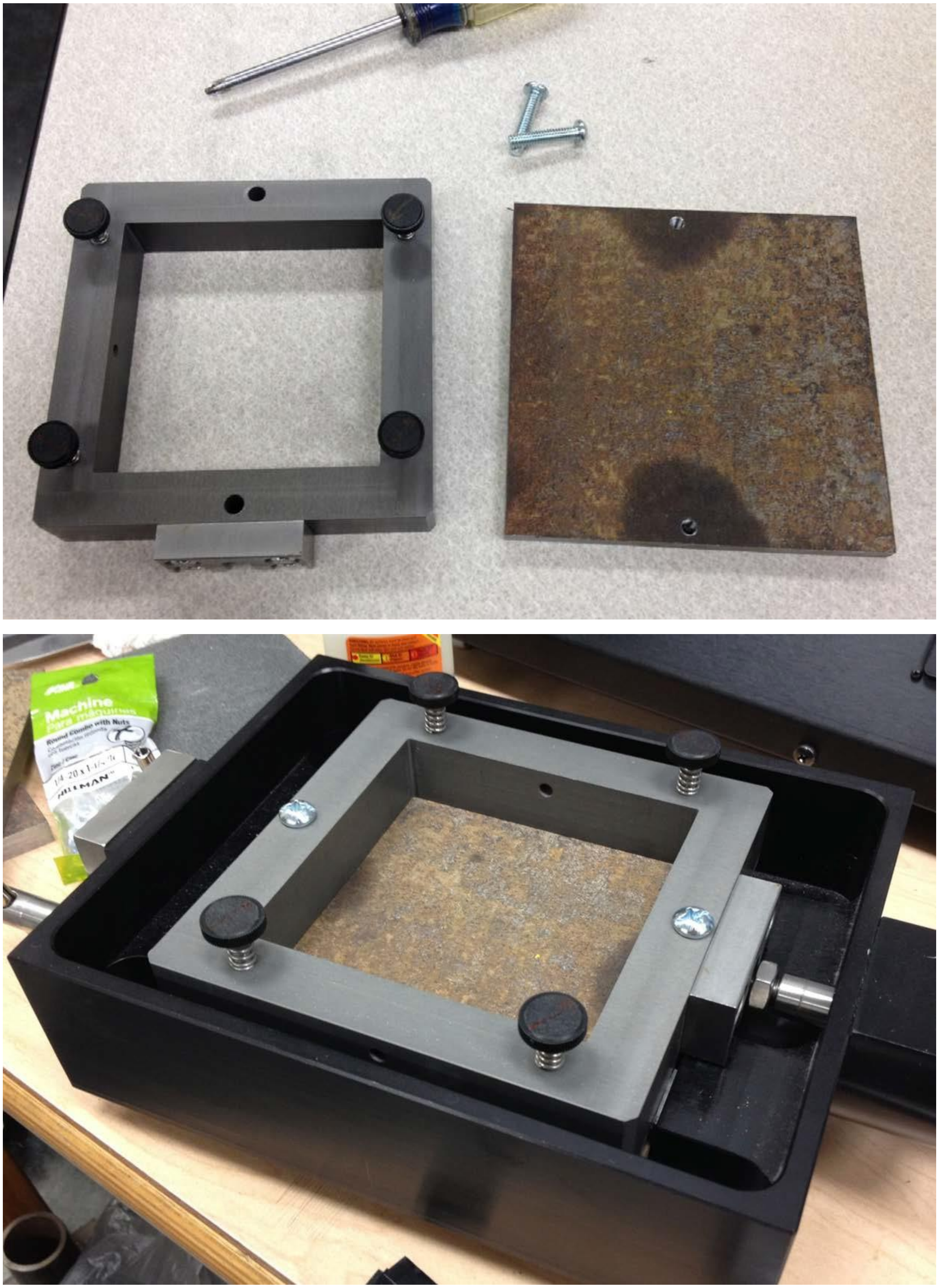


Figure B-17. Images of interface shear test setup, above: steel coupon, top half of shear box, below: assembled box

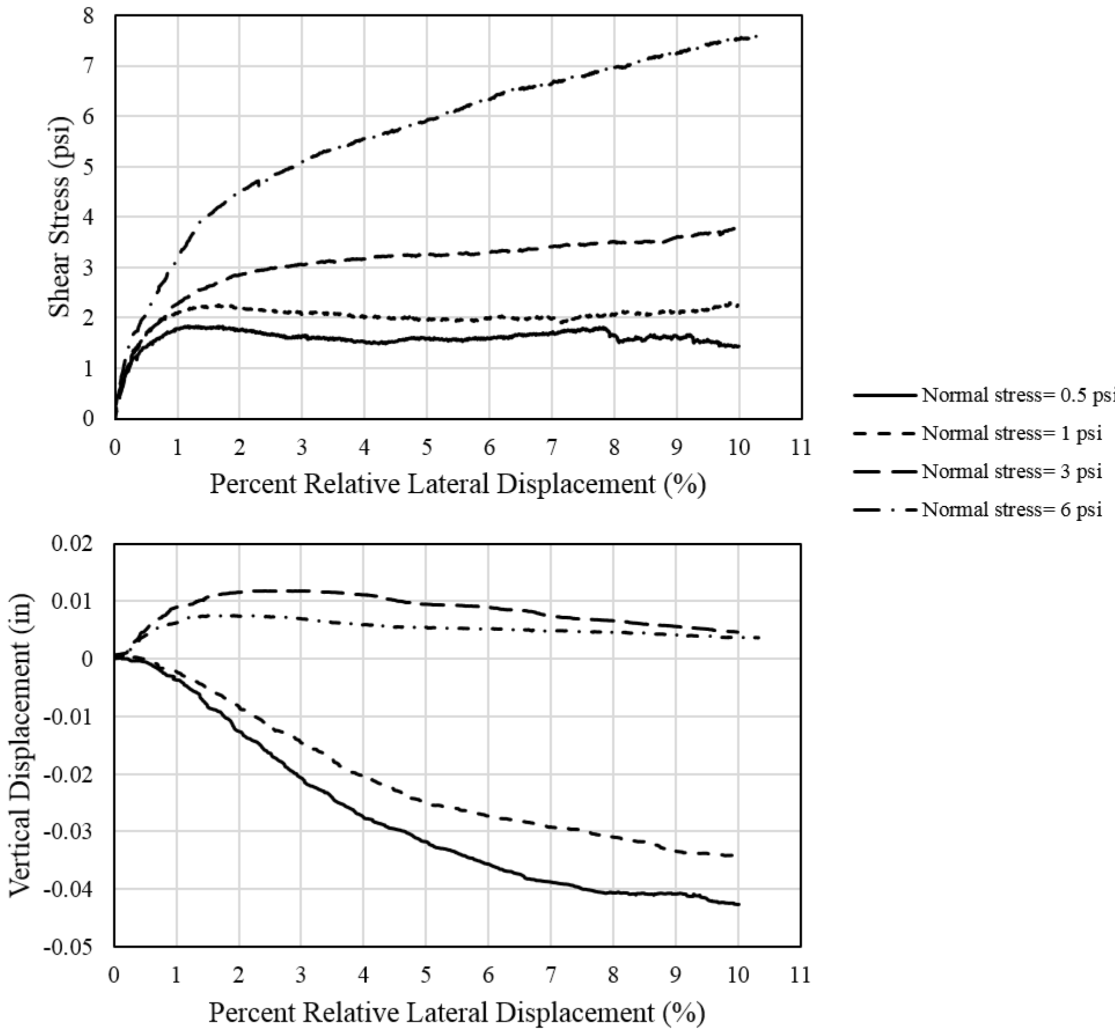


Figure B-18. Direct shear test results performed using backfill soil used at UNCC Highbay

## B.2. Overview of Data Analysis for UNCC Highbay Testing of Sheet Piles

### B.2.1. Assessment of Strains Measured Above Ground

This section presents documentation of the procedures developed and used by the research team to perform the raw, strain gage data processing on the results obtained from pile load testing at the UNCC Highbay. The processing included steps to address:

- Non-uniform load distribution across the four sheet piles
- Nonlinear strain profiles across sheet pile cross sections (such that simple averaging of strain gages installed on each flange will not null bending strain)

This analysis made use of twelve resistive strain gages installed 0.51 m above grade after pile installation across the sheet pile wall (as shown in Figure 3-9). Figure B-19 presents the time histories obtained from these twelve sensors, and negative values for strain indicate compression (Note: Pile 3 represents the heavily instrumented pile towards the inside of the wall and Pile 1 represents the heavily instrumented pile towards the outside of the wall). This time history demonstrates higher strain measurements were experienced towards the east flange of the piles as compared to the west flange, likely due to some eccentricity in the applied loading. Additionally, the measured strains show that the distribution of strain across the sheet piles is not linear, with strain measured in the web exceeding measured values at the flanges. As a result, simply averaging strains measured from the east and west flanges will not result in a cancelation of bending strains and will likely underestimate axial force at each elevation.

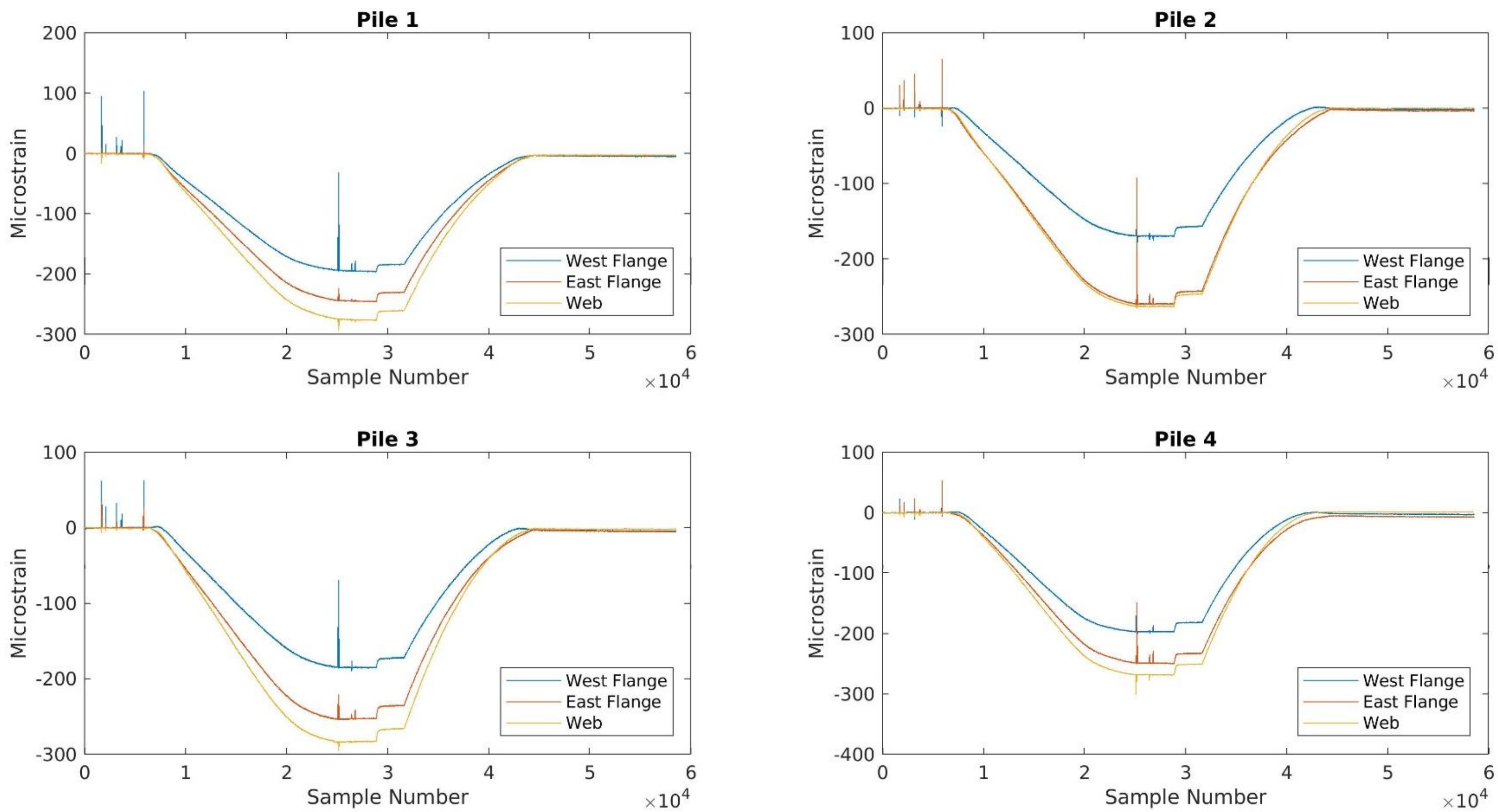


Figure B-19. Time history obtained from twelve strain gages installed 0.51 m above grade

In an attempt to address this issue with the strain measurements available (limited to the measurements on each flange below the ground line), a weighted average of the strains measured on each flange was used to determine the axial strains, and correspondingly axial force, at each elevation. Mathematically, the determination of the axial strain from strain gage measurements at each flange was determined by:

$$\varepsilon_{axial} = \varepsilon_{west} + \alpha(\varepsilon_{east} - \varepsilon_{west}) \tag{B.1}$$

Where $\alpha$ is a weighting factor. The determination of this weighting factor was performed through optimization of the correlation of axial strain determined by the total measured force $\left(\varepsilon = \dfrac{P}{EA}\right)$ and the axial strain calculated by this relative weighting equation averaged over the four piles using strain gage data from the gages installed above grade. Through this optimization, the weighting factor was determined as $\alpha$ = 0.335. Use of this weighting factor leads to strong correlation between the estimated axial force from the strain data above grade with the measured axial force, without any additional post-processing of the strain measurements (no detrending applied). Figure B-20 presents the measured load applied to the piles compared to force calculated using strain data with optimized weighing factor and a simple averaging of strain ($\alpha$ = 0.5). As can be seen, the strain data provides a much better prediction of measured load when corrected with a weighting factor of $\alpha$ = 0.335.

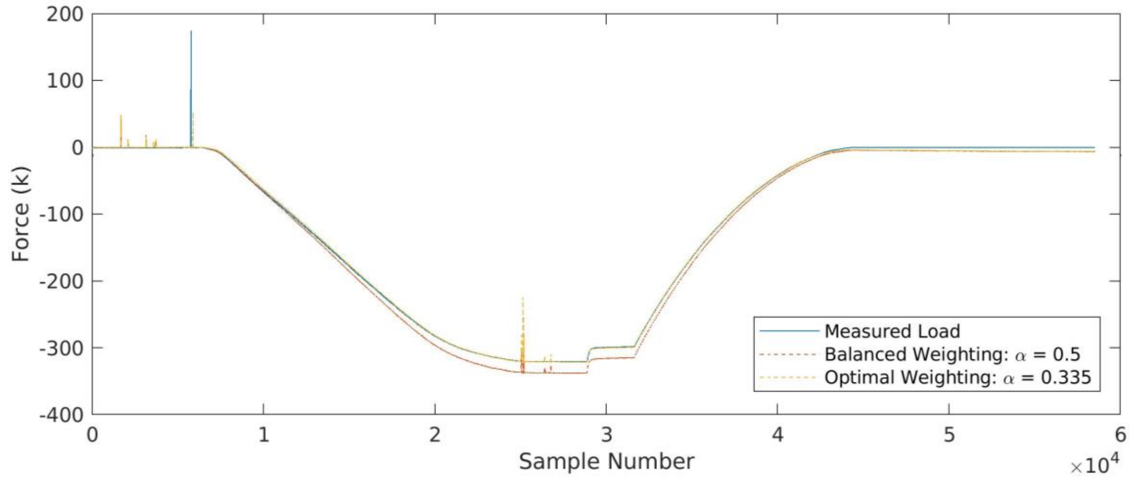


Figure B-20. Comparison of measured load to load predicted using strain gage measurements acquired from the flanges of all four piles above grade (Note: area includes cover plates)

With the weighting factor determined for the estimation of axial strain using measured strains at the flanges, the load distribution across the four piles in the group was investigated. Figure B-21 presents the estimated total axial force using the estimated axial strains from the individual piles. This figure provides information on the relative load distribution across the four piles and suggest that the exterior piles are carrying slightly greater load than the interior piles. Since there is some apparent nonuniform load distribution across the four piles, individual correction factors were developed for each pile to increase the accuracy of estimating the total load on the pile group using strains measured from individual piles. This step is necessary for the load transfer analysis since only two of the four piles featured strain gages installed along the depth of the pile. Through the use of the correction factor, $\beta$, the axial force can be determined as:

$$P = \beta \varepsilon_{axial} EA \tag{B.2}$$

Correction factors were determined for each pile by optimizing the correlation of the measured load with the total axial force estimated by (B.2). Figure B-22 presents the estimated total axial force using the developed correction factors for the two piles with strain gages installed below grade. The correlation obtained with the measured force is strong for both instrumented piles and the correction factors are each within 3% of unity.

### B.2.2. Load Transfer Estimates

With the weighting and correction factors developed in the previous section, the magnitude of axial force at each instrumented elevation of pile 3 could be determined using:

$$P = 1.005\left[\varepsilon_{west} + 0.335(\varepsilon_{east} - \varepsilon_{west})\right]EA \quad \text{(B.3)}$$

And, likewise, from Pile 1 using:

$$P = 0.98\left[\varepsilon_{west} + 0.335(\varepsilon_{east} - \varepsilon_{west})\right]EA \quad \text{(B.4)}$$

Pile 3 was instrumented with 8 pairs of resistive strain gages installed on the flanges at uniform intervals over the embedded depth. Pile 1 was instrumented with a sparser array of 4 pairs of resistive strain gages installed on the flanges at uniform intervals over the embedded depth. Strain gages at locations 8, 16, and 24 (all located at the toe of the pile) did not function during the load test, but the remainder of the gages produces reasonable strain time histories over the course of the load test. This degree of gage survivability permitted for direct measurement of the axial load transfer over all gages locations down to the depth of the pair directly above the lowest elevation of gages. For the estimation of the axial force at the toe of the pile in the absence of direct strain measurements at the toe, the force could be estimated by a linear extrapolation of the load transfer curve using the measurements at the two elevations directly above the non-functioning gages. In general, the progressions of axial force with depth are consistent with expectations, with the exception of the axial force estimated at elevations 0 and 1 when the weighted averaging was used. For this case, there was a slight increase in the estimated axial force over this depth. One notable issue identified in the axial force estimates is that the axial forces predicted using the original resistive strain gages place above the ground line were slightly less than the measured axial force. In an attempt to compensate for this error the magnitudes of all of the estimated axial forces were increased by a common factor to shift the estimated axial force above the ground line to match the measured force. When axial force estimates are developed with the simple average, the correction factor required is 1.04 and when axial force estimates are developed with the weighted average, the correction factor required is 1.06.

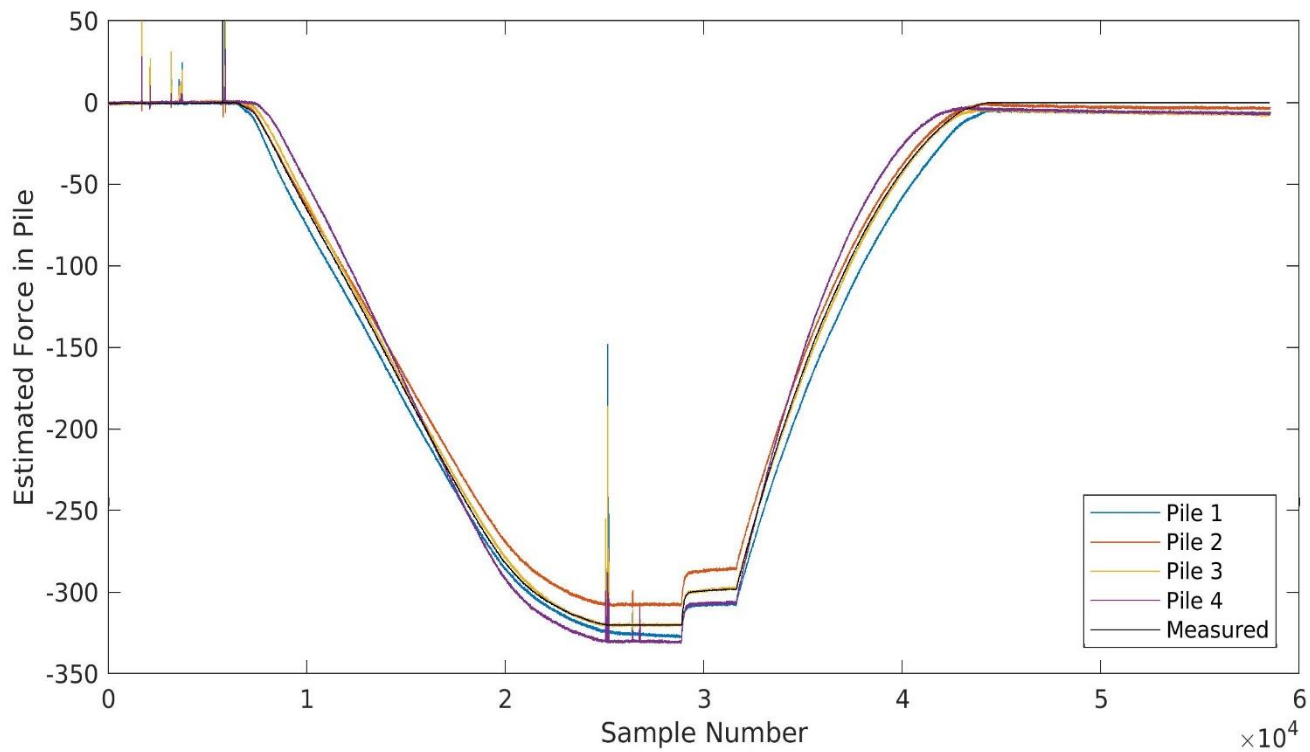


Figure B-21. Comparison of estimated force using axial strains from individual piles (Note: area includes cover plates)

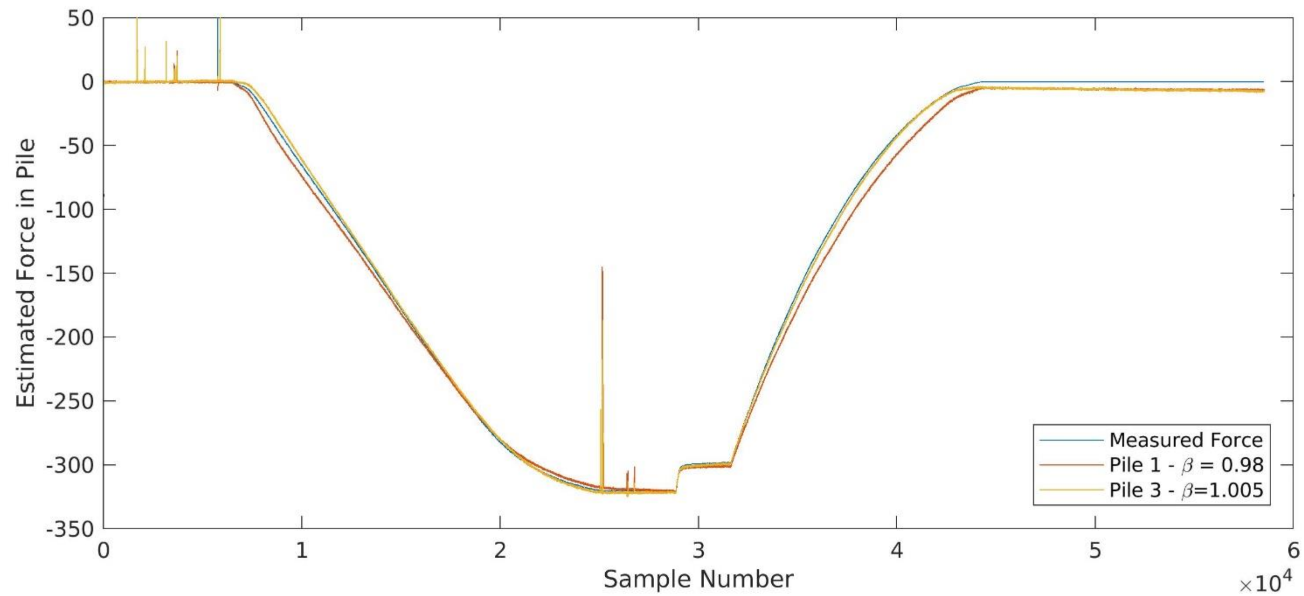


Figure B-22. Load distribution factors applied to pile force estimates for instrumented piles

## APPENDIX C. SUPPLEMENTAL INFORMATION- FIELD SITE

Figure C-1. Field site at ICE in Matthews, North Carolina, during site selection process


Figure C-2. Field site after site characterization geotechnical testing

a.) CME 550X rig used for SPT and CPT testing

b.) Performing SPT boring

c.) Soft soil encountered during SPT boring

Figure C-3. Images of SPT borings conducted at ICE field site, tests performed by S&ME (Charlotte office)

a.) CME 550X rig used for pushing SCPTu cone and rods

b.) SCPTu cone with saturated porous element around pore pressure sensors

c.) Placing SCPTu cone prior to sounding

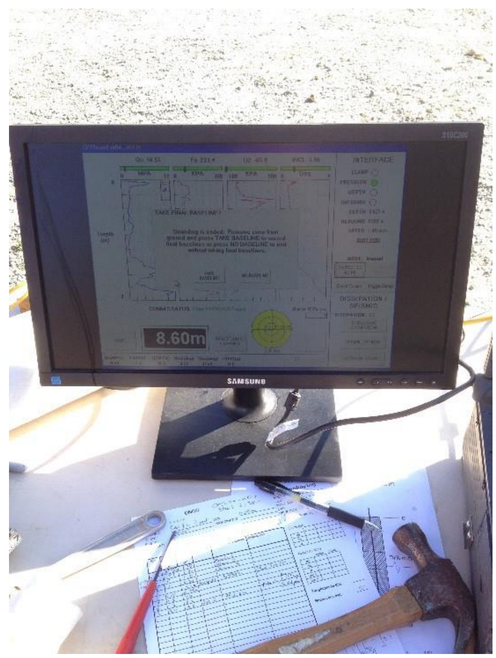


d.) Results from SCPTu test at end of sounding

Figure C-4. Images of SCPTu soundings conducted at ICE field site, tests performed with S&ME (Charlotte office)


a.) MASW equipment

b.) MASW seismic source

c.) Array for MASW

d.) Additional array for MASW testing

Figure C-5. Images of MASW conducted at ICE field site, tests performed by S&ME (Charlotte office)

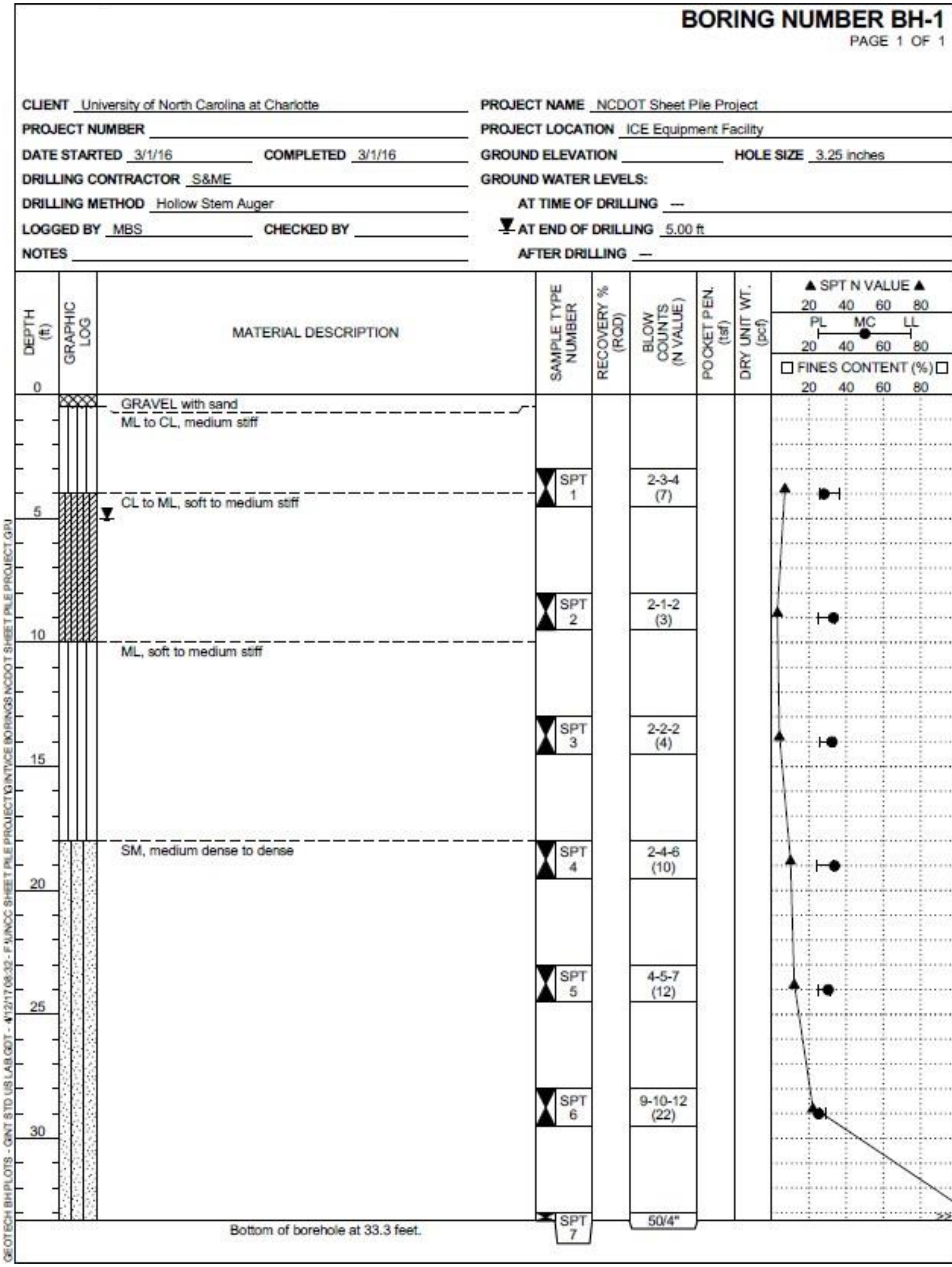


Figure C-6. Boring log for borehole BH-1 (adjacent to sheet pile)

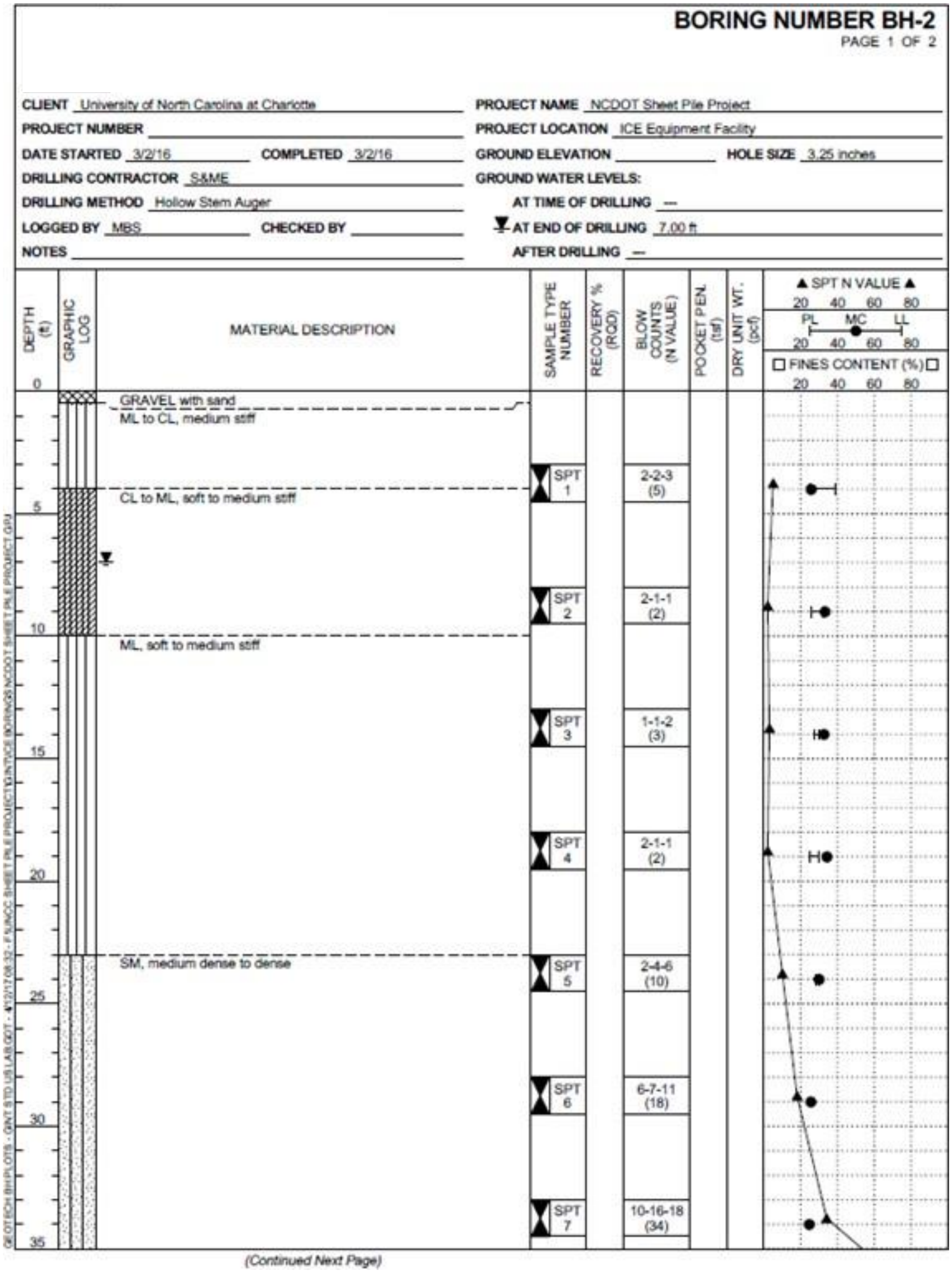


Figure C-7. Page 1 of 2 of boring log for borehole BH-2 (adjacent to H-pile)

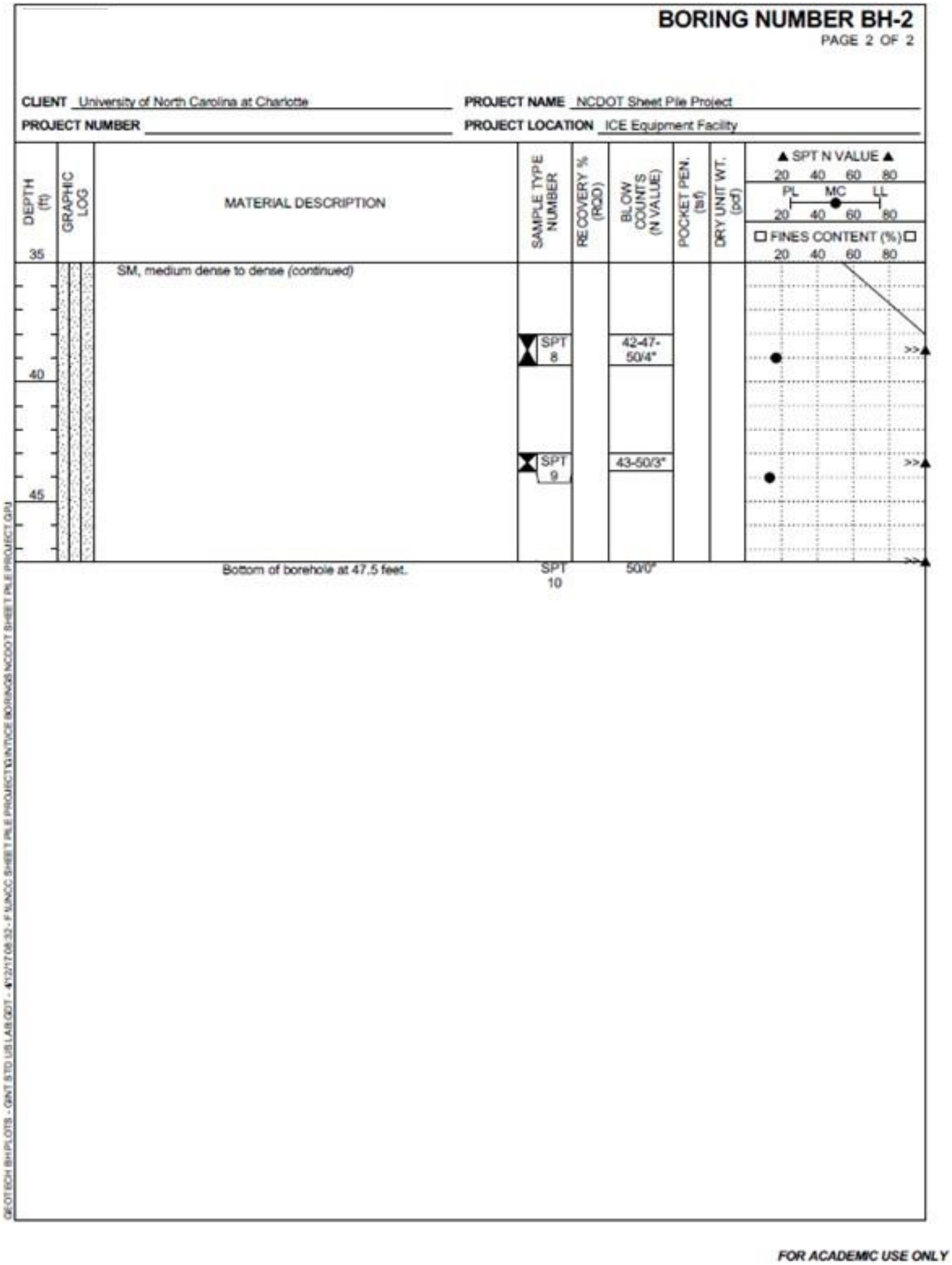


Figure C-8. Page 2 of 2 of boring log for borehole BH-2 (adjacent to H-pile)

Figure C-9. Image of instrumented H-pile for field load testing program

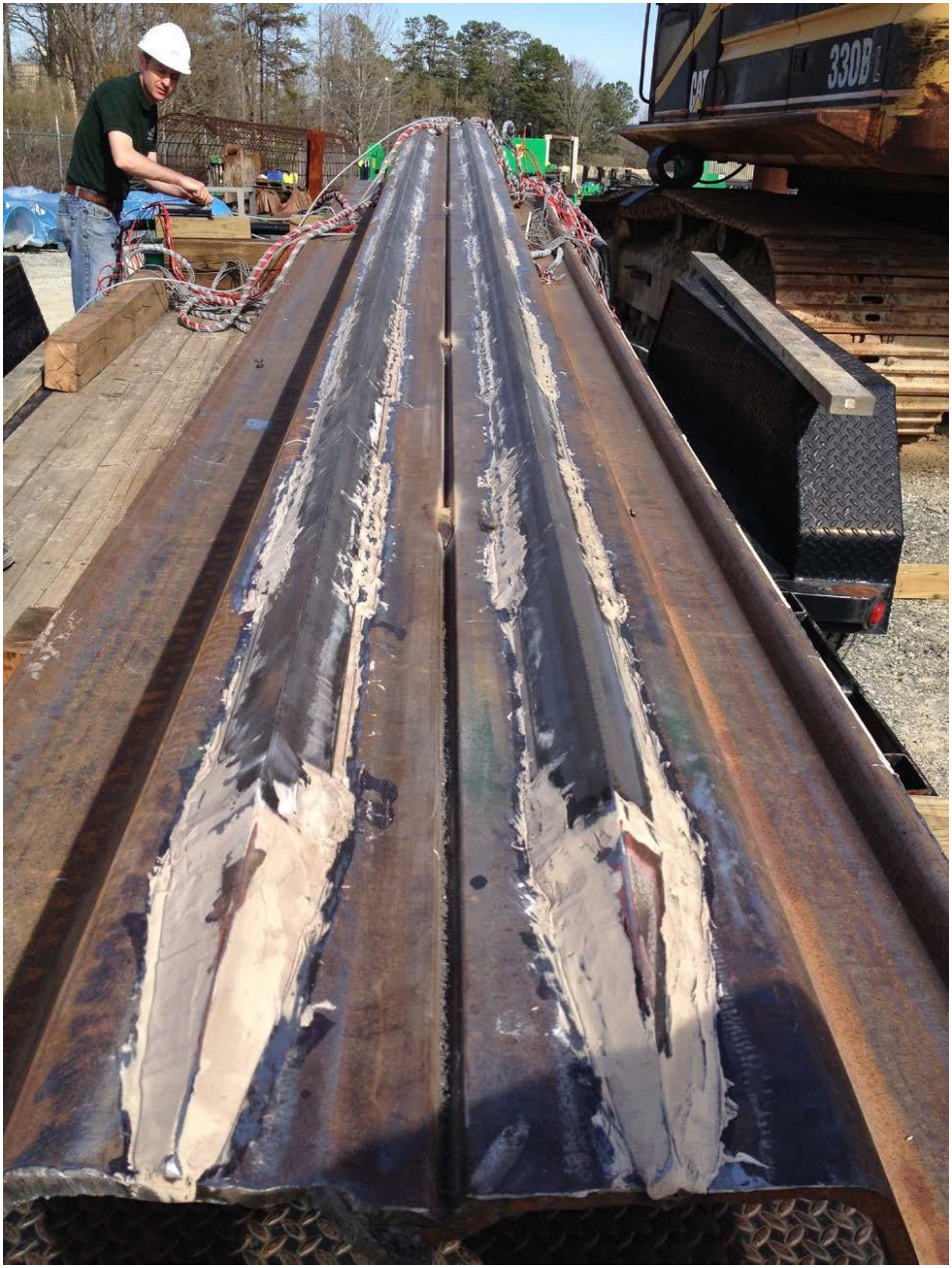


Figure C-10. Image of instrumented sheet piles for field load testing program

Figure C-11. Image of PDA instrumentation during impact driving of sheet piles at ICE field site, PDA testing performed in conjunction with GRL

Figure C-12. Photo of impact driving and PDA instrumentation during restrike testing of sheet piles at ICE field site

a.) Piles and beam for reaction frame, steel beams for reaction piles provided by Skyline Steel, LLC

b.) Beams for reaction frame, provided by Lee Construction Company

Figure C-13. Images of steel beams used for construction of reaction frame at ICE field site, steel provided by Skyline Steel, LLC, and Lee Construction Company

Figure C-14. Image of steel beams used for piles and installation guide frame constructed by ICE for reaction pile driving

Figure C-15. Image of transfer beams bolted to reaction frame, installation of reaction pile and placement of transfer beams courtesy of ICE


Figure C-16. Images of assembled reaction frame and driven H-pile for load testing

Figure C-17. Side view of test piles and reaction frame at ICE field site

a.) Oblique view of reaction frame over HP 12x53 test pile with reference beams

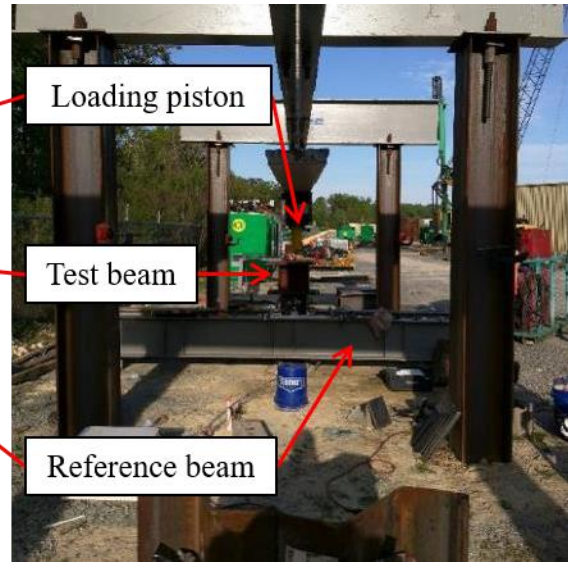


b.) Side view of reaction frame over HP 12x53 test pile with reference beams

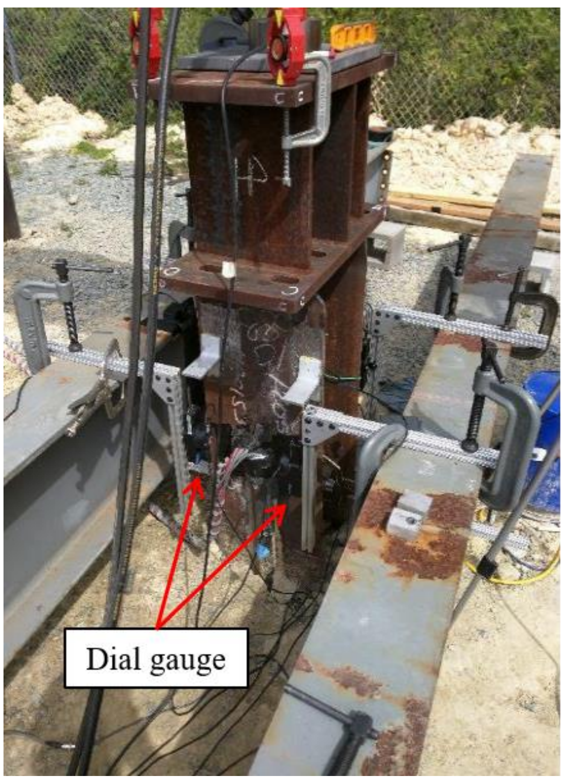


c.) Close up on HP 12x53 test pile showing instrumentation

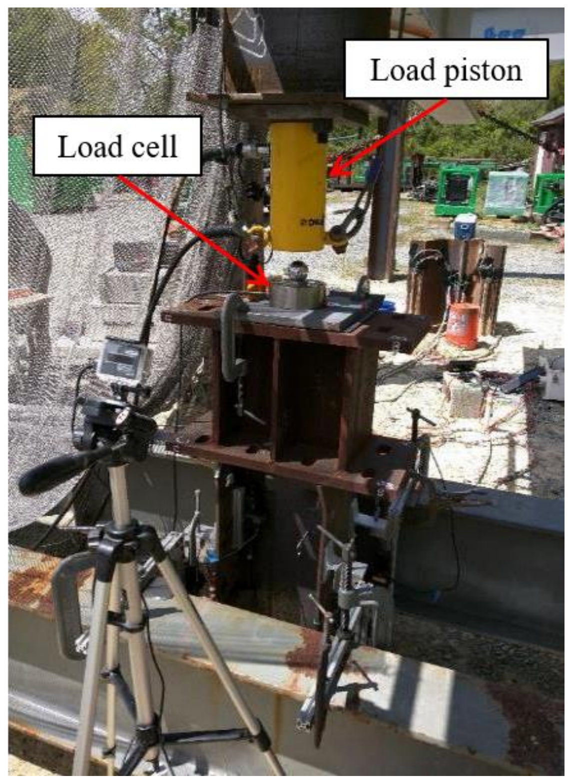


d.) Side view of same test pile showing the load piston and load cell.

Figure C-18. Images of test setup used for testing of H-pile at ICE field site

Figure C-19. Image of static load test setup for sheet pile at ICE field site

# APPENDIX D. SUPPLEMENTAL INFORMATION- STATIC METHODS

## D.1. Static Capacity Estimates Based on SPT Measurements

This section considers methods for pile load capacity based on SPT data. Several methods exist in the literature for determining pile load capacity based on this information. A few of the most popular and commonly used methods are summarized here and are considered in more depth as part of this research. The SPT based methods were performed as described in the report FHWA-NHI-05-042, Design and Construction of Driven Pile Foundations – Volume 1 (2006).

### D.1.1. Meyerhof Method

The Meyerhof Method (Meyerhof 1959) is a popular empirical static method for determining pile capacity, it provides an accessible estimate of pile capacity and the required information for the method is typically available from routine site investigation. It is best suited for cohesionless soils and requires SPT information, specifically $(N_1)_{60}$ values. This method is popular partly due to the availability of SPT test results and ease of use. Values for $f_s$ in units of kPa are obtained directly from $(N_1)_{60}$ values which are multiplied by a factor of 1 for non-displacement piles or 2 for displacement piles, $f_s$ values are limited by a maximum value of 100 kPa. For piles driven into a uniform bearing layer, the toe resistance, in units of kPa, can be determined as:

$$q_t = \frac{40\left(\left(\bar{N}_1\right)_{60}\right)_B D_B}{b} \leq 400\left(\left(\bar{N}_1\right)_{60}\right)_B \;;\left(=300\left(\left(\bar{N}_1\right)_{60}\right)_B \text{ for non-plasatic silts}\right) \quad \text{(D.1)}$$

Or for the case where a weaker soil layer overlays the bearing stratum and the interface is near the elevation of the pile toe:

$$q_t = 400\left(\left(\bar{N}_1\right)_{60}\right)_O + \frac{\left(40\left(\left(\bar{N}_1\right)_{60}\right)_B - 40\left(\left(\bar{N}_1\right)_{60}\right)_O\right)D_B}{b} \le 400\left(\left(\bar{N}_1\right)_{60}\right)_B \qquad \text{(D.2)}$$

,

$\left(\left(\bar{N}_1\right)_{60}\right)_B$ = Average corrected SPT blow count for bearing layer of soil,

$D_B$ = Embedment depth of pile into bearing stratum (m),

$b$ = Pile diameter (m), and

$\left(\left(\bar{N}_1\right)_{60}\right)_O$ = Average corrected SPT blow count for soil layer above bearing layer.

For Equation (D.1), the limiting value is reached within ten pile diameters of embedment into the bearing layer. Also, $\left(\left(\bar{N}_1\right)_{60}\right)_B$ should be calculated based on the zone of soil extending three diameters below the pile toe. This method provides a quick, easy to calculate value for pile capacity and is based on numerous pile load tests. Appropriate static capacity values will depend upon the quality of the SPT data and corrected values.

### D.1.2. Beta (Effective Stress) Method

The Beta method is a semi-empirical method which is best suited for cohesionless soils but can also be used for cohesive soil. This method is best suited for drained, long term conditions. Shaft resistance is a function of effective overburden pressure, the earth pressure coefficient, and the soil-pile interface friction angle. Toe resistance is a function of effective overburden pressure at the toe and a toe bearing coefficient which is a function of soil type and the angle of internal friction. The equations for calculating unit resistances are provided below:

$$f_s = \beta \bar{p}_0 \qquad \text{(D.3)}$$

where,

$\beta$ = Bjerrum-Burland beta coefficient = $K_s \tan(\delta)$,

$\bar{p}_0$ = Average of effective overburden pressure along the shaft of the pile,

$K_s$ = Earth pressure coefficient, and

$\delta$ = Soil-pile interface friction angle.

$$q_t = N_t p_t \tag{D.4}$$

where,

$N_t$ = Toe bearing capacity coefficient, and

$p_t$ = Effective overburden pressure at the pile toe.

Limiting values are not applied for shaft or toe bearing resistances. Typical values for $N_t$ range from 30 to 120 for sedimentary and cohesionless soils. Softer clays tend to have values around 30 or lower and very dense soils can have values equal to and much higher than 120. It is recommended that local experience be used when selecting parameter values. Additionally, confirmation of parameters for use in the equations is recommended through the comparison of static capacity calculations with static load test results.

### D.1.3. Nordlund Method

The Nordlund method (Nordlund 1963) is a semi-empirical method best suited for capacity estimates for piles driven into cohesionless soils. The method is based upon numerous pile load tests and can account for different pile geometries and materials. This method is best suited for piles ranging in width from 250 to 500 mm and will tend to over predict capacity for piles with widths greater than 600 mm. The method suggests that shaft resistance is a function of the friction angle of the soil, the soil to pile friction angle, the geometry of the pile (taper, length, and perimeter), the effective unit weight of the soil, and the volume of soil displaced. The equation for this method is provided below:

$$Q_u = \sum_{d=0}^{d=D} K_\delta C_F p_d \frac{\sin(\delta+\omega)}{cos(\omega)} C_d \Delta d + \alpha_t N'_q A_t p_t \qquad \text{(D.5)}$$

where,

$d$ = Depth,

$D$ = Embedded depth of pile,

$K_\delta$ = Coefficient of lateral earth pressure at depth *d*,

$C_F$ = Correction factor for $K_\delta$, to be used when $\delta \neq \phi$,

$p_d$ = Effective overburden pressure at the center of depth increment *d*,

$\delta$ = Friction angle between pile and soil,

$\phi$ = Internal friction angle for soil,

$\omega$ = Angle of pile taper, measured from the vertical,

$C_d$ = Pile perimeter at depth *d*,

$\Delta d$ = Length of a pile segment,

$\alpha_t$ = Dimensionless factor, a function of the pile depth-width relationship,

$N'_q$ = Bearing capacity factor,

$A_t$ = Pile toe area, and

$p_t$ = Effective overburden pressure at the pile toe.

This method utilizes values of the soil friction angle, ideally these values are provided by laboratory measurements but in the absence of this information they can be estimated based on SPT data. A limiting value of 150 kPa is recommended for the effective overburden pressure at the pile toe, limiting values for shaft resistance are not provided. The accuracy of the parameters outlined above, especially soil friction angle, will influence the accuracy of predicted capacities when using this method.

### D.1.4. Brown Method

The Brown Method (Brown et al. 2001) is an empirical method for determining pile capacity estimates and is best suited for cohesionless soils. The load tests used to develop the method incorporated various pile types including closed and open end pipe piles, H-piles, and precast concrete piles. The method also provides values accounting for compression or tension loading as well as impact or vibratory driving. Shaft resistance provided by the soil is determined using empirical factors obtained from the load test database and information regarding the soil conditions, as well as assumptions regarding plugging behavior when determining shaft bearing area. Values for empirical factors are provided in Table D-1. The equation for shaft resistance capacity is as follows:

$$R_s = f_s \cdot A_s \tag{D.6}$$

where,

$f_s = F_{vs}\left(A_b + B_b N_{60}\right)$,

$F_{vs}$ = Empirical reduction factor, 1.0 for impact driving, 0.68 for vibratory driving,

$A_b$ and $B_b$ = Empirical constants based on soil type,

$N_{60}$ = SPT N corrected for 60% energy transfer, with minimum and maximum values of 3 and 50, respectively, and

$A_s$ = Pile shaft area using outside shaft area only for pipe piles or outside area assuming full box plug for H-piles.

The calculation of toe resistance incorporates plugging behavior for pipe piles and partial plugging behavior for H-piles. Toe capacity is determined using the following equation:

$$R_t = q_t\left(A_t + A_{tp}F_p\right) \tag{D.7}$$

where,

$q_t = 0.17N_{60}$ for impact driven piles, multiply by 0.56 for vibratory driven piles (MPa),

$A_t$ = Cross sectional area of steel,

$A_{tp}$ = soil plug area at the pile toe, and

$F_p$ = Plug mobilization factor, 0.42 for open end pipe piles, 0.67 for H-piles.

Table D-1. Empirical factors used for determination of shaft resistance through the Brown Method (Hannigan et al. 2006)

| Loading Condition | Installation Method | Soil Type | $F_{vs}$ | $A_b$ (kPa) | $B_b$ (kPa/$N_{60}$) |
|---|---|---|---|---|---|
| Compression | Impact | Clay to Sand | 1.0 | 26.6 | 1.92 |
| | | Gravelly Sand to Boulders | | 42.6 | 42.6 |
| | | Rock | | 138.0 | 138.0 |
| Tension | | Clay to Sand | | 25.0 | 1.8 |
| | | Gravelly Sand to Boulders | | 40.0 | 0.0 |
| | | Rock | | 130.0 | 0.0 |
| | Vibratory | Clay to Sand | 0.68 | 25.0 | 0.0376 |
| | | Gravelly Sand to Boulders | | 40.0 | 0.0 |

| | | | | | |
|---|---|---|---|---|---|
| | | Rock | | 130.0 | 0.0 |

## D.2. Static Capacity Estimates Based on CPT Measurements

This section considers methods for pile load capacity based on CPT data. A CPT sounding can represent an especially useful dataset when predicting pile axial load capacities. The sensor used to perform the test can be thought of as a model pile during driving and can experience stresses similar to what a pile may encounter during a pile load test. For a given soil profile a CPT test yields continuous values for frictional ($f_s$) and tip ($q_t$) resistance for the length of the sounding, these measured resistances can be considered similar to the two sources of resistance which in summation provide pile load capacity. The following sections present these methods in more detail. The LCPC and De Ruiter and Beringen methods were preformed as described in “Cone Penetration Testing in Geotechnical Practice” by T. Lunne, P.K. Robertson, and J.J.M. Powell (1997). The Nottingham and Schmertmann and Elasami and Fellenius methods were preformed as described in the report FHWA-NHI-05-042, Design and Construction of Driven Pile Foundations – Volume 1 (2006).

### D.2.1. Laboratoire Central des Ponts et Chaussees (LCPC)

The Laboratoire Central des Ponts et Chaussees (LCPC) method was developed by Bustamante and Gianeselli (1982) and is an empirical method developed using the results from 197 pile load tests on various pile and soil types. The method utilizes primarily $q_c$ values to develop both shaft and toe resistance values for the pile. Values for shaft resistance depend upon pile type and installation method. The method determines shaft resistance by dividing $q_c$ by an $\alpha$ value, which is a function of pile and soil type, maximum $f_s$ values are provided by the authors.

Tip resistance involves an interpretation procedure that averages $q_c$ values 1.5 times the diameter above and below the installation depth of the pile toe to obtain an equivalent average cone resistance, $q_{ca}$. This averaging procedure is outlined by Lunne et al. (1997) . This averaged $q_{ca}$ value is then multiplied by an end-bearing coefficient, $k_c$, to obtain unit end-bearing resistance, $q_p$. Values for $k_c$ are a function of soil and pile type. The method suggests using the cross sectional area of steel for the pile toe area unless past experience or a compelling reason suggests a plug is forming. If the plugged area is used, the corresponding plugged perimeter should be used to determine the shaft bearing resistance. Table D-2 presents factors for the calculations used for this method.

Table D-2. Values for limiting values of $f_p$ and $\alpha$ based on measured soil $q_c$ values and soil type for driven metal piles (Lunne et al. 1997)

| Soil Description | $q_c$ (MPa) | Values for driven metal piles | | |
|---|---|---|---|---|
| | | α | Maximum value of $f_p$ (MPa) | $k_c$ |
| Soft clay and mud | < 1 | 30 | 0.015 | 0.5 |
| Moderately compact clay | 1 to 5 | 80 | 0.035 | 0.45 |
| Silt and loose sand | ≤ 5 | 120 | 0.035 | 0.5 |
| Compact to stiff clay and compact silt | > 5 | 120 | 0.035 | 0.55 |
| Soft chalk | ≤ 5 | 120 | 0.035 | 0.3 |
| Moderately compact sand and gravel | 5 to 12 | 200 | 0.08 | 0.5 |
| Weathered to fragmented chalk | > 5 | 80 | 0.12 | 0.4 |
| Compact to very compact sand and gravel | > 12 | 200 | 0.12 | 0.4 |

### D.2.2. Nottingham and Schmertmann

The Nottingham and Schmertmann method (Nottingham 1975) is an empirical procedure which considers the pile material and geometry. This method utilizes sleeve resistance measured from the CPT for determining shaft resistance as follows:

$$R_s = K\left[\frac{1}{2}\left(\overline{f_s}A_s\right)_{0\,to\,8b} + \left(\overline{f_s}A_s\right)_{8b\,to\,D}\right] \tag{D.8}$$

where,

$K$ = The ratio of unit pile shaft resistance to unit cone sleeve friction, and is a function of pile embedment, diameter, material, and type of penetrometer used for testing,

$\overline{f_s}$ = Average unit sleeve friction over the depth interval denoted in subscript, no limiting value applied,

$b$ = Pile diameter (or width), and

$D$ = Pile embedment length.

In the absence of sleeve friction data, the shaft resistance can be estimated using the cone toe resistance as follows:

$$R_s = C_f \sum q_c A_s \tag{D.9}$$

where,

$C_f$ = A factor based on material and type of pile,

$q_c$ = Average toe resistance along the pile length, and

$A_s$ = Pile-soil surface area.

For shaft resistance in cohesive soils, the shaft resistance can be obtained as follows:

$$R_s = \alpha' \overline{f_s} A_s \tag{D.10}$$

where,

$\alpha'$ = The ratio of pile shaft resistance to cone sleeve friction for the region of soil 8 pile diameters (or widths) above the pile toe, and 3.75 pile diameters below the pile toe.

Values for toe resistance are determined using a ‘minimum path’ rule for averaging CPT tip resistance measured values. A limiting value for CPT measured $q_c$ between 5,000 and 15,000 kPa is recommended, unless local experience suggests otherwise. For the scenario of mechanical cone resistance in cohesive soils, the $q_t$ value should be reduced by 40 percent due to end-bearing effects on the base of the friction sleeve. Specific considerations regarding plugging are not provided, however careful consideration of this behavior is recommended when choosing values for toe bearing area.

### D.2.3. De Ruiter and Beringen

The De Ruiter and Beringen method (De Ruiter and Beringen 1979) provides different procedures for determining capacity for both sand and clay soil profiles. For clay soils, the method first determines undrained shear strength, $s_u$, along the shaft based on CPT $q_c$ measurements. It is recommended that the $s_u$ value be obtained by dividing $q_c$ by a cone factor, $N_k$, which is equal to 15 to 20. Unit shaft resistance is obtained by multiplying $s_u$ by an $\alpha$ factor which depends on if the soil is normally or over consolidated. For toe resistance in clay, $s_u$ is multiplied by a factor of $N_c$ which is equal to 9 for this method.

For sand soil, unit skin friction equals the minimum of four numbers as determined in Table D-3. Values for toe resistance are determined based on averaged $q_c$ values taken above and below the pile tip, the procedure uses the minimum path rule and is described by Lunne et al. (1997) . OCR influences pile capacity for sand soil, the authors found. Limiting values for unit toe resistance in sand are provided based on the

OCR, and in all cases resistance values can't exceed 15 MPa. Figure D-1 presents these limiting values.

Table D-3. Values for shaft and toe resistances from De Ruiter and Beringen method (obtained from Lunne et al. (1997) )

| | Sand | Clay |
|---|---|---|
| Unit skin friction, $f_p$ | Minimum of:<br>• $f_1$= 0.12 MPa<br>• $f_2$= CPT sleeve friction, $f_s$<br>• $f_3$= $q_c$/300 (compression)<br>• $f_4$= $q_c$/400 (tension) | $f = \alpha \cdot s_u$<br>Where:<br>$\alpha$= 1 for N.C. clay,<br>$\alpha$= 0.5 for O.C. clay |
| Unit end-bearing, $q_p$ | Use minimum value obtained from averaging procedure described by authors and value obtained from Figure D-1 | $q_p = N_c \cdot s_u$<br>Where:<br>$N_c$= 9,<br>$s_u$= $q_c$/$N_k$,<br>$N_k$= 15 to 20 |

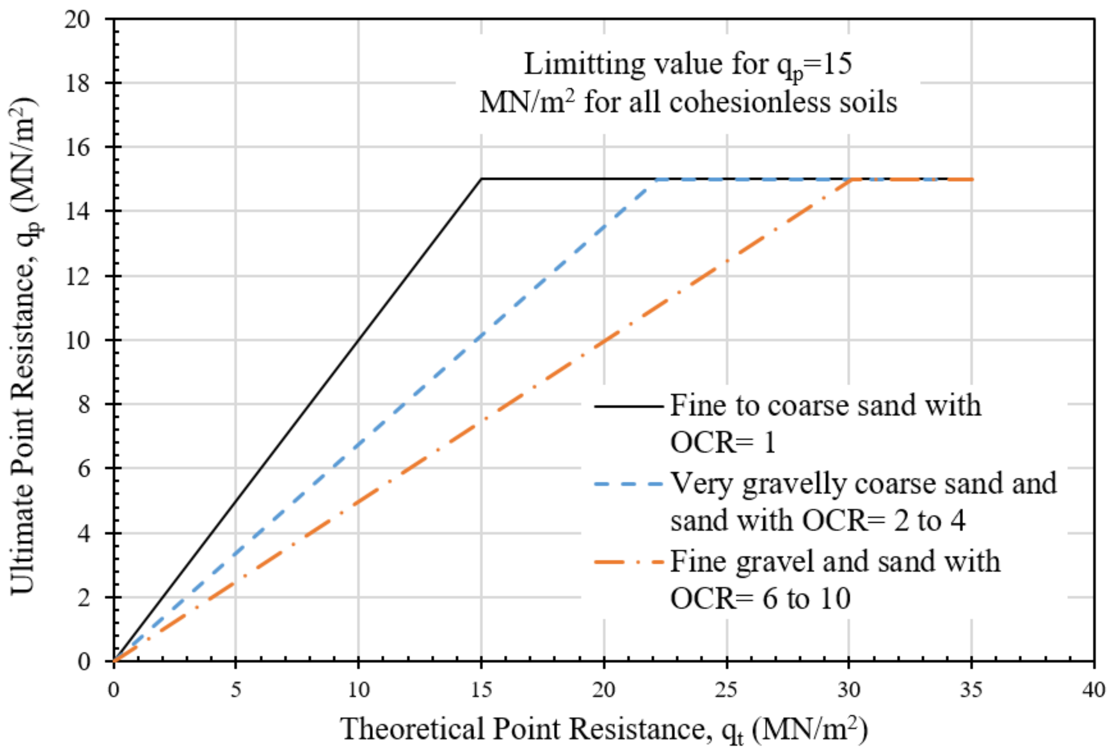


Figure D-1. Limiting values for $q_p$ for sand soils (obtained from De Ruiter and Beringen (1979) )

D.3. Elsami and Fellenius Method

The Elsami and Fellenius method (Eslami and Fellenius 1997) was developed based on 102 pile load tests which include a wide range of soil profiles and embedment depths. The method uses measured cone tip resistance for determining unit shaft and toe resistances. Shaft resistance is determined through the following equation:

$$f_s = C_{sc} q_E \tag{D.11}$$

where,

$C_{sc}$ = A shaft correlation coefficient, a function of soil type, and

$q_E$ = The cone tip resistance after correction for pore pressures and effective stress.

For toe resistance, values are obtained from the following equation:

$$q_t = C_{tc} q_{Eg} \tag{D.12}$$

where,

$C_{tc}$ = toe correction coefficient, a function of pile diameter and usually equal to 1, (for pile diameters greater than 400 mm $C_{tc} = \frac{1}{3}b$ (m)) and,

$q_{Eg}$ = Cone tip resistance, corrected for pore pressure and effective stress, geometrically averaged over the influence zone.

The zone of influence used for determining $q_t$ is based on pile diameter (or width). For the scenario of a weak stratum overlying a dense stratum this zone ranges from 4b below the toe to 8b above. For the scenario of a dense stratum overlying a weak stratum this zone ranges from 4b below the toe to 2b above.